



Lecture Notes for the 2017 School for Experimental High Energy Physics Students

**Lecturers: A Banfi, DG Cerdeño, C Englert, S Badger,
C Maxwell
Compiler : N. Konstantinidis**

September 2017

©2017 Science and Technology Facilities Council



This work is licensed under a [Creative Commons Attribution 3.0 Unported License](https://creativecommons.org/licenses/by/3.0/).

Enquiries concerning this report should be addressed to:

RAL Library
STFC Rutherford Appleton Laboratory
Harwell Oxford
Didcot
OX11 0QX

Tel: +44(0)1235 445384
Fax: +44(0)1235 446403
email: libraryral@stfc.ac.uk

Science and Technology Facilities Council reports are available online at: <http://epubs.stfc.ac.uk>

ISSN 1358-6254

Neither the Council nor the Laboratory accept any responsibility for loss or damage arising from the use of information contained in any of their reports or in any communication about their tests or investigations.

Science and Technology Facilities Council

**Lecture Notes for the 2017
School for Experimental High
Energy Physics Students**

**University of Lancaster
3 - 15 September 2017**

**Lecturers: A. Banfi, D. G. Cerdeño, C. Englert, S. Badger, C. Maxwell
Compiler: N. Konstantinidis**

CONTENTS

Pages

LECTURE COURSES

| | |
|---|-----------|
| Quantum Field Theory Dr C. Englert | 1 - 52 |
| An Introduction to QED & QCD Dr A. Banfi | 53 - 97 |
| The Standard Model Dr C. Maxwell | 98 - 133 |
| Phenomenology Dr S. Badger | 134 - 212 |
| Dark Matter Dr D. G. Cerdeño | 213 - 242 |

QUANTUM FIELD THEORY

Dr Christoph Englert (University of Glasgow)

Contents

| | | |
|----------|--|-----------|
| 1 | Introduction | 5 |
| 1.1 | Classical Mechanics | 6 |
| 1.2 | Quantum mechanics..... | 9 |
| 1.3 | The Schrödinger picture..... | 10 |
| 1.4 | The Heisenberg picture..... | 11 |
| 1.5 | The quantum harmonic oscillator | 12 |
| 1.6 | Relativistic Quantum Mechanics | 13 |
| 2 | Classical Field Theory..... | 15 |
| 2.1 | Example: Model of an Elastic Rod..... | 15 |
| 2.2 | Relativistic Fields | 17 |
| 2.3 | Plane wave solutions to the Klein-Gordon equation..... | 19 |
| 2.4 | Symmetries and Conservation Laws | 19 |
| 3 | Quantum Field Theory: Free Fields..... | 21 |
| 3.1 | Canonical Field Quantisation..... | 21 |
| 3.2 | Creation and annihilation operators | 23 |
| 3.3 | Energy of the vacuum state and renormalisation | 24 |
| 3.4 | Fock space and Particles | 26 |
| 4 | Quantum Field Theory: Interacting Fields | 28 |
| 4.1 | The S-matrix..... | 28 |
| 4.2 | More on time evolution: Dirac picture | 31 |
| 4.3 | S-matrix and Green's functions | 33 |
| 4.4 | How to compute Green's functions | 36 |
| 5 | Perturbation Theory | 38 |
| 5.1 | Wick's Theorem..... | 39 |
| 5.2 | The Feynman propagator | 40 |
| 5.3 | Two-particle scattering to $O(\lambda)$ | 41 |
| 5.4 | Graphical representation of the Wick expansion: Feynman rules..... | 43 |
| 5.5 | Feynman rules in momentum space | 45 |
| 5.6 | S-matrix and truncated Green's functions | 46 |
| 6 | Summary..... | 48 |
| | Acknowledgments | 50 |
| A | Books on QFT | 50 |
| | References..... | 50 |
| B | Notation and conventions | 52 |

Quantum Field Theory

Christoph Englert¹

These notes are a write-up of lectures given at the RAL school for High Energy Physicists, which took place at Warwick in 2014. The aim is to introduce the canonical quantisation approach to QFT, and derive the Feynman rules for a scalar field.

1 Introduction

Quantum Field Theory is a highly important cornerstone of modern physics. It underlies, for example, the description of elementary particles i.e. the Standard Model of particle physics is a QFT. There is currently no observational evidence to suggest that QFT is insufficient in describing particle behaviour, and indeed many theories for beyond the Standard Model physics (e.g. supersymmetry, extra dimensions) are QFTs. There are some theoretical reasons, however, for believing that QFT will not work at energies above the Planck scale, at which gravity becomes important. Aside from particle physics, QFT is also widely used in the description of condensed matter systems, and there has been a fruitful interplay between the fields of condensed matter and high energy physics.

We will see that the need for QFT arises when one tries to unify special relativity and quantum mechanics, which explains why theories of use in high energy particle physics are quantum field theories. Historically, Quantum Electrodynamics (QED) emerged as the prototype of modern QFT's. It was developed in the late 1940s and early 1950s chiefly by Feynman, Schwinger and Tomonaga, and has the distinction of being the most accurately verified theory of all time: the anomalous magnetic dipole moment of the electron predicted by QED agrees with experiment with a stunning accuracy of one part in 10^{10} ! Since then, QED has been understood as forming part of a larger theory, the Standard Model of particle physics, which also describes the weak and strong nuclear forces. As you will learn at this school, electromagnetism and the weak interaction can be unified into a single “electroweak” theory, and the theory of the strong force is described by Quantum Chromodynamics (QCD). QCD has been verified in a wide range of contexts, albeit not as accurately as QED (due to the fact that the QED force is much weaker, allowing more accurate calculations to be carried out).

As is clear from the above discussion, QFT is a type of theory, rather than a particular theory. In this course, our aim is to introduce what a QFT is, and how to derive scattering amplitudes in perturbation theory (in the form of Feynman rules). For this purpose, it is sufficient to consider the simple example of a single, real scalar field. More physically relevant examples will be dealt with

¹SUPA, School of Physics and Astronomy, University of Glasgow.
Email: christoph.englert@glasgow.ac.uk

in the other courses. Throughout, we will follow the so-called canonical quantisation approach to QFT, rather than the path integral approach. Although the latter approach is more elegant, it is less easily presented in such a short course.

The structure of these notes is as follows. In the rest of the introduction, we review those aspects of classical and quantum mechanics which are relevant in discussing QFT. In particular, we go over the Lagrangian formalism in point particle mechanics, and see how this can also be used to describe classical fields. We then look at the quantum mechanics of non-relativistic point particles, and recall the properties of the quantum harmonic oscillator, which will be useful in what follows. We then briefly show how attempts to construct a relativistic analogue of the Schrödinger equation lead to inconsistencies. Next, we discuss classical field theory, deriving the equations of motion that a relativistic scalar field theory has to satisfy, and examining the relationship between symmetries and conservation laws. We then discuss the quantum theory of free fields, and interpret the resulting theory in terms of particles, before showing how to describe interactions via the S -matrix and its relation to Green's functions. Finally, we describe how to obtain explicit results for scattering amplitudes using perturbation theory, which leads (via Wick's theorem) to Feynman diagrams.

1.1 Classical Mechanics

Let us begin this little review by considering the simplest possible system in classical mechanics, a single point particle of mass m in one dimension, whose coordinate and velocity are functions of time, $x(t)$ and $\dot{x}(t) = dx(t)/dt$, respectively. Let the particle be exposed to a time-independent potential $V(x)$. Its motion is then governed by Newton's law

$$m \frac{d^2x}{dt^2} = -\frac{\partial V}{\partial x} = F(x), \quad (1)$$

where $F(x)$ is the force exerted on the particle. Solving this equation of motion involves two integrations, and hence two arbitrary integration constants to be fixed by initial conditions. Specifying, e.g., the position $x(t_0)$ and velocity $\dot{x}(t_0)$ of the particle at some initial time t_0 completely determines its motion: knowing the initial conditions and the equations of motion, we also know the evolution of the particle at all times (provided we can solve the equations of motion).

We can also derive the equation of motion using an entirely different approach, via the Lagrangian formalism. This is perhaps more abstract than Newton's force-based approach, but in fact is easier to generalise and technically more simple in complicated systems (such as field theory!), not least because it avoids us having to think about forces at all.

First, we introduce the *Lagrangian*

$$L(x, \dot{x}) = T - V = \frac{1}{2}m\dot{x}^2 - V(x), \quad (2)$$

which is a function of coordinates and velocities, and given by the difference between the kinetic and potential energies of the particle. Next, we define the *action*

$$S = \int_{t_0}^{t_1} dt L(x, \dot{x}). \quad (3)$$

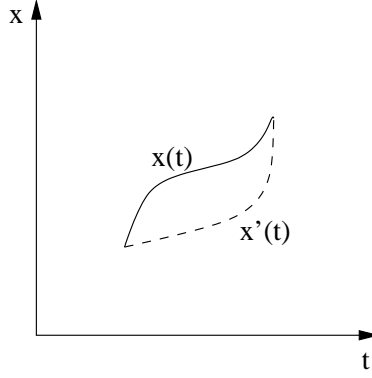


Figure 1: *Variation of particle trajectory with identified initial and end points.*

The equations of motion are then given by the *principle of least action*, which says that the trajectory $x(t)$ followed by the particle is precisely that such that S is extremised². To verify this in the present case, let us rederive Newton's Second Law.

First let us suppose that $x(t)$ is indeed the trajectory that extremises the action, and then introduce a small perturbation

$$x(t) \rightarrow x(t) + \delta x(t), \quad (4)$$

such that the end points are fixed:

$$\left. \begin{array}{l} x'(t_1) = x(t_1) \\ x'(t_2) = x(t_2) \end{array} \right\} \Rightarrow \delta x(t_1) = \delta x(t_2) = 0. \quad (5)$$

This sends S to some $S + \delta S$, where $\delta S = 0$ if S is extremised. One may Taylor expand to give

$$\begin{aligned} S + \delta S &= \int_{t_1}^{t_2} L(x + \delta x, \dot{x} + \delta \dot{x}) dt, \quad \delta \dot{x} = \frac{d}{dt} \delta x \\ &= \int_{t_1}^{t_2} \left\{ L(x, \dot{x}) + \frac{\partial L}{\partial x} \delta x + \frac{\partial L}{\partial \dot{x}} \delta \dot{x} + \dots \right\} dt \\ &= S + \frac{\partial L}{\partial \dot{x}} \delta x \Big|_{t_1}^{t_2} + \int_{t_1}^{t_2} \left\{ \frac{\partial L}{\partial x} - \frac{d}{dt} \frac{\partial L}{\partial \dot{x}} \right\} \delta x dt, \end{aligned} \quad (6)$$

where we performed an integration by parts on the last term in the second line. The second and third term in the last line are the variation of the action, δS , under variations of the trajectory, δx . The second term vanishes because of the boundary conditions for the variation, and we are left with the third. Now the Principle of Least Action demands $\delta S = 0$. For the remaining integral to vanish for arbitrary δx is only possible if the integrand vanishes, leaving us with the Euler-Lagrange equation:

$$\frac{\partial L}{\partial x} - \frac{d}{dt} \frac{\partial L}{\partial \dot{x}} = 0. \quad (7)$$

²The name of the principle comes from the fact that, in most cases, S is indeed minimised.

If we insert the Lagrangian of our point particle, Eq. (2), into the Euler-Lagrange equation we obtain

$$\begin{aligned}\frac{\partial L}{\partial x} &= -\frac{\partial V(x)}{\partial x} = F \\ \frac{d}{dt} \frac{\partial L}{\partial \dot{x}} &= \frac{d}{dt} m\dot{x} = m\ddot{x} \\ \Rightarrow m\ddot{x} &= F = -\frac{\partial V}{\partial x} \quad (\text{Newton's law}).\end{aligned}\tag{8}$$

Hence, we have derived the equation of motion (the Euler-Lagrange equation) using the Principal of Least Action and found it to be equivalent to Newton's Second Law. The benefit of the former is that it can be easily generalised to other systems in any number of dimensions, multi-particle systems, or systems with an infinite number of degrees of freedom, where the latter are needed for field theory.

For example, a general system of point particles has a set $\{q_i\}$ of *generalised coordinates*, which may not be simple positions but also angles etc. The equations of motion are then given by

$$\frac{d}{dt} \frac{\partial L}{\partial \dot{q}_i} = \frac{\partial L}{\partial q_i},$$

by analogy with the one-dimensional case. That is, each coordinate has its own Euler-Lagrange equation (which may nevertheless depend on the other coordinates, so that the equations of motion are coupled). Another advantage of the Lagrangian formalism is that the relationship between symmetries and conserved quantities is readily understood - more on this later.

First, let us note that there is yet another way to think about classical mechanics (that we will see again in quantum mechanics / field theory), namely via the Hamiltonian formalism. Given a Lagrangian depending on generalised coordinates $\{q_i\}$, we may define the *conjugate momenta*

$$p_i = \frac{\partial L}{\partial \dot{q}_i}$$

e.g. in the simple one-dimensional example given above, there is a single momentum $p = m\dot{x}$ conjugate to x . We recognise as the familiar definition of momentum, but it is not always true that $p_i = m\dot{q}_i$.

We may now define the *Hamiltonian*

$$H(\{q_i\}, \{p_i\}) = \sum_i \dot{q}_i p_i - L(\{q_i\}, \{\dot{q}_i\}).$$

As an example, consider again

$$L = \frac{1}{2}m\dot{x}^2 - V(x).$$

It is easy to show from the above definition that

$$H = \frac{1}{2}m\dot{x}^2 + V(x),$$

which we recognise as the total energy of the system. From the definition of the Hamiltonian one may derive (problem 1.1)

$$\frac{\partial H}{\partial q_i} = -\dot{p}_i, \quad \frac{\partial H}{\partial p_i} = \dot{q}_i,$$

which constitute *Hamilton's equations*. These are useful in proving the relation between symmetries and conserved quantities. For example, one readily sees from the above equations that the momentum p_i is conserved if H does not depend explicitly on q_i . That is, conservation of momentum is related to invariance under spatial translations, if q_i can be interpreted as a simple position coordinate.

1.2 Quantum mechanics

Having set up some basic formalism for classical mechanics, let us now move on to quantum mechanics. In doing so we shall use *canonical quantisation*, which is historically what was used first and what we shall later use to quantise fields as well. We remark, however, that one can also quantise a theory using path integrals.

Canonical quantisation consists of two steps. Firstly, the dynamical variables of a system are replaced by operators, which we denote by a hat. Secondly, one imposes commutation relations on these operators,

$$[\hat{x}_i, \hat{p}_j] = i\hbar \delta_{ij} \quad (9)$$

$$[\hat{x}_i, \hat{x}_j] = [\hat{p}_i, \hat{p}_j] = 0. \quad (10)$$

The physical state of a quantum mechanical system is encoded in state vectors $|\psi\rangle$, which are elements of a Hilbert space \mathcal{H} . The hermitian conjugate state is $\langle\psi| = (|\psi\rangle)^\dagger$, and the modulus squared of the scalar product between two states gives the probability for the system to go from state 1 to state 2,

$$|\langle\psi_1|\psi_2\rangle|^2 = \text{probability for } |\psi_1\rangle \rightarrow |\psi_2\rangle. \quad (11)$$

On the other hand physical observables O , i.e. measurable quantities, are given by the expectation values of hermitian operators, $\hat{O} = \hat{O}^\dagger$,

$$O = \langle\psi|\hat{O}|\psi\rangle, \quad O_{12} = \langle\psi_2|\hat{O}|\psi_1\rangle. \quad (12)$$

Hermiticity ensures that expectation values are real, as required for measurable quantities. Due to the probabilistic nature of quantum mechanics, expectation values correspond to statistical averages, or mean values, with a variance

$$(\Delta O)^2 = \langle\psi|(\hat{O} - O)^2|\psi\rangle = \langle\psi|\hat{O}^2|\psi\rangle - \langle\psi|\hat{O}|\psi\rangle^2. \quad (13)$$

An important concept in quantum mechanics is that of eigenstates of an operator, defined by

$$\hat{O}|\psi\rangle = O|\psi\rangle. \quad (14)$$

Evidently, between eigenstates we have $\Delta O = 0$. Examples are coordinate eigenstates, $\hat{\mathbf{x}}|\mathbf{x}\rangle = \mathbf{x}|\mathbf{x}\rangle$, and momentum eigenstates, $\hat{\mathbf{p}}|\mathbf{p}\rangle = \mathbf{p}|\mathbf{p}\rangle$, describing a particle at position \mathbf{x} or with momentum \mathbf{p} , respectively. However, a state vector cannot be simultaneous eigenstate of non-commuting

operators. This leads to the Heisenberg uncertainty relation for any two non-commuting operators \hat{A}, \hat{B} ,

$$\Delta A \Delta B \geq \frac{1}{2} |\langle \psi | [\hat{A}, \hat{B}] | \psi \rangle|. \quad (15)$$

Finally, sets of eigenstates can be orthonormalized and we assume completeness, i.e. they span the entire Hilbert space,

$$\langle \mathbf{p}' | \mathbf{p} \rangle = \delta(\mathbf{p} - \mathbf{p}'), \quad 1 = \int d^3 p |\mathbf{p}\rangle \langle \mathbf{p}|. \quad (16)$$

As a consequence, an arbitrary state vector can always be expanded in terms of a set of eigenstates. We may then define the *position space wavefunction*

$$\psi(\mathbf{x}) = \langle \mathbf{x} | \psi \rangle,$$

so that

$$\begin{aligned} \langle \psi_1 | \psi_2 \rangle &= \int d^3 \mathbf{x} \langle \psi_1 | \mathbf{x} \rangle \langle \mathbf{x} | \psi_2 \rangle \\ &= \int d^3 \mathbf{x} \psi_1^*(\mathbf{x}) \psi_2(\mathbf{x}). \end{aligned} \quad (17)$$

Acting on the wavefunction, the explicit form of the position and momentum operators is

$$\hat{\mathbf{x}} = \mathbf{x}, \quad \hat{\mathbf{p}} = -i\hbar \nabla, \quad (18)$$

so that the Hamiltonian operator is

$$\hat{H} = \frac{\hat{\mathbf{p}}^2}{2m} + V(\mathbf{x}) = -\frac{\hbar^2 \nabla^2}{2m} + V(\mathbf{x}). \quad (19)$$

Having quantised our system, we now want to describe its time evolution. This can be done in different “pictures”, depending on whether we consider the state vectors or the operators (or both) to depend explicitly on t , such that expectation values remain the same. Two extreme cases are those where the operators do not depend on time (the *Schrödinger picture*), and when the state vectors do not depend on time (the *Heisenberg picture*). We discuss these two choices in the following sections.

1.3 The Schrödinger picture

In this approach state vectors are functions of time, $|\psi(t)\rangle$, while operators are time independent, $\partial_t \hat{O} = 0$. The time evolution of a system is described by the Schrödinger equation³,

$$i\hbar \frac{\partial}{\partial t} \psi(\mathbf{x}, t) = \hat{H} \psi(\mathbf{x}, t). \quad (20)$$

If at some initial time t_0 our system is in the state $\Psi(\mathbf{x}, t_0)$, then the time dependent state vector

$$\Psi(\mathbf{x}, t) = e^{-\frac{i}{\hbar} \hat{H}(t-t_0)} \Psi(\mathbf{x}, t_0) \quad (21)$$

³Note that the Hamiltonian could itself have some time dependence in general, even in the Schrödinger picture, if the potential of a system depends on time. Here we assume that this is not the case.

solves the Schrödinger equation for all later times t .

The expectation value of some hermitian operator \hat{O} at a given time t is then defined as

$$\langle \hat{O} \rangle_t = \int d^3x \Psi^*(\mathbf{x}, t) \hat{O} \Psi(\mathbf{x}, t), \quad (22)$$

and the normalisation of the wavefunction is given by

$$\int d^3x \Psi^*(\mathbf{x}, t) \Psi(\mathbf{x}, t) = \langle 1 \rangle_t. \quad (23)$$

Since $\Psi^* \Psi$ is positive, it is natural to interpret it as the *probability density* for finding a particle at position \mathbf{x} . Furthermore one can derive a conserved current \mathbf{j} , as well as a continuity equation by considering

$$\Psi^* \times (\text{Schr.Eq.}) - \Psi \times (\text{Schr.Eq.})^*. \quad (24)$$

The continuity equation reads

$$\frac{\partial}{\partial t} \rho = -\nabla \cdot \mathbf{j} \quad (25)$$

where the density ρ and the current \mathbf{j} are given by

$$\rho = \Psi^* \Psi \quad (\text{positive}), \quad (26)$$

$$\mathbf{j} = \frac{\hbar}{2im} (\Psi^* \nabla \Psi - (\nabla \Psi^*) \Psi) \quad (\text{real}). \quad (27)$$

Now that we have derived the continuity equation let us discuss the probability interpretation of Quantum Mechanics in more detail. Consider a finite volume V with boundary S . The integrated continuity equation is

$$\begin{aligned} \int_V \frac{\partial \rho}{\partial t} d^3x &= - \int_V \nabla \cdot \mathbf{j} d^3x \\ &= - \int_S \mathbf{j} \cdot d^2\mathbf{o} \end{aligned} \quad (28)$$

where in the last line we have used Gauss's theorem. Using Eq. (23) the left-hand side can be rewritten and we obtain

$$\frac{\partial}{\partial t} \langle 1 \rangle_t = - \int_S \mathbf{j} \cdot d^2\mathbf{o} = 0. \quad (29)$$

In other words, provided that $\mathbf{j} = 0$ everywhere at the boundary S , we find that the time derivative of $\langle 1 \rangle_t$ vanishes. Since $\langle 1 \rangle_t$ represents the total probability for finding the particle anywhere inside the volume V , we conclude that this probability must be conserved: particles cannot be created or destroyed in our theory. Non-relativistic Quantum Mechanics thus provides a consistent formalism to describe a single particle. The quantity $\Psi(\mathbf{x}, t)$ is interpreted as a one-particle wave function.

1.4 The Heisenberg picture

Here the situation is the opposite to that in the Schrödinger picture, with the state vectors regarded as constant, $\partial_t |\Psi_H\rangle = 0$, and operators which carry the time dependence, $\hat{O}_H(t)$. This is the concept

which later generalises most readily to field theory. We make use of the solution Eq. (21) to the Schrödinger equation in order to *define* a Heisenberg state vector through

$$\Psi(x, t) = e^{-\frac{i}{\hbar}\hat{H}(t-t_0)}\Psi(x, t_0) \equiv e^{-\frac{i}{\hbar}\hat{H}(t-t_0)}\Psi_H(x), \quad (30)$$

i.e. $\Psi_H(\mathbf{x}) = \Psi(\mathbf{x}, t_0)$. In other words, the Schrödinger vector at some time t_0 is defined to be equivalent to the Heisenberg vector, and the solution to the Schrödinger equation provides the transformation law between the two for all times. This transformation of course leaves the physics, i.e. expectation values, invariant,

$$\langle \Psi(t) | \hat{O} | \Psi(t) \rangle = \langle \Psi(t_0) | e^{\frac{i}{\hbar}\hat{H}(t-t_0)} \hat{O} e^{-\frac{i}{\hbar}\hat{H}(t-t_0)} | \Psi(t_0) \rangle = \langle \Psi_H | \hat{O}_H(t) | \Psi_H \rangle, \quad (31)$$

with

$$\hat{O}_H(t) = e^{\frac{i}{\hbar}\hat{H}(t-t_0)} \hat{O} e^{-\frac{i}{\hbar}\hat{H}(t-t_0)}. \quad (32)$$

From this last equation it is now easy to derive the equivalent of the Schrödinger equation for the Heisenberg picture, the Heisenberg equation of motion for operators:

$$i\hbar \frac{d\hat{O}_H(t)}{dt} = [\hat{O}_H, \hat{H}]. \quad (33)$$

Note that all commutation relations, like Eq. (9), with time dependent operators are now intended to be valid for all times. Substituting \hat{x}, \hat{p} for \hat{O} into the Heisenberg equation readily leads to

$$\begin{aligned} \frac{d\hat{x}_i}{dt} &= \frac{\partial \hat{H}}{\partial \hat{p}_i}, \\ \frac{d\hat{p}_i}{dt} &= -\frac{\partial \hat{H}}{\partial \hat{x}_i}, \end{aligned} \quad (34)$$

the quantum mechanical equivalent of the Hamilton equations of classical mechanics.

1.5 The quantum harmonic oscillator

Because of similar structures later in quantum field theory, it is instructive to also briefly recall the harmonic oscillator in one dimension. Its Hamiltonian is given by

$$\hat{H}(\hat{x}, \hat{p}) = \frac{1}{2} \left(\frac{\hat{p}^2}{m} + m\omega^2 \hat{x}^2 \right). \quad (35)$$

Employing the canonical formalism we have just set up, we easily identify the momentum operator to be $\hat{p}(t) = m\partial_t \hat{x}(t)$, and from the Hamilton equations we find the equation of motion to be $\partial_t^2 \hat{x} = -\omega^2 \hat{x}$, which has the well known plane wave solution $\hat{x} \sim \exp i\omega t$.

An alternative path useful for later field theory applications is to introduce new operators, expressed in terms of the old ones,

$$\hat{a} = \frac{1}{\sqrt{2}} \left(\sqrt{\frac{m\omega}{\hbar}} \hat{x} + i\sqrt{\frac{1}{m\omega\hbar}} \hat{p} \right), \quad \hat{a}^\dagger = \frac{1}{\sqrt{2}} \left(\sqrt{\frac{m\omega}{\hbar}} \hat{x} - i\sqrt{\frac{1}{m\omega\hbar}} \hat{p} \right). \quad (36)$$

Using the commutation relation for \hat{x}, \hat{p} , one readily derives (see the preschool problems)

$$[\hat{a}, \hat{a}^\dagger] = 1, \quad [\hat{H}, \hat{a}] = -\hbar\omega \hat{a}, \quad [\hat{H}, \hat{a}^\dagger] = \hbar\omega \hat{a}^\dagger. \quad (37)$$

With the help of these the Hamiltonian can be rewritten in terms of the new operators:

$$\hat{H} = \frac{1}{2}\hbar\omega \left(\hat{a}^\dagger \hat{a} + \hat{a} \hat{a}^\dagger \right) = \left(\hat{a}^\dagger \hat{a} + \frac{1}{2} \right) \hbar\omega. \quad (38)$$

With this form of the Hamiltonian it is easy to construct a complete basis of energy eigenstates $|n\rangle$,

$$\hat{H}|n\rangle = E_n|n\rangle. \quad (39)$$

Using the above commutation relations, one finds

$$\hat{a}^\dagger \hat{H}|n\rangle = (\hat{H} \hat{a}^\dagger - \hbar\omega \hat{a}^\dagger)|n\rangle = E_n \hat{a}^\dagger|n\rangle, \quad (40)$$

and therefore

$$\hat{H} \hat{a}^\dagger|n\rangle = (E_n + \hbar\omega) \hat{a}^\dagger|n\rangle. \quad (41)$$

Thus, the state $\hat{a}^\dagger|n\rangle$ has energy $E_n + \hbar\omega$, so that \hat{a}^\dagger may be regarded as a “creation operator” for a quantum with energy $\hbar\omega$. Along the same lines one finds that $\hat{a}|n\rangle$ has energy $E_n - \hbar\omega$, and \hat{a} is an “annihilation operator”.

Let us introduce a vacuum state $|0\rangle$ with no quanta excited, for which $\hat{a}|0\rangle = 0$, because there cannot be any negative energy states. Acting with the Hamiltonian on that state we find

$$\hat{H}|0\rangle = \hbar\omega/2, \quad (42)$$

i.e. the quantum mechanical vacuum has a non-zero energy, known as vacuum oscillation or *zero point energy*. Acting with a creation operator onto the vacuum state one easily finds the state with one quantum excited, and this can be repeated n times to get

$$\begin{aligned} |1\rangle &= \hat{a}^\dagger|0\rangle \quad , \quad E_1 = (1 + \frac{1}{2})\hbar\omega, \quad \dots \\ |n\rangle &= \frac{\hat{a}^\dagger}{\sqrt{n}}|n-1\rangle = \frac{1}{\sqrt{n!}}(\hat{a}^\dagger)^n|0\rangle \quad , \quad E_n = (n + \frac{1}{2})\hbar\omega. \end{aligned} \quad (43)$$

The root of the factorial is there to normalise all eigenstates to one. Finally, the *number operator* $\hat{N} = \hat{a}^\dagger \hat{a}$ returns the number of quanta in a given energy eigenstate,

$$\hat{N}|n\rangle = n|n\rangle. \quad (44)$$

1.6 Relativistic Quantum Mechanics

So far we have only considered non-relativistic particles. In this section, we see what happens when we try to formulate a relativistic analogue of the Schrödinger equation. First, note that we can derive the non-relativistic equation starting from the energy relation

$$E = \frac{\mathbf{p}^2}{2m} + V(\mathbf{x}) \quad (45)$$

and replacing variables by their appropriate operators acting on a position space wavefunction $\psi(\mathbf{x}, t)$

$$E \rightarrow i\hbar \frac{\partial}{\partial t}, \quad \mathbf{p} \rightarrow -i\hbar \nabla, \quad \mathbf{x} \rightarrow \mathbf{x} \quad (46)$$

to give

$$\left[-\frac{\hbar^2}{2m} \nabla^2 + V(\mathbf{x}) \right] \psi(\mathbf{x}, t) = i\hbar \frac{\partial \psi(\mathbf{x}, t)}{\partial t}. \quad (47)$$

As we have already seen, there is a corresponding positive definite probability density

$$\rho = |\psi(\mathbf{x}, t)|^2 \geq 0, \quad (48)$$

with corresponding current

$$\mathbf{j} = \frac{\hbar}{2im} (\psi^* \nabla \psi - (\nabla \psi^*) \psi). \quad (49)$$

Can we also make a relativistic equation? By analogy with the above, we may start with the relativistic energy relation

$$E^2 = c^2 \mathbf{p}^2 + m^2 c^4, \quad (50)$$

and making the appropriate operator replacements leads to the equation

$$\left(\frac{1}{c^2} \frac{\partial^2}{\partial t^2} - \nabla^2 + \frac{m^2 c^2}{\hbar^2} \right) \phi(\mathbf{x}, t) \quad (51)$$

for some wavefunction $\phi(\mathbf{x}, t)$. This is the *Klein-Gordon* equation, and one may try to form a probability density and current, as in the non-relativistic case. Firstly, one notes that to satisfy relativistic invariance, the probability density should be the zeroth component of a 4-vector $j^\mu = (\rho, \mathbf{j})$ satisfying

$$\partial_\mu j^\mu = 0. \quad (52)$$

In fact, one finds

$$\rho = \frac{i\hbar}{2m} \left(\phi^* \frac{\partial \phi}{\partial t} - \phi \frac{\partial \phi^*}{\partial t} \right), \quad (53)$$

with \mathbf{j} given as before. This is not positive definite! That is, this may (and will) become negative in general, so we cannot interpret this as the probability density of a single particle.

There is another problem with the Klein-Gordon equation as it stands, that is perhaps less abstract to appreciate. The relativistic energy relation gives

$$E = \pm \sqrt{c^2 \mathbf{p}^2 + m^2 c^4}, \quad (54)$$

and thus one has positive and negative energy solutions. For a free particle, one could restrict to having positive energy states only. However, an interacting particle may exchange energy with its environment, and there is nothing to stop it cascading down to energy states of more and more negative energy, thus emitting infinite amounts of energy.

We conclude that the Klein-Gordon equation does not make sense as a consistent quantum theory of a single particle. We thus need a different approach in unifying special relativity and quantum mechanics. This, as we will see, is QFT, in which we will be able to reinterpret the Klein-Gordon function as a field $\phi(\mathbf{x}, t)$ describing many particles.

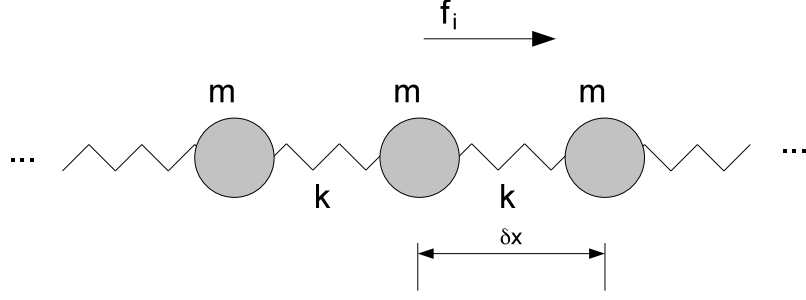


Figure 2: System of masses m joined by springs (of constant k), whose longitudinal displacements are $\{f_i\}$, and whose separation at rest is δx .

From now on, it will be extremely convenient to work in *natural units*, in which one sets $\hbar = c = 1$. The correct factors can always be reinstated by dimensional analysis. In these units, the Klein-Gordon equation becomes

$$(\square + m^2)\phi(\mathbf{x}, t) = 0, \quad (55)$$

where

$$\square = \partial^\mu \partial_\mu = \frac{\partial}{\partial t^2} - \nabla^2. \quad (56)$$

2 Classical Field Theory

In the previous section, we have seen how to describe point particles, both classically and quantum mechanically. In this section, we discuss classical field theory, as a precursor to considering quantum fields. A *field* associates a mathematical object (e.g. scalar, vector, tensor, spinor...) with every point in spacetime. Examples are the temperature distribution in a room (a scalar field), or the \mathbf{E} and \mathbf{B} fields in electromagnetism (vector fields). Just as point particles can be described by Lagrangians, so can fields, although it is more natural to think in terms of *Lagrangian densities*.

2.1 Example: Model of an Elastic Rod

Let us consider a particular example, namely a set of point masses connected together by springs, as shown in figure 2. Assume the masses m are equal, as also are the force constants of the springs k . Furthermore, we assume that the masses may move only longitudinally, where the i^{th} displacement is f_i , and that the separation of adjacent masses is δx when all f_i are zero. This system is an approximation to an elastic rod, with a displacement field $f(x, t)$. To see what this field theory looks like, we may first write the total kinetic and potential energies as

$$T = \sum_i \frac{1}{2} m \dot{f}_i^2, \quad V = \sum_i \frac{1}{2} k (f_{i+1} - f_i)^2 \quad (57)$$

respectively, where we have used Hooke's Law for the potential energy. Thus, the Lagrangian is

$$L = T - V = \sum_i \left[\frac{1}{2} m \dot{f}_i^2 - \frac{1}{2} k (f_{i+1} - f_i)^2 \right]. \quad (58)$$

Clearly this system becomes a better approximation to an elastic rod as the continuum limit is approached, in which the number of masses $N \rightarrow \infty$ and the separation $\delta x \rightarrow 0$. We can then rewrite the Lagrangian as

$$L = \sum_i \delta x \left[\frac{1}{2} \left(\frac{m}{\delta x} \right) \dot{f}_i^2 - \frac{1}{2} (k \delta x) \left(\frac{f_{i+1} - f_i}{\delta x} \right)^2 \right]. \quad (59)$$

We may recognise

$$\lim_{\delta x \rightarrow 0} m / \delta x = \rho \quad (60)$$

as the density of the rod, and also define the tension

$$\kappa = \lim_{\delta x \rightarrow 0} k \delta x. \quad (61)$$

Furthermore, the position index i gets replaced by the continuous variable x , and one has

$$\lim_{\delta x \rightarrow 0} \frac{f_{i+1} - f_i}{\delta x} = \frac{\partial f(x, t)}{\partial x}. \quad (62)$$

Finally, the sum over i becomes an integral so that the continuum Lagrangian is

$$L = \int dx \left[\frac{1}{2} \rho \dot{f}(x, t)^2 - \frac{1}{2} \kappa \left(\frac{\partial f}{\partial x} \right)^2 \right]. \quad (63)$$

This is the Lagrangian for the displacement field $f(x, t)$. It depends on a function of f and \dot{f} which is integrated over all space coordinates (in this case there is only one, the position along the rod). We may therefore write the Lagrangian manifestly as

$$L = \int dx \mathcal{L}[f(x, t), \dot{f}(x, t)], \quad (64)$$

where \mathcal{L} is the *Lagrangian density*

$$\mathcal{L}[f(x, t), \dot{f}(x, t)] = \frac{1}{2} \rho \dot{f}^2(x, t) - \frac{1}{2} \kappa \left(\frac{\partial f}{\partial x} \right)^2. \quad (65)$$

It is perhaps clear from the above example that for any field, there will always be an integration over all space dimensions, and thus it is more natural to think about the Lagrangian density rather than the Lagrangian itself. Indeed, we may construct the following dictionary between quantities in point particle mechanics, and corresponding field theory quantities (which may or may not be helpful to you in remembering the differences between particles and fields...!).

| | | |
|----------------------|-------------------------|------|
| Classical Mechanics: | Classical Field Theory: | |
| $x(t)$ | $\phi(x, t)$ | (66) |
| $\dot{x}(t)$ | $\dot{\phi}(x, t)$ | |

| | | |
|-----------|----------------|------|
| Index i | Coordinate x | (67) |
|-----------|----------------|------|

| | | |
|-----------------|---------------------------------|------|
| $L(x, \dot{x})$ | $\mathcal{L}[\phi, \dot{\phi}]$ | (68) |
|-----------------|---------------------------------|------|

Note that the action for the above field theory is given, as usual, by the time integral of the Lagrangian:

$$S = \int dt L = \int dt \int dx L[f, \dot{f}]. \quad (69)$$

2.2 Relativistic Fields

In the previous section we saw how fields can be described using Lagrangian densities, and illustrated this with a non-relativistic example. Rather than derive the field equations for this case, we do this explicitly here for relativistic theories, which we will be concerned with for the rest of the course (and, indeed, the school).

In special relativity, coordinates are combined into four-vectors, $x^\mu = (t, x_i)$ or $x = (t, \mathbf{x})$, whose length $x^2 = t^2 - \mathbf{x}^2$ is invariant under Lorentz transformations

$$x'^\mu = \Lambda^\mu{}_\nu x^\nu. \quad (70)$$

A general function transforms as $f(x) \rightarrow f'(x')$, i.e. both the function and its argument transform. A Lorentz scalar is a function $\phi(x)$ which at any given point in space-time will have the same amplitude, regardless of which inertial frame it is observed in. Consider a space-time point given by x in the unprimed frame, and $x'(x)$ in the primed frame, where the function $x'(x)$ can be derived from eq. (70). Observers in both the primed and unprimed frames will see the same amplitude $\phi(x)$, although an observer in the primed frame will prefer to express this in terms of his or her own coordinate system x' , hence will see

$$\phi(x) = \phi(x(x')) = \phi'(x'), \quad (71)$$

where the latter equality defines ϕ' .

Equation (71) defines the transformation law for a Lorentz scalar. A vector function transforms as

$$V'^\mu(x') = \Lambda^\mu{}_\nu V^\nu(x). \quad (72)$$

We will work in particular with $\partial_\mu \phi(x)$, where $x \equiv x^\mu$ denotes the 4-position. Note in particular that

$$\begin{aligned} (\partial_\mu \phi)(\partial^\mu \phi) &= \left(\frac{\partial \phi}{\partial t} \right)^2 - \nabla \phi \cdot \nabla \phi \\ \partial_\mu \partial^\mu \phi &= \frac{\partial^2 \phi}{\partial t^2} - \nabla^2 \phi. \end{aligned}$$

In general, a relativistically invariant scalar field theory has action

$$S = \int d^4x \mathcal{L}[\phi, \partial_\mu \phi], \quad (73)$$

where

$$\int d^4x \equiv \int dt d^3\mathbf{x}, \quad (74)$$

and \mathcal{L} is the appropriate Lagrangian density. We can find the equations of motion satisfied by the field ϕ using, as in point particle mechanics, the principle of least action. The field theory form of this is that the field $\phi(x)$ is such that the action of eq. (73) is extremised. Assuming $\phi(x)$ is indeed such a field, we may introduce a small perturbation

$$\phi(x) \rightarrow \phi(x) + \delta\phi(x), \quad (75)$$

which correspondingly perturbs the action according to

$$S \rightarrow S + \delta S = \int d^4x \left[\mathcal{L}(\phi, \partial_\mu \phi) + \frac{\partial \mathcal{L}}{\partial \phi} \delta \phi + \frac{\partial \mathcal{L}}{\partial (\partial_\mu \phi)} \delta (\partial_\mu \phi) \right]. \quad (76)$$

Recognising the first term as the unperturbed action, one thus finds

$$\begin{aligned} \delta S &= \int d^4x \left[\frac{\partial \mathcal{L}}{\partial \phi} \delta \phi + \frac{\partial \mathcal{L}}{\partial (\partial_\mu \phi)} \delta (\partial_\mu \phi) \right] \\ &= \left[\frac{\partial \mathcal{L}}{\partial (\partial_\mu \phi)} \delta \phi \right]_{\text{boundary}} + \int d^4x \left[\frac{\partial \mathcal{L}}{\partial \phi} - \partial_\mu \left(\frac{\partial \mathcal{L}}{\partial (\partial_\mu \phi)} \right) \right] \delta \phi, \end{aligned}$$

where we have integrated by parts in the second line. Assuming the fields die away at infinity so that $\delta \phi = 0$ at the boundary of spacetime, the principle of least action $\delta S = 0$ implies

$$\partial_\mu \left(\frac{\partial \mathcal{L}}{\partial (\partial_\mu \phi)} \right) = \frac{\partial \mathcal{L}}{\partial \phi}. \quad (77)$$

This is the *Euler-Lagrange field equation*. It tells us, given a particular Lagrangian density (which defines a particular field theory) the classical equation of motion which must be satisfied by the field ϕ . As a specific example, let us consider the Lagrangian density

$$\mathcal{L} = \frac{1}{2} (\partial_\mu \phi) (\partial^\mu \phi) - \frac{1}{2} m^2 \phi^2, \quad (78)$$

from which one finds

$$\frac{\partial \mathcal{L}}{\partial (\partial_\mu \phi)} = \partial^\mu \phi, \quad \frac{\partial \mathcal{L}}{\partial \phi} = -m^2 \phi, \quad (79)$$

so that the Euler-Lagrange equation gives

$$\partial_\mu \partial^\mu \phi + m^2 \phi = (\square + m^2) \phi(x) = 0. \quad (80)$$

This is the Klein-Gordon equation! The above Lagrangian density thus corresponds to the classical field theory of a Klein-Gordon field. We see in particular that the coefficient of the quadratic term in the Lagrangian can be interpreted as the mass.

By analogy with point particle mechanics, one can define a *canonical momentum field* conjugate to ϕ :

$$\pi(x) = \frac{\partial \mathcal{L}}{\partial \dot{\phi}}. \quad (81)$$

Then one can define the *Hamiltonian density*

$$\mathcal{H}[\phi, \pi] = \pi \dot{\phi} - \mathcal{L}, \quad (82)$$

such that

$$H = \int d^3x \mathcal{H}(\pi, \phi) \quad (83)$$

is the Hamiltonian (total energy carried by the field). For example, the Klein-Gordon field has conjugate momentum $\pi = \dot{\phi}$, and Hamiltonian density

$$\mathcal{H} = \frac{1}{2} [\pi^2(x) + (\nabla \phi)^2 + m^2 \phi^2]. \quad (84)$$

2.3 Plane wave solutions to the Klein-Gordon equation

Let us consider real solutions to Eq. (80), characterised by $\phi^*(x) = \phi(x)$. To find them we try an ansatz of plane waves

$$\phi(x) \propto e^{i(k^0 t - \mathbf{k} \cdot \mathbf{x})}. \quad (85)$$

The Klein-Gordon equation is satisfied if $(k^0)^2 - \mathbf{k}^2 = m^2$ so that

$$k^0 = \pm \sqrt{\mathbf{k}^2 + m^2}. \quad (86)$$

Defining the energy as

$$E(\mathbf{k}) = \sqrt{\mathbf{k}^2 + m^2} > 0, \quad (87)$$

we obtain two types of solution which read

$$\phi_+(x) \propto e^{i(E(\mathbf{k})t - \mathbf{k} \cdot \mathbf{x})}, \quad \phi_-(x) \propto e^{-i(E(\mathbf{k})t - \mathbf{k} \cdot \mathbf{x})}. \quad (88)$$

We may interpret these as positive and negative energy solutions, such that it does not matter which branch of the square root we take in eq. (87) (it is conventional, however, to define energy as a positive quantity). The general solution is a superposition of ϕ_+ and ϕ_- . Using

$$E(\mathbf{k})t - \mathbf{k} \cdot \mathbf{x} = k^\mu k_\mu = k_\mu k^\mu = k \cdot x \quad (89)$$

this solution reads

$$\phi(x) = \int \frac{d^3 k}{(2\pi)^3 2E(\mathbf{k})} \left(e^{ik \cdot x} \alpha^*(\mathbf{k}) + e^{-ik \cdot x} \alpha(\mathbf{k}) \right), \quad (90)$$

where $\alpha(\mathbf{k})$ is an arbitrary complex coefficient. Note that the coefficients of the positive and negative exponentials are related by complex conjugation. This ensures that the field $\phi(x)$ is real (as can be easily verified from eq. (90)), consistent with the Lagrangian we wrote down. Such a field has applications in e.g. the description of neutral mesons. We can also write down a Klein-Gordon Lagrangian for a complex field ϕ . This is really two independent fields (i.e. ϕ and ϕ^*), and thus can be used to describe a system of two particles (e.g. charged meson pairs). To simplify the discussion in this course, we will explicitly consider the real Klein-Gordon field. Note that the factors of 2 and π in eq. (90) are conventional, and the inverse power of the energy is such that the measure of integration is Lorentz invariant (problem 2.1), so that the whole solution is written in a manifestly Lorentz invariant way.

2.4 Symmetries and Conservation Laws

As was the case in point particle mechanics, one may relate symmetries of the Lagrangian density to conserved quantities in field theory. For example, consider the invariance of \mathcal{L} under space-time translations

$$x^\mu \rightarrow x^\mu + \epsilon^\mu, \quad (91)$$

where ϵ^μ is constant. Under such a transformation one has

$$\mathcal{L}(x^\mu + \epsilon^\mu) = \mathcal{L}(x^\mu) + \epsilon^\mu \partial_\mu \mathcal{L}(x^\mu) + \dots \quad (92)$$

$$\phi(x^\mu + \epsilon^\mu) = \phi(x^\mu) + \epsilon^\mu \partial_\mu \phi(x^\mu) + \dots \quad (93)$$

$$\partial_\nu \phi(x^\mu + \epsilon^\mu) = \partial_\nu \phi(x^\mu) + \epsilon^\mu \partial_\mu \partial_\nu \phi(x^\mu) + \dots, \quad (94)$$

$$(95)$$

where we have used Taylor's theorem. But if \mathcal{L} does not explicitly depend on x^μ (i.e. only through ϕ and $\partial_\mu\phi$) then one has

$$\begin{aligned}\mathcal{L}(x^\mu + \epsilon^\mu) &= \mathcal{L}[\phi(x^\mu + \epsilon^\mu), \partial_\nu\phi(x^\mu + \epsilon^\mu)] \\ &= \mathcal{L} + \frac{\partial\mathcal{L}}{\partial\phi}\delta\phi + \frac{\partial\mathcal{L}}{\partial(\partial_\nu\phi)}\delta(\partial_\nu\phi) + \dots\end{aligned}\tag{96}$$

$$= \mathcal{L} + \frac{\partial\mathcal{L}}{\partial\phi}\epsilon^\mu\partial_\mu\phi + \frac{\partial\mathcal{L}}{\partial(\partial_\nu\phi)}\epsilon^\mu\partial_\mu\partial_\nu\phi + \dots,\tag{97}$$

where we have used the fact that $\delta\phi = \epsilon^\mu\partial_\mu\phi$ in the third line, and all functions on the right-hand side are evaluated at x^μ . One may replace $\partial\mathcal{L}/\partial\phi$ by the LHS of the Euler-Lagrange equation to get

$$\begin{aligned}\mathcal{L}(x^\mu + \epsilon^\mu) &= \mathcal{L} + \partial_\nu\frac{\partial\mathcal{L}}{\partial(\partial_\nu\phi)}\epsilon^\mu\partial_\mu\phi + \frac{\partial\mathcal{L}}{\partial(\partial_\nu\phi)}\epsilon^\mu\partial_\mu\partial_\nu\phi + \dots \\ &= \mathcal{L} + \partial_\nu\left[\frac{\partial\mathcal{L}}{\partial(\partial_\nu\phi)}\partial_\mu\phi\right]\epsilon^\mu,\end{aligned}\tag{98}$$

and equating this with the alternative expression above, one finds

$$\partial_\nu\left[\frac{\partial\mathcal{L}}{\partial(\partial_\nu\phi)}\partial_\mu\phi\right]\epsilon^\mu = \epsilon^\mu\partial_\mu\mathcal{L}.\tag{99}$$

If this is true for all ϵ^μ , then one has

$$\partial^\nu\Theta_{\nu\mu} = 0,\tag{100}$$

where

$$\Theta_{\nu\mu} = \frac{\partial\mathcal{L}}{\partial(\partial_\nu\phi)}\partial_\mu\phi - g_{\mu\nu}\mathcal{L}\tag{101}$$

is the *energy-momentum tensor*. We can see how this name arises by considering the components explicitly, for the case of the Klein Gordon field. One then finds

$$\Theta_{00} = \frac{\partial\mathcal{L}}{\partial\dot{\phi}}\dot{\phi} - g_{00}\mathcal{L} = \pi\dot{\phi} - \mathcal{L} = \mathcal{H},\tag{102}$$

$$\Theta_{0j} = \frac{\partial\mathcal{L}}{\partial\dot{\phi}}\partial_j\phi - g_{0j}\mathcal{L} = \pi\partial_j\phi \quad (j = 1 \dots 3).\tag{103}$$

One then sees that Θ_{00} is the energy density carried by the field. Its conservation can then be shown by considering

$$\begin{aligned}\frac{\partial}{\partial t}\int_V d^3x \Theta_{00} &= \int_V d^3x \partial^0\Theta_{00} \\ &= \int_V d^3x \partial^j\Theta_{j0} = \int_S dS_j \cdot \Theta_{0j} = 0,\end{aligned}\tag{104}$$

where we have used Eq. (100) in the second line. The Hamiltonian density is a conserved quantity, provided that there is no energy flow through the surface S which encloses the volume V . In a

similar manner one can show that the 3-momentum p_j , which is related to Θ_{0j} , is conserved as well. It is then useful to define a conserved energy-momentum four-vector

$$P_\mu = \int d^3x \Theta_{0\mu}. \quad (105)$$

In analogy to point particle mechanics, we thus see that invariances of the Lagrangian density correspond to conservation laws. An entirely analogous procedure leads to conserved quantities like angular momentum and spin. Furthermore one can study so-called internal symmetries, i.e. ones which are not related to coordinate but other transformations. Examples are conservation of all kinds of charges, isospin, etc.

We have thus established the Lagrange-Hamilton formalism for classical field theory: we derived the equation of motion (Euler-Lagrange equation) from the Lagrangian and introduced the conjugate momentum. We then defined the Hamiltonian (density) and considered conservation laws by studying the energy-momentum tensor $\Theta_{\mu\nu}$.

3 Quantum Field Theory: Free Fields

3.1 Canonical Field Quantisation

In the previous sections we have reviewed the classical and quantum mechanics of point particles, and also classical field theory. We used the canonical quantisation procedure in discussing quantum mechanics, whereby classical variables are replaced by operators, which have non-trivial commutation relations. In this section, we see how to apply this procedure to fields, taking the explicit example of the Klein-Gordon field discussed previously. This is, as yet, a non-interacting field theory, and we will discuss how to deal with interactions later on in the course.

The Klein-Gordon Lagrangian density has the form

$$\mathcal{L} = \frac{1}{2} \partial^\mu \phi \partial_\mu \phi - \frac{1}{2} m^2 \phi^2. \quad (106)$$

We have seen that in field theory the field $\phi(x)$ plays the role of the coordinates in ordinary point particle mechanics, and we defined a canonically conjugate momentum, $\pi(x) = \partial \mathcal{L} / \partial \dot{\phi} = \dot{\phi}(x)$. We then continue the analogy to point mechanics through the quantisation procedure, i.e. we now take our canonical variables to be operators,

$$\phi(x) \rightarrow \hat{\phi}(x), \quad \pi(x) \rightarrow \hat{\pi}(x). \quad (107)$$

Next we impose equal-time commutation relations on them,

$$\left[\hat{\phi}(\mathbf{x}, t), \hat{\pi}(\mathbf{y}, t) \right] = i \delta^3(\mathbf{x} - \mathbf{y}), \quad (108)$$

$$\left[\hat{\phi}(\mathbf{x}, t), \hat{\phi}(\mathbf{y}, t) \right] = \left[\hat{\pi}(\mathbf{x}, t), \hat{\pi}(\mathbf{y}, t) \right] = 0. \quad (109)$$

As in the case of quantum mechanics, the canonical variables commute among themselves, but not the canonical coordinate and momentum with each other. Note that the commutation relation is entirely analogous to the quantum mechanical case. There would be an \hbar , if it hadn't been set to

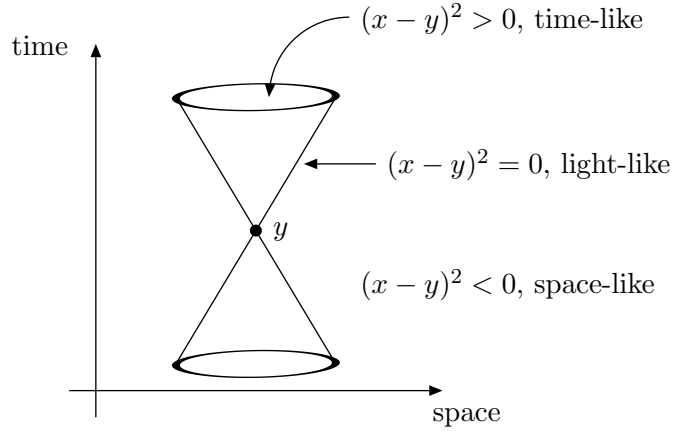


Figure 3: The light cone about y . Events occurring at points x and y are said to be time-like (space-like) if x is inside (outside) the light cone about y .

one earlier, and the delta-function accounts for the fact that we are dealing with fields. It is zero if the fields are evaluated at different space-time points.

After quantisation, our fields have turned into field operators. Note that within the relativistic formulation they depend on time, and hence they are Heisenberg operators.

In the previous paragraph we have formulated commutation relations for fields evaluated at equal time, which is clearly a special case when considering fields at general x, y . The reason has to do with maintaining causality in a relativistic theory. Let us recall the light cone about an event at y , as in Fig. 3. One important postulate of special relativity states that no signal and no interaction can travel faster than the speed of light. This has important consequences about the way in which different events can affect each other. For instance, two events which are characterised by space-time points x^μ and y^μ are said to be causal if the distance $(x - y)^2$ is time-like, i.e. $(x - y)^2 > 0$. By contrast, two events characterised by a space-like separation, i.e. $(x - y)^2 < 0$, cannot affect each other, since the point x is not contained inside the light cone about y .

In non-relativistic Quantum Mechanics the commutation relations among operators indicate whether precise and independent measurements of the corresponding observables can be made. If the commutator does not vanish, then a measurement of one observable affects that of the other. From the above it is then clear that the issue of causality must be incorporated into the commutation relations of the relativistic version of our quantum theory: whether or not independent and precise measurements of two observables can be made depends also on the separation of the 4-vectors characterising the points at which these measurements occur. Clearly, events with space-like separations cannot affect each other, and hence all fields must commute,

$$\left[\hat{\phi}(x), \hat{\phi}(y) \right] = [\hat{\pi}(x), \hat{\pi}(y)] = \left[\hat{\phi}(x), \hat{\pi}(y) \right] = 0 \quad \text{for} \quad (x - y)^2 < 0. \quad (110)$$

This condition is sometimes called micro-causality. Writing out the four-components of the time interval, we see that as long as $|t' - t| < |\mathbf{x} - \mathbf{y}|$, the commutator vanishes in a finite interval $|t' - t|$. It also vanishes for $t' = t$, as long as $\mathbf{x} \neq \mathbf{y}$. Only if the fields are evaluated at an equal space-time point can they affect each other, which leads to the equal-time commutation relations above. They can also affect each other everywhere within the light cone, i.e. for time-like intervals. It is not

hard to show that in this case (e.g. problem 3.1)

$$\left[\hat{\phi}(x), \hat{\phi}(y)\right] = [\hat{\pi}(x), \hat{\pi}(y)] = 0, \quad \text{for } (x-y)^2 > 0 \quad (111)$$

$$\left[\hat{\phi}(x), \hat{\pi}(y)\right] = \frac{i}{2} \int \frac{d^3 \mathbf{p}}{(2\pi)^3} \left(e^{ip \cdot (x-y)} + e^{-ip \cdot (x-y)} \right). \quad (112)$$

n.b. since the 4-vector dot product $p \cdot (x-y)$ depends on $p_0 = \sqrt{\mathbf{p}^2 + m^2}$, one cannot trivially carry out the integrals over $d^3 \mathbf{p}$ here.

3.2 Creation and annihilation operators

After quantisation, the Klein-Gordon equation we derived earlier turns into an equation for operators. For its solution we simply promote the classical plane wave solution, Eq. (90), to operator status,

$$\hat{\phi}(x) = \int \frac{d^3 k}{(2\pi)^3 2E(\mathbf{k})} \left(e^{ik \cdot x} \hat{a}^\dagger(\mathbf{k}) + e^{-ik \cdot x} \hat{a}(\mathbf{k}) \right). \quad (113)$$

Note that the complex conjugation of the Fourier coefficient turned into hermitian conjugation for an operator.

Let us now solve for the operator coefficients of the positive and negative energy solutions. In order to do so, we invert the Fourier integrals for the field and its time derivative,

$$\int d^3 x \hat{\phi}(\mathbf{x}, t) e^{ikx} = \frac{1}{2E} \left[\hat{a}(\mathbf{k}) + \hat{a}^\dagger(\mathbf{k}) e^{2ik_0 x_0} \right], \quad (114)$$

$$\int d^3 x \dot{\hat{\phi}}(\mathbf{x}, t) e^{ikx} = -\frac{i}{2} \left[\hat{a}(\mathbf{k}) - \hat{a}^\dagger(\mathbf{k}) e^{2ik_0 x_0} \right], \quad (115)$$

and then build the linear combination $iE(k)(114)-(115)$ to find

$$\int d^3 x \left[iE(k) \hat{\phi}(\mathbf{x}, t) - \dot{\hat{\phi}}(\mathbf{x}, t) \right] e^{ikx} = i \hat{a}(\mathbf{k}), \quad (116)$$

Following a similar procedure for $\hat{a}^\dagger(k)$, and using $\hat{\pi}(x) = \dot{\hat{\phi}}(x)$ we find

$$\hat{a}(\mathbf{k}) = \int d^3 x \left[E(k) \hat{\phi}(\mathbf{x}, t) + i \hat{\pi}(\mathbf{x}, t) \right] e^{ikx}, \quad (117)$$

$$\hat{a}^\dagger(\mathbf{k}) = \int d^3 x \left[E(k) \hat{\phi}(\mathbf{x}, t) - i \hat{\pi}(\mathbf{x}, t) \right] e^{-ikx}. \quad (118)$$

Note that, as Fourier coefficients, these operators do not depend on time, even though the right hand side does contain time variables. Having expressions in terms of the canonical field variables $\hat{\phi}(x), \hat{\pi}(x)$, we can now evaluate the commutators for the Fourier coefficients. Expanding everything out and using the commutation relations Eq. (109), we find

$$\left[\hat{a}^\dagger(\mathbf{k}_1), \hat{a}^\dagger(\mathbf{k}_2) \right] = 0 \quad (119)$$

$$\left[\hat{a}(\mathbf{k}_1), \hat{a}(\mathbf{k}_2) \right] = 0 \quad (120)$$

$$\left[\hat{a}(\mathbf{k}_1), \hat{a}^\dagger(\mathbf{k}_2) \right] = (2\pi)^3 2E(\mathbf{k}_1) \delta^3(\mathbf{k}_1 - \mathbf{k}_2) \quad (121)$$

We easily recognise these for every \mathbf{k} to correspond to the commutation relations for the harmonic oscillator, Eq. (37). This motivates us to also express the Hamiltonian and the energy momentum four-vector of our quantum field theory in terms of these operators. To do this, first note that the Hamiltonian is given by the integral of the Hamiltonian density (eq. (84)) over all space. One may then substitute eq. (113) to yield (see the problem sheet)

$$\hat{H} = \frac{1}{2} \int \frac{d^3k}{(2\pi)^3 2E(\mathbf{k})} E(\mathbf{k}) \left(\hat{a}^\dagger(\mathbf{k}) \hat{a}(\mathbf{k}) + \hat{a}(\mathbf{k}) \hat{a}^\dagger(\mathbf{k}) \right), \quad (122)$$

$$\hat{\mathbf{P}} = \frac{1}{2} \int \frac{d^3k}{(2\pi)^3 2E(\mathbf{k})} \mathbf{k} \left(\hat{a}^\dagger(\mathbf{k}) \hat{a}(\mathbf{k}) + \hat{a}(\mathbf{k}) \hat{a}^\dagger(\mathbf{k}) \right). \quad (123)$$

We thus find that the Hamiltonian and the momentum operator are nothing but a continuous sum of excitation energies/momenta of one-dimensional harmonic oscillators! After a minute of thought this is not so surprising. We expanded the solution of the Klein-Gordon equation into a superposition of plane waves with momenta \mathbf{k} . But of course a plane wave solution with energy $E(\mathbf{k})$ is also the solution to a one-dimensional harmonic oscillator with the same energy. Hence, our free scalar field is simply a collection of infinitely many harmonic oscillators distributed over the whole energy/momentum range. These energies sum up to that of the entire system. We have thus reduced the problem of handling our field theory to oscillator algebra. From the harmonic oscillator we know already how to construct a complete basis of energy eigenstates, and thanks to the analogy of the previous section we can take this over to our quantum field theory.

3.3 Energy of the vacuum state and renormalisation

In complete analogy we begin again with the postulate of a vacuum state $|0\rangle$ with norm one, which is annihilated by the action of the operator a ,

$$\langle 0|0\rangle = 1, \quad \hat{a}(\mathbf{k})|0\rangle = 0 \quad \text{for all } \mathbf{k}. \quad (124)$$

Let us next evaluate the energy of this vacuum state, by taking the expectation value of the Hamiltonian,

$$E_0 = \langle 0|\hat{H}|0\rangle = \frac{1}{2} \int \frac{d^3k}{(2\pi)^3 2E(\mathbf{k})} E(\mathbf{k}) \left\{ \langle 0|\hat{a}^\dagger(\mathbf{k}) \hat{a}(\mathbf{k})|0\rangle + \langle 0|\hat{a}(\mathbf{k}) \hat{a}^\dagger(\mathbf{k})|0\rangle \right\}. \quad (125)$$

The first term in curly brackets vanishes, since a annihilates the vacuum. The second can be rewritten as

$$\hat{a}(\mathbf{k}) \hat{a}^\dagger(\mathbf{k})|0\rangle = \left\{ \left[\hat{a}(\mathbf{k}), \hat{a}^\dagger(\mathbf{k}) \right] + \hat{a}^\dagger(\mathbf{k}) \hat{a}(\mathbf{k}) \right\} |0\rangle. \quad (126)$$

It is now the second term which vanishes, whereas the first can be replaced by the value of the commutator. Thus we obtain

$$E_0 = \langle 0|\hat{H}|0\rangle = \delta^3(0) \frac{1}{2} \int d^3k E(\mathbf{k}) = \delta^3(0) \frac{1}{2} \int d^3k \sqrt{\mathbf{k}^2 + m^2} = \infty, \quad (127)$$

which means that the energy of the ground state is infinite! This result seems rather paradoxical, but it can be understood again in terms of the harmonic oscillator. Recall that the simple quantum mechanical oscillator has a finite zero-point energy. As we have seen above, our field theory corresponds to an infinite collection of harmonic oscillators, i.e. the vacuum receives an infinite number of zero point contributions, and its energy thus diverges.

This is the first of frequent occurrences of infinities in quantum field theory. Fortunately, it is not too hard to work around this particular one. Firstly, we note that nowhere in nature can we observe absolute values of energy, all we can measure are energy differences relative to some reference scale, at best the one of the vacuum state, $|0\rangle$. In this case it does not really matter what the energy of the vacuum is. This then allows us to redefine the energy scale, by always subtracting the (infinite) vacuum energy from any energy we compute. This process is called “renormalisation”.

We then *define* the renormalised vacuum energy to be zero, and take it to be the expectation value of a renormalised Hamiltonian,

$$E_0^R \equiv \langle 0 | \hat{H}^R | 0 \rangle = 0. \quad (128)$$

According to this recipe, the renormalised Hamiltonian is our original one, minus the (unrenormalised) vacuum energy,

$$\hat{H}^R = \hat{H} - E_0 \quad (129)$$

$$\begin{aligned} &= \frac{1}{2} \int \frac{d^3 k}{(2\pi)^3 2E(\mathbf{k})} E(\mathbf{k}) \left\{ \hat{a}^\dagger(\mathbf{k}) \hat{a}(\mathbf{k}) + \hat{a}(\mathbf{k}) \hat{a}^\dagger(\mathbf{k}) - \langle 0 | \hat{a}^\dagger(\mathbf{k}) \hat{a}(\mathbf{k}) + \hat{a}(\mathbf{k}) \hat{a}^\dagger(\mathbf{k}) | 0 \rangle \right\} \\ &= \frac{1}{2} \int \frac{d^3 k}{(2\pi)^3 2E(\mathbf{k})} E(\mathbf{k}) \left\{ 2\hat{a}^\dagger(\mathbf{k}) \hat{a}(\mathbf{k}) + [\hat{a}(\mathbf{k}), \hat{a}^\dagger(\mathbf{k})] - \langle 0 | [\hat{a}(\mathbf{k}), \hat{a}^\dagger(\mathbf{k})] | 0 \rangle \right\}. \end{aligned} \quad (130)$$

Here the subtraction of the vacuum energy is shown explicitly, and we can rewrite it as

$$\begin{aligned} \hat{H}^R &= \int \frac{d^3 p}{(2\pi)^3 2E(\mathbf{p})} E(\mathbf{p}) \hat{a}^\dagger(\mathbf{p}) \hat{a}(\mathbf{p}) \\ &\quad + \frac{1}{2} \int \frac{d^3 p}{(2\pi)^3 2E(\mathbf{p})} E(\mathbf{p}) \left\{ [\hat{a}(\mathbf{p}), \hat{a}^\dagger(\mathbf{p})] - \langle 0 | [\hat{a}(\mathbf{p}), \hat{a}^\dagger(\mathbf{p})] | 0 \rangle \right\} \\ &= \int \frac{d^3 p}{(2\pi)^3 2E(\mathbf{p})} E(\mathbf{p}) \hat{a}^\dagger(\mathbf{p}) \hat{a}(\mathbf{p}) + \hat{H}^{\text{vac}} \end{aligned} \quad (131)$$

The operator \hat{H}^{vac} ensures that the vacuum energy is properly subtracted: if $|\psi\rangle$ and $|\psi'\rangle$ denote arbitrary N -particle states, then one can convince oneself that $\langle \psi' | \hat{H}^{\text{vac}} | \psi \rangle = 0$. In particular we now find that

$$\langle 0 | \hat{H}^R | 0 \rangle = 0, \quad (132)$$

as we wanted. A simple way to automatise the removal of the vacuum contribution is to introduce *normal ordering*. Normal ordering means that all annihilation operators appear to the right of any creation operator. The notation is

$$: \hat{a} \hat{a}^\dagger : = \hat{a}^\dagger \hat{a}, \quad (133)$$

i.e. the normal-ordered operators are enclosed within colons. For instance

$$: \frac{1}{2} \left(\hat{a}^\dagger(\mathbf{p}) \hat{a}(\mathbf{p}) + \hat{a}(\mathbf{p}) \hat{a}^\dagger(\mathbf{p}) \right) : = \hat{a}^\dagger(\mathbf{p}) \hat{a}(\mathbf{p}). \quad (134)$$

It is important to keep in mind that \hat{a} and \hat{a}^\dagger *always* commute inside $: \cdots :$. This is true for an arbitrary string of \hat{a} and \hat{a}^\dagger . With this definition we can write the normal-ordered Hamiltonian as

$$\begin{aligned} : \hat{H} : &= : \frac{1}{2} \int \frac{d^3 p}{(2\pi)^3 2E(\mathbf{p})} E(\mathbf{p}) \left(\hat{a}^\dagger(\mathbf{p}) \hat{a}(\mathbf{p}) + \hat{a}(\mathbf{p}) \hat{a}^\dagger(\mathbf{p}) \right) : \\ &= \int \frac{d^3 p}{(2\pi)^3 2E(\mathbf{p})} E(\mathbf{p}) \hat{a}^\dagger(\mathbf{p}) \hat{a}(\mathbf{p}), \end{aligned} \quad (135)$$

and thus have the relation

$$\hat{H}^R =: \hat{H} : + \hat{H}^{\text{vac}}. \quad (136)$$

Hence, we find that

$$\langle \psi' | : \hat{H} : | \psi \rangle = \langle \psi' | \hat{H}^R | \psi \rangle, \quad (137)$$

and, in particular, $\langle 0 | : \hat{H} : | 0 \rangle = 0$. The normal ordered Hamiltonian thus produces a renormalised, sensible result for the vacuum energy.

3.4 Fock space and Particles

After this lengthy grappling with the vacuum state, we can continue to construct our basis of states in analogy to the harmonic oscillator, making use of the commutation relations for the operators \hat{a}, \hat{a}^\dagger . In particular, we define the state $|\mathbf{k}\rangle$ to be the one obtained by acting with the operator $\hat{a}^\dagger(\mathbf{k})$ on the vacuum,

$$|\mathbf{k}\rangle = \hat{a}^\dagger(\mathbf{k})|0\rangle. \quad (138)$$

Using the commutator, its norm is found to be

$$\langle \mathbf{k} | \mathbf{k}' \rangle = \langle 0 | \hat{a}(\mathbf{k}) \hat{a}^\dagger(\mathbf{k}') | 0 \rangle = \langle 0 | [\hat{a}(\mathbf{k}), \hat{a}^\dagger(\mathbf{k}')] | 0 \rangle + \langle 0 | \hat{a}^\dagger(\mathbf{k}') \hat{a}(\mathbf{k}) | 0 \rangle \quad (139)$$

$$= (2\pi)^3 2E(\mathbf{k}) \delta^3(\mathbf{k} - \mathbf{k}'), \quad (140)$$

since the last term in the first line vanishes ($\hat{a}(\mathbf{k})$ acting on the vacuum). Next we compute the energy of this state, making use of the normal ordered Hamiltonian,

$$: \hat{H} : |\mathbf{k}\rangle = \int \frac{d^3 k'}{(2\pi)^3 2E(\mathbf{k}')} E(\mathbf{k}') \hat{a}^\dagger(\mathbf{k}') \hat{a}(\mathbf{k}') \hat{a}^\dagger(\mathbf{k}) | 0 \rangle \quad (141)$$

$$= \int \frac{d^3 k'}{(2\pi)^3 2E(\mathbf{k}')} E(\mathbf{k}') (2\pi)^3 2E(\mathbf{k}) \delta^3(\mathbf{k} - \mathbf{k}') \hat{a}^\dagger(\mathbf{k}) | 0 \rangle \quad (142)$$

$$= E(\mathbf{k}) \hat{a}^\dagger(\mathbf{k}) | 0 \rangle = E(\mathbf{k}) |\mathbf{k}\rangle, \quad (143)$$

and similarly one finds

$$: \hat{\mathbf{P}} : |\mathbf{k}\rangle = \mathbf{k} |\mathbf{k}\rangle. \quad (144)$$

Observing that the normal ordering did its job and we obtain renormalised, finite results, we may now interpret the state $|\mathbf{k}\rangle$. It is a one-particle state for a relativistic particle of mass m and momentum \mathbf{k} , since acting on it with the energy-momentum operator returns the relativistic one particle energy-momentum dispersion relation, $E(\mathbf{k}) = \sqrt{\mathbf{k}^2 + m^2}$. The $\hat{a}^\dagger(\mathbf{k}), \hat{a}(\mathbf{k})$ are creation and annihilation operators for particles of momentum \mathbf{k} .

In analogy to the harmonic oscillator, the procedure can be continued to higher states. One easily checks that (problem 3.4)

$$: \hat{P}^\mu : \hat{a}^\dagger(\mathbf{k}_2) \hat{a}^\dagger(\mathbf{k}_1) | 0 \rangle = (k_1^\mu + k_2^\mu) \hat{a}^\dagger(\mathbf{k}_2) \hat{a}^\dagger(\mathbf{k}_1) | 0 \rangle, \quad (145)$$

and so the state

$$|\mathbf{k}_2, \mathbf{k}_1\rangle = \frac{1}{\sqrt{2!}} \hat{a}^\dagger(\mathbf{k}_2) \hat{a}^\dagger(\mathbf{k}_1) | 0 \rangle \quad (146)$$

is a two-particle state (the factorial is there to have it normalised in the same way as the one-particle state), and so on for higher states. These are called *Fock states* in the textbooks (formally

speaking, a Fock space is a tensor product of Hilbert spaces, where the latter occur in ordinary Quantum Mechanics).

At long last we can now see how the field in our free quantum field theory is related to particles. A particle of momentum \mathbf{k} corresponds to an excited Fourier mode of a field. Since the field is a superposition of all possible Fourier modes, one field is enough to describe all possible configurations representing one or many particles of the same kind in any desired momentum state.

There are some rather profound ideas here about how nature works at fundamental scales. In classical physics we have matter particles, and forces which act on those particles. These forces can be represented by fields, such that fields and particles are distinct concepts. In non-relativistic quantum mechanics, one unifies the concept of waves and particles (particles can have wave-like characteristics), but fields are still distinct (e.g. one may quantise a particle in an electromagnetic field in QM, provided the latter is treated classically). Taking into account the effects of relativity for both particles and fields, one finds in QFT that all particles are excitation quanta of fields. That is, the concepts of *field* and *particle* are no longer distinct, but actually manifestations of the same thing, namely quantum fields. In this sense, QFT is more fundamental than either of its preceding theories. Each force field and each matter field have particles associated with it.

Returning to our theory for the free Klein-Gordon field, let us investigate what happens under interchange of the two particles. Since $[\hat{a}^\dagger(\mathbf{k}_1), \hat{a}^\dagger(\mathbf{k}_2)] = 0$ for all $\mathbf{k}_1, \mathbf{k}_2$, we see that

$$|\mathbf{k}_2, \mathbf{k}_1\rangle = |\mathbf{k}_1, \mathbf{k}_2\rangle, \quad (147)$$

and hence the state is symmetric under interchange of the two particles. Thus, the particles described by the scalar field are bosons.

Finally we complete the analogy to the harmonic oscillator by introducing a number operator

$$\hat{N}(\mathbf{k}) = \hat{a}^\dagger(\mathbf{k})\hat{a}(\mathbf{k}), \quad \hat{\mathcal{N}} = \int d^3k \hat{a}^\dagger(\mathbf{k})\hat{a}(\mathbf{k}), \quad (148)$$

which gives us the number of bosons described by a particular Fock state,

$$\hat{\mathcal{N}}|0\rangle = 0, \quad \hat{\mathcal{N}}|\mathbf{k}\rangle = |\mathbf{k}\rangle, \quad \hat{\mathcal{N}}|\mathbf{k}_1 \dots \mathbf{k}_n\rangle = n|\mathbf{k}_1 \dots \mathbf{k}_n\rangle. \quad (149)$$

Of course the normal-ordered Hamiltonian can now simply be given in terms of this operator,

$$:\hat{H}:= \int \frac{d^3k}{(2\pi)^3} \frac{1}{2E(\mathbf{k})} E(\mathbf{k}) \hat{N}(\mathbf{k}), \quad (150)$$

i.e. when acting on a Fock state it simply sums up the energies of the individual particles to give

$$:\hat{H}: |\mathbf{k}_1 \dots \mathbf{k}_n\rangle = (E(\mathbf{k}_1) + \dots E(\mathbf{k}_n)) |\mathbf{k}_1 \dots \mathbf{k}_n\rangle. \quad (151)$$

This concludes the quantisation of our free scalar field theory. We have followed the canonical quantisation procedure familiar from quantum mechanics. Due to the infinite number of degrees of freedom, we encountered a divergent vacuum energy, which we had to renormalise. The renormalised Hamiltonian and the Fock states that we constructed describe free relativistic, uncharged spin zero particles of mass m , such as neutral pions, for example.

If we want to describe charged pions as well, we need to introduce complex scalar fields, the real and imaginary parts being necessary to describe opposite charges. For particles with spin we need

still more degrees of freedom and use vector or spinor fields, which have the appropriate rotation and Lorentz transformation properties. For fermion fields (which satisfy the Dirac equation rather than the Klein-Gordon equation), one finds that the condition of a positive-definite energy density requires that one impose anti-commutation relations rather than commutation relations. This in turn implies that multiparticle states are antisymmetric under interchange of identical fermions, which we recognise as the Pauli exclusion principle. Thus, not only does QFT provide a consistent theory of relativistic multiparticle systems; it also allows us to “derive” the Pauli principle, which is put in by hand in non-relativistic quantum mechanics.

More details on vector and spinor fields can be found in the other courses at this school. Here, we continue to restrict our attention to scalar fields, so as to more clearly illustrate what happens when interactions are present.

4 Quantum Field Theory: Interacting Fields

So far we have seen how to quantise the Klein-Gordon Lagrangian, and seen that this describes free scalar particles. For interesting physics, however, we need to know how to describe interactions, which lead to nontrivial scattering processes. This is the subject of this section.

From now on we shall always discuss quantised real scalar fields. It is then convenient to drop the “hats” on the operators that we have considered up to now. Interactions can be described by adding a term \mathcal{L}_{int} to the Lagrangian density, so that the full result \mathcal{L} is given by

$$\mathcal{L} = \mathcal{L}_0 + \mathcal{L}_{\text{int}} \quad (152)$$

where

$$\mathcal{L}_0 = \frac{1}{2} \partial_\mu \phi \partial^\mu \phi - \frac{1}{2} m^2 \phi^2 \quad (153)$$

is the free Lagrangian density discussed before. The Hamiltonian density of the interaction is related to \mathcal{L}_{int} simply by

$$\mathcal{H}_{\text{int}} = \mathcal{H} - \mathcal{H}_0, \quad (154)$$

where \mathcal{H}_0 is the free Hamiltonian. If the interaction Lagrangian only depends on ϕ (we will consider such a case later in the course), one has

$$\mathcal{H}_{\text{int}} = -\mathcal{L}_{\text{int}}, \quad (155)$$

as can be easily shown from the definition above. We shall leave the details of \mathcal{L}_{int} unspecified for the moment. What we will be concerned with mostly are scattering processes, in which two initial particles with momenta \mathbf{p}_1 and \mathbf{p}_2 scatter, thereby producing a number of particles in the final state, characterised by momenta $\mathbf{k}_1, \dots, \mathbf{k}_n$. This is schematically shown in Fig. 4. Our task is to find a description of such a scattering process in terms of the underlying quantum field theory.

4.1 The S -matrix

The timescales over which interactions happen are extremely short. The scattering (interaction) process takes place during a short interval around some particular time t with $-\infty \ll t \ll \infty$.

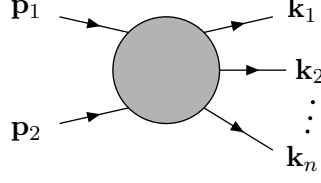


Figure 4: Scattering of two initial particles with momenta \mathbf{p}_1 and \mathbf{p}_2 into n particles with momenta $\mathbf{k}_1, \dots, \mathbf{k}_n$ in the final state.

Long before t , the incoming particles evolve independently and freely. They are described by a field operator ϕ_{in} defined through

$$\lim_{t \rightarrow -\infty} \phi(x) = \phi_{\text{in}}(x), \quad (156)$$

which acts on a corresponding basis of $|\text{in}\rangle$ states. Long after the collision the particles in the final state evolve again like in the free theory, and the corresponding operator is

$$\lim_{t \rightarrow +\infty} \phi(x) = \phi_{\text{out}}(x), \quad (157)$$

acting on states $|\text{out}\rangle$. The fields ϕ_{in} , ϕ_{out} are the asymptotic limits of the Heisenberg operator ϕ . They both satisfy the free Klein-Gordon equation, i.e.

$$(\square + m^2)\phi_{\text{in}}(x) = 0, \quad (\square + m^2)\phi_{\text{out}}(x) = 0. \quad (158)$$

Operators describing free fields can be expressed as a superposition of plane waves (see Eq. (113)). Thus, for ϕ_{in} we have

$$\phi_{\text{in}}(x) = \int \frac{d^3k}{(2\pi)^3 2E(\mathbf{k})} \left(e^{ik \cdot x} a_{\text{in}}^\dagger(\mathbf{k}) + e^{-ik \cdot x} a_{\text{in}}(\mathbf{k}) \right), \quad (159)$$

with an entirely analogous expression for $\phi_{\text{out}}(x)$. Note that the operators a^\dagger and a also carry subscripts “in” and “out”.

The above discussion assumes that the interaction is such that we can talk about free particles at asymptotic times $t \rightarrow \pm\infty$ i.e. that the interaction is only present at intermediate times. This is not always a reasonable assumption e.g. it does not encompass the phenomenon of bound states, in which incident particles form a composite object at late times, which no longer consists of free particles. Nevertheless, the assumption will indeed allow us to discuss scattering processes, which is the aim of this course. Note that we can only talk about well-defined particle states at $t \rightarrow \pm\infty$ (the states labelled by “in” and “out” above), as only at these times do we have a free theory, and thus know what the spectrum of states is (using the methods of section 3). At general times t , the interaction is present, and it is not possible in general to solve for the states of the quantum field theory. Remarkably, we will end up seeing that we can ignore all the complicated stuff at intermediate times, and solve for scattering probabilities purely using the properties of the asymptotic fields.

At the asymptotic times $t = \pm\infty$, we can use the creation operators a_{in}^\dagger and a_{out}^\dagger to build up Fock states from the vacuum. For instance

$$a_{\text{in}}^\dagger(\mathbf{p}_1) a_{\text{in}}^\dagger(\mathbf{p}_2)|0\rangle = |\mathbf{p}_1, \mathbf{p}_2; \text{in}\rangle, \quad (160)$$

$$a_{\text{out}}^\dagger(\mathbf{k}_1) \cdots a_{\text{out}}^\dagger(\mathbf{k}_n)|0\rangle = |\mathbf{k}_1, \dots, \mathbf{k}_n; \text{out}\rangle. \quad (161)$$

We must now distinguish between Fock states generated by a_{in}^\dagger and a_{out}^\dagger , and therefore we have labelled the Fock states accordingly. In eqs. (160) and (161) we have assumed that there is a stable and unique vacuum state of the free theory (the vacuum at general times t will be that of the full interacting theory, and thus differ from this in general):

$$|0\rangle = |0; \text{in}\rangle = |0; \text{out}\rangle. \quad (162)$$

Mathematically speaking, the a_{in}^\dagger 's and a_{out}^\dagger 's generate two different bases of the Fock space. Since the physics that we want to describe must be independent of the choice of basis, expectation values expressed in terms of “in” and “out” operators and states must satisfy

$$\langle \text{in} | \phi_{\text{in}}(x) | \text{in} \rangle = \langle \text{out} | \phi_{\text{out}}(x) | \text{out} \rangle. \quad (163)$$

Here $|\text{in}\rangle$ and $|\text{out}\rangle$ denote generic “in” and “out” states. We can relate the two bases by introducing a unitary operator S such that

$$\phi_{\text{in}}(x) = S \phi_{\text{out}}(x) S^\dagger \quad (164)$$

$$|\text{in}\rangle = S |\text{out}\rangle, \quad |\text{out}\rangle = S^\dagger |\text{in}\rangle, \quad S^\dagger S = 1. \quad (165)$$

S is called the S -matrix or S -operator. Note that the plane wave solutions of ϕ_{in} and ϕ_{out} also imply that

$$a_{\text{in}}^\dagger = S a_{\text{out}}^\dagger S^\dagger, \quad \hat{a}_{\text{in}} = S \hat{a}_{\text{out}} S^\dagger. \quad (166)$$

By comparing “in” with “out” states one can extract information about the interaction – this is the very essence of detector experiments, where one tries to infer the nature of the interaction by studying the products of the scattering of particles that have been collided with known energies. As we will see below, this information is contained in the elements of the S -matrix.

By contrast, in the absence of any interaction, i.e. for $\mathcal{L}_{\text{int}} = 0$ the distinction between ϕ_{in} and ϕ_{out} is not necessary. They can thus be identified, and then the relation between different bases of the Fock space becomes trivial, $S = 1$, as one would expect.

What we are ultimately interested in are transition amplitudes between an initial state i of, say, two particles of momenta $\mathbf{p}_1, \mathbf{p}_2$, and a final state f , for instance n particles of unequal momenta. The transition amplitude is then given by

$$\langle f, \text{out} | i, \text{in} \rangle = \langle f, \text{out} | S | i, \text{out} \rangle = \langle f, \text{in} | S | i, \text{in} \rangle \equiv S_{fi}. \quad (167)$$

The S -matrix element S_{fi} therefore describes the transition amplitude for the scattering process in question. The scattering cross section, which is a measurable quantity, is then proportional to $|S_{fi}|^2$. All information about the scattering is thus encoded in the S -matrix, which must therefore be closely related to the interaction Hamiltonian density \mathcal{H}_{int} . However, before we try to derive the relation between S and \mathcal{H}_{int} we have to take a slight detour.

4.2 More on time evolution: Dirac picture

The operators $\phi(\mathbf{x}, t)$ and $\pi(\mathbf{x}, t)$ which we have encountered are Heisenberg fields and thus time-dependent. The state vectors are time-independent in the sense that they do not satisfy a non-trivial equation of motion. Nevertheless, state vectors in the Heisenberg picture can carry a time label. For instance, the “in”-states of the previous subsection are defined at $t = -\infty$. The relation of the Heisenberg operator $\phi_H(x)$ with its counterpart ϕ_S in the Schrödinger picture is given by

$$\phi_H(\mathbf{x}, t) = e^{iHt} \phi_S e^{-iHt}, \quad H = H_0 + H_{\text{int}}, \quad (168)$$

Note that this relation involves the *full* Hamiltonian $H = H_0 + H_{\text{int}}$ in the interacting theory. We have so far found solutions to the Klein-Gordon equation in the free theory, and so we know how to handle time evolution in this case. However, in the interacting case the Klein-Gordon equation has an extra term,

$$(\square + m^2)\phi(x) + \frac{\partial V_{\text{int}}(\phi)}{\partial \phi} = 0, \quad (169)$$

due to the potential of the interactions. Apart from very special cases of this potential, the equation cannot be solved anymore in closed form, and thus we no longer know the time evolution. It is therefore useful to introduce a new quantum picture for the interacting theory, in which the time dependence is governed by H_0 only. This is the so-called Dirac or Interaction picture. The relation between fields in the Interaction picture, ϕ_I , and in the Schrödinger picture, ϕ_S , is given by

$$\phi_I(\mathbf{x}, t) = e^{iH_0 t} \phi_S e^{-iH_0 t}. \quad (170)$$

At $t = -\infty$ the interaction vanishes, i.e. $H_{\text{int}} = 0$, and hence the fields in the Interaction and Heisenberg pictures are identical, i.e. $\phi_H(\mathbf{x}, t) = \phi_I(\mathbf{x}, t)$ for $t \rightarrow -\infty$. The relation between ϕ_H and ϕ_I can be worked out easily:

$$\begin{aligned} \phi_H(\mathbf{x}, t) &= e^{iHt} \phi_S e^{-iHt} \\ &= e^{iHt} e^{-iH_0 t} \underbrace{e^{iH_0 t} \phi_S e^{-iH_0 t}}_{\phi_I(\mathbf{x}, t)} e^{iH_0 t} e^{-iHt} \\ &= U^{-1}(t) \phi_I(\mathbf{x}, t) U(t), \end{aligned} \quad (171)$$

where we have introduced the unitary operator $U(t)$

$$U(t) = e^{iH_0 t} e^{-iHt}, \quad U^\dagger U = 1. \quad (172)$$

The field $\phi_H(\mathbf{x}, t)$ contains the information about the interaction, since it evolves over time with the full Hamiltonian. In order to describe the “in” and “out” field operators, we can now make the following identifications:

$$t \rightarrow -\infty : \phi_{\text{in}}(\mathbf{x}, t) = \phi_I(\mathbf{x}, t) = \phi_H(\mathbf{x}, t), \quad (173)$$

$$t \rightarrow +\infty : \phi_{\text{out}}(\mathbf{x}, t) = \phi_H(\mathbf{x}, t). \quad (174)$$

Furthermore, since the fields ϕ_I evolve over time with the free Hamiltonian H_0 , they always act in the basis of “in” vectors, such that

$$\phi_{\text{in}}(\mathbf{x}, t) = \phi_I(\mathbf{x}, t), \quad -\infty < t < \infty. \quad (175)$$

The relation between ϕ_I and ϕ_H at any time t is given by

$$\phi_I(\mathbf{x}, t) = U(t) \phi_H(\mathbf{x}, t) U^{-1}(t). \quad (176)$$

As $t \rightarrow \infty$ the identifications of eqs. (174) and (175) yield

$$\phi_{\text{in}} = U(\infty) \phi_{\text{out}} U^\dagger(\infty). \quad (177)$$

From the definition of the S -matrix, Eq. (164) we then read off that

$$\lim_{t \rightarrow \infty} U(t) = S. \quad (178)$$

We have thus derived a formal expression for the S -matrix in terms of the operator $U(t)$, which tells us how operators and state vectors deviate from the free theory at time t , measured relative to $t_0 = -\infty$, i.e. long before the interaction process.

An important boundary condition for $U(t)$ is

$$\lim_{t \rightarrow -\infty} U(t) = 1. \quad (179)$$

What we mean here is the following: the operator U actually describes the evolution relative to some initial time t_0 , which we will normally suppress, i.e. we write $U(t)$ instead of $U(t, t_0)$. We regard t_0 merely as a time label and fix it at $-\infty$, where the interaction vanishes. Equation (179) then simply states that U becomes unity as $t \rightarrow t_0$, which means that in this limit there is no distinction between Heisenberg and Dirac fields.

Using the definition of $U(t)$, Eq. (172), it is an easy exercise to derive the equation of motion for $U(t)$:

$$i \frac{d}{dt} U(t) = H_{\text{int}}(t) U(t), \quad H_{\text{int}}(t) = e^{iH_0 t} H_{\text{int}} e^{-iH_0 t}. \quad (180)$$

The time-dependent operator $H_{\text{int}}(t)$ is defined in the interaction picture, and depends on the fields $\phi_{\text{in}}, \pi_{\text{in}}$ in the “in” basis. Let us now solve the equation of motion for $U(t)$ with the boundary condition $\lim_{t \rightarrow -\infty} U(t) = 1$. Integrating Eq. (180) gives

$$\begin{aligned} \int_{-\infty}^t \frac{d}{dt_1} U(t_1) dt_1 &= -i \int_{-\infty}^t H_{\text{int}}(t_1) U(t_1) dt_1 \\ U(t) - U(-\infty) &= -i \int_{-\infty}^t H_{\text{int}}(t_1) U(t_1) dt_1 \\ \Rightarrow U(t) &= 1 - i \int_{-\infty}^t H_{\text{int}}(t_1) U(t_1) dt_1. \end{aligned} \quad (181)$$

The right-hand side still depends on U , but we can substitute our new expression for $U(t)$ into the integrand, which gives

$$\begin{aligned} U(t) &= 1 - i \int_{-\infty}^t H_{\text{int}}(t_1) \left\{ 1 - i \int_{-\infty}^{t_1} H_{\text{int}}(t_2) U(t_2) dt_2 \right\} dt_1 \\ &= 1 - i \int_{-\infty}^t H_{\text{int}}(t_1) dt_1 - \int_{-\infty}^t dt_1 H_{\text{int}}(t_1) \int_{-\infty}^{t_1} dt_2 H_{\text{int}}(t_2) U(t_2), \end{aligned} \quad (182)$$

where $t_2 < t_1 < t$. This procedure can be iterated further, so that the n th term in the sum is

$$(-i)^n \int_{-\infty}^t dt_1 \int_{-\infty}^{t_1} dt_2 \cdots \int_{-\infty}^{t_{n-1}} dt_n H_{\text{int}}(t_1) H_{\text{int}}(t_2) \cdots H_{\text{int}}(t_n). \quad (183)$$

This iterative solution could be written in much more compact form, were it not for the fact that the upper integration bounds were all different, and that the ordering $t_n < t_{n-1} < \dots < t_1 < t$ had to be obeyed. Time ordering is an important issue, since one has to ensure that the interaction Hamiltonians act at the proper time, thereby ensuring the causality of the theory. By introducing the time-ordered product of operators, one can use a compact notation, such that the resulting expressions still obey causality. The time-ordered product of two fields $\phi(t_1)$ and $\phi(t_2)$ is defined as

$$\begin{aligned} T\{\phi(t_1)\phi(t_2)\} &= \begin{cases} \phi(t_1)\phi(t_2) & t_1 > t_2 \\ \phi(t_2)\phi(t_1) & t_1 < t_2 \end{cases} \\ &\equiv \theta(t_1 - t_2)\phi(t_1)\phi(t_2) + \theta(t_2 - t_1)\phi(t_2)\phi(t_1), \end{aligned} \quad (184)$$

where θ denotes the step function. The generalisation to products of n operators is obvious. Using time ordering for the n th term of Eq. (183) we obtain

$$\frac{(-i)^n}{n!} \prod_{i=1}^n \int_{-\infty}^t dt_i T\{H_{\text{int}}(t_1) H_{\text{int}}(t_2) \cdots H_{\text{int}}(t_n)\}. \quad (185)$$

Here we have replaced each upper limit of integration with t . Each specific ordering in the time-ordered product gives a term identical to eq. (183), where applying the T operator corresponds to setting the upper limit of integration to the relevant t_i in each integral. However, we have overcounted by a factor $n!$, corresponding to the number of ways of ordering the fields in the time ordered product. Thus one must divide by $n!$ as shown. We may recognise eq. (185) as the n th term in the series expansion of an exponential, and thus can finally rewrite the solution for $U(t)$ in compact form as

$$U(t) = T \exp \left\{ -i \int_{-\infty}^t H_{\text{int}}(t') dt' \right\}, \quad (186)$$

where the “ T ” in front ensures the correct time ordering.

4.3 S -matrix and Green’s functions

The S -matrix, which relates the “in” and “out” fields before and after the scattering process, can be written as

$$S = 1 + iT, \quad (187)$$

where T is commonly called the T -matrix. The fact that S contains the unit operator means that also the case where none of the particles scatter is encoded in S . On the other hand, the non-trivial case is described by the T -matrix, and this is what we are interested in. So far we have derived an expression for the S -matrix in terms of the interaction Hamiltonian, and we could use this in principle to calculate scattering processes. However, there is a slight complication owing to the fact that the vacuum of the free theory is not the same as the true vacuum of the full, interacting

theory. Instead, we will follow the approach of Lehmann, Symanzik and Zimmerman, which relates the S -matrix to n -point Green's functions

$$G_n(x_1, \dots, x_n) = \langle 0 | T(\phi(x_1) \dots \phi(x_n)) | 0 \rangle \quad (188)$$

i.e. vacuum expectation values of Heisenberg fields. We will see later how to calculate these in terms of vacuum expectation values of “in” fields (i.e. in the free theory).

In order to relate S -matrix elements to Green's functions, we have to express the “in/out”-states in terms of creation operators $a_{\text{in/out}}^\dagger$ and the vacuum, then express the creation operators by the fields $\phi_{\text{in/out}}$, and finally use the time evolution to connect those with the fields ϕ in our Lagrangian. Let us consider again the scattering process depicted in Fig. 4. The S -matrix element in this case is

$$\begin{aligned} S_{\text{fi}} &= \langle \mathbf{k}_1, \mathbf{k}_2, \dots, \mathbf{k}_n; \text{out} | \mathbf{p}_1, \mathbf{p}_2; \text{in} \rangle \\ &= \langle \mathbf{k}_1, \mathbf{k}_2, \dots, \mathbf{k}_n; \text{out} | a_{\text{in}}^\dagger(\mathbf{p}_1) | \mathbf{p}_2; \text{in} \rangle, \end{aligned} \quad (189)$$

where a_{in}^\dagger is the creation operator pertaining to the “in” field ϕ_{in} . Our task is now to express a_{in}^\dagger in terms of ϕ_{in} , and repeat this procedure for all other momenta labelling our Fock states.

The following identities will prove useful

$$\begin{aligned} a^\dagger(\mathbf{p}) &= i \int d^3x \{ (\partial_0 e^{-iq \cdot x}) \phi(x) - e^{-iq \cdot x} (\partial_0 \phi(x)) \} \\ &\equiv -i \int d^3x e^{-iq \cdot x} \overleftrightarrow{\partial}_0 \phi(x), \end{aligned} \quad (190)$$

$$\begin{aligned} \hat{a}(\mathbf{p}) &= -i \int d^3x \{ (\partial_0 e^{iq \cdot x}) \phi(x) - e^{iq \cdot x} (\partial_0 \phi(x)) \} \\ &\equiv i \int d^3x e^{iq \cdot x} \overleftrightarrow{\partial}_0 \phi(x). \end{aligned} \quad (191)$$

The S -matrix element can then be rewritten as

$$\begin{aligned} S_{\text{fi}} &= -i \int d^3x_1 e^{-ip_1 \cdot x_1} \overleftrightarrow{\partial}_0 \langle \mathbf{k}_1, \dots, \mathbf{k}_n; \text{out} | \phi_{\text{in}}(x_1) | \mathbf{p}_2; \text{in} \rangle \\ &= -i \lim_{t_1 \rightarrow -\infty} \int d^3x_1 e^{-ip_1 \cdot x_1} \overleftrightarrow{\partial}_0 \langle \mathbf{k}_1, \dots, \mathbf{k}_n; \text{out} | \phi(x_1) | \mathbf{p}_2; \text{in} \rangle, \end{aligned} \quad (192)$$

where in the last line we have used Eq. (156) to replace ϕ_{in} by ϕ . We can now rewrite $\lim_{t_1 \rightarrow -\infty}$ using the following identity, which holds for an arbitrary, differentiable function $f(t)$, whose limit $t \rightarrow \pm\infty$ exists:

$$\lim_{t \rightarrow -\infty} f(t) = \lim_{t \rightarrow +\infty} f(t) - \int_{-\infty}^{+\infty} \frac{df}{dt} dt. \quad (193)$$

The S -matrix element then reads

$$\begin{aligned} S_{\text{fi}} &= -i \lim_{t_1 \rightarrow +\infty} \int d^3x_1 e^{-ip_1 \cdot x_1} \overleftrightarrow{\partial}_0 \langle \mathbf{k}_1, \dots, \mathbf{k}_n; \text{out} | \phi(x_1) | \mathbf{p}_2; \text{in} \rangle \\ &\quad + i \int_{-\infty}^{+\infty} dt_1 \frac{\partial}{\partial t_1} \left\{ \int d^3x_1 e^{-ip_1 \cdot x_1} \overleftrightarrow{\partial}_0 \langle \mathbf{k}_1, \dots, \mathbf{k}_n; \text{out} | \phi(x_1) | \mathbf{p}_2; \text{in} \rangle \right\}. \end{aligned} \quad (194)$$

The first term in this expression involves $\lim_{t_1 \rightarrow +\infty} \phi = \phi_{\text{out}}$, which gives rise to a contribution

$$\propto \left\langle \mathbf{k}_1, \dots, \mathbf{k}_n; \text{out} \left| a_{\text{out}}^\dagger(\mathbf{p}_1) \right| \mathbf{p}_2; \text{in} \right\rangle. \quad (195)$$

This is non-zero only if \mathbf{p}_1 is equal to one of $\mathbf{k}_1, \dots, \mathbf{k}_n$. This, however, means that the particle with momentum \mathbf{p}_1 does not scatter, and hence the first term does not contribute to the T -matrix of Eq. (187). We are then left with the following expression for S_{fi} :

$$S_{\text{fi}} = -i \int d^4 x_1 \left\langle \mathbf{k}_1, \dots, \mathbf{k}_n; \text{out} \left| \partial_0 \left\{ (\partial_0 e^{-ip_1 \cdot x_1}) \phi(x_1) - e^{-ip_1 \cdot x_1} (\partial_0 \phi(x_1)) \right\} \right| \mathbf{p}_2; \text{in} \right\rangle. \quad (196)$$

The time derivatives in the integrand can be worked out:

$$\begin{aligned} & \partial_0 \left\{ (\partial_0 e^{-ip_1 \cdot x_1}) \phi(x_1) - e^{-ip_1 \cdot x_1} (\partial_0 \phi(x_1)) \right\} \\ &= -[E(\mathbf{p}_1)]^2 e^{-ip_1 \cdot x_1} \phi(x_1) - e^{-ip_1 \cdot x_1} \partial_0^2 \phi(x_1) \\ &= -\left\{ ((-\nabla^2 + m^2) e^{-ip_1 \cdot x_1}) \phi(x_1) + e^{-ip_1 \cdot x_1} \partial_0^2 \phi(x_1) \right\}, \end{aligned} \quad (197)$$

where we have used that $-\nabla^2 e^{-ip_1 \cdot x_1} = \mathbf{p}_1^2 e^{-ip_1 \cdot x_1}$. For the S -matrix element one obtains

$$\begin{aligned} S_{\text{fi}} &= i \int d^4 x_1 e^{-ip_1 \cdot x_1} \left\langle \mathbf{k}_1, \dots, \mathbf{k}_n; \text{out} \left| (\partial_0^2 - \nabla^2 + m^2) \phi(x_1) \right| \mathbf{p}_2; \text{in} \right\rangle \\ &= i \int d^4 x_1 e^{-ip_1 \cdot x_1} (\square_{x_1} + m^2) \left\langle \mathbf{k}_1, \dots, \mathbf{k}_n; \text{out} \left| \phi(x_1) \right| \mathbf{p}_2; \text{in} \right\rangle, \end{aligned} \quad (198)$$

where we have used integration by parts twice so that ∇^2 acts on $\phi(x_1)$ rather than on $e^{-ip_1 \cdot x_1}$. What we have obtained after this rather lengthy step of algebra is an expression in which the (Heisenberg) field operator is sandwiched between Fock states, one of which has been reduced to a one-particle state. We can now successively eliminate all momentum variables from the Fock states, by repeating the procedure for the momentum \mathbf{p}_2 , as well as the n momenta of the “out” state. The final expression for S_{fi} is

$$\begin{aligned} S_{\text{fi}} &= (i)^{n+2} \int d^4 x_1 \int d^4 x_2 \int d^4 y_1 \cdots \int d^4 y_n e^{(-ip_1 \cdot x_1 - ip_2 \cdot x_2 + ik_1 \cdot y_1 + \cdots + ik_n \cdot y_n)} \\ &\quad \times (\square_{x_1} + m^2) (\square_{x_2} + m^2) (\square_{y_1} + m^2) \cdots (\square_{y_n} + m^2) \\ &\quad \times \left\langle 0; \text{out} \left| T\{\phi(y_1) \cdots \phi(y_n) \phi(x_1) \phi(x_2)\} \right| 0; \text{in} \right\rangle, \end{aligned} \quad (199)$$

where the time-ordering inside the vacuum expectation value (VEV) ensures that causality is obeyed. The above expression is known as the *Lehmann-Symanzik-Zimmermann* (LSZ) *reduction formula*. It relates the formal definition of the scattering amplitude to a vacuum expectation value of time-ordered fields. Since the vacuum is uniquely the same for “in/out”, the VEV in the LSZ formula for the scattering of two initial particles into n particles in the final state is recognised as the $(n+2)$ -point Green’s function:

$$G_{n+2}(y_1, y_2, \dots, y_n, x_1, x_2) = \left\langle 0 \left| T\{\phi(y_1) \cdots \phi(y_n) \phi(x_1) \phi(x_2)\} \right| 0 \right\rangle. \quad (200)$$

You will note that we still have not calculated or evaluated anything, but merely rewritten the expression for the scattering matrix elements. Nevertheless, the LSZ formula is of tremendous

importance and a central piece of QFT. It provides the link between fields in the Lagrangian and the scattering amplitude S_{fi}^2 , which yields the cross section, measurable in an experiment. Up to here no assumptions or approximations have been made, so this connection between physics and formalism is rather tight. It also illustrates a profound phenomenon of QFT and particle physics: the scattering properties of particles, in other words their interactions, are encoded in the vacuum structure, i.e. the vacuum is non-trivial!

4.4 How to compute Green's functions

Of course, in order to calculate cross sections, we need to compute the Green's functions. Alas, for any physically interesting and interacting theory this cannot be done exactly, contrary to the free theory discussed earlier. Instead, approximation methods have to be used in order to simplify the calculation, while hopefully still giving reliable results. Or one reformulates the entire QFT as a lattice field theory, which in principle allows to compute Green's functions without any approximations (in practice this still turns out to be a difficult task for physically relevant systems). This is what many theorists do for a living. But the formalism stands, and if there are discrepancies between theory and experiments, one “only” needs to check the accuracy with which the Green's functions have been calculated or measured, before approving or discarding a particular Lagrangian.

In the next section we shall discuss how to compute the Green's function of scalar field theory in perturbation theory. Before we can tackle the actual computation, we must take a further step. Let us consider the n -point Green's function

$$G_n(x_1, \dots, x_n) = \langle 0 | T \{ \phi(x_1) \cdots \phi(x_n) \} | 0 \rangle. \quad (201)$$

The fields ϕ which appear in this expression are Heisenberg fields, whose time evolution is governed by the full Hamiltonian $H_0 + H_{\text{int}}$. In particular, the ϕ 's are *not* the ϕ_{in} 's. We know how to handle the latter, because they correspond to a free field theory, but not the former, whose time evolution is governed by the interacting theory, whose solutions we do not know. Let us thus start to isolate the dependence of the fields on the interaction Hamiltonian. Recall the relation between the Heisenberg fields $\phi(t)$ and the “in”-fields⁴

$$\phi(t) = U^{-1}(t) \phi_{\text{in}}(t) U(t). \quad (202)$$

We now assume that the fields are properly time-ordered, i.e. $t_1 > t_2 > \dots > t_n$, so that we can forget about writing $T(\dots)$ everywhere. After inserting Eq. (202) into the definition of G_n one obtains

$$G_n = \langle 0 | U^{-1}(t_1) \phi_{\text{in}}(t_1) U(t_1) U^{-1}(t_2) \phi_{\text{in}}(t_2) U(t_2) \cdots \\ \times U^{-1}(t_n) \phi_{\text{in}}(t_n) U(t_n) | 0 \rangle. \quad (203)$$

Now we introduce another time label t such that $t \gg t_1$ and $-t \ll t_1$. For the n -point function we now obtain

$$G_n = \left\langle 0 \left| U^{-1}(t) \left\{ U(t) U^{-1}(t_1) \phi_{\text{in}}(t_1) U(t_1) U^{-1}(t_2) \phi_{\text{in}}(t_2) U(t_2) \cdots \right. \right. \right. \\ \left. \left. \left. \times U^{-1}(t_n) \phi_{\text{in}}(t_n) U(t_n) U^{-1}(-t) \right\} U(-t) \right| 0 \right\rangle. \quad (204)$$

⁴Here and in the following we suppress the spatial argument of the fields for the sake of brevity.

The expression in curly braces is now time-ordered by construction. An important observation at this point is that it involves pairs of U and its inverse, for instance

$$U(t)U^{-1}(t_1) \equiv U(t, t_1). \quad (205)$$

One can easily convince oneself that $U(t, t_1)$ provides the net time evolution from t_1 to t . We can now write G_n as

$$G_n = \left\langle 0 \left| U^{-1}(t) T \left\{ \phi_{\text{in}}(t_1) \cdots \phi_{\text{in}}(t_n) \underbrace{U(t, t_1) U(t_1, t_2) \cdots U(t_n, -t)}_{U(t, -t)} \right\} U(-t) \right| 0 \right\rangle, \quad (206)$$

where we have used the fact that we may commute the U operators within the time-ordered product. Let us now take $t \rightarrow \infty$. The relation between $U(t)$ and the S -matrix Eq. (178), as well as the boundary condition Eq. (179) tell us that

$$\lim_{t \rightarrow \infty} U(-t) = 1, \quad \lim_{t \rightarrow \infty} U(t, -t) = S, \quad (207)$$

which can be inserted into the above expression. We still have to work out the meaning of $\langle 0|U^{-1}(\infty)$ in the expression for G_n . In a paper by Gell-Mann and Low it was argued that the time evolution operator must leave the vacuum invariant (up to a phase), which justifies the ansatz

$$\langle 0|U^{-1}(\infty) = K \langle 0|, \quad (208)$$

with K being the phase⁵. Multiplying this relation with $|0\rangle$ from the right gives

$$\langle 0|U^{-1}(\infty)|0\rangle = K \langle 0|0\rangle = K. \quad (209)$$

Furthermore, Gell-Mann and Low showed that

$$\langle 0|U^{-1}(\infty)|0\rangle = \frac{1}{\langle 0|U(\infty)|0\rangle}, \quad (210)$$

which implies

$$K = \frac{1}{\langle 0|S|0\rangle}. \quad (211)$$

After inserting all these relations into the expression for G_n we obtain

$$G_n(x_1, \dots, x_n) = \frac{\langle 0|T \{ \phi_{\text{in}}(x_1) \cdots \phi_{\text{in}}(x_n) S \} |0\rangle}{\langle 0|S|0\rangle}. \quad (212)$$

The S -matrix is given by

$$S = T \exp \left\{ -i \int_{-\infty}^{+\infty} H_{\text{int}}(t) dt \right\}, \quad H_{\text{int}} = H_{\text{int}}(\phi_{\text{in}}, \pi_{\text{in}}), \quad (213)$$

and thus we have finally succeeded in expressing the n -point Green's function exclusively in terms of the “in”-fields. This completes the derivation of a relation between the general definition of the scattering amplitude S_{fi} and the VEV of time-ordered “in”-fields. This has been a long and

⁵As hinted at earlier, K relates the vacuum of the free theory to the true vacuum of the interacting theory.

technical discussion, but the main points are the following:

Scattering probabilities are related to S -matrix elements. To calculate S -matrix elements for an n particle scattering process, one must first calculate the n particle Green's function (eq. (212)). Then one plugs this into the LSZ formula (eq. (199)).

In fact, the Green's functions cannot be calculated exactly using eq. (212). Instead, one can only obtain answers in the limit in which the interaction strength λ is small. This is the subject of the following sections.

5 Perturbation Theory

In this section we are going to calculate the Green's functions of scalar quantum field theory explicitly. We will specify the interaction Lagrangian in detail and use an approximation known as perturbation theory. At the end we will derive a set of rules, which represent a systematic prescription for the calculation of Green's functions, and can be easily generalised to apply to other, more complicated field theories. These are the famous *Feynman rules*.

We start by making a definite choice for the interaction Lagrangian \mathcal{L}_{int} . Although one may think of many different expressions for \mathcal{L}_{int} , one has to obey some basic principles: firstly, \mathcal{L}_{int} must be chosen such that the potential it generates is bounded from below – otherwise the system has no ground state. Secondly, our interacting theory should be *renormalisable*. Despite being of great importance, the second issue will not be addressed in these lectures. The requirement of renormalisability arises because the non-trivial vacuum, much like a medium, interacts with particles to modify their properties. Moreover, if one computes quantities like the energy or charge of a particle, one typically obtains a divergent result⁶. There are classes of quantum field theories, called renormalisable, in which these divergences can be removed by suitable redefinitions of the fields and the parameters (masses and coupling constants).

For our theory of a real scalar field in four space-time dimensions, it turns out that the only interaction term which leads to a renormalisable theory must be quartic in the fields. Thus we choose

$$\mathcal{L}_{\text{int}} = -\frac{\lambda}{4!}\phi^4(x), \quad (214)$$

where the coupling constant λ describes the strength of the interaction between the scalar fields, much like, say, the electric charge describing the strength of the interaction between photons and electrons. The factor $4!$ is for later convenience. The full Lagrangian of the theory then reads

$$\mathcal{L} = \mathcal{L}_0 + \mathcal{L}_{\text{int}} = \frac{1}{2}(\partial_\mu\phi)^2 - \frac{1}{2}m^2\phi^2 - \frac{\lambda}{4!}\phi^4, \quad (215)$$

and the explicit expressions for the interaction Hamiltonian and the S -matrix are

$$\begin{aligned} \mathcal{H}_{\text{int}} &= -\mathcal{L}_{\text{int}}, & H_{\text{int}} &= \frac{\lambda}{4!} \int d^3x \phi_{\text{in}}^4(\mathbf{x}, t) \\ S &= T \exp \left\{ -i \frac{\lambda}{4!} \int d^4x \phi_{\text{in}}^4(x) \right\}. \end{aligned} \quad (216)$$

⁶This is despite the subtraction of the vacuum energy discussed earlier.

The n -point Green's function is

$$G_n(x_1, \dots, x_n) = \frac{\sum_{r=0}^{\infty} \left(-\frac{i\lambda}{4!}\right)^r \frac{1}{r!} \left\langle 0 \left| T \left\{ \phi_{\text{in}}(x_1) \cdots \phi_{\text{in}}(x_n) \left(\int d^4y \phi_{\text{in}}^4(y) \right)^r \right\} \right| 0 \right\rangle}{\sum_{r=0}^{\infty} \left(-\frac{i\lambda}{4!}\right)^r \frac{1}{r!} \left\langle 0 \left| T \left(\int d^4y \phi_{\text{in}}^4(y) \right)^r \right| 0 \right\rangle}. \quad (217)$$

This expression cannot be dealt with as it stands. In order to evaluate it we must expand G_n in powers of the coupling λ and truncate the series after a finite number of terms. This only makes sense if λ is sufficiently small. In other words, the interaction Lagrangian must act as a small perturbation on the system. As a consequence, the procedure of expanding Green's functions in powers of the coupling is referred to as *perturbation theory*. We will see that there is a natural diagrammatic representation of this expansion (Feynman diagrams). First, we need to know how to calculate the vacuum expectation values of time ordered products. This is the subject of the next section.

5.1 Wick's Theorem

The n -point Green's function in Eq. (217) involves the time-ordered product over at least n fields. There is a method to express VEV's of n fields, i.e. $\langle 0 | T \{ \phi_{\text{in}}(x_1) \cdots \phi_{\text{in}}(x_n) \} | 0 \rangle$ in terms of VEV's involving two fields only. This is known as Wick's theorem.

Let us for the moment ignore the subscript "in" and return to the definition of normal-ordered fields. The normal-ordered product $:\phi(x_1)\phi(x_2):$ differs from $\phi(x_1)\phi(x_2)$ by the vacuum expectation value, i.e.

$$\phi(x_1)\phi(x_2) = :\phi(x_1)\phi(x_2): + \langle 0 | \phi(x_1)\phi(x_2) | 0 \rangle. \quad (218)$$

We are now going to combine normal-ordered products with time ordering. The time-ordered product $T\{\phi(x_1)\phi(x_2)\}$ is given by

$$\begin{aligned} T\{\phi(x_1)\phi(x_2)\} &= \phi(x_1)\phi(x_2)\theta(t_1 - t_2) + \phi(x_2)\phi(x_1)\theta(t_2 - t_1) \\ &= :\phi(x_1)\phi(x_2): \left(\theta(t_1 - t_2) + \theta(t_2 - t_1) \right) \\ &\quad + \langle 0 | \phi(x_1)\phi(x_2)\theta(t_1 - t_2) + \phi(x_2)\phi(x_1)\theta(t_2 - t_1) | 0 \rangle. \end{aligned} \quad (219)$$

Here we have used the important observation that

$$:\phi(x_1)\phi(x_2): = :\phi(x_2)\phi(x_1):, \quad (220)$$

which means that normal-ordered products of fields are automatically time-ordered.⁷ Equation (219) is Wick's theorem for the case of two fields:

$$T\{\phi(x_1)\phi(x_2)\} = :\phi(x_1)\phi(x_2): + \langle 0 | T \{ \phi(x_1)\phi(x_2) \} | 0 \rangle. \quad (221)$$

For the case of three fields, Wick's theorem yields

$$\begin{aligned} T\{\phi(x_1)\phi(x_2)\phi(x_3)\} &= :\phi(x_1)\phi(x_2)\phi(x_3): + :\phi(x_1): \langle 0 | T \{ \phi(x_2)\phi(x_3) \} | 0 \rangle \\ &\quad + :\phi(x_2): \langle 0 | T \{ \phi(x_1)\phi(x_3) \} | 0 \rangle + :\phi(x_3): \langle 0 | T \{ \phi(x_1)\phi(x_2) \} | 0 \rangle \end{aligned} \quad (222)$$

⁷The reverse is, however, not true!

At this point the general pattern becomes clear: any time-ordered product of fields is equal to its normal-ordered version plus terms in which pairs of fields are removed from the normal-ordered product and sandwiched between the vacuum to form 2-point functions. Then one sums over all permutations. Without proof we give the expression for the general case of n fields (n even):

$$\begin{aligned}
T\{\phi(x_1)\cdots\phi(x_n)\} = & \\
& : \phi(x_1)\cdots\phi(x_n) : \\
& + : \phi(x_1)\cdots\widehat{\phi(x_i)}\cdots\widehat{\phi(x_j)}\cdots\phi(x_n) : \langle 0|T\{\phi(x_i)\phi(x_j)\}|0\rangle + \text{perms.} \\
& + : \phi(x_1)\cdots\widehat{\phi(x_i)}\cdots\widehat{\phi(x_j)}\cdots\widehat{\phi(x_k)}\cdots\widehat{\phi(x_l)}\cdots\phi(x_n) : \\
& \quad \times \langle 0|T\{\phi(x_i)\phi(x_j)\}|0\rangle\langle 0|T\{\phi(x_k)\phi(x_l)\}|0\rangle + \text{perms.} \\
& + \dots + \\
& + \langle 0|T\{\phi(x_1)\phi(x_2)\}|0\rangle\langle 0|T\{\phi(x_3)\phi(x_4)\}|0\rangle\cdots\langle 0|T\{\phi(x_{n-1})\phi(x_n)\}|0\rangle \\
& + \text{perms..}
\end{aligned} \tag{223}$$

The symbol $\widehat{\phi(x_i)}$ indicates that $\phi(x_i)$ has been removed from the normal-ordered product. Let us now go back to $\langle 0|T\{\phi(x_1)\cdots\phi(x_n)\}|0\rangle$. If we insert Wick's theorem, then we find that only the contribution in the last line of Eq. (223) survives: by definition the VEV of a normal-ordered product of fields vanishes, and it is precisely the last line of Wick's theorem in which no normal-ordered products are left. The only surviving contribution is that in which all fields have been paired or "contracted". Sometimes a contraction is represented by the notation:

$$\underbrace{\phi(x_i)\phi(x_j)} \equiv \langle 0|T\{\phi(x_i)\phi(x_j)\}|0\rangle, \tag{224}$$

i.e. the pair of fields which is contracted is joined by the braces. Wick's theorem can now be rephrased as

$$\langle 0|T\{\phi(x_1)\cdots\phi(x_n)\}|0\rangle = \text{sum of all possible contractions of } n \text{ fields.} \tag{225}$$

An example of this result is the 4-point function

$$\begin{aligned}
\langle 0|T\{\phi(x_1)\phi(x_2)\phi(x_3)\phi(x_4)\}|0\rangle = & \underbrace{\phi(x_1)\phi(x_2)}\underbrace{\phi(x_3)\phi(x_4)} \\
& + \underbrace{\phi(x_1)\phi(x_2)\phi(x_3)}\phi(x_4) + \underbrace{\phi(x_1)\phi(x_2)\phi(x_4)}\phi(x_3)
\end{aligned} \tag{226}$$

5.2 The Feynman propagator

Using Wick's Theorem one can relate any n -point Green's functions to an expression involving only 2-point functions. Let us have a closer look at

$$G_2(x, y) = \langle 0|T\{\phi_{\text{in}}(x)\phi_{\text{in}}(y)\}|0\rangle. \tag{227}$$

We can now insert the solution for ϕ in terms of \hat{a} and \hat{a}^\dagger . If we assume $t_x > t_y$ then $G_2(x, y)$ can be written as

$$\begin{aligned} G_2(x, y) &= \int \frac{d^3p \, d^3q}{(2\pi)^6 4E(\mathbf{p})E(\mathbf{q})} \\ &\quad \times \left\langle 0 \left| \left(\hat{a}^\dagger(\mathbf{p}) e^{ip \cdot x} + \hat{a}(\mathbf{p}) e^{-ip \cdot x} \right) \left(\hat{a}^\dagger(\mathbf{q}) e^{iq \cdot y} + \hat{a}(\mathbf{q}) e^{-iq \cdot y} \right) \right| 0 \right\rangle \\ &= \int \frac{d^3p \, d^3q}{(2\pi)^6 4E(\mathbf{p})E(\mathbf{q})} e^{-ip \cdot x + iq \cdot y} \left\langle 0 \left| \hat{a}(\mathbf{p}) \hat{a}^\dagger(\mathbf{q}) \right| 0 \right\rangle. \end{aligned} \quad (228)$$

This shows that G_2 can be interpreted as the amplitude for a meson which is created at y and destroyed again at point x . We can now replace $\hat{a}(\mathbf{p})\hat{a}^\dagger(\mathbf{q})$ by its commutator:

$$\begin{aligned} G_2(x, y) &= \int \frac{d^3p \, d^3q}{(2\pi)^6 4E(\mathbf{p})E(\mathbf{q})} e^{-ip \cdot x + iq \cdot y} \left\langle 0 \left| [\hat{a}(\mathbf{p}), \hat{a}^\dagger(\mathbf{q})] \right| 0 \right\rangle \\ &= \int \frac{d^3p}{(2\pi)^3 2E(\mathbf{p})} e^{-ip \cdot (x-y)}, \end{aligned} \quad (229)$$

and the general result, after restoring time-ordering, reads

$$G_2(x, y) = \int \frac{d^3p}{(2\pi)^3 2E(\mathbf{p})} \left(e^{-ip \cdot (x-y)} \theta(t_x - t_y) + e^{ip \cdot (x-y)} \theta(t_y - t_x) \right). \quad (230)$$

Furthermore, using contour integration one can show that this expression can be rewritten as a 4-dimensional integral

$$G_2(x, y) = i \int \frac{d^4p}{(2\pi)^4} \frac{e^{-ip \cdot (x-y)}}{p^2 - m^2 + i\epsilon}, \quad (231)$$

where ϵ is a small parameter which ensures that G_2 does not develop a pole. This calculation has established that $G_2(x, y)$ actually depends only on the difference $(x - y)$. Equation (231) is called the *Feynman propagator* $G_F(x - y)$:

$$G_F(x - y) \equiv \langle 0 | T \{ \phi(x) \phi(y) \} | 0 \rangle = i \int \frac{d^4p}{(2\pi)^4} \frac{e^{-ip \cdot (x-y)}}{p^2 - m^2 + i\epsilon}. \quad (232)$$

The Feynman propagator is a Green's function of the Klein-Gordon equation, i.e. it satisfies

$$(\Box_x + m^2) G_F(x - y) = -i\delta^4(x - y), \quad (233)$$

and describes the propagation of a meson between the space-time points x and y .

5.3 Two-particle scattering to $\mathcal{O}(\lambda)$

Let us now consider a scattering process in which two incoming particles with momenta \mathbf{p}_1 and \mathbf{p}_2 scatter into two outgoing ones with momenta \mathbf{k}_1 and \mathbf{k}_2 , as shown in Fig. 5. The S -matrix element in this case is

$$\begin{aligned} S_{\text{fi}} &= \langle \mathbf{k}_1, \mathbf{k}_2; \text{out} | \mathbf{p}_1, \mathbf{p}_2; \text{in} \rangle \\ &= \langle \mathbf{k}_1, \mathbf{k}_2; \text{in} | S | \mathbf{p}_1, \mathbf{p}_2; \text{in} \rangle, \end{aligned} \quad (234)$$

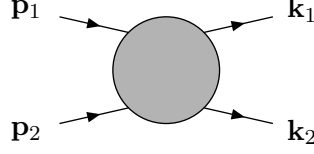


Figure 5: Scattering of two initial particles with momenta \mathbf{p}_1 and \mathbf{p}_2 into 2 particles with momenta \mathbf{k}_1 and \mathbf{k}_2 .

and $S = 1 + iT$. The LSZ formula Eq. (199) tells us that we must compute G_4 in order to obtain S_{fi} . Let us work out G_4 in powers of λ using Wick's theorem.

Suppressing the subscripts “in” from now on, the expression we have to evaluate order by order in λ is

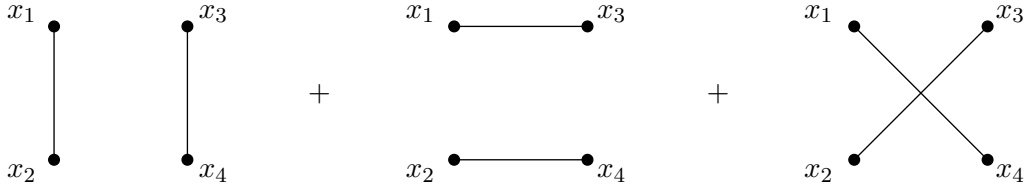
$$G_4(x_1, \dots, x_4) \quad (235)$$

$$= \frac{\sum_{r=0}^{\infty} \left(-\frac{i\lambda}{4!}\right)^r \frac{1}{r!} \left\langle 0 \left| T \left\{ \phi(x_1)\phi(x_2)\phi(x_3)\phi(x_4) \left(\int d^4y \phi^4(y) \right)^r \right\} \right| 0 \right\rangle}{\sum_{r=0}^{\infty} \left(-\frac{i\lambda}{4!}\right)^r \frac{1}{r!} \left\langle 0 \left| T \left(\int d^4y \phi^4(y) \right)^r \right| 0 \right\rangle}.$$

At $\mathcal{O}(\lambda^0)$, the denominator is 1, and the numerator gives

$$\begin{aligned} \langle 0 | T \{ \phi(x_1)\phi(x_2)\phi(x_3)\phi(x_4) \} | 0 \rangle &= G_F(x_1 - x_2) G_F(x_3 - x_4) + G_F(x_1 - x_3) G_F(x_2 - x_4) \\ &\quad + G_F(x_1 - x_4) G_F(x_2 - x_3), \end{aligned} \quad (236)$$

where we have used Wick's theorem. We may represent this graphically as follows:

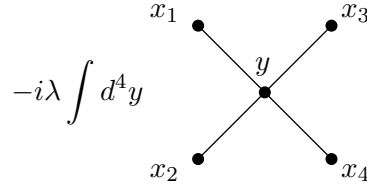


But this is the same answer as if we had set $\lambda = 0$, so $\mathcal{O}(\lambda^0)$ does not describe scattering and hence is not a contribution to the T -matrix.

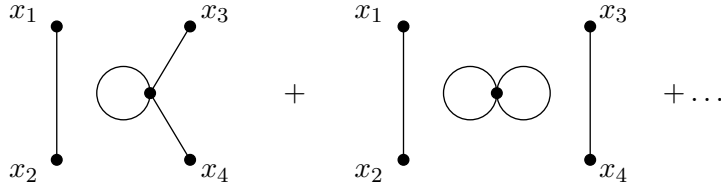
The first non-trivial scattering happens at $\mathcal{O}(\lambda)$. For example, the expansion of the above formula includes the contribution (from the numerator)

$$\begin{aligned} -\frac{i\lambda}{4!} \langle 0 | T [\phi(x_1) \dots \phi(x_4) \int d^4y \phi^4(y) | 0 \rangle &= -\frac{i\lambda}{4!} \int d^4y 4! G_F(x_1 - y) G_F(x_2 - y) G_F(x_3 - y) \\ &\quad \times G_F(x_4 - y), \end{aligned} \quad (237)$$

where the $4!$ inside the integral arises from all possible contractions in Wick's theorem. This has the graphical representation



where each line corresponds to a propagator, and we have assigned a vertex to each space-time point. Also at this order, we have the graphs



We will see later on that neither of these graphs contributes to the S -matrix element (after substituting the Green's function into the LSZ formula of eq. (199)), as they are not fully connected. By this we mean that not all external particle vertices are connected to the same graph. At yet higher orders, we may have graphs which involve fully connected pieces, dressed by additional “vacuum bubbles” (such as that which is sitting in the middle of the right-most figure above). These vacuum bubbles are cancelled by the denominator in eq. (212) which, given that it contains no external fields, generates all possible vacuum graphs. The presence of these vacuum graphs explains why the vacuum of the interacting theory is different to that of the free theory, as mentioned earlier.

To summarise, the final answer for the scattering amplitude to $O(\lambda)$ is given by Eq. (237).

5.4 Graphical representation of the Wick expansion: Feynman rules

We have already encountered the graphical representation of the expansion of Green's functions in perturbation theory after applying Wick's theorem. It is possible to formulate a simple set of rules which allow us to draw the graphs directly without using Wick's theorem and to write down the corresponding algebraic expressions.

We again consider a neutral scalar field whose Lagrangian is

$$\mathcal{L} = \frac{1}{2} \partial_\mu \phi \partial^\mu \phi - \frac{1}{2} m^2 \phi^2 - \frac{\lambda}{4!} \phi^4. \quad (238)$$

Suppose now that we want to compute the $O(\lambda^m)$ contribution to the n -point Green's function $G_n(x_1, \dots, x_n)$. This is achieved by going through the following steps:

(1) Draw all *distinct* diagrams with n external lines and m 4-fold vertices:

- Draw n dots and label them x_1, \dots, x_n (external points)
- Draw m dots and label them y_1, \dots, y_m (vertices)

- Join the dots according to the following rules:
 - only one line emanates from each x_i
 - exactly four lines run into each y_j
 - the resulting diagram must be connected, i.e. there must be a continuous path between any two points.

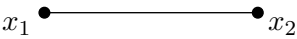
(2) Assign a factor $-\frac{i\lambda}{4!} \int d^4 y_i$ to the vertex at y_i

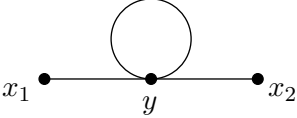
(3) Assign a factor $G_F(x_i - y_j)$ to the line joining x_i and y_j

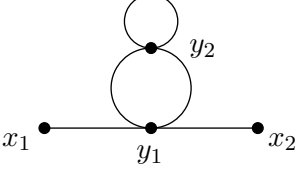
(4) Multiply by the number of contractions \mathcal{C} from the Wick expansion which lead to the same diagram.

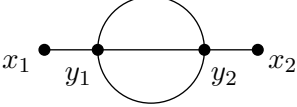
These are the Feynman rules for scalar field theory in *position space*.

Let us look at an example, namely the 2-point function. According to the Feynman rules the contributions up to order λ^2 are as follows:

O(1):  $= G_F(x_1 - x_2)$

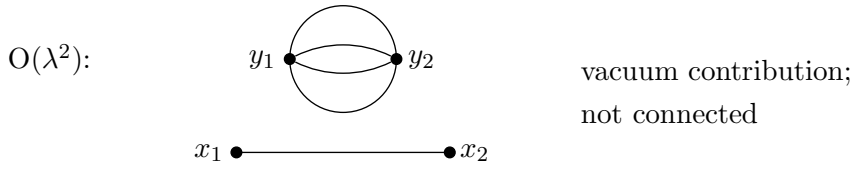
O(λ):  $= \frac{i\lambda}{2} \int d^4 y G_F(x_1 - y) G_F(x_2 - y) G_F(0)$

O(λ^2):  $= -\frac{\lambda^2}{4} \int d^4 y \int d^4 z G_F(x_1 - y) G_F(x_2 - y) \times G_F^2(y - z) G_F(0)$

O(λ^2):  $= \mathcal{C} \left(-\frac{i\lambda}{4!} \right)^2 \int d^4 y_1 d^4 y_2 G_F(x_1 - y_1) [G_F(y_1 - y_2)]^3 G_F(y_2 - x_2)$

The combinatorial factor for this contribution is worked out as $\mathcal{C} = 4 \cdot 4!$. Note that the same graph, but with the positions of y_1 and y_2 interchanged is topologically distinct. Numerically it has the same value as the above graph, and so the corresponding expression has to be multiplied by a factor 2.

Another contribution at order λ^2 is



This contribution must be discarded, since not all of the points are connected via a continuous line.

5.5 Feynman rules in momentum space

It is often simpler to work in momentum space, and hence we will discuss the derivation of Feynman rules in this case. This also reflects what is typically done in scattering experiments (i.e. incoming and outgoing particles have definite momentum). If one works in momentum space, the Green's functions are related to those in position space by a Fourier transform

$$\tilde{G}_n(p_1, \dots, p_n) = \int d^4x_1 \cdots \int d^4x_n e^{ip_1 \cdot x_1 + \dots + ip_n \cdot x_n} G_n(x_1, \dots, x_n). \quad (239)$$

The Feynman rules then serve to compute the Green's function $\tilde{G}_n(p_1, \dots, p_n)$ order by order in the coupling.

Let us see how this works for the $2 \rightarrow 2$ scattering example we considered above. At $\mathcal{O}(\lambda)$ this was given in eq. (237), which we may simplify slightly to

$$-i\lambda \int d^4y G_F(x_1 - y) G_F(x_2 - y) G_F(x_3 - y) G_F(x_4 - y). \quad (240)$$

We may now substitute in the momentum space form of each propagator (eq. (232)) to give

$$\begin{aligned} & -i\lambda \int d^4y \left(\prod_{i=1}^4 \int \frac{d^4p_i}{(2\pi)^4} \frac{i}{p_i^2 - m^2 + i\epsilon} \right) e^{-i \sum_i p_i \cdot (x_i - y)} \\ & = -i\lambda (2\pi)^4 \delta^4(p_1 + p_2 + p_3 + p_4) \left(\prod_{i=1}^4 \int \frac{d^4p_i}{(2\pi)^4} \frac{i}{p_i^2 - m^2 + i\epsilon} \right) e^{-i \sum_i p_i \cdot x_i}, \end{aligned}$$

where we have carried out the y integration in the second line. Substituting this into eq. (239) and carrying out the integrals over each x_i , one finds

$$\begin{aligned} \tilde{G}_4(p_1, \dots, p_n) & = -i\lambda (2\pi)^4 \delta^4(p_1 + p_2 + p_3 + p_4) \left(\prod_i \int \frac{d^4p_i}{(2\pi)^4} \frac{i}{p_i^2 - m^2 + i\epsilon} (2\pi)^4 \delta(p_i) \right) \\ & = -i\lambda (2\pi)^4 \delta^4(p_1 + p_2 + p_3 + p_4) \prod_i \frac{i}{p_i^2 - m^2 + i\epsilon} \end{aligned}$$

We will not repeat the above derivation for a general Green's function. Rather, we now state the Feynman rules in momentum space, and the reader may easily verify that the above example is a special case.

Feynman rules (momentum space)

(1) Draw all *distinct* diagrams with n external lines and m 4-fold vertices:

- Assign momenta p_1, \dots, p_n to the external lines
- Assign momenta k_j to the internal lines

(2) Assign to each external line a factor

$$\frac{i}{p_k^2 - m^2 + i\epsilon}$$

(3) Assign to each internal line a factor

$$\int \frac{d^4 k_j}{(2\pi)^4} \frac{i}{k_j^2 - m^2 + i\epsilon}$$

(4) Each vertex contributes a factor

$$-\frac{i\lambda}{4!}(2\pi)^4 \delta^4 \left(\sum \text{momenta} \right),$$

(the delta function ensures that momentum is conserved at each vertex).

(5) Multiply by the combinatorial factor \mathcal{C} , which is the number of contractions leading to the same momentum space diagram (note that \mathcal{C} may be different from the combinatorial factor for the same diagram considered in position space!)

Alternatively, one may rephrase (4) and (5) as follows:

(4*) Each vertex carries a factor

$$-i\lambda(2\pi)^4 \delta^4 \left(\sum \text{momenta} \right),$$

(5*) Divide by the *symmetry factor* i.e. the dimension of the group of symmetry transformations that leaves the diagram invariant.

5.6 S -matrix and truncated Green's functions

The final topic in these lectures is the derivation of a simple relation between the S -matrix element and a particular momentum space Green's function, which has its external legs amputated: the so-called truncated Green's function. This further simplifies the calculation of scattering amplitudes using Feynman rules.

Let us return to the LSZ formalism and consider the scattering of m initial particles (momenta $\mathbf{p}_1, \dots, \mathbf{p}_m$) into n final particles with momenta $\mathbf{k}_1, \dots, \mathbf{k}_n$. The LSZ formula (eq. (199)) tells us that the S -matrix element is given by

$$\begin{aligned} & \left\langle \mathbf{k}_1, \dots, \mathbf{k}_n; \text{out} \middle| \mathbf{p}_1, \dots, \mathbf{p}_m; \text{in} \right\rangle \\ &= (i)^{n+m} \int \prod_{i=1}^m d^4 x_i \int \prod_{j=1}^n d^4 y_j \exp \left\{ -i \sum_{i=1}^m p_i \cdot x_i + i \sum_{j=1}^n k_j \cdot y_j \right\} \\ & \quad \times \prod_{i=1}^m (\square_{x_i} + m^2) \prod_{j=1}^n (\square_{y_j} + m^2) G_{n+m}(x_1, \dots, x_m, y_1, \dots, y_n). \end{aligned} \quad (241)$$

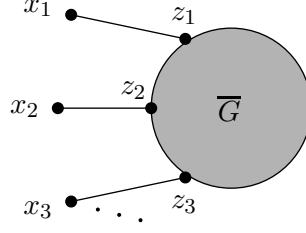


Figure 6: The construction of the truncated Green's function in position space.

Let us have a closer look at $G_{n+m}(x_1, \dots, x_m, y_1, \dots, y_n)$. As shown in Fig. 6 it can be split into Feynman propagators, which connect the external points to the vertices at z_1, \dots, z_{n+m} , and a remaining Green's function \overline{G}_{n+m} , according to

$$G_{n+m} = \int d^4 z_1 \cdots d^4 z_{n+m} G_F(x_1 - z_1) \cdots G_F(y_n - z_{n+m}) \overline{G}_{n+m}(z_1, \dots, z_{n+m}), \quad (242)$$

where, perhaps for obvious reasons, \overline{G}_{n+m} is called the *truncated* Green's function. Putting Eq. (242) back into the LSZ expression for the S -matrix element, and using that

$$(\square_{x_i} + m^2) G_F(x_i - z_i) = -i\delta^4(x_i - z_i) \quad (243)$$

one obtains

$$\begin{aligned} & \langle \mathbf{k}_1, \dots, \mathbf{k}_n; \text{out} | \mathbf{p}_1, \dots, \mathbf{p}_m; \text{in} \rangle \\ &= (i)^{n+m} \int \prod_{i=1}^m d^4 x_i \int \prod_{j=1}^n d^4 y_j \exp \left\{ -i \sum_{i=1}^m p_i \cdot x_i + i \sum_{j=1}^n k_j \cdot y_j \right\} \\ & \quad \times (-i)^{n+m} \int d^4 z_1 \cdots d^4 z_{n+m} \delta^4(x_1 - z_1) \cdots \delta^4(y_n - z_{n+m}) \overline{G}_{n+m}(z_1, \dots, z_{n+m}). \end{aligned} \quad (244)$$

After performing all the integrations over the z_k 's, the final relation becomes

$$\begin{aligned} & \langle \mathbf{k}_1, \dots, \mathbf{k}_n; \text{out} | \mathbf{p}_1, \dots, \mathbf{p}_m; \text{in} \rangle \\ &= \int \prod_{i=1}^m d^4 x_i \prod_{j=1}^n d^4 y_j \exp \left\{ -i \sum_{i=1}^m p_i \cdot x_i + i \sum_{j=1}^n k_j \cdot y_j \right\} \\ & \quad \times \overline{G}_{n+m}(x_1, \dots, x_m, y_1, \dots, y_n) \\ &\equiv \overline{\mathcal{G}}_{n+m}(p_1, \dots, p_m, k_1, \dots, k_n), \end{aligned} \quad (245)$$

where $\overline{\mathcal{G}}_{n+m}$ is the truncated $n+m$ -point function in momentum space. This result shows that the scattering matrix element is directly given by the truncated Green's function in momentum space. In other words, calculating the S -matrix is much the same as calculating the Green's function, but without the free propagators associated with the external legs. Note that this renders zero any graph which is not fully connected - any diagram in which not all external points are connected to the same graph vanishes upon multiplication by the $(p_i^2 + m^2)$ factors. This is what allowed us to neglect such graphs in the previous section.

6 Summary

That completes this introductory look at quantum field theory. Although we did not get as far as some of the more relevant physical applications of QFT, we have looked in detail at what a QFT is, and how the description of scattering amplitudes leads to Feynman diagrams. To recap how we did this:

1. We reviewed the Lagrangian formalism for classical field theory, and also the canonical quantisation approach to quantum mechanics.
2. We constructed the Lagrangian for a relativistic field theory (the free Klein-Gordon field), and applied the techniques of canonical quantisation to this field theory.
3. States in this theory were found to represent particle excitations, such that a particle of momentum \mathbf{p} was found to be a quantum of excitation in the relevant Fourier mode of the field.
4. We then studied the interacting theory, arguing that at initial and final times (when the interaction dies away) we can work with free fields. These were related by an operator S , whose matrix elements represented the transition probability to go from a given initial to a given final state.
5. Using the interaction picture for time evolution, we found an expression for the S matrix in terms of an evolution operator U , describing how the fields at general time t deviate from the initial free fields.
6. We also found a formula which related S matrix elements to n -particle Green's functions (vacuum expectation values of time-ordered fields). This was the LSZ formula of eq. (199).
7. We related the Green's functions involving Heisenberg fields to those involving the “in” fields at time $t \rightarrow -\infty$ (eq. (212)).
8. We then found how to compute these Green's functions in perturbation theory, valid when the strength of the interaction is weak. This involved having to calculate vacuum expectation values of time-ordered products, for which we could use Wick's theorem.
9. We developed a graphical representation of Wick's theorem, which led to simple rules (Feynman rules) for the calculation of Green's functions in position or momentum space.
10. These can easily be converted to S matrix elements by truncating the free propagators associated with the external lines.

Needless to say, there are many things we did not have time to talk about. Some of these will be explored by the other courses at this school:

- Here we calculated S -matrix elements without explaining how to turn these into decay rates or cross-sections, which are the measurable quantities. This is dealt with in the QED / QCD course.

- The Klein-Gordon field involves particles of spin zero, which are bosons. One may also construct field theories for fermions of spin $\frac{1}{2}$, and vector bosons (spin 1). Physical examples include QED and QCD.
- Fields may have internal symmetries (e.g. local gauge invariance). Again, see the QED / QCD and Standard Model courses.
- Diagrams involving loops are divergent, ultimately leading to infinite renormalisation of the couplings and masses. The renormalisation procedure can only be carried out in certain theories. The Standard Model is one example, but other well-known physical theories (e.g. general relativity) fail this criterion.
- There is an alternative formulation of QFT in terms of path integrals (i.e. sums over all possible configurations of fields). This alternative formulation involves some extra conceptual overhead, but allows a much more straightforward derivation of the Feynman rules. More than this, the path integral approach makes many aspects of field theory manifest i.e. is central to our understanding of what a quantum field theory is. This will not be covered at all in this school, but the interested student will find many excellent textbooks on the subject.

There are other areas which are not covered at this school, but nonetheless are indicative of the fact that field theory is still very much an active research area, with many exciting new developments:

- Calculating Feynman diagrams at higher orders is itself a highly complicated subject, and there are a variety of interesting mathematical ideas (e.g. from number theory and complex analysis) involved in current research.
- Sometimes perturbation theory is not well-behaved, in that there are large coefficients at each order of the expansion in the coupling constant. Often the physics of these large contributions can be understood, and summed up to all orders in the coupling. This is known as *resummation*, and is crucial to obtaining sensible results for many cross-sections, especially in QCD.
- Here we have “solved” for scattering probabilities using a perturbation expansion. It is sometimes possible to numerically solve the theory fully non-perturbatively. Such approaches are known as lattice field theory, due to the fact that one discretizes space and time into a lattice of points. It is then possible (with enough supercomputing power!) to calculate things like hadron masses, which are completely incalculable in perturbation theory.
- Here we set up QFT in Minkowski (flat space). If one attempts to do the same thing in curved space (i.e. a strong gravitational field), many weird things happen that give us tantalising hints of what a quantum field of gravity should look like.
- There are some very interesting recent correspondences between certain limits of certain string theories, and a particular quantum field theory in the strong coupling limit. This has allowed us to gain new insights into nonperturbative field theory from an analytic point of view, and there have been applications in heavy ion physics and even condensed matter systems.

I could go on of course, and many of the more formal developments of current QFT research are perhaps not so interesting to a student in experimental particle physics. However, at the present

time some of the more remarkable and novel extensions to the Standard Model (SUSY, extra dimensions) are not only testable, but are actively being looked for. Thus QFT, despite its age, is very much at the forefront of current research efforts and may yet surprise us!

Acknowledgments

I am very grateful to Chris White and Mrinal Dasgupta for providing a previous set of lecture notes, on which these notes are heavily based.

A Books on QFT

There are numerous textbooks already and a surprisingly high number of new books are appearing all the time. As with anything in theoretical physics, exploring a multitude of approaches to a certain field is encouraged.

In the following list, [1] is said to be a good introductory text and a lot of my colleagues use this one for their introduction to QFT classes. Mark has also put a “try-before-buy” version on his webpage, which is an early version of the entire textbook. You can judge yourself if it’s worth the investment.

My first encounter with QFT was [2]. It’s a very good book that heavily makes use of the Path Integral Formalism (not discussed in these lectures), it also includes topics which are normally not featured in general purpose QFT books (e.g. SUSY, topological aspects). A modern classic is [3], which many use as a standard text. It covers a lot of ground and develops an intuitive approach to QFT (but you aren’t spared the hard bits!). It also touches other areas where QFT finds application (e.g. Statistical Physics). In my opinion, it isn’t very good to look things up because Peskin’s pedagogical approach forces logically-connected topics to be scattered across the text. Unless you are very familiar with the book, it can take ages to find certain things again. My personal favorite by far is [4], probably owing to the authors’ focus on particle theory applications of QFT. But you’ll probably need a bit of exposure to one of the introductory texts to fully appreciate the depth and technical details that the authors have put into it. Yes, it’s expensive (like most of the Graduate-level textbooks), but having an advanced QFT book by a bunch of German authors on your shelf will not go unnoticed by your colleagues. Another good text is [5]. Finally, those who are not faint of heart and who like their field theory from the horse’s mouth may like to consult Weinberg’s monumental three volume set [6].

References

- [1] M. Srednicki, *Quantum Field Theory*, CUP 2007.
- [2] L. Ryder, *Quantum Field Theory*, CUP 1985.
- [3] M.E. Peskin and D.V. Schroeder, *An Introduction to Quantum Field Theory*, Addison Wesley 1995.
- [4] M. Böhm, A. Denner, H. Joos, *Gauge Theories*, Teubner 2001.
- [5] T.-P. Cheng, L.-F. Li, *Gauge Theories of Elementary Particle Physics*, Clarendon 1982.

- [6] S. Weinberg, *The Quantum Theory of Fields*, CUP 1995.

B Notation and conventions

4-vectors:

$$\begin{aligned}x^\mu &= (x^0, \mathbf{x}) = (t, \mathbf{x}) \\x_\mu &= g_{\mu\nu} x^\nu = (x^0, -\mathbf{x}) = (t, -\mathbf{x}) \\ \text{Metric tensor: } g_{\mu\nu} &= g^{\mu\nu} = \begin{pmatrix} 1 & 0 & 0 & 0 \\ 0 & -1 & 0 & 0 \\ 0 & 0 & -1 & 0 \\ 0 & 0 & 0 & -1 \end{pmatrix}\end{aligned}$$

Scalar product:

$$\begin{aligned}x^\mu x_\mu &= x^0 x_0 + x^1 x_1 + x^2 x_2 + x^3 x_3 \\ &= t^2 - \mathbf{x}^2\end{aligned}$$

Gradient operators:

$$\begin{aligned}\partial^\mu &\equiv \frac{\partial}{\partial x_\mu} = \left(\frac{\partial}{\partial t}, -\nabla \right) \\ \partial_\mu &\equiv \frac{\partial}{\partial x^\mu} = \left(\frac{\partial}{\partial t}, \nabla \right) \\ \text{d'Alembertian: } \partial^\mu \partial_\mu &= \frac{\partial^2}{\partial t^2} - \nabla^2 \equiv \square\end{aligned}$$

Momentum operator:

$$\hat{p}^\mu = i\hbar \partial^\mu = \left(i\hbar \frac{\partial}{\partial t}, -i\hbar \nabla \right) = \left(\hat{E}, \hat{\mathbf{p}} \right) \quad (\text{as it should be})$$

δ -functions:

$$\begin{aligned}\int d^3p f(\mathbf{p}) \delta^3(\mathbf{p} - \mathbf{q}) &= f(\mathbf{q}) \\ \int d^3x e^{-i\mathbf{p}\cdot\mathbf{x}} &= (2\pi)^3 \delta^3(\mathbf{p}) \\ \int \frac{d^3p}{(2\pi)^3} e^{-i\mathbf{p}\cdot\mathbf{x}} &= \delta^3(\mathbf{x})\end{aligned}$$

(similarly in four dimensions)

Note:

$$\begin{aligned}\delta(x^2 - x_0^2) &= \delta\{(x - x_0)(x + x_0)\} \\ &= \frac{1}{2x} \{\delta(x - x_0) + \delta(x + x_0)\}\end{aligned}$$

AN INTRODUCTION TO QED & QCD

Dr Andrea Banfi (University of Sussex)

Contents

| | |
|--|-----------|
| Outline of Lectures | 57 |
| Textbooks | 58 |
| 1 Relativistic Quantum Mechanics..... | 59 |
| 1.1 The Klein-Gordon Equation | 59 |
| 1.2 The Dirac Equation | 60 |
| 2 Spin..... | 63 |
| 2.1 Plane Wave Solutions of the Dirac Equation | 64 |
| 2.2 Spin | 65 |
| 2.3 Working with Dirac Spinors | 66 |
| 2.4 Lorentz transformations on spinors | 67 |
| 3 Quantum Electro-Dynamics | 68 |
| 3.1 The QED Lagrangian..... | 69 |
| 3.2 Feynman Rules | 70 |
| 4 Calculation of Cross Sections | 75 |
| 4.1 Phase Space Integrals | 75 |
| 4.2 Return to Coulomb Scattering | 76 |
| 4.3 The Coulomb Potential | 77 |
| 4.4 e^+e^- Annihilation | 78 |
| 5 Photon Scattering..... | 79 |
| 5.1 Photon Polarisation | 79 |
| 5.2 Compton Scattering..... | 81 |
| 6 Strong interactions..... | 83 |
| 6.1 QCD Lagrangian | 83 |
| 6.2 Gauge Invariance | 86 |
| 7 Renormalization..... | 91 |
| 7.1 Dimensional regularisation and renormalisation scale | 91 |
| 7.2 Running Coupling | 93 |
| Summary | 97 |
| Acknowledgments | 97 |

| |
|---|
| <p style="text-align: center;">QED and QCD HEP Summer School 2016</p> |
|---|

This course gives an introduction to the ingredients of gauge theories which are necessary to calculate cross sections for particular processes. The section headings are given below:

Outline of Lectures:

1. Relativistic Quantum Mechanics
2. Spin
3. Relativistic Electromagnetism
4. Coulomb Scattering, $e\mu \rightarrow e\mu$
5. Compton Scattering, $e\gamma \rightarrow e\gamma$
6. Colour
7. Renormalisation

This course runs in parallel with the Quantum Field Theory course, from which we will use some results. Some topics mentioned in this course will be covered in more detail in the Standard Model and Phenomenology courses next week.

Textbooks:

These notes are intended to be self-contained, but only provide a short introduction to a complex and fascinating topic. You may find the following textbooks useful:

1. Aitchison and Hey, *Gauge Theories in Particle Physics*, CRC Press.
2. Halzen and Martin, *Quarks and Leptons*, Wiley.
3. Peskin and Schröder, *An Introduction to Quantum Field Theory*, ABP.
4. Ryder, *Quantum Field Theory*, CUP.
5. Srednicki, *Quantum Field Theory*, CUP.
6. Schwartz, *Quantum Field Theory and the Standard Model*, CUP.

The first two are more practical and closer to the spirit of this course while the other contain many more mathematical details. The last one is very recent. If you are particularly interested in (or confused by) a particular topic, I encourage you to take a look at it. If there are other textbooks which you find particularly helpful, please tell me and I will update the list.

These notes are based heavily on the content of previous versions of this course, in particular the 2013 version by Jennifer Smillie. Throughout, we will use “natural units” where $\hbar = c = 1$ and the metric signature $(+ - - -)$.

Please email any comments, questions or corrections to **a.banfi@sussex.ac.uk**.

Andrea Banfi
May 25, 2016

1 Relativistic Quantum Mechanics

In order to describe the dynamics of particles involved in high-energy collisions we must be able to combine the theory of phenomena occurring at the smallest scales, i.e. quantum mechanics, with the description of particles moving close to the speed of light, i.e. special relativity. To do this we must develop wave equations which are relativistically invariant (i.e. invariant under Lorentz transformations). In this section we will derive relativistic equations of motion for scalar particles (spin-0) and particles with spin-1/2.

1.1 The Klein-Gordon Equation

We start with the Hamiltonian for a particle in classical mechanics:

$$E = \frac{\mathbf{p}^2}{2m} + V(\mathbf{x}). \quad (1)$$

To convert this into a wave equation, we make the replacements $E \rightarrow i\partial_t$ and $\mathbf{p} \rightarrow -i\nabla$, so that a plane-wave solution

$$\phi(t, \mathbf{x}) \propto e^{-i(Et - \mathbf{p} \cdot \mathbf{x})} = e^{-ip \cdot x} \quad (2)$$

has the energy-momentum relation given in eq. (1). Applied to a general wavefunction ϕ , a linear superposition of plane waves, this gives

$$i\partial_t \phi(t, \mathbf{x}) = \left(-\frac{1}{2m} \nabla^2 + V(\mathbf{x}) \right) \phi(t, \mathbf{x}) = H \phi(t, \mathbf{x}), \quad (3)$$

where H is the so-called Hamiltonian. We recognise this as the Schrödinger Equation, the cornerstone of Quantum Mechanics. From this form, we can deduce that eq. (3) cannot be relativistically invariant because time appears only through a first-order derivative on the left-hand side while space appears as a second-order derivative on the right-hand side. Yet we know that if we make a Lorentz transformation in the x direction for example, this would mix the x and t components and therefore they cannot have different rôles.

The problem with the Schrödinger Equation arose because we started from a non-relativistic energy-momentum relation. Let us then start from the relativistic equation for energy. For a particle with 4-momentum $p^\mu = (E, \mathbf{p})$ and mass m ,

$$E^2 = m^2 + \mathbf{p}^2. \quad (4)$$

Again we convert this to an operator equation by setting $p_\mu = i\partial_\mu$ so that the corresponding wave equation for an arbitrary scalar wavefunction $\phi(\mathbf{x}, t)$ gives

$$(\partial_t^2 - \nabla^2 + m^2) \phi(t, \mathbf{x}) = (\partial_\mu \partial^\mu + m^2) \phi(x) = (\square + m^2) \phi(x) = 0, \quad (5)$$

where we have introduced the four-vector $x^\mu = (t, \mathbf{x})$. This is the “Klein-Gordon equation” which is the equation of motion for a free scalar field. We can explicitly check that this is indeed Lorentz invariant. Under a Lorentz transformation

$$x^\mu \rightarrow x'^\mu = \Lambda^\mu_\nu x^\nu \quad \Rightarrow \quad \partial_\mu \rightarrow \partial'_\mu = (\Lambda^{-1})^\rho_\mu \partial_\rho, \quad (6)$$

The field ϕ is a scalar, i.e. it has the transformation property

$$\phi(x) \rightarrow \phi'(x') = \phi'(\Lambda x) = \phi(x). \quad (7)$$

Therefore, in the primed system,

$$\begin{aligned} (\partial'_\mu \partial'^\mu + m^2) \phi'(x') &= [(\Lambda^{-1})^\rho_\mu \partial_\rho (\Lambda^{-1})^\sigma_\nu \partial_\sigma g^{\mu\nu} + m^2] \phi'(\Lambda x) \\ &= [\partial_\rho \partial_\sigma g^{\rho\sigma} + m^2] \phi(x) = 0, \end{aligned} \quad (8)$$

and the equation still holds.

1.2 The Dirac Equation

The Klein-Gordon equation admits negative-energy solutions, because the energy E appearing in the plane-wave in eq. (2) can have the two values $\pm \sqrt{\mathbf{p}^2 + m^2}$. Dirac sought to find an alternative relativistic equation which was linear in ∂_t like the Schrödinger equation (this was an attempt to solve the problem of negative-energy solutions to eq. (5) – in fact he didn’t solve this problem, but a different one). If the equation is linear in ∂_t , it must also be linear in ∇ if it is to be invariant under Lorentz transformations. We therefore start with the general form

$$i\partial_t \psi(t, \mathbf{x}) = (-i\boldsymbol{\alpha} \cdot \nabla + \beta m) \psi(t, \mathbf{x}). \quad (9)$$

Dirac also required that the solutions of his equation would be a solution of the Klein-Gordon equation as well, or equivalently, the energy relation eq. (4) was the correct energy-momentum relation for plane wave solutions $e^{-ip \cdot x}$ of the Dirac equation. To see what constraints this imposes, we must square eq. (9):

$$\begin{aligned} -\partial_t^2 \psi(t, \mathbf{x}) &= i\partial_t (-i\boldsymbol{\alpha} \cdot \nabla + \beta m) \psi(t, \mathbf{x}) \\ &= (-i\boldsymbol{\alpha} \cdot \nabla + \beta m)^2 \psi(t, \mathbf{x}) \\ &= [-\alpha^i \alpha^j \nabla^i \nabla^j - i(\beta \alpha^i + \alpha^i \beta) m \nabla^i + \beta^2 m^2] \psi(t, \mathbf{x}). \end{aligned} \quad (10)$$

However, the Klein-Gordon equation requires that the right-hand side is equal to $[-\nabla^2 + m^2]\psi(t, \mathbf{x})$ and therefore $\boldsymbol{\alpha}$ and β must satisfy

$$\alpha^i \alpha^j + \alpha^j \alpha^i = \{\alpha^i, \alpha^j\} = 2\delta^{ij}, \quad \beta \alpha^i + \alpha^i \beta = \{\alpha^i, \beta\} = 0, \quad \beta^2 = 1. \quad (11)$$

If α^i and β are just numbers, these equations cannot be solved. Dirac solved them by instead taking α^i and β to be $n \times n$ matrices, and $\psi(t, \mathbf{x})$ to be a column vector. Even now, the solution is not immediate. One can show that the conditions in eq. (11) require

$$\text{Tr } \alpha^i = 0 = \text{Tr } \beta, \quad (12)$$

and further that the eigenvalues of the above matrices are ± 1 . This in turn means that n must be even (do you understand why?). In 2-dimensions, there are still not enough linearly independent matrices to satisfy eq. (11). There do exist solutions in four dimensions. One such solution is

$$\alpha = \begin{pmatrix} 0 & \boldsymbol{\sigma} \\ \boldsymbol{\sigma} & 0 \end{pmatrix}, \quad \beta = \begin{pmatrix} \mathbb{1}_2 & 0 \\ 0 & -\mathbb{1}_2 \end{pmatrix}, \quad (13)$$

where $\boldsymbol{\sigma}$ are the usual Pauli matrices and $\mathbb{1}_2$ represents the 2×2 identity matrix. Now we have formed an equation which may be thought of as a square-root of the Klein-Gordon equation, but which is not obviously Lorentz invariant. To show that, we first define the new matrices

$$\gamma^0 = \beta, \quad \boldsymbol{\gamma} = \beta \boldsymbol{\alpha}. \quad (14)$$

Then we form $\gamma^\mu = (\gamma^0, \boldsymbol{\gamma})$ where the μ is a Lorentz index. Each component is a 4×4 matrix. In terms of the γ -matrices, one can write the conditions in eq. (11) in a Lorentz covariant form

$$\{\gamma^\mu, \gamma^\nu\} = \gamma^\mu \gamma^\nu + \gamma^\nu \gamma^\mu = 2g^{\mu\nu}. \quad (15)$$

This is an example of a Clifford algebra. Any matrices satisfying this condition in eq. (15) may be used to construct the Dirac equation. The representation in eqs. (13) and (14) is just one example, known as the Dirac representation. Note, for example, that any other matrices satisfying

$$\alpha'_i = \mathbf{U} \alpha_i \mathbf{U}^{-1}, \quad \text{and} \quad \beta' = \mathbf{U} \beta \mathbf{U}^{-1}, \quad (16)$$

where \mathbf{U} is a unitary matrix, will also be suitable.

Multiplying through by γ^0 , we may rewrite the eq. (9) in a covariant form as

$$(i\gamma^\mu \partial_\mu - m\mathbb{1}_4)\psi(t, \mathbf{x}) = (i\not{\partial} - m)\psi(x) = 0, \quad (17)$$

where $\not{\partial}$, a vector with a slash, is a short-hand notation for $\gamma^\mu a_\mu$. The equation above is known as the Dirac equation. In momentum space, i.e. after a Fourier transformation, $\partial_\mu \rightarrow -ip_\mu$, and the Dirac equation becomes

$$(\gamma^\mu p_\mu - m\mathbb{1}_4)\tilde{\psi}(p) = (\not{p} - m)\tilde{\psi}(p) = 0, \quad (18)$$

where $\tilde{\psi}(p)$ is the Fourier transform of a solution of the Dirac equation $\psi(x)$.

We mentioned in passing that $\psi(t, \mathbf{x})$ is a column vector rather than a scalar. This means that it contains more than one degree of freedom. Dirac exploited this property to interpret his equation as the wave equation for spin-1/2 particles, fermions, which can be either spin-up or spin-down. The column vector ψ is known as a Dirac spinor.

Comparing eq. (9) to the Schrödinger equation in eq. (3) gives the Hamiltonian for a free spin-1/2 particle:

$$H_{\text{Dirac}} = -i\boldsymbol{\alpha} \cdot \nabla + \beta m. \quad (19)$$

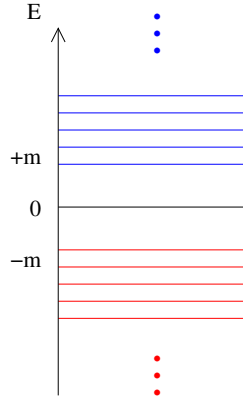


Figure 1: The energy levels in the Dirac sea picture. They must satisfy $|E| > m$, but negative-energy states are allowed. The vacuum is the state in which all negative-energy levels are filled.

The trace of the Hamiltonian gives the sum of the energy eigenvalues. The condition that the matrices α and β are traceless therefore means that the eigenvalues of H_{Dirac} must sum to zero. Therefore, like the Klein-Gordon equation, also the Dirac equation has negative-energy solutions.

Dirac himself proposed a solution for this problem which became known as the “Dirac sea”. He accepted the existence of negative-energy states, but took the vacuum as the state in which all these states are filled, see fig. 1. There is a conceptual problem with this in that the vacuum has infinite negative charge and energy. However, any observation relies only on energy differences, so this picture can give an acceptable theory.

As the negative-energy states are already full, the Pauli exclusion principle forbids any positive-energy electron to fall into one of the negative-energy states. If instead energy is supplied, an electron is excited from a negative-energy state to a positive-energy state and an “electron-hole” pair is created. The absence of the negative-energy electron, the hole, is interpreted as the presence of a state with positive energy and positive charge, i.e. a positron. Dirac predicted the existence of the positron in 1927 and this particle was discovered five years later.

However, Dirac’s argument only holds for spin-1/2 particles which obey the Pauli exclusion principle. A consistent solution for all particles is provided by Quantum Field Theory in a picture developed by Feynman and Stückelberg, in which positive-energy particles travel only *forward* in time, whereas negative-energy particles travel only *backwards* in time. In this way, a negative-energy particle with momentum p^μ , travelling backward in time, is re-interpreted as a positive energy anti-particle with momentum $-p^\mu$ travelling forward in time. Let us see how this picture naturally arises by considering two processes, the scattering $e^-\mu^- \rightarrow e^-\mu^-$, and Compton scattering $e^-\gamma \rightarrow e^-\gamma$. In non-relativistic quantum mechanics, the scattering $e^-\mu^- \rightarrow e^-\mu^-$ corresponds to the scattering of an electron from an external Coulomb potential. This is represented on the left-hand side of fig. 2. The horizontal axis represents the time at which a give elementary process occurs.

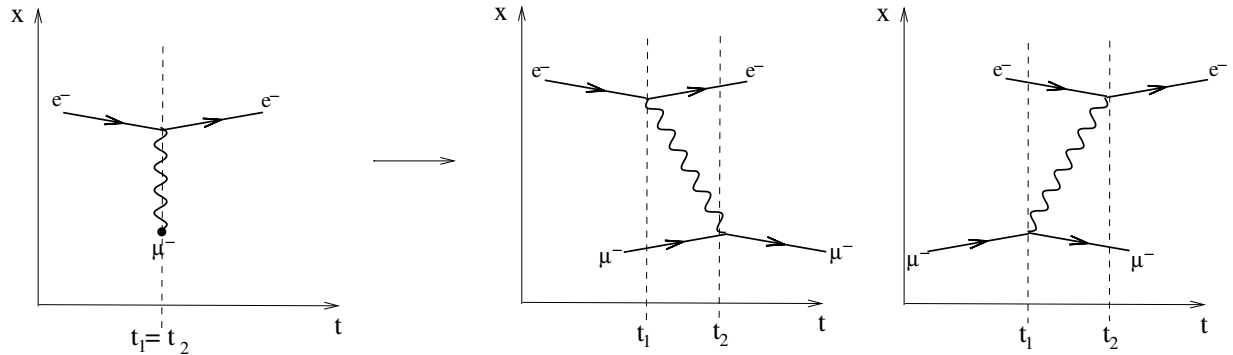


Figure 2: A pictorial representation of the scattering $e^-\mu^- \rightarrow e^-\mu^-$ in non-relativistic quantum mechanics (left) and in Quantum Field Theory (right).

In non-relativistic quantum mechanics, scattering happens instantaneously, so that the time t_1 at which a photon is emitted by the incoming electron coincides with the time t_2 in which it is absorbed by a muon, which stays at rest as a source of a static potential. In quantum field theory the scattering cannot occur instantaneously, because we need to take into account the fact that the photon mediating the scattering travels at the speed of light. The corresponding scattering amplitude is given by the sum of the contributions of the two diagrams on the right-hand side of fig. 2. It is clear that, in the limit in which c can be taken to be infinite, the two diagrams coincide and give the non-relativistic contribution. From the point of view of the electron, the first diagram can be interpreted as the emission of a positive-energy photon at $t = t_1$ that travels forward in time, and is later absorbed by a muon at $t = t_2$. The second diagram has an awkward interpretation from the point of view of the electron, because it corresponds to the emission of a negative-energy photon at $t = t_2$ that travels *backwards* in time. However, the graph makes perfectly sense if one considers that it is the muon that emits a photon a time t_1 , which is later reabsorbed by the electron at a time t_2 . A similar interpretation can be applied to the Compton scattering diagrams in Fig. 3, and clarifies the Feynman and Stückelberg interpretation of negative-energy states. In the left diagram, an electron emits a photon at time t_1 and later, at time t_2 absorbs another one. In the right-hand diagram it appears as if an electron emits a photon and then travels backwards in time to absorb another photon. Feynman and Stückelberg reasoned instead that the incoming photon split into an electron-positron pair and then at a later time, the positron annihilates the other electron, emitting a photon.

2 Spin

In the previous section, we introduced a Dirac spinor as a solution to the Dirac equation in the form of a column vector. In this section, we will discuss the explicit form of the solutions to the Dirac equation, and verify that they indeed correspond to the wave functions for particles with spin-1/2.

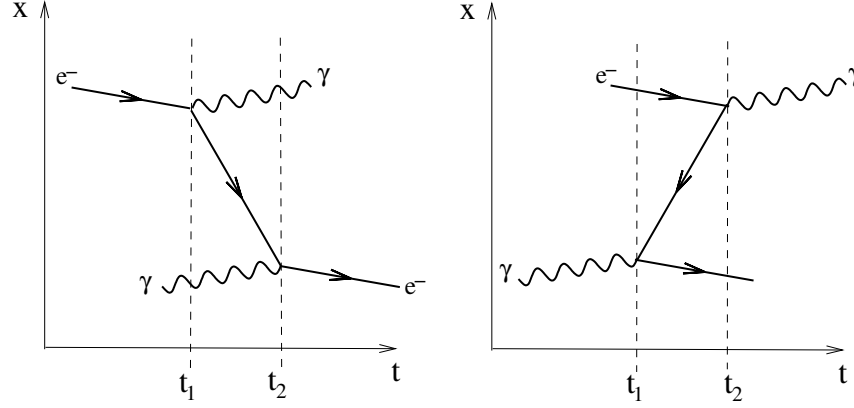


Figure 3: Diagrams illustrating the Feynman-Stückelberg interpretation of negative-energy particles, which correspond to those travelling backwards in time, as in the right-hand diagram. They interpreted a negative-energy particle travelling backwards as a positive-energy anti-particle travelling forwards in time, see text.

2.1 Plane-Wave Solutions of the Dirac Equation

We begin by seeking plane-wave solutions to the Dirac Equation. Given the 2×2 block nature of the γ -matrices, we will start with the form

$$\psi(x) = \begin{pmatrix} \chi(\mathbf{p}) \\ \phi(\mathbf{p}) \end{pmatrix} e^{-ip \cdot x}, \quad (20)$$

where χ and ϕ are two-component spinors. Substituting this into eq. (18) and using eqs. (13) and (14), we find

$$p^0 \begin{pmatrix} \chi \\ \phi \end{pmatrix} = \begin{pmatrix} m & \boldsymbol{\sigma} \cdot \mathbf{p} \\ \boldsymbol{\sigma} \cdot \mathbf{p} & -m \end{pmatrix} \begin{pmatrix} \chi \\ \phi \end{pmatrix}, \quad (21)$$

or equivalently

$$\begin{aligned} (\boldsymbol{\sigma} \cdot \mathbf{p}) \phi &= (p^0 - m) \chi \\ (\boldsymbol{\sigma} \cdot \mathbf{p}) \chi &= (p^0 + m) \phi. \end{aligned} \quad (22)$$

From the identity $(\boldsymbol{\sigma} \cdot \mathbf{p})^2 = \mathbf{p}^2$, these equations are only consistent for particles with $p^0 = \pm \sqrt{\mathbf{p}^2 + m^2}$ (consistent with having solutions of the Klein-Gordon equation).

For a massive fermion at rest ($\mathbf{p} = 0$), we have

$$p^0 \chi = m \chi \quad \text{and} \quad p^0 \phi = -m \phi. \quad (23)$$

Positive-energy solutions $\psi_+^{\mathbf{p}=0}$ must therefore have $\phi = 0$ and negative energy solutions $\psi_-^{\mathbf{p}=0}$ have $\chi = 0$, as follows:

$$\psi_+^{\mathbf{p}=0} = \begin{pmatrix} \chi \\ 0 \end{pmatrix} e^{-imt}, \quad \text{and} \quad \psi_-^{\mathbf{p}=0} = \begin{pmatrix} 0 \\ \phi \end{pmatrix} e^{imt}. \quad (24)$$

For particles which are not at rest ($\mathbf{p} \neq 0$), the solution is then dictated by eq. (22), with the requirement that it reduces to eq. (24) for $\mathbf{p} = 0$. For positive-energy solutions, we therefore write

$$\psi_+(x) = \mathcal{N} \left(\frac{\chi_r}{\frac{\boldsymbol{\sigma} \cdot \mathbf{p}}{E+m} \chi_r} \right) e^{-ip \cdot x} \equiv u_r(\mathbf{p}) e^{-ip \cdot x}, \quad p^0 = E \equiv \sqrt{\mathbf{p}^2 + m^2}, \quad (25)$$

where $r = 1, 2$ and \mathcal{N} is a normalisation conventionally chosen such that $u_r^\dagger(\mathbf{p}) u_s(\mathbf{p}) = 2E \delta^{rs}$, which gives $\mathcal{N} = \sqrt{E+m}$. The spinors χ_1 and χ_2 cover the two (spin) degrees of freedom:

$$\chi_1 = \begin{pmatrix} 1 \\ 0 \end{pmatrix}, \quad \text{and} \quad \chi_2 = \begin{pmatrix} 0 \\ 1 \end{pmatrix}. \quad (26)$$

Similarly, negative-energy solutions are conventionally written as

$$\psi_-(x) = \mathcal{N} \left(\frac{\frac{\boldsymbol{\sigma} \cdot \mathbf{p}}{E+m} \phi_r}{\phi_r} \right) e^{ip \cdot x} \equiv v_r(\mathbf{p}) e^{ip \cdot x}, \quad p^0 = E, \quad (27)$$

with the spinors ϕ_1 and ϕ_2 again covering the two (spin) degrees of freedom:

$$\phi_1 = \begin{pmatrix} 1 \\ 0 \end{pmatrix}, \quad \text{and} \quad \phi_2 = \begin{pmatrix} 0 \\ 1 \end{pmatrix}. \quad (28)$$

The spinors $u(\mathbf{p})$ and $v(\mathbf{p})$ therefore represent particle and anti-particle solutions with momentum \mathbf{p} and energy $E = \sqrt{\mathbf{p}^2 + m^2}$.

2.2 Spin

Each Dirac spinor has two linearly independent solutions which we stated earlier corresponded to the two possible spin states of a fermion. In this subsection we will define the corresponding spin operator. If we again consider a particle at rest we have

$$u_1 = \begin{pmatrix} 1 \\ 0 \\ 0 \\ 0 \end{pmatrix}, \quad \text{and} \quad u_2 = \begin{pmatrix} 0 \\ 1 \\ 0 \\ 0 \end{pmatrix}. \quad (29)$$

These have eigen-values $\pm \frac{1}{2}$ under the matrix

$$\frac{1}{2} \begin{pmatrix} \sigma_z & 0 \\ 0 & 0 \end{pmatrix}. \quad (30)$$

One can repeat the same thing for anti-particles and generalise to all the Pauli matrices to deduce the “spin operator”

$$\mathbf{S} = \frac{1}{2} \begin{pmatrix} \boldsymbol{\sigma} & 0 \\ 0 & \boldsymbol{\sigma} \end{pmatrix}. \quad (31)$$

You can check explicitly that $\mathbf{S}^2 = \frac{3}{4}\mathbf{1}_4$, as we would expect. Therefore, for particles at rest, $\mathbf{p} = 0$, the top two components of ψ_+ describe fermions with $S_z = +1/2$ (spin up) and $S_z = -1/2$ (spin down) respectively.

In case of a general \mathbf{p} one can consider the projection of the spin-operator along the direction of motion of a particle, i.e. $\mathbf{p}/|\mathbf{p}|$. This gives the helicity operator, $h(\mathbf{p})$

$$h(\mathbf{p}) = \begin{pmatrix} \frac{\boldsymbol{\sigma} \cdot \mathbf{p}}{|\mathbf{p}|} & \mathbf{0} \\ \mathbf{0} & \frac{\boldsymbol{\sigma} \cdot \mathbf{p}}{|\mathbf{p}|} \end{pmatrix}. \quad (32)$$

This operator satisfies $h(\mathbf{p})^2 = 1$, and hence its eigenvalues are ± 1 .

2.3 Working with Dirac Spinors

So far we have discussed Dirac spinors, ψ , describing spin-1/2 particles and how Dirac used his equation to predict anti-particles. To generate an equation for anti-particles, we first take the Hermitian conjugate of the Dirac equation and find

$$\psi^\dagger(-i\gamma^0 \overleftarrow{\partial}_0 + i\gamma^i \overleftarrow{\partial}_i - m) = 0, \quad (33)$$

where the arrows over the derivatives just mean they act on the left, and we have used the fact that $\gamma^{0\dagger} = \gamma^0$ and $\gamma^{i\dagger} = -\gamma^i$. All matrices have to be written on the right because they are multiplying matrices and ψ^\dagger is a row-vector. The above equation does not seem Lorentz covariant. This can be rectified by multiplying the equation by γ^0 on the right-hand side and using $[\gamma^0, \gamma^i] = 0$. Then we have

$$(\psi^\dagger \gamma^0)(-i \overleftarrow{\not{\partial}} - m) = 0, \quad \text{or} \quad \bar{\psi}(i \overleftarrow{\not{\partial}} + m) = 0. \quad (34)$$

The interpretation of the above equation is that the field $\bar{\psi} \equiv \psi^\dagger \gamma^0$ represents an anti-particle.

By construction, the spinors $u(\mathbf{p})$ and $v(\mathbf{p})$ satisfy their respective Dirac equations in momentum space:

$$(\not{p} - m)u(\mathbf{p}) = 0, \quad (\not{p} + m)v(\mathbf{p}) = 0. \quad (35)$$

They also satisfy a number of relations which will prove very useful in calculations of scattering amplitudes. Firstly, they are orthonormal:

$$\begin{aligned} \bar{u}_r(\mathbf{p})u_s(\mathbf{p}) &= 2m \delta^{rs} = -\bar{v}_r(\mathbf{p})v_s(\mathbf{p}), \\ \bar{u}_r(\mathbf{p})v_s(\mathbf{p}) &= 0 = -\bar{v}_r(\mathbf{p})u_s(\mathbf{p}). \end{aligned} \quad (36)$$

If instead one takes the outer product of spinor and anti-spinor, they also satisfy the following completeness relations:

$$\sum_{r=1}^2 u_r(\mathbf{p})\bar{u}_r(\mathbf{p}) = (\not{p} + m) \quad \text{and} \quad \sum_{r=1}^2 v_r(\mathbf{p})\bar{v}_r(\mathbf{p}) = (\not{p} - m). \quad (37)$$

These relations can be checked explicitly (see problem sheet).

2.4 Lorentz transformations on spinors

Let us consider the Lorentz transformation of eq. (6). The field ψ has the transformation property

$$\psi(x) \rightarrow \psi'(x') = \psi'(\Lambda x) = S(\Lambda)\psi(x) \quad \Rightarrow \quad \bar{\psi}(x) \rightarrow \bar{\psi}'(x') = \bar{\psi}(x)\gamma^0 S^\dagger(\Lambda)\gamma^0, \quad (38)$$

with $S(\Lambda)$ a suitable 4×4 matrix. Its explicit form is derived by imposing that the Dirac equation is Lorentz invariant:

$$(i\partial'_\mu \gamma^\mu - m) \psi'(x') = (i(\Lambda^{-1})^\nu_\mu \partial_\nu \gamma^\mu - m) S(\Lambda)\psi(x). \quad (39)$$

Imposing that $S(\Lambda)$ satisfies

$$\gamma^\mu S(\Lambda) = S(\Lambda)\Lambda^\mu_\rho \gamma^\rho, \quad (40)$$

we obtain

$$\begin{aligned} (i\partial'_\mu \gamma^\mu - m) \psi'(x') &= S(\Lambda) [i(\Lambda^{-1})^\nu_\mu \partial_\nu \gamma^\mu - m] \psi(x) \\ &= S(\Lambda)(i\partial_\nu \gamma^\nu - m)\psi(x) = 0, \end{aligned} \quad (41)$$

so that $\psi'(x')$ is a solution of the transformed Dirac equation, provided $\psi(x)$ is a solution of the original one.

Eq. (40) is enough to construct the matrices $S(\Lambda)$. By direct inspection one observes that

$$S^\dagger(\Lambda) = \gamma^0 S^{-1}(\Lambda) \gamma^0 \quad \Rightarrow \quad \bar{\psi}'(x') = S^{-1}(\Lambda) \bar{\psi}(x). \quad (42)$$

The fact that $S^{-1}(\Lambda) \neq S^\dagger(\Lambda)$ is not surprising, and is due to the fact that the Lorentz group is non-compact, and therefore it does not admit unitary finite-dimensional representations.

One can construct bi-linear products $\bar{\psi}\Gamma\psi$, with Γ a 4×4 matrix. We now show that Γ can be decomposed into a set of bi-linears, each having a definite transformation property under the Lorentz group. Since Γ is 4×4 matrix, we expect to find 16 such bi-linear products, constructed out of linearly independent matrices. Already we can find 5 such bi-linears:

$$\begin{aligned} \bar{\psi}\psi &\rightarrow \bar{\psi}S^{-1}(\Lambda)S(\Lambda)\psi = \bar{\psi}\psi && \text{(scalar)}, \\ \bar{\psi}\gamma^\mu\psi &\rightarrow \bar{\psi}S^{-1}(\Lambda)\gamma^\mu S(\Lambda)\psi = \Lambda^\mu_\nu (\bar{\psi}\gamma^\nu\psi) && \text{(vector)}, \end{aligned} \quad (43)$$

We can construct 6 more matrices by considering

$$\Sigma^{\mu\nu} = \frac{i}{4}[\gamma^\mu, \gamma^\nu]. \quad (44)$$

Note that $\gamma^\mu\gamma^\nu$ is not linearly independent from the previous matrices because $\{\gamma^\mu\gamma^\nu\} = 2g^{\mu\nu}\mathbb{1}$. This gives

$$\bar{\psi}\Sigma^{\mu\nu}\psi \rightarrow \bar{\psi}S^{-1}(\Lambda)\frac{i}{4}[\gamma^\mu, \gamma^\nu]S(\Lambda)\psi = \Lambda^\mu_\rho \Lambda^\nu_\sigma (\bar{\psi}\Sigma^{\rho\sigma}\psi) \quad \text{(tensor)}. \quad (45)$$

In addition to the four γ -matrices, we can construct their product which is conventionally known as γ^5 :

$$\gamma^5 \equiv i\gamma^0\gamma^1\gamma^2\gamma^3 = \frac{i}{4!} \epsilon_{\mu\nu\rho\sigma} \gamma^\mu \gamma^\nu \gamma^\rho \gamma^\sigma = \begin{pmatrix} -\mathbb{1}_2 & 0 \\ 0 & \mathbb{1}_2 \end{pmatrix}, \quad (46)$$

which satisfies

$$(\gamma^5)^2 = \mathbb{1}, \quad \{\gamma^5, \gamma^\mu\} = 0, \quad (\gamma^5)^\dagger = \gamma^5. \quad (47)$$

The factor of i is to make then matrix Hermitian. Using γ^5 , we can construct 5 more bi-linears

$$\begin{aligned} \bar{\psi} \gamma^5 \psi &\rightarrow \bar{\psi} S^{-1}(\Lambda) i \epsilon_{\mu\nu\rho\sigma} \gamma^\mu \gamma^\nu \gamma^\rho \gamma^\sigma S(\Lambda) \psi \\ &= i \epsilon_{\mu\nu\rho\sigma} \Lambda_\alpha^\mu \Lambda_\beta^\nu \Lambda_\gamma^\rho \Lambda_\delta^\sigma (\bar{\psi} \gamma^\alpha \gamma^\beta \gamma^\gamma \gamma^\delta \psi) \\ &= \det(\Lambda) \bar{\psi} i \epsilon_{\alpha\beta\gamma\delta} \gamma^\alpha \gamma^\beta \gamma^\gamma \gamma^\delta \psi = \det(\Lambda) \bar{\psi} \gamma^5 \psi \quad (\text{pseudo-scalar}), \\ \bar{\psi} \gamma^5 \gamma^\mu \psi &\rightarrow \det(\Lambda) \Lambda_\nu^\mu (\bar{\psi} \gamma^5 \gamma^\nu \psi) \quad (\text{pseudo-vector}). \end{aligned} \quad (48)$$

We have then found a set of 16 linearly independent matrices (check that they are linearly independent!)

$$\mathbb{1}, \gamma^5, \gamma^\mu, \gamma^\mu \gamma^5, \Sigma^{\mu\nu} = \frac{i}{4} [\gamma^\mu, \gamma^\nu], \quad (49)$$

so that any bi-linear $\bar{\psi} \Gamma \psi$ can be written as a sum of terms with definite transformation properties, i.e. transforming in a clear way as a scalar, pseudo-scalar, vector, pseudo-vector and tensor. (This is why the Feynman rule for a pseudo-scalar interacting with a particle-anti-particle pair has a γ^5 for example.)

The most common use of γ^5 is in the projectors $P_L = (1 - \gamma^5)/2$ and $P_R = (1 + \gamma^5)/2$. You can check explicitly that these behave like projectors (ie. $P^2 = P$ and $P_L P_R = 0$). When these act upon a Dirac spinor they project out either the component with “left-handed” *chirality* or with “right-handed” chirality. These projectors therefore appear when considering weak interactions, for example, as W bosons only couple to left-handed particles. One has to take care when defining the handedness of antiparticles because

$$\bar{\psi}_L = \psi_L^\dagger \gamma^0 = \psi^\dagger P_L \gamma^0 = \psi^\dagger \gamma^0 P_R = \bar{\psi} P_R. \quad (50)$$

A left-handed anti-particle appears with a right-handed projection operator next to it and vice-versa.

3 Quantum Electro-Dynamics

In this section, we will develop the theory of quantum electro-dynamics (QED) which describes the interaction between electrically charged fermions and a vector field (the photon A^μ).

3.1 The QED Lagrangian

In this course, we have so far considered spin-0 and spin-1/2 particles. We will postpone a detailed discussion of spin-1 particles until section 5.1. For the time being, we start from the Maxwell's equations in the vacuum in relativistic notation:

$$\partial_\mu F^{\mu\nu} = J^\nu, \quad \text{where} \quad F^{\mu\nu} = \partial^\mu A^\nu - \partial^\nu A^\mu, \quad (51)$$

and J^ν is a conserved current, i.e. satisfying $\partial_\nu J^\nu = 0$. Maxwell's equations can be derived from the Lagrangian

$$\mathcal{L} = \mathcal{L}_{\text{em}} + \mathcal{L}_{\text{int}}, \quad \mathcal{L}_{\text{em}} = -\frac{1}{4}F^{\mu\nu}F_{\mu\nu}, \quad \mathcal{L}_{\text{int}} = -J^\mu A_\mu, \quad (52)$$

by applying Euler-Lagrange equations

$$\partial_\mu \frac{\partial \mathcal{L}}{\partial(\partial_\mu A_\nu)} - \frac{\partial \mathcal{L}}{\partial A_\nu} = -\partial_\mu F^{\mu\nu} + J^\nu = 0. \quad (53)$$

The Dirac equation for ψ and its equivalent for $\bar{\psi}$ can be derived from the Lagrangian

$$\mathcal{L}_{\text{Dirac}} = \bar{\psi}(i\gamma^\mu \partial_\mu - m)\psi. \quad (54)$$

The starting point for the QED Lagrangian is then the sum of \mathcal{L}_{em} and $\mathcal{L}_{\text{Dirac}}$. However, in order to make the theory describe interactions, we must include a term which couples A^μ to ψ and $\bar{\psi}$. If we wish Maxwell's equation to be valid, this term has to be of the form $\mathcal{L}_{\text{int}} = -J^\mu A_\mu$, with J^μ a conserved vector current. We then observe that the vector current $J^\mu = \bar{\psi} \gamma^\mu \psi$ is conserved if ψ is a solution of Dirac equation. In fact

$$\partial_\mu J^\mu = \bar{\psi} \overleftarrow{\partial} \psi + \bar{\psi} (\partial \psi) = (-m\bar{\psi}) + \bar{\psi} (m\psi) = 0. \quad (55)$$

Therefore, a good candidate for the electromagnetic current describing an electron of charge $-e$ is

$$J^\mu = -e \bar{\psi} \gamma^\mu \psi, \quad (56)$$

where $-e$ multiplies the vector current so as to be sure that the resulting Coulomb potential arising from the solution of the static Maxwell's equations is the expected one. Using the above current, we obtain:

$$\mathcal{L} = \mathcal{L}_{\text{em}} + \mathcal{L}_{\text{Dirac}} + \mathcal{L}_{\text{int}} = -\frac{1}{4}F^{\mu\nu}F_{\mu\nu} + \bar{\psi}(i\partial - m)\psi + e\bar{\psi} \gamma^\mu \psi A_\mu. \quad (57)$$

Notice that \mathcal{L} is invariant with respect to the “gauge” transformations

$$\psi(x) \rightarrow \psi'(x) = e^{-ie\alpha(x)}\psi(x), \quad A_\mu(x) \rightarrow A'_\mu(x) = A_\mu(x) + \partial_\mu \alpha(x). \quad (58)$$

Notice that the addition of the interaction term \mathcal{L}_{int} is equivalent to the replacement

$$\partial_\mu \rightarrow D_\mu = \partial_\mu - ieA_\mu. \quad (59)$$

This prescription is known as “minimal coupling” and automatically ensures that the Lagrangian is gauge invariant. The use of gauge invariance to introduce interactions will be covered in detail in the Standard Model course next week. This gives

$$\mathcal{L} = -\frac{1}{4}F^{\mu\nu}F_{\mu\nu} + \bar{\psi}(i\gamma^\mu(\partial_\mu + ieA_\mu)\psi). \quad (60)$$

The fact that \mathcal{L} is invariant under the gauge transformations in eq. (62) means that A^μ contains unphysical degrees of freedom. This is clear in view of the fact that a massless vector field contains two physical polarisations, whereas A^μ has four degrees of freedom. In order to eliminate this degeneracy, a “gauge-fixing” condition is imposed. A possible choice of a gauge condition is the so-called Coulomb gauge, in which $\nabla \cdot \mathbf{A} = 0$. Although this condition eliminates the two additional degrees of freedom, it breaks Lorentz covariance. A common choice that preserves Lorentz covariance is the Lorentz gauge:

$$\partial_\mu A^\mu = 0. \quad (61)$$

This corresponds to choosing the gauge parameter α such that $\square\alpha = -\partial_\mu A^\mu$ above. In this gauge, the Maxwell equations become $\square A^\nu = 0$.

Notice that the Lorentz gauge condition reduces the number of degrees of freedom in A from four to three. Even now though A^μ is not unique. A transformation of the form

$$A_\mu \rightarrow A'_\mu = A_\mu + \partial_\mu \chi, \quad \square\chi = 0, \quad (62)$$

will also leave the Lagrangian unchanged. At classical level we can eliminate the extra polarisation “by hand”, but at quantum level this cannot be done without giving up covariant canonical commutation rules. The way out, which can only be summarised, is to add a gauge-fixing Lagrangian \mathcal{L}_{gf} , so that the full QED Lagrangian becomes

$$\mathcal{L}_{\text{QED}} = \mathcal{L}_{\text{em}} + \mathcal{L}_{\text{Dirac}} + \mathcal{L}_{\text{int}} + \mathcal{L}_{\text{gf}}, \quad \mathcal{L}_{\text{gf}} = -\frac{1}{2\xi}(\partial_\mu A^\mu)^2. \quad (63)$$

Using this Lagrangian as a starting point, and an extra condition on physical states, only the two physical polarisations propagate on-shell. Notice that setting $\xi = 0$ corresponds to enforcing the Lorentz gauge condition $\partial_\mu A^\mu = 0$, otherwise the equations of motions give $\square\partial_\mu A^\mu = 0$, i.e. $\partial_\mu A^\mu$ is a free field.

3.2 Feynman Rules

Feynman developed a method of organising the calculation of scattering amplitudes in terms of diagrams. Starting from a set of vertices (or interactions), each corresponding to a term in the Lagrangian and a set of links (or propagators), you build every possible diagram corresponding to your initial and final state. Each piece comes with a “rule” and the combination of these give the scattering amplitude (actually $i\mathcal{M}$).

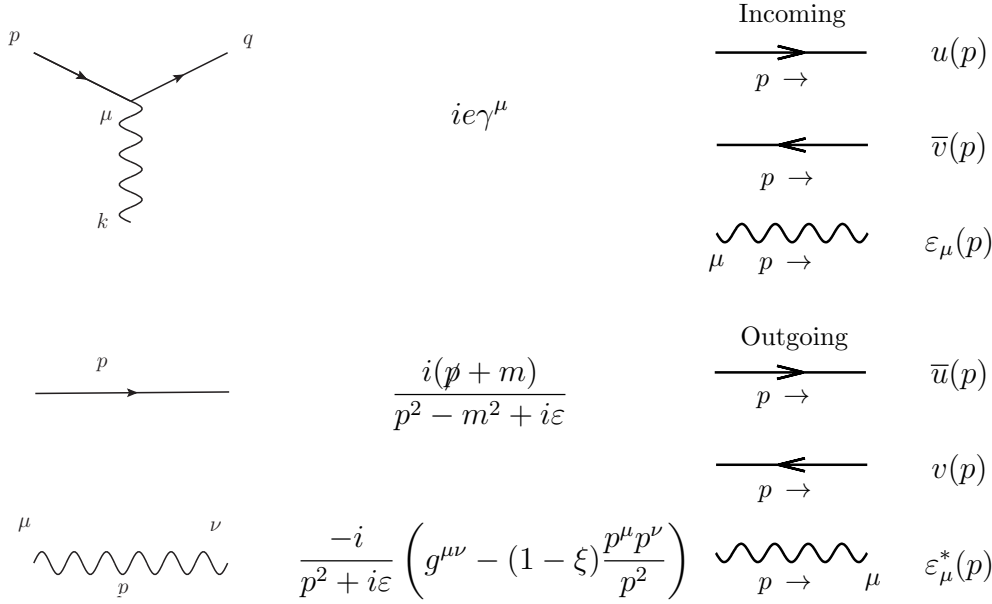


Figure 4: The Feynman rules for QED. Wavy lines represent a photon and straight lines represent any charged fermion. The arrow on the straight line tells you it is a particle or anti-particle depending on whether it is with or against momentum flow. The polarisation vectors $\varepsilon_\mu(p)$ will be discussed in section 5.2.

In the quantum field theory course at this school, you learn how to derive the “Feynman rules” for scalar ϕ^4 theory. The principles are the same here so in this course we will state the Feynman rules for QED and learn how to work with them. The Feynman rules are shown in figure 4. The left-hand column represents internal parts of the diagram while the right-hand column gives the rules for external fermions and photons.

A few comments are necessary here:

1. Individual pieces of a Feynman diagram are a mixture of matrices, vectors, co-vectors and scalars. They do not commute. The final amplitude is a number and therefore you must follow each fermion line from a spinor (either outgoing particle or incoming anti-particle) through the series of matrices to finish on an anti-spinor (either incoming particle or out-going anti-particle). This corresponds to working backwards along the fermion line. We will see this in the examples which follow. Similarly, all Lorentz indices corresponding to photons have to be contracted.
2. The photon propagator term has a free parameter ξ . This is due to the gauge freedom we discussed in the previous section. It does not represent a physical degree of freedom and therefore any calculation of a physical observable will be independent of ξ . We will most commonly work in Feynman gauge $\xi = 1$.
3. The propagators come with factors of $i\varepsilon$ in the denominator, otherwise they would have poles on the real axis and any integral over p would not be well-defined. The

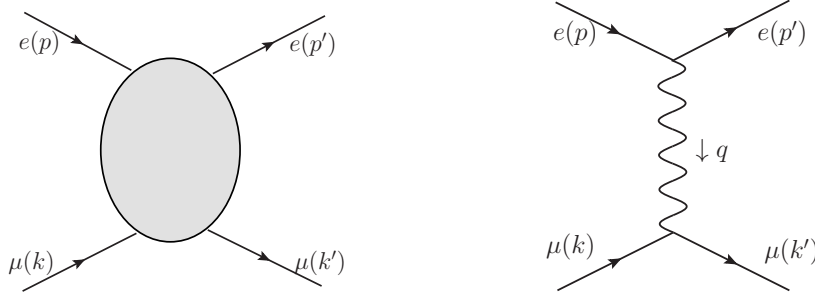


Figure 5: Building the leading-order Feynman diagram for Coulomb scattering. We start from the initial and final states on the left-hand side. The diagram on the right is the only way to connect these with up to two vertices.

factor of $i\varepsilon$ prescribes which direction to travel around the poles. This choice corresponds to the “Feynman prescription”, which ensures causality.

4. The interaction vertex contains only one flavour of fermion. We know that the emission of a photon does not change an electron to a quark for example.
5. There are additional factors of (-1) in the following scenarios:
 - (a) an anti-fermion line runs continuously from an initial to a final state;
 - (b) there is a closed fermion loop;
 - (c) between diagrams with identical fermions in the final state.

These arise from the anti-commutation properties of fermionic operators which is beyond the scope of this course. This sign can be important to get the relative phase between diagrams correct, as happens for instance in Bhabha scattering.

Examples: Coulomb Scattering

As a first example, we consider Coulomb scattering:

$$e(p) \mu(k) \rightarrow e(p') \mu(k'). \quad (64)$$

We start by drawing the external particles, see left-hand side of fig. 5. We now want to find all possible ways to connect these. There is no direct interaction between an electron and a muon but both interact with a photon, so a possible connected diagram is the one shown on the right-hand side. In fact, this is the only possible diagram with no more than two vertices. The number of vertices is directly related to the powers of the coupling e and therefore the diagram shown on the right is the leading-order (or tree-level) process.

If we consider $e(p) e(k) \rightarrow e(p') e(k')$ or $e^+(p) e^-(k) \rightarrow e^+(p') e^-(k')$ instead, there are two diagrams with two vertices, i.e. at $\mathcal{O}(e^2)$ (try this!). Both have to be added before squaring the amplitude to have the tree-level contribution to the cross section.

If we allow ourselves more than two vertices, there are many more diagrams we can draw. Since the number of external particles doesn't increase, these must contain closed loops and, therefore, they represent higher-loop processes. In this course, we will limit ourselves to tree-level processes. Loop-diagrams will be covered in the phenomenology course.

Now we will construct the tree-level amplitude for Coulomb scattering from the rules in Fig. 4. Keeping in mind the earlier warning about the ordering of matrices and spinors, we take each fermion line in turn. The electron line gives

$$\bar{u}(p') (ie\gamma^\mu) u(p). \quad (65)$$

In spin-space, this is co-vector–matrix–vector, which is a number. In Lorentz space it has one free index μ and is therefore a vector. Similarly, for the muon line we get

$$\bar{u}(k') (ie\gamma^\nu) u(k). \quad (66)$$

Lastly, for the propagator with momentum $q = p' - p = k - k'$ in Feynman gauge, we get

$$\frac{-ig_{\mu\nu}}{q^2 + i\varepsilon}, \quad (67)$$

so that the full amplitude is

$$i\mathcal{M} = ie^2 [\bar{u}(p') \gamma^\mu u(p)] \frac{g_{\mu\nu}}{q^2} [\bar{u}(k') \gamma^\nu u(k)]. \quad (68)$$

We will drop the $i\varepsilon$ from now on, as we will not need it in this example.

Just as in quantum mechanics, in order to compute the probability of this process happening, we must calculate $|\mathcal{M}|^2$. We will now add specific indices to label the spins, r, r', s, s' . In order to describe an unpolarised physical scattering process, we will average over initial-state spins and sum over final-state spins. This convention is represented by a bar as follows:

$$\begin{aligned} \overline{|\mathcal{M}|^2} &= \frac{1}{2} \sum_{r=1}^2 \frac{1}{2} \sum_{s=1}^2 \sum_{r'=1}^2 \sum_{s'=1}^2 |\mathcal{M}|^2 \\ &= \frac{1}{4} \frac{e^4}{(q^2)^2} \sum_{r,r'} [\bar{u}_{r'}(p') \gamma^\mu u_r(p)] [\bar{u}_{r'}(p') \gamma^\rho u_r(p)]^* \\ &\quad \times \sum_{s,s'} [\bar{u}_{s'}(k') \gamma_\mu u_s(k)] [\bar{u}_{s'}(k') \gamma_\rho u_s(k)]^*, \end{aligned} \quad (69)$$

where we have explicitly evaluated the metric contractions for brevity.

To evaluate the products in eq. (69) we will use the results from section 2.1. We will take the pieces corresponding to the electron line first. Since $[\bar{u}_{r'}(p') \gamma^\rho u_r(p)]^*$ is a number, its complex conjugate is its hermitian conjugate. Therefore

$$[\bar{u}_{r'}(p') \gamma^\rho u_r(p)]^* = u_r^\dagger(p) \gamma^{\rho\dagger} \gamma^{0\dagger} u_{r'}(p') = u_r^\dagger(p) \gamma^0 \gamma^\rho u_{r'}(p') = \bar{u}_r(p) \gamma^\rho u_{r'}(p'), \quad (70)$$

where we have used $\gamma^{\nu\dagger} = \gamma^0 \gamma^\nu \gamma^0$, which you showed on the problem sheet. We now use eq. (37) to find

$$\begin{aligned} \sum_{r,r'} [\bar{u}_{r'}(p') \gamma^\mu u_r(p)] [\bar{u}_{r'}(p') \gamma^\rho u_r(p)]^* &= \sum_{r,r'} \bar{u}_{r'}(p') \gamma^\mu u_r(p) \bar{u}_r(p) \gamma^\rho u_{r'}(p') \\ &= \sum_{r'} \bar{u}_{r'}(p') \gamma^\mu (\not{p} + m) \gamma^\rho u_{r'}(p'). \end{aligned} \quad (71)$$

We will use m for the electron mass and M for the muon mass. It is now useful to add a component index in spinor-space like you would do in normal linear algebra. Schematically we have

$$\sum_{r'} \bar{u}_{r'i} \Gamma_{ij} u_{r'j}, \quad (72)$$

where Γ represents the chain of γ -matrices in eq. (71). Now that we are explicitly labelling the components, we can swap the order of the terms to get

$$\sum_{r'} \Gamma_{ij} u_{r'j} \bar{u}_{r'i} = \Gamma_{ij} (\not{p}' + m)_{ji} = \text{Tr}(\gamma^\mu (\not{p}' + m) \gamma^\rho (\not{p}' + m)). \quad (73)$$

We could have anticipated that we would get a trace as we need to get a single number from a series of matrices. Working from the anti-commutation relations, one can readily show the following identities (see problem sheet):

$$\begin{aligned} \text{Tr}(\text{odd number of } \gamma \text{ matrices}) &= 0, & \text{Tr}(\gamma^\mu \gamma^\nu) &= 4g^{\mu\nu}, \\ \text{Tr}(\gamma^\mu \gamma^\nu \gamma^\rho \gamma^\sigma) &= 4(g^{\mu\nu} g^{\rho\sigma} - g^{\mu\rho} g^{\nu\sigma} + g^{\mu\sigma} g^{\nu\rho}). \end{aligned} \quad (74)$$

Therefore, eq. (73) equals

$$4p_\nu p'_\sigma (g^{\mu\nu} g^{\rho\sigma} - g^{\mu\rho} g^{\nu\sigma} + g^{\mu\sigma} g^{\nu\rho}) + 4m^2 g^{\mu\rho}. \quad (75)$$

The same series of steps gives

$$\sum_{s,s'} [\bar{u}_{s'}(k') \gamma_\mu u_s(k)] [\bar{u}_{s'}(k') \gamma_\rho u_s(k)]^* = 4k^\alpha k'^\beta (g_{\mu\alpha} g_{\rho\beta} - g_{\mu\rho} g_{\alpha\beta} + g_{\mu\beta} g_{\alpha\rho}) + 4M^2 g_{\mu\rho}. \quad (76)$$

Substituting these results into eq. (69) gives

$$|\overline{\mathcal{M}}|^2 = \frac{8e^4}{(q^2)^2} ((pk)(p'k') + (pk')(p'k) + 2m^2 M^2 - M^2(pp') - m^2(kk')). \quad (77)$$

We will now rewrite the invariants which appear in the above equation in terms of the centre-of-mass energy squared, s and the exchanged momentum-squared, $q^2 = t$. We have

$$\begin{aligned} 2(pk) &= (p+k)^2 - m^2 - M^2 = s - m^2 - M^2, & 2(p'k') &= s - m^2 - M^2 \\ 2(pp') &= -(p-p')^2 + 2m^2 = -q^2 + 2m^2, & 2(kk') &= -q^2 + 2M^2 \\ 2(pk') &= 2p \cdot (p+k-p') = s + q^2 - m^2 - M^2, & 2(p'k) &= s + q^2 - m^2 - M^2, \end{aligned} \quad (78)$$

which finally gives

$$|\overline{\mathcal{M}}|^2 = \frac{2e^4}{(q^2)^2} \left((s - m^2 - M^2)^2 + (s + q^2 - m^2 - M^2)^2 + 2q^2(m^2 + M^2) \right). \quad (79)$$

This expression can be further simplified by introducing the further invariant $u = (p - k')^2 = (p' - k)^2$:

$$|\overline{\mathcal{M}}|^2 = \frac{2e^4}{t^2} \left((s - m^2 - M^2)^2 + (u - m^2 - M^2)^2 + 2t(m^2 + M^2) \right). \quad (80)$$

The above equation gives the probability that the corresponding process occurs at a given point in phase space. In the next section, we will derive how to calculate a total cross section (or a total decay width) from amplitudes squared.

4 Calculation of Cross Sections

Ultimately it is not the amplitude we really want to calculate, but its integral over phase space to give the total cross section if it is a scattering process or the total decay width if it is a decay.

4.1 Phase Space Integrals

We must integrate over all the allowed phase space, which means all possible momentum configurations of the final-state particles. This result, divided by the flux of incoming particles, will give the total cross section.

In principle, we must integrate over over a 4-dimensional phase space for each particle f in the final state, but we must impose that each satisfies its on-shell condition $p_f^2 = m_f^2$. We therefore must have

$$\begin{aligned} \prod_f \int \frac{d^4 p_f}{(2\pi)^4} (2\pi) \delta(p_f^2 - m^2) \Theta(p_f^0) &= \prod_f \int \frac{d^4 p_f}{(2\pi)^4} (2\pi) \delta((p_f^0)^2 - \mathbf{p}_f^2 - m^2) \Theta(p_f^0) \\ &= \prod_f \int \frac{d^3 \mathbf{p}_f}{(2\pi)^3 (2E_f)}, \end{aligned} \quad (81)$$

where $E_f = \sqrt{\mathbf{p}_f^2 + m^2}$. Although the final expression explicitly separates the dependence on E and \mathbf{p} , it is still Lorentz invariant as the original expression is clearly Lorentz invariant. Eq. (81) is frequently referred to as the Lorentz Invariant Phase Space measure (LIPS). The factors of 2π correspond to the conventions used for momentum space integrations in QFT.

We now need to normalise this expression to the flux of incoming particles. This is done by multiplying by the flux factor, \mathcal{F} . For the scattering of two incoming particles, this is

usually written as

$$\mathcal{F} = \frac{1}{4E_a E_b |\mathbf{v}_a - \mathbf{v}_b|}, \quad (82)$$

where E_i and \mathbf{v}_i are the energy and velocity of each incoming particle.¹ A neater, equivalent form which explicitly demonstrates the Lorentz invariance of this quantity is

$$\mathcal{F} = \frac{1}{4\sqrt{(p_a p_b)^2 - m_a^2 m_b^2}}. \quad (83)$$

In the massless limit $s \gg m_1, m_2$, this simplifies to $\mathcal{F} \simeq 1/(2s)$. Finally, we must impose total conservation of momentum to find

$$\sigma = \mathcal{F} \left(\prod_f \int \frac{d^3 \mathbf{p}_f}{(2\pi)^3 (2E_f)} \right) |\overline{\mathcal{M}}|^2 (2\pi)^4 \delta^4 \left(\sum_f p_f - p_1 - p_2 \right). \quad (84)$$

If you wish to calculate a total decay width instead, the expression is very similar. The only difference is that the flux factor becomes

$$\mathcal{F} = \frac{1}{2M}, \quad (85)$$

where M is the mass of the decaying particle. The total decay width, Γ , is therefore given by

$$\Gamma = \frac{1}{2M} \left(\prod_f \int \frac{d^3 \mathbf{p}_f}{(2\pi)^3 (2E_f)} \right) |\overline{\mathcal{M}}|^2 (2\pi)^4 \delta^4 \left(\sum_f p_f - p_M \right). \quad (86)$$

4.2 Return to Coulomb Scattering

We may now calculate the relativistic cross section for Coulomb scattering, using our result from section 3.2. Eq. (84) applied to this example gives

$$\sigma = \mathcal{F} \int \frac{d^3 \mathbf{p}'}{(2\pi)^3 (2E'_p)} \frac{d^3 \mathbf{k}'}{(2\pi)^3 (2E'_k)} |\overline{\mathcal{M}}|^2 (2\pi)^4 \delta^4 (p' + k' - p - k). \quad (87)$$

As this expression is Lorentz invariant, we are free to choose which frame to evaluate it in. This is an extremely powerful tool to evaluate these integrals, as a careful choice can lead to considerable simplifications. We will choose the centre-of-mass frame here so that $\mathbf{p} = -\mathbf{k}$. We can easily do the \mathbf{k}' integration using three of the δ -functions to give

$$\sigma = \mathcal{F} \int \frac{d^3 \mathbf{p}'}{(2\pi)^3 4E'_p E'_k} |\overline{\mathcal{M}}|^2 (2\pi) \delta(E'_p + E'_k - E_p - E_k). \quad (88)$$

¹You can find a motivation for the flux factor in Aitchison and Hey and a more complete derivation in Peskin and Schröder chapter 4.5.

We will proceed by transforming to spherical polar coordinates, $d^3\mathbf{p}' = |\mathbf{p}'|^2 d|\mathbf{p}'| d\Omega$, where we have written the solid angle, $\sin\theta d\theta d\phi$, as $d\Omega$:

$$\sigma = \frac{\mathcal{F}}{(2\pi)^2} \int d\Omega d|\mathbf{p}'| \frac{|\mathbf{p}'|^2}{4E'_p E'_k} |\overline{\mathcal{M}}|^2 \delta(E'_p + E'_k - E_p - E_k). \quad (89)$$

We now make the change of variable $|\mathbf{p}'| \rightarrow E = E'_p + E'_k$, which has Jacobian factor

$$\frac{\partial E}{\partial |\mathbf{p}'|} = \frac{E|\mathbf{p}'|}{E'_p E'_k} \quad (90)$$

to get

$$\sigma = \frac{\mathcal{F}}{(2\pi)^2} \int d\Omega dE \frac{|\mathbf{p}'|}{4E} |\overline{\mathcal{M}}|^2 \delta(E - \sqrt{s}) = \frac{\mathcal{F}}{(2\pi)^2} \int d\Omega \frac{|\mathbf{p}'|}{4\sqrt{s}} |\overline{\mathcal{M}}|^2, \quad (91)$$

where it is understood that $\mathbf{k}' = -\mathbf{p}'$ with $|\mathbf{p}'|$ determined from $E = \sqrt{s}$. The only undefined variables are the angles which remain to be integrated over. We could now substitute the expression for $|\overline{\mathcal{M}}|^2$ explicitly in terms of these angles but it is actually informative to instead study the differential cross section

$$\frac{d\sigma}{d\Omega} = \frac{\mathcal{F}}{16\pi^2} \frac{|\mathbf{p}'|}{\sqrt{s}} |\overline{\mathcal{M}}|^2. \quad (92)$$

We will now consider the high energy limit where $s \gg m_e^2, m_\mu^2$. In this limit, the three Mandelstam invariants are given by

$$s = 4\mathbf{p}^2, \quad t = -4\mathbf{p}^2 \sin^2(\theta/2), \quad u = -4\mathbf{p}^2 \cos^2(\theta/2), \quad (93)$$

which gives

$$|\overline{\mathcal{M}}|^2 \simeq 2e^4 \frac{s^2 + u^2}{t^2} = \frac{2e^4}{\sin^4(\theta/2)} \left(1 + \cos^4 \frac{\theta}{2}\right). \quad (94)$$

Note that this amplitude squared has no dependence on the azimuthal angle ϕ . Using the conventional notation $\alpha = e^2/(4\pi)$, we obtain

$$\frac{d\sigma}{d\Omega} \simeq \frac{\alpha^2}{2s} \frac{1 + \cos^4(\theta/2)}{\sin^4(\theta/2)}. \quad (95)$$

4.3 The Coulomb Potential

The same calculation may be used to calculate the cross section for the scattering of a relativistic particle from an external Coulomb potential by working in the rest frame of the muon and taking $m_\mu \rightarrow \infty$. This is illustrated in fig. 6.

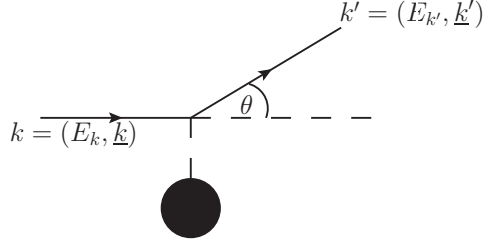


Figure 6: Scattering by an external Coulomb potential.

Repeating the same calculation in this limit yields

$$\begin{aligned} \frac{d\sigma}{d\Omega} &= \frac{\alpha^2}{4\mathbf{k}^2 \mathbf{v}^2 \sin^4(\theta/2)} (1 - \mathbf{v}^2 \sin^2(\theta/2)) \\ &= \left(\frac{d\sigma}{d\Omega} \right)_R (1 - \mathbf{v}^2 \sin^2(\theta/2)) , \end{aligned} \quad (96)$$

where $\mathbf{v} = |\mathbf{k}|/E_k$ and

$$\left(\frac{d\sigma}{d\Omega} \right)_R = \frac{\alpha^2}{4\mathbf{k}^2 \mathbf{v}^2 \sin^4(\theta/2)} \quad (97)$$

is the Rutherford cross section which was calculated in preschool problem 9. The extra \mathbf{v}^2 -term in eq. (96) then gives the relativistic correction to this. This result is entirely due to the electron being a spin-1/2 particle. If it were spin-0 instead, $|\overline{\mathcal{M}}|^2$ would look much simpler as there are no fermion traces to be performed and in that case we would find that there is no relativistic correction.

4.4 e^+e^- Annihilation

The calculation we have just performed is almost identical to $e^+(p') e^-(p) \rightarrow \mu^+(k) \mu^-(k')$. Although this now involves anti-particles, there is still one single diagram at leading-order and the trace algebra is very similar. Indeed we can re-interpret the incoming e^+ as an outgoing e^- with momentum $-p'$, and the outgoing μ^+ as an incoming μ^- with momentum $-k$. Then we do find explicitly that

$$\overline{|\mathcal{M}_{e^+(p')e^-(p) \rightarrow \mu^+(k')\mu^-(k)}|^2} = \overline{|\mathcal{M}_{e^-(p)\mu^-(-k) \rightarrow e^-(-p')\mu^-(k')}|^2} . \quad (98)$$

This is an example of “crossing symmetry”. Note in general that there is an additional minus sign for each fermion which swaps from the initial to final state or vice versa. This is because, for example,

$$\sum_r u_r(p') \bar{u}_r(p') = \not{p}' + m \longrightarrow \sum_r v_r(-p') \bar{v}_r(-p') = -\not{p}' - m = -(\not{p}' + m) . \quad (99)$$

In this case there are two minus signs whose combined effect gives just one.

If in e^+e^- -annihilation we take the approximation $m_e = 0$, we find

$$|\overline{\mathcal{M}}|^2 = \frac{8e^4}{s^2} [(pk)^2 + (pk')^2 + m_\mu^2(kk)'] , \quad (100)$$

Once again, choosing to work in the centre-of-mass frame, we find

$$\left(\frac{d\sigma}{d\Omega}\right)_{e^+e^- \rightarrow \mu^+\mu^-} = \frac{\alpha^2}{4s} \sqrt{1 - \frac{4m_\mu^2}{s}} \left(1 + \frac{4m_\mu^2}{s} + \left(1 - \frac{4m_\mu^2}{s}\right) \cos^2 \theta\right) . \quad (101)$$

If we again take the high-energy limit where $s \gg m_\mu^2$, this reduces to

$$\left(\frac{d\sigma}{d\Omega}\right)_{e^+e^- \rightarrow \mu^+\mu^-} = \frac{\alpha^2}{4s} (1 + \cos^2 \theta) . \quad (102)$$

We can now convert the above result to a total cross section by performing the integral over the solid angle. This gives

$$\sigma(e^+e^- \rightarrow \mu^+\mu^-) \simeq \frac{4\pi\alpha^2}{3s} . \quad (103)$$

Now, when an electron and positron annihilate, other fermions may be produced. If these are quarks, they are then observed in the detector as hadrons. The same calculation gives

$$\sigma(e^+e^- \rightarrow \text{hadrons}) = \frac{4\pi\alpha^2}{3s} N_c \sum_{i=1}^{n_f} Q_i^2 , \quad (104)$$

plus higher-order corrections, where there are N_c colours in each of the n_f massless flavours of quarks with charge Q_i . Therefore the ratio

$$R = \frac{\sigma(e^+e^- \rightarrow \mu^+\mu^-)}{\sigma(e^+e^- \rightarrow \text{hadrons})} \quad (105)$$

has been used to measure the number of colours to be $N_c = 3$.

5 Photon Scattering

In this section we will calculate the scattering amplitude for $e\gamma \rightarrow e\gamma$. In order to do that we need first to consider how to treat incoming and outgoing photons.

5.1 Photon Polarisation

We seek to find a plane-wave solution corresponding to a free photon (like our treatment for Dirac particles in section 2.1). It will have the form

$$A^\mu(x) = \varepsilon^\mu(k) e^{-ik \cdot x} , \quad (106)$$

where $\varepsilon^\mu(k)$ is the polarisation vector of the photon. In the Lorentz gauge of eq. (61), the photon equation of motion in eq. (51) is

$$\square A^\mu = 0, \quad (107)$$

and is automatically satisfied by a solution of the form in eq. (106), provided $k^2 = 0$. The Lorentz gauge condition gives an additional constraint on the polarisation vector

$$k \cdot \varepsilon(k) = 0. \quad (108)$$

However, there is still freedom here because, given a polarisation vector ε which solves this equation, any other vector of the form $\varepsilon' = \varepsilon + \lambda k$ will also be a solution, which corresponds to the propagation of an extra unphysical longitudinal photon, with a polarisation proportional to k_μ . This freedom is usually used to set $\varepsilon^0 = 0$ such that $\mathbf{k} \cdot \boldsymbol{\varepsilon} = 0$ so that the two physical polarisations ε^α , with $\alpha = 1, 2$, are in the transverse direction, and are chosen to be orthonormal. A useful relation we will use in the following is

$$\sum_{\alpha=1}^2 \varepsilon^{\alpha i}(k) \varepsilon^{\alpha j}(k) = \delta^{ij} - \hat{k}^i \hat{k}^j, \quad \text{where} \quad \hat{k}^i = \frac{k^i}{|\mathbf{k}|} = \frac{k^i}{k^0}. \quad (109)$$

The Feynman rule for an incoming photon is simply $\varepsilon^\mu(k)$ while for an outgoing photon it is $\varepsilon^{*\mu}(k)$, as shown in Fig. 4.

As for fermion spins, for unpolarised processes you compute the total cross section by averaging over incoming polarisations and summing over outgoing polarisations. Let us consider the case of a general process with one external incoming photon. The matrix element would have the form

$$i\mathcal{M} = \mathcal{A}^\mu \varepsilon_\mu(k). \quad (110)$$

The left-hand side is a physical quantity, hence it should give the same result for any choice of the gauge. Had we chosen $\varepsilon + \lambda k$ instead, this implies that $\mathcal{A}^\mu k_\mu$ has to vanish. This is a ‘‘Ward Identity’’ for QED, and is therefore a test of gauge-invariance.

Squaring the scattering-amplitude over the physical polarisations gives

$$\begin{aligned} \sum_{\alpha=1}^2 |\mathcal{A}^\mu \varepsilon_\mu^\alpha(k)|^2 &= \sum_{\alpha=1}^2 \mathcal{A}^\mu \mathcal{A}^{*\nu} \varepsilon_\mu^\alpha(k) \varepsilon_\nu^{*\alpha}(k) \\ &= A^i A^j (\delta^{ij} - \hat{k}^i \hat{k}^j), \end{aligned} \quad (111)$$

using eq. (109). The equation $\mathcal{A}^\mu k_\mu = 0$ implies $A^i \hat{k}^i = A^0$ and hence

$$\sum_{\alpha=1}^2 |\mathcal{A}^\mu \varepsilon_\mu^\alpha(k)|^2 = A^i A^i - A^0 A^0 = -A^\mu A^\nu g_{\mu\nu}. \quad (112)$$

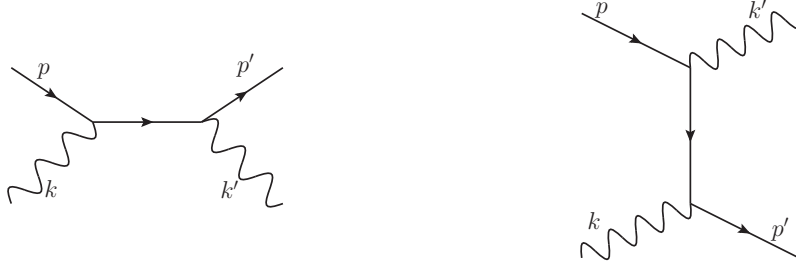


Figure 7: The two tree-level diagrams for $e(p) \gamma(k) \rightarrow e(p') \gamma(k')$.

This could be done for each photon in turn if there were more in the process, and we find the general result that

$$\sum_{\alpha=1}^2 \varepsilon_{\mu}^{\alpha} \varepsilon_{\nu}^{*\alpha} \rightarrow -g_{\mu\nu} . \quad (113)$$

We have used the \rightarrow notation of Peskin and Schröder here as the result is not an exact equality in the absence of the rest of the matrix element, but the result is nonetheless true in any practical calculation.

5.2 Compton Scattering

There are two diagrams at leading order for this process, shown in Fig. 7. Following the Feynman rules in Fig. 4 and the rules for external photons in the previous subsection, we find that the sum of the two diagrams gives

$$i\mathcal{M} = -ie^2 \varepsilon^{*\mu}(k') \varepsilon^{\nu}(k) \bar{u}(p') \left(\gamma_{\mu} \frac{\not{p} + \not{k} + m}{(p+k)^2 - m^2} \gamma_{\nu} + \gamma_{\nu} \frac{\not{p} - \not{k}' + m}{(p-k')^2 - m^2} \gamma_{\mu} \right) u(p) . \quad (114)$$

You can check explicitly that the above amplitude does indeed satisfy the appropriate QED Ward Identities, i.e. replacing $\varepsilon^{\nu}(k)$ with k^{ν} gives $\mathcal{M} = 0$, and similarly when replacing $\varepsilon^{*\mu}(k')$ with k'^{μ} (see tutorial sheet).

We now square the amplitude to get

$$\begin{aligned} |\overline{\mathcal{M}}|^2 &= \frac{1}{2} \sum_{\gamma \text{ pol}} \frac{1}{2} \sum_{e \text{ spin}} |\mathcal{M}|^2 \\ &= 2e^4 \left(\frac{(pk)}{(pk')} + \frac{(pk')}{(pk)} + 2m^2 \left(\frac{1}{(pk)} - \frac{1}{(pk')} \right) + m^4 \left(\frac{1}{(pk)} - \frac{1}{(pk')} \right)^2 \right) . \end{aligned} \quad (115)$$

The calculation of the spin traces in this case requires the identities

$$\gamma_{\mu} \gamma^{\mu} = 4 , \quad \gamma_{\mu} \gamma^{\rho} \gamma^{\mu} = -2\gamma^{\rho} , \quad (116)$$

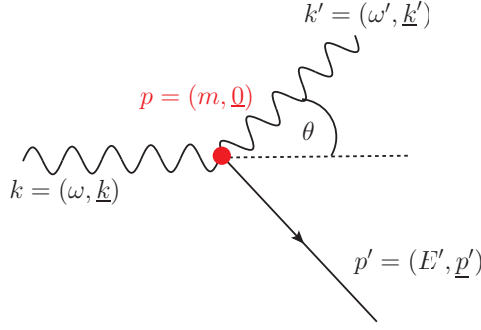


Figure 8: The Compton scattering process in the rest frame of the incoming electron.

from the problem sheet. We will again choose a suitable reference frame to simplify the calculation. In this case, it is convenient to work in the rest frame of the incoming electron as shown in fig. 8. We can use energy conservation to compute ω' :

$$\begin{aligned} m^2 = p'^2 &= (p + k - k')^2 = m^2 + 2m(\omega - \omega') - 2\omega\omega'(1 - \cos\theta) \\ \Rightarrow \quad \omega' &= \frac{\omega}{1 + (\omega/m)(1 - \cos\theta)}. \end{aligned} \quad (117)$$

In this frame, we therefore have

$$|\overline{\mathcal{M}}|^2 = 2e^4 \left(\frac{\omega}{\omega'} + \frac{\omega'}{\omega} - \sin^2\theta \right). \quad (118)$$

The explicit dependence on the electron mass cancels with the factors of m in ω' . It is however present in the flux factor $\mathcal{F} = 1/(4m\omega)$. We now compute the integral over the phase space to get

$$\sigma = \frac{1}{4m\omega} \int \frac{d^3\mathbf{p}'}{(2\pi)^3(2E')} \frac{d^3\mathbf{k}'}{(2\pi)^3(2\omega')} 2e^4 \left(\frac{\omega}{\omega'} + \frac{\omega'}{\omega} - \sin^2\theta \right) (2\pi)^4 \delta^4(p' + k' - p - k). \quad (119)$$

We can again do the integral over $d^3\mathbf{k}'$ using the spatial parts of the δ -function. Then we transfer to spherical polars and find

$$\frac{d\sigma}{d\Omega} = \frac{\alpha^2}{2m^2} \left(\frac{\omega'}{\omega} \right)^2 \left(\frac{\omega}{\omega'} + \frac{\omega'}{\omega} - \sin^2\theta \right). \quad (120)$$

A nice check of this result is to take the low-energy limit where $\omega \ll m$. Then $\omega \simeq \omega'$ and we find

$$\frac{d\sigma}{d\Omega} = \frac{\alpha^2}{2m^2} (1 + \cos^2\theta). \quad (121)$$

This is the Thomson cross section for the scattering of classical electromagnetic radiation by a free electron. In the other limit, the high-energy limit where $\omega \gg m$, we have

$$\omega' \simeq \frac{m}{1 - \cos\theta} \quad \Rightarrow \quad \frac{d\sigma}{d\Omega} \simeq \frac{\alpha^2}{2m\omega} \frac{1}{1 - \cos\theta}. \quad (122)$$

and the cross section is strongly peaked for small angles. This leads to a logarithmic enhancement when you perform the angular integration. These “collinear” logarithms arise whenever massless particles are emitted; this will be discussed in more detail in the phenomenology course.

Note that, since $\omega > \omega'$, eq. (122) holds strictly for $(1 - \cos \theta) > m/\omega$. For smaller angles, eq. (121) holds and

$$\frac{d\sigma}{d\Omega} \simeq \frac{\alpha^2}{m^2}. \quad (123)$$

The forward (small scattering angle) Compton scattering cross section is then a valuable method to measure the QED coupling α .

6 Strong Interactions

In this section we will develop the theory of the strong interactions, quantum chromodynamics (QCD). The major difference between QED and QCD is that the gluons are self-interacting because they also carry colour charge (unlike the charge-neutral photon).

6.1 QCD Lagrangian

The particles which carry colour charge are

Spin-1/2: six families of quarks (up, charge and top with electric charge +2/3; down, strange and bottom with electric charge -1/3)
For each flavour, there are $N_c = 3$ of these.

Spin-1: $8 = (N_c^2 - 1)$ massless gluons.

The QCD Lagrangian for a quark of mass m is

$$\mathcal{L}_{\text{QCD}} = -\frac{1}{4}F^{a\mu\nu}F_{\mu\nu}^a + \bar{\psi}_i(i\not{D}_{ij} - m\delta_{ij})\psi_j, \quad (124)$$

with $D_{ij}^\mu = \partial^\mu\delta_{ij} + ig_s t_{ij}^a A^{a\mu}, \quad F_{\mu\nu}^a = \partial_\mu A_\nu^a - \partial_\nu A_\mu^a + g_s f^{abc} A_\mu^b A_\nu^c.$

The a , i and j indices are gauge group indices which are discussed further below. The sum over these is implicit in eq. (124). Each t^a is a 3×3 matrix in colour space. The t^a matrices do not commute with each other, but obey the following algebra

$$[t^a, t^b] = if^{abc}t^c, \quad (125)$$

which is reminiscent of the algebra of angular momentum operators, $[J_i, J_j] = i\varepsilon_{ijk}J_k$. Here, in place of the alternating tensor ε_{ijk} , we have the “structure constants” f^{abc} (which also appear in $F_{\mu\nu}^a$). These are also completely anti-symmetric under the swapping of any pair of indices.

Just as the J_i generate the rotation group, $SU(2)$, the t^a generate the colour symmetry group, $SU(3)$. We choose to take the Pauli matrices as a representation of $SU(2)$. For $SU(3)$ we choose to take the representation where $t^a = \frac{1}{2}\lambda^a$ and the λ^a are the Gell-Mann matrices:

$$\begin{aligned}\lambda^1 &= \begin{pmatrix} 0 & 1 & 0 \\ 1 & 0 & 0 \\ 0 & 0 & 0 \end{pmatrix}, & \lambda^2 &= \begin{pmatrix} 0 & -i & 0 \\ i & 0 & 0 \\ 0 & 0 & 0 \end{pmatrix}, & \lambda^3 &= \begin{pmatrix} 1 & 0 & 0 \\ 0 & -1 & 0 \\ 0 & 0 & 0 \end{pmatrix}, \\ \lambda^4 &= \begin{pmatrix} 0 & 0 & 1 \\ 0 & 0 & 0 \\ 1 & 0 & 0 \end{pmatrix}, & \lambda^5 &= \begin{pmatrix} 0 & 0 & -i \\ 0 & 0 & 0 \\ i & 0 & 0 \end{pmatrix}, & \lambda^6 &= \begin{pmatrix} 0 & 0 & 0 \\ 0 & 0 & 1 \\ 0 & 1 & 0 \end{pmatrix}, \\ \lambda^7 &= \begin{pmatrix} 0 & 0 & 0 \\ 0 & 0 & -i \\ 0 & i & 0 \end{pmatrix}, & \lambda^8 &= \frac{1}{\sqrt{3}} \begin{pmatrix} 1 & 0 & 0 \\ 0 & 1 & 0 \\ 0 & 0 & -2 \end{pmatrix}.\end{aligned}\tag{126}$$

In practice, we are not interested in calculating one particular colour component and instead work with sums over all colours which ultimately leads to traces over the t^a -matrices. We will see explicit examples of this in the sections that follow and here just collect some useful identities:

$$\begin{aligned}\text{Tr}(t^a) &= 0, & \text{Tr}(t^a t^b) &= \frac{1}{2}\delta^{ab}, & \sum_a t_{ij}^a t_{jk}^a &= C_F \delta_{ik}, & \sum_{a,b} f^{abc} f^{abd} &= C_A \delta^{cd}, \\ \text{where } C_F &= \frac{4}{3}, & C_A &= 3.\end{aligned}\tag{127}$$

Notice that we have labelled with $a = 1, \dots, 8$ the gluon indices and with $i = 1, \dots, 3$ the quark indices. Particular care must be taken when these identities combine to give a trace of a δ -function:

$$\begin{aligned}\delta^{aa} &= N_c^2 - 1 = 8 \quad (\text{the number of gluons}) \\ \delta_{ii} &= N_c = 3 \quad (\text{the number of quarks}).\end{aligned}\tag{128}$$

The QCD Lagrangian \mathcal{L}_{QCD} is invariant under the infinitesimal “gauge” transformations

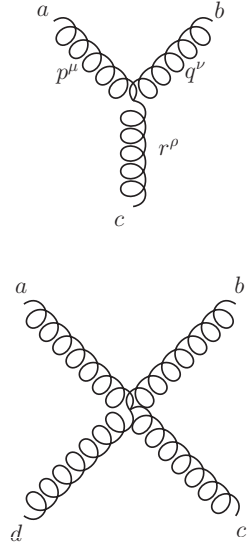
$$\begin{aligned}\psi_i(x) &\rightarrow (\delta_{ij} - ig_s \theta^a(x) t_{ij}^a) \psi(x), \\ A_\mu^a(x) &\rightarrow A_\mu^a(x) + D_\mu^{ab} \theta^b(x),\end{aligned}\tag{129}$$

where D_μ^{ab} is the covariant derivative in the “adjoint” representation, the one under which the gluon fields transforms under $SU(3)$, as opposed to the “fundamental” representation, which rules the transformation of quark fields. In particular, the adjoint covariant derivative is given by

$$D_\mu^{ab} = \partial_\mu \delta^{ab} + ig_s A_\mu^c (T^c)^{ab}, \quad (T^c)^{ab} = if^{acb} = -if^{abc}.\tag{130}$$

The matrices T^a , as needed for any generator of a representation of $SU(3)$, satisfy the same commutation rules as t^a :

$$[T^a, T^b] = if^{abc} T^c.\tag{131}$$



$$g_s f^{abc} (g^{\mu\nu} (p - q)^\rho + g^{\nu\rho} (q - r)^\mu + g^{\rho\mu} (r - p)^\nu)$$

$$-ig_s^2 (f^{abe} f^{cde} (g^{\mu\rho} g^{\nu\sigma} - g^{\mu\sigma} g^{\nu\rho})$$

$$+ f^{ace} f^{bde} (g^{\mu\nu} g^{\rho\sigma} - g^{\mu\sigma} g^{\nu\rho})$$

$$+ f^{ade} f^{bce} (g^{\mu\nu} g^{\rho\sigma} - g^{\mu\rho} g^{\nu\sigma}))$$

Figure 11: Three and four gluon vertices which arise from eq. (124). All momenta are taken to be incoming.

Returning to the Lagrangian, in QCD $F_{\mu\nu}^a$ has an extra term compared to QED, as required by gauge invariance. (Technically this term is present for QED too, but QED is an “Abelian” gauge theory which means that the structure constants are zero). Multiplying out $F^{a\mu\nu} F_{\mu\nu}^a$ give extra terms with 3 and 4 gauge fields. These correspond to new three- and four-gluon vertices as shown in fig. 11.

6.2 Gauge Invariance

The presence of the non-commuting colour matrices illustrates that $SU(3)$ is a non-Abelian gauge group. We can see the effect of this by studying the QCD equivalent of photon pair production, $q(p) \bar{q}(p') \rightarrow g(k) g(k')$, shown in fig. 12. In QED, the matrix element squared

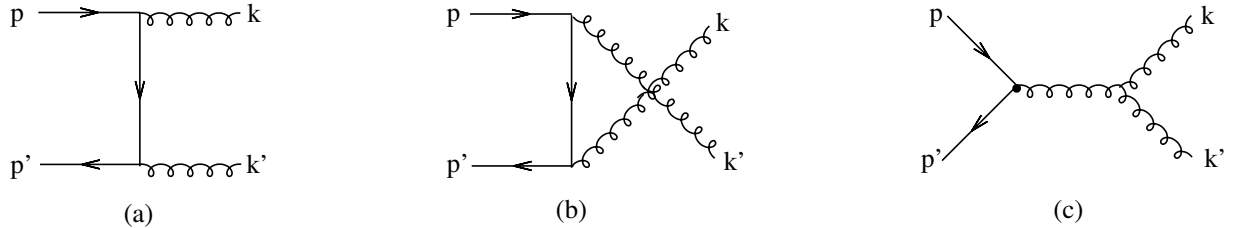


Figure 12: Feynman diagrams for the process $q\bar{q} \rightarrow gg$.

for this process can be obtained from that of Compton scattering via crossing.

One immediate effect is obvious – there is now a third diagram including the three-gluon

vertex. If we sum the contributions from the first two diagrams we find

$$\begin{aligned}\mathcal{M}^{(a)+(b)} &= \mathcal{A}_{\mu\nu}^{(a)+(b)} \varepsilon^{*\mu}(k) \varepsilon'^{\nu}(k'), \\ \mathcal{A}_{\mu\nu}^{(a)+(b)} &= -ig_s^2 \bar{v}(p') \left(\gamma_\nu t^b \frac{\not{p} - \not{k}}{(p-k)^2} \gamma_\mu t^a + \gamma_\mu t^a \frac{\not{p} - \not{k}'}{(p-k')^2} \gamma_\nu t^b \right) u(p),\end{aligned}\tag{135}$$

where we have implicitly assumed that gluon k has colour a and polarisation index μ , and gluon k' has colour b and polarisation index ν . At this order, see eq. (133), gauge invariance corresponds to testing whether the replacement $\epsilon_\mu \rightarrow \epsilon_\mu + \lambda k_\mu$ leaves the amplitude invariant. This is equivalent to testing the condition for the Ward Identity, $\mathcal{A}_{\mu\nu}^{(a)+(b)} k^\mu = 0$:

$$\mathcal{A}_{\mu\nu}^{(a)+(b)} k^\mu = -ig_s^2 [t^a, t^b] \bar{v}(p') \gamma_\nu u(p) \neq 0.\tag{136}$$

The non-zero commutator makes these diagrams alone not gauge-invariant. Adding diagram (c) gives a contribution which exactly cancels this (try this!) but yields another term proportional to k'_μ . This vanishes when we remember the whole expression is contracted with $\varepsilon'^{\nu}(k')$, and so gauge invariance is only obeyed once we project onto physical polarisations. This wasn't necessary in QED.

Recall in the QED case in section 3.2, we used $\mathcal{A}_{\mu\nu} k^\mu = 0$ to show that, in practical calculations, we can always make the replacement

$$\sum_{\alpha=1}^2 \varepsilon_\mu^\alpha \varepsilon_\nu^{*\alpha} \rightarrow -g_{\mu\nu}.\tag{137}$$

Although the right-hand summed all polarisations and not only the physical transverse ones, in actual calculations the unphysical longitudinal gluon polarisations automatically cancelled. This is no longer the case in QCD, where one has to sum strictly over physical polarisations. However, this can make calculations more cumbersome, so it might still be useful to sum over all polarisations, and to cancel in some way the unphysical degrees of freedom. How this cancellation is performed depends on the gauge. In covariant gauges, like the Feynman gauge, this is done by introducing extra fields, called the ghost fields. The alternative is to use the so-called physical gauges, that ensure that that only physical degrees of freedom propagate on shell.

Ghost Fields

To understand how the cancellation of unphysical polarisations actually arises in a covariant gauge, we need to revert to the case of photon pair production in QED. When we make the replacement in eq. (137), we are exploiting the fact that QED is unitary, i.e. probability is conserved through time evolution. A non-trivial implication of unitarity is that, at the lowest order in perturbation theory, twice the imaginary part of the forward amplitude for the process $e^+e^- \rightarrow e^+e^-$ has to be equal to amplitude squared for the process $e^+e^- \rightarrow \gamma\gamma$, when we integrate over the photon phase space and sum over *physical* photon polarisations. This is illustrated in Fig. 13, which shows the only intermediate

$$2\text{Im} \left(\text{Diagram 1} + \text{Diagram 2} \right) = \left| \text{Diagram with shaded blob} \right|^2$$

Figure 13: Unitarity relation for the process $e^+e^- \rightarrow \gamma\gamma$. The shaded blob represent the sum of all possible subdiagrams that can give rise to two photons in the final state at the lowest order in perturbation theory.

states that, at the considered order in perturbation theory, give a non-zero imaginary part, namely two virtual photons. Furthermore, it is possible to show that the imaginary part of any Feynman diagram is obtained by putting on shell in all possible ways the intermediate propagators (i.e. cutting the diagram) by replacing $i/(p^2 - m^2 + i\varepsilon)$ in each of them by $(2\pi)\Theta(p_0)\delta(p^2 - m^2)$. This divides each Feynman diagram into two subdiagrams on either side of the cut. On one side of the cut, one uses standard Feynman rules. On the other sides, one needs to apply complex conjugation to all Feynman vertices and propagators. Cuts of a diagram that conflict with energy-momentum conservation do not give any contribution to the imaginary part. The result of this cutting procedure for the present case is illustrated in Fig. 14. The dashed line on the right-hand side of the figure represents the only cut of the diagram that gives a non-zero imaginary part, obtained by putting on shell the intermediate photon propagators. If the amplitude is computed in the Feynman

$$2\text{Im} \left(\text{Diagram with two blobs} \right) = \text{Diagram with dashed cut line}$$

Figure 14: Pictorial representation of the cutting rules needed to compute the imaginary part of the forward amplitude $e^+e^- \rightarrow e^+e^-$ mediated by two virtual photons. The shaded blob represents the sum all possible subdiagrams that can give two photons in the intermediate state, that is, the two diagrams on the left-hand side of Fig. 13.

gauge, for an intermediate photon of momentum k , we have to perform the replacement

$$-g_{\mu\mu'} \frac{i}{k^2 + i\varepsilon} \rightarrow -g_{\mu\mu'} (2\pi)\Theta(k_0)\delta(k^2). \quad (138)$$

Let us call $A^{\mu\nu}$ the contribution to the diagram on the left of the cut in Fig. 14. From the Ward identity $k_\mu A^{\mu\nu} = 0$, we obtain that the contribution of gluon k to the imaginary part of the amplitude becomes

$$\int \frac{d^4k}{(2\pi)^4} (-g_{\mu\mu'}) (2\pi)\Theta(k_0)\delta(k^2) A^{\mu\nu} = \int \frac{d^3k}{(2\pi)^3 2k_0} A^{\mu\nu} \sum_{\alpha=1}^2 \epsilon_\mu^\alpha(k) \epsilon_{\mu'}^{*\alpha}(k), \quad (139)$$

where $\alpha = 1, 2$ is the index labelling photon physical polarisations. This verifies explicitly the unitary relation represented in Fig. 13. The latter means that, in QED, making the replacement in eq. (137) corresponds to exploiting the unitarity of the theory to compute an amplitude squared through the imaginary part of the corresponding forward amplitude.

In the case of QCD, as we have seen in the previous section, the fact that $k_\mu \mathcal{A}^{\mu\nu} \neq 0$ implies that the amplitude squared for the process $q\bar{q} \rightarrow gg$ is not given by the imaginary part of the forward amplitude $q\bar{q} \rightarrow q\bar{q}$, when only gluons are considered as intermediate states. In fact, the cut forward amplitude contains the contribution of non-physical longitudinal polarisations, which do not contribute to the amplitude squared for $q\bar{q} \rightarrow gg$. This would violate unitarity, so there has to be additional fields that are responsible for the cancellation of the contribution of non-physical polarisations in the imaginary part of the forward amplitude. These new fields are called ghosts. They are scalar fields, but satisfy Pauli exclusion principle like fermions. They transform under $SU(3)$ in the same way as gluons, i.e. in the adjoint representation. The Feynman rules for ghosts are shown in fig. 15. They can propagate and couple to gluons, but never appear in physical final states. If

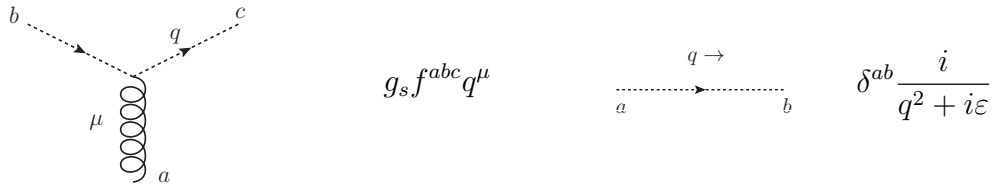


Figure 15: The Feynman rules for ghost fields, which are constructed explicitly to cancel unphysical degrees of freedom.

we now consider the imaginary part of the forward $q\bar{q}$ amplitude, at the lowest order in perturbation theory we need to include not only gluons as intermediate states, but ghosts as well, as pictorially illustrated in Fig. 16. The ghost-antighost loop contributes to the imaginary part of the forward amplitude with a factor (-1) , just like a normal fermion loop, so as to cancel the contribution of the unphysical longitudinal gluon polarisations when summing over all diagrams. The resulting imaginary part equals the amplitude squared for the process $q\bar{q} \rightarrow gg$, integrated over the gluon phase space and summed over physical gluon polarisations, as required by unitarity of QCD.

Physical Gauges

Alternatively, we can impose a so-called “physical gauge” condition on the gluon fields to eliminate unphysical polarisations from the start. This eliminates the need for ghosts, which do not interact with gluons anymore, but complicates the gluon propagator. In place of the Lorentz gauge condition $\partial^\mu A_\mu^a = 0$, we impose

$$A_\mu^a n^\mu = 0, \quad (140)$$

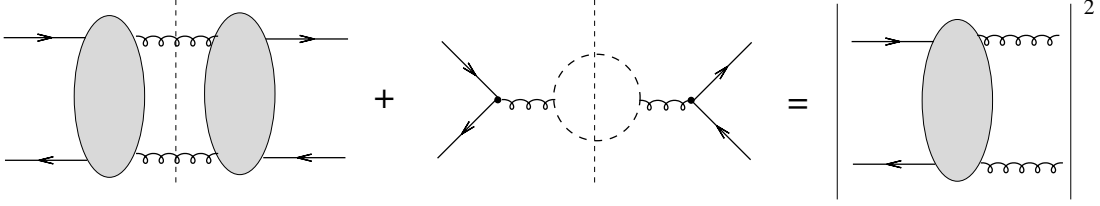


Figure 16: Pictorial representation of the unitarity constraint for QCD discussed in the text. Longitudinal polarisations for on-shell gluons in the cut amplitude on the left-hand side of the equality are cancelled by the contribution of the ghost-antighost loop. Each blob represents the sum of the three diagrams in Fig. 12.

for some arbitrary reference vector n^μ . This is done by adding the gauge-fixing Lagrangian

$$\mathcal{L}_{\text{gf}} = -\frac{1}{2\xi}(A_\mu^a n^\mu)^2, \quad (141)$$

and taking the limit $\xi \rightarrow 0$, thus enforcing the gauge condition in eq. (140).

The new expression for the propagator (for $\xi = 0$) is shown in fig. 17. When we use a

$$\overset{\mu}{\underbrace{\text{oooooo}}_a} \xrightarrow{q} \overset{\nu}{\underbrace{\text{oooooo}}_b} \quad \delta^{ab} \frac{i}{q^2 + i\varepsilon} \left(-g^{\mu\nu} + \frac{q^\mu n^\nu + q^\nu n^\mu}{(qn)} - n^2 \frac{q^\mu q^\nu}{(qn)^2} \right)$$

Figure 17: The gluon propagator when working in a physical gauge, $A_\mu^a n^\mu = 0$.

physical gauge, whenever we sum over polarisations, we can make the replacement

$$\sum_{\alpha=1}^2 \varepsilon_\mu^\alpha(q) \varepsilon_\nu^{*\alpha}(q) \rightarrow -g_{\mu\nu} + \frac{q^\mu n^\nu + q^\nu n^\mu}{(qn)} - n^2 \frac{q^\mu q^\nu}{(qn)^2}. \quad (142)$$

The different choices of reference vector n^μ correspond to different choices of the gauge. One can explicitly check that results for physical quantities, such as cross sections, are independent of this choice.

A relevant example of a physical gauge is the light-cone gauge, in which $n^2 = 0$. In such a gauge, if we have an on-shell gluon $q = (\omega, \mathbf{q})$, we can choose $n = (1, -\mathbf{q}/\omega)$. In this case

$$-g_{\mu\nu} + \frac{q^\mu n^\nu + q^\nu n^\mu}{(qn)} = \sum_{\alpha=1}^2 \varepsilon_\mu^\alpha(q) \varepsilon_\nu^{*\alpha}(q), \quad (143)$$

so that the replacement gives exactly the sum over the physical polarisations introduced in section 5.1. The expression in eq. (143) is the one that must be used in covariant gauges if one does not want to introduce unphysical amplitudes squared with ghosts in the final state.



Figure 18: Sample “loop” Feynman diagrams: (a) one of the one-loop corrections to Coulomb scattering and (b) a one-loop correction to the photon propagator.

7 Renormalisation

7.1 Dimensional regularisation and renormalisation scale

As mentioned in section 3.2, starting from the Feynman rules one can construct diagrams with loops, as for example the diagrams shown in fig. 18. The presence of loops means that momentum-conservation at each interaction vertex is no longer sufficient to determine the momentum in each leg. For example, k can take any value in the diagrams shown in fig. 18. We must therefore integrate over all possible values of unconstrained loop momenta. For example, the result for the diagram in fig. 18(b) is

$$(ie)^2 \int \frac{d^4 k}{(2\pi)^4} \frac{\text{Tr}[\gamma_\mu(\not{k} + \not{p} + m)\gamma_\nu(\not{k} + m)]}{(k^2 - m^2)((k + p)^2 - m^2)}, \quad (144)$$

with p the photon momentum and d the number of space-time dimensions. As the integral runs over all values of k , it includes very large values of k . Counting the powers of k , there are six of them in the numerator and four in the denominator, which implies that this integral diverges. In general, for any integral of the form

$$\int \frac{d^d k}{(2\pi)^4} \frac{N(k)}{M(k)} \quad (145)$$

we define the superficial degree of divergence, D , to be the result of the naïve power-counting:

$$D = d + (\text{powers of } k \text{ in } N) - (\text{powers of } k \text{ in } M). \quad (146)$$

If $D \geq 0$, then the integral is said to be superficially divergent. Such divergences are called ultra-violet (UV) because they arise whenever loop momenta get large. The boundary case of $D = 0$ is a logarithmic divergence (think of $\int dk \, 1/k$). The term “superficial” is used because there can be other factors which can affect the actual degree of divergence. In the example above, gauge invariance actually implies that the final result of the integral in eq. (144) must be proportional to $(p^2 g_{\mu\nu} - p_\mu p_\nu)$. Therefore the divergence is only logarithmic, and not quadratic as it appears from naïve power counting.

The main point, though, is not the degree of divergence, but the fact that one finds divergences at all. These higher-loop corrections were supposed to be corrections in the

perturbative series, hence smaller than those appearing at the previous perturbative order. For many years, this caused a major problem for the development of perturbation theory. However, there exists a well-defined procedure to “remove” these divergences which is called renormalisation. The basic idea behind renormalisation is that the parameters appearing in the Lagrangian do not need to be physical quantities, but their value is determined by comparing perturbative predictions to actual experimental data. For instance, the value of e can be extracted by measuring the Compton differential cross section at small angles. Therefore, infinities that eventually appear in perturbative calculations can be in principle reabsorbed in a redefinition of the parameters entering the Lagrangian. In practice, this amounts to rescaling all quantities in the Lagrangian by a “renormalisation constant”, Z . For instance, for a field ϕ we have

$$\phi \longrightarrow \phi_0 = Z_\phi \phi_R. \quad (147)$$

The field ϕ_0 is called “bare” field, as opposed to the “renormalised” field ϕ_R , and Z_ϕ is called renormalisation constant. This procedure has to be repeated for all fields, masses and coupling constants. Provided that *all* infinities in the theory can be removed with a finite number of renormalisation constants Z , then the theory is said to be renormalisable. After the renormalisation constants have been fixed, we can calculate all physical quantities in terms of the renormalised quantities and the results will be both finite and unambiguously defined.

The renormalisation constants are calculated according to some procedure that is called “renormalisation scheme”. This consists in computing a suitable set of correlation functions, and imposing that these functions are finite at any order in perturbation theory. In this procedure one finds divergent integrals, which have to be regularised in some way. The regularisation actually provide means to parameterise the divergence. One approach is to implement a momentum cut-off, Λ , so as to artificially remove the region with large momentum. The most common approach though is called “dimensional regularisation”. Here we decrease the term d in eq. (146) to a lower value, so that we calculate all integrals in $d = 4 - 2\epsilon$ dimensions instead of $d = 4$. The integration measure becomes

$$\frac{d^4 k}{(2\pi)^4} \longrightarrow \frac{d^{4-2\epsilon} k}{(2\pi)^{4-2\epsilon}}, \quad (148)$$

and for each dimensionless coupling g_R one performs the replacement

$$g_R \rightarrow \mu^{\frac{4-d}{2}} g_R(\mu) = \mu^\epsilon g_R(\mu). \quad (149)$$

The factor of μ^ϵ is essential to preserve the correct dimensions of the bare coupling in d dimensions. The renormalised coupling g_R stays dimensionless and depends now on the scale μ . The latter quantity is the famous renormalisation scale and it is the price that we pay for renormalisation as our finite calculations are now all dependent upon μ .

To summarise, the steps to perform renormalisation within dimensional regularisation are:

1. Compute all integrals in terms of renormalised quantities.

2. All UV divergences appear as $1/\epsilon$ -poles.
3. Define the renormalisation functions Z so as to cancel the poles in ϵ (and maybe some finite terms).

After renormalisation, eq. (147) depends on both ϵ and μ , as follows:

$$\phi_0(\epsilon) = Z_\phi(\mu, \epsilon) \phi_R(\mu), \quad (150)$$

and a similar expression holds for all couplings and masses. Both ϕ_0 and Z are infinite for $\epsilon \rightarrow 0$, whereas $\phi_R(\mu)$ stays finite, but depends on the unphysical renormalisation scale μ .

In a renormalised theory then, even tree-level diagrams depend on the renormalisation scale, through the coupling for example. The dependence on the renormalisation scale would disappear only if we were able to calculate physical quantities to all orders in perturbation theory. Although this is unpractical, calculating one or two extra orders in perturbation theory can reduce the dependence considerably. However, this does mean that any theoretical calculation now depends on a free parameter, and it is exactly this parameter which leads to a way to estimate the “theory uncertainty”. In fact, consider an observable $O(\alpha_R(\mu), \mu, \{Q_i\})$, where $\{Q_i\}$ is a set of characteristic scales for the process. If we know $O^{(n)}$, the perturbative expansion of O at order n in perturbation theory, we have

$$O^{(n)}(\alpha_R(\mu'), \mu', \{Q_i\}) = O^{(n)}(\alpha_R(\mu), \mu, \{Q_i\}) + \mathcal{O}(\alpha_R^{n+1}(\mu)), \quad (151)$$

so that the variation of μ around some central value μ_0 produces automatically a higher-order term. Notice that $O^{(n)}(\alpha_R(\mu), \mu, \{Q_i\})$ might contain $\ln(Q_i/\mu)$. This is why the central scale μ_0 is normally chosen of the order of the typical value that the scales Q_i can assume. For example in $gg \rightarrow H$, one would typically take $\mu_0 \sim m_H$.

The obvious way to gauge how the strength of the dependence on the scale in a calculation is to vary the scale and see how the result varies. If the dependence is very weak, the result will be negligible. If the dependence is very strong, the variation will be large. The consensus of the community is to quote the theoretical uncertainty when the central scale is varied by a factor of 2 in each direction. One should remember that this is only an uncertainty of the dependence on the renormalisation scale and not a strict error bar. This is illustrated by the plot in fig. 19, which is taken from Gehrmann-De Ridder, Gehrmann, Glover & Pires, arXiv:1301.7310. It shows the scale dependence for inclusive jet production in the gluon-gluon channel at LO, NLO and NNLO. Indeed the variation decreases each time indicating that the sensitivity to the scale is decreasing. The fact that the lines do not overlap is a clear sign that these uncertainty bands are not error bands.

7.2 Running Coupling

Suppose we have chosen a renormalisation scale μ . How do we measure a coupling $\alpha_R(\mu)$? We normally consider an observable $O(\alpha_R(\mu'), \mu', \{Q_i\})$, compute it at the highest possible

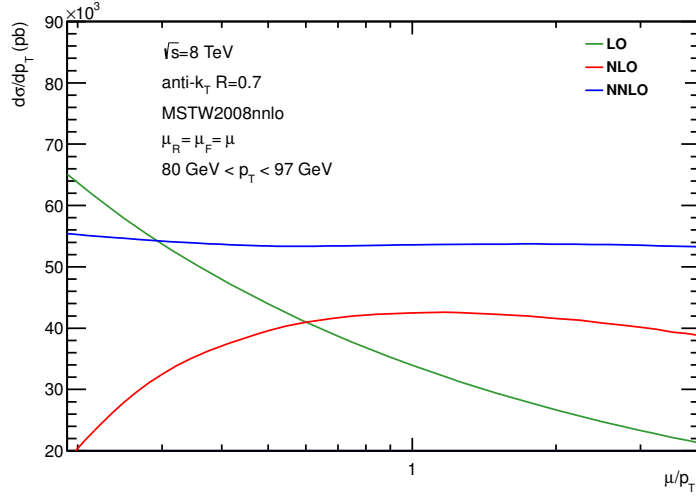


Figure 19: Plot showing the scale dependence for inclusive jet production at LO, NLO and NNLO, taken from Gehrmann-De Ridder, Gehrmann, Glover & Pires, arXiv:1301.7310.

order in perturbation theory, and compare the obtained number with experimental data:

$$O^{(n)}(\alpha_R(\mu'), \mu', \{Q_i\}) = O_{\text{exp}} \Rightarrow \alpha_R(\mu). \quad (152)$$

By doing this for various observables, characterised by different typical scales μ , one can actually measure the dependence of the coupling on the renormalisation scale μ . This dependence can be predicted theoretically, and the comparison of the predicted dependence with the one that is actually observed represents one of the most stringent tests of the validity of a given QFT. This is illustrated for QCD in fig. 20, where one sees an astonishing agreement between the predicted “running” of the QCD coupling with the renormalisation scale Q , and what is observed in experimental data.

The theoretical object that dictates how a coupling evolves with the renormalisation scale is the beta function $\beta(\alpha_R)$, defined as

$$\mu^2 \frac{\partial \alpha_R}{\partial \mu^2} = \beta(\alpha_R) = -\beta_0 \alpha_R^2 - \beta_1 \alpha_R^3 + \dots \quad (153)$$

There are various ways to compute the beta function, which in general depends on the renormalisation scheme used. However, one can show that the first two coefficient of the beta function, β_0 and β_1 , are independent of the renormalisation scheme. If we consider a scheme tied to dimensional regularisation (e.g. the so-called $\overline{\text{MS}}$ scheme), one has the relation

$$\alpha_0(\epsilon) = \mu^{2\epsilon} Z_g^2(\epsilon, \mu^2) \alpha_R(\mu^2), \quad (154)$$

where $\alpha_0 = g_0^2/(4\pi)$ and $\alpha_R = g_R^2/(4\pi)$. The crucial observation is that the bare coupling α_0 does not depend on μ . Therefore, its logarithmic derivative with respect to μ^2 is zero:

$$0 = \mu^2 \frac{\partial \alpha_0}{\partial \mu^2} = \mu^{2\epsilon} Z_g^2(\epsilon, \mu^2) \left[\left(\epsilon + \frac{\mu^2}{Z_g^2} \frac{\partial Z_g^2}{\partial \mu^2} \right) \alpha_R + \mu^2 \frac{\partial \alpha_R}{\partial \mu^2} \right]. \quad (155)$$

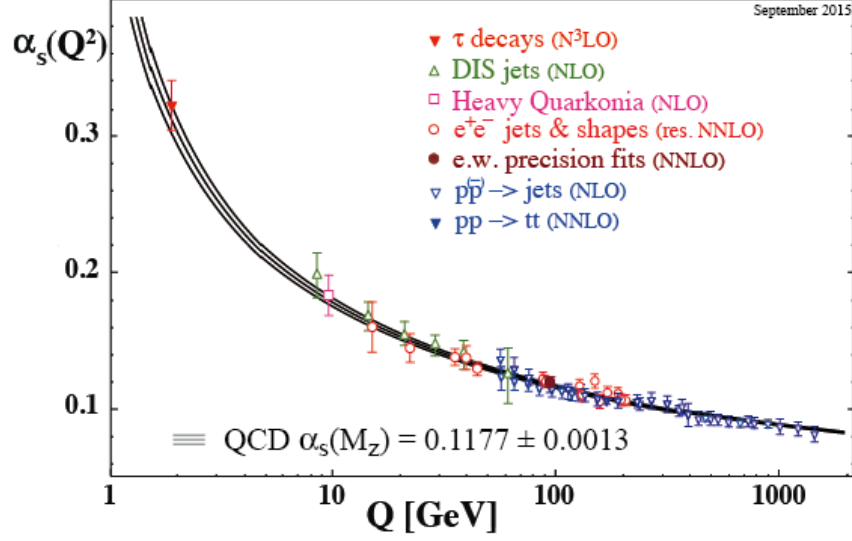


Figure 20: The QCD coupling α_s as a function of the renormalisation scale Q , in theory and experiment, taken from arXiv:1512.0519.

This gives

$$\mu^2 \frac{\partial \alpha_R}{\partial \mu^2} = - \left(\epsilon + \frac{\mu^2}{Z_g^2} \frac{\partial Z_g^2}{\partial \mu^2} \right) \alpha_R \equiv \beta(\epsilon, \alpha_R) \rightarrow \beta(\alpha_R) = - \lim_{\epsilon \rightarrow 0} \frac{\mu^2}{Z_g^2} \frac{\partial Z_g^2}{\partial \mu^2} \alpha_R, \quad \epsilon \rightarrow 0. \quad (156)$$

In any scheme based on dimensional regularisation we have

$$Z_g(\epsilon, \mu^2) = 1 + \frac{\alpha_R(\mu^2)}{\epsilon} Z_g^{(1)} + \dots \quad (157)$$

Therefore the first term of the beta function is just obtained from the $1/\epsilon$ pole of Z_g , as follows

$$\beta(\alpha_R) = - \lim_{\epsilon \rightarrow 0} \frac{\mu^2}{Z_g^2} \frac{\partial Z_g^2}{\partial \mu^2} \alpha_R = - \lim_{\epsilon \rightarrow 0} \frac{2Z_g^{(1)}}{\epsilon} \underbrace{\mu^2 \frac{\partial \alpha_R}{\partial \mu^2}}_{=-\epsilon \alpha_R} \alpha_R = -\beta_0 \alpha_R^2 \quad \Rightarrow \quad \beta_0 = -2Z_g^{(1)}. \quad (158)$$

The calculation of $Z_g^{(1)}$ can be performed using any quantity that involves an interaction vertex. A way that is common to both QED and QCD is to consider the renormalised interaction Lagrangian

$$\mathcal{L}_{\text{int}} \rightarrow Z_g Z_2 \sqrt{Z_3} (g_R \bar{\psi}_R \mathcal{A}_R \psi_R) = Z_1 (g_R \bar{\psi}_R \mathcal{A}_R \psi_R), \quad \Rightarrow \quad Z_g = \frac{Z_1}{Z_2 \sqrt{Z_3}}. \quad (159)$$

Here we have used the ubiquitous notation $Z_\psi = \sqrt{Z_2}$ and $Z_A = \sqrt{Z_3}$. The function Z_1 contains all UV divergences associated with loop corrections to the interaction vertex, whereas Z_2 and Z_3 contain UV divergences arising in the calculations of the fermion

and gauge-boson propagators respectively. In QED, a powerful Ward identity implies $Z_1 = Z_2$, so that the beta function can be calculated just from all the loop corrections to the propagator in the unrenormalised theory. For the case of QED

$$\beta_0 = -2Z_g^{(1)} = Z_3^{(1)} = -\frac{1}{3\pi}. \quad (160)$$

Inserting this expression in the beta function we obtain

$$\beta_{\text{QED}}(\alpha) = \frac{1}{3\pi}\alpha^2. \quad (161)$$

which means that the QED coupling, at least until the beta function is dominated by its first term, becomes stronger with energy.

In QCD instead the Ward identity $Z_1 = Z_2$ does not hold any more. However, it holds at least for the part of these renormalisation functions that depends on C_F . Since, at one loop, $Z_2^{(1)}$ is proportional to C_F , its contribution to the beta function cancels exactly with the abelian contribution to $Z_1^{(1)}$. Therefore, the only contributions to the QCD beta function at one loop come from the renormalisation function of the gluon $Z_3^{(1)}$ and the non-abelian part of $Z_1^{(1)}$, which we call $Z_1^{(1)}|_{\text{n.a.}}$. The two depend on the gauge, but this gauge dependence cancels in the combination

$$\beta_0 = -2Z_g^{(1)} = Z_3^{(1)} - 2Z_1^{(1)}|_{\text{n.a.}}. \quad (162)$$

For instance, in the Feynman gauge

$$Z_3^{(1)} = \frac{\alpha_s}{\epsilon} \frac{5C_A - 2n_f}{12\pi}, \quad Z_1^{(1)} = -\frac{\alpha_s}{\epsilon} \frac{C_F + C_A}{4\pi}, \quad (163)$$

where $\alpha_s = g_s^2/(4\pi)$ and n_f is the number of massless (a.k.a. “active”) quark flavours contributing to the renormalisation of the gluon propagator. This gives

$$\beta_{\text{QCD}}(\alpha_s) = -\frac{11C_A - 2n_f}{12\pi}\alpha_s^2 = -\frac{21}{12\pi}\alpha_s^2, \quad (164)$$

where the latter expression corresponds to the actual value of the beta function for $n_f = 6$ active flavours, as is the case at very high momentum scales. The fact that the beta function of QCD is negative when α_s is small means that the QCD coupling decreases with energy. This property is known as asymptotic freedom, and is crucial to be able to compute hadronic cross sections in terms of quarks and gluons. In fact, when probed at short distances, hadrons appear as made up of pointlike constituents, quarks and gluons, which interact very feebly. Therefore, the Feynman rules we have learnt so far are enough to compute high-energy observables, for instance jet cross sections, as will be explained in the phenomenology course. At larger distances, the QCD coupling becomes stronger and stronger, at a point that quarks and gluons bind together to form hadrons. This phenomenon is known as confinement.

Summary

This has been a very quick tour through some very important, deep and interesting material. I hope it has provided some insight into the quantum field theory descriptions of QED and QCD, and provided you with useful tools for the future.

Acknowledgements

It has been a pleasure to give this course at the 2016 HEP Summer School. I would like to thank Nikos Konstantinidis for directing this successful school, the other lecturers and tutors for making this such an interesting and entertaining fortnight, and the students for engaging with the courses.

THE STANDARD MODEL

Dr Chris Maxwell (University of Durham)

Contents

| | | |
|----------|---|------------|
| 1 | Abelian and non-Abelian local gauge theories..... | 103 |
| 1.1 | QED Lagrangian from local gauge invariance | 103 |
| 1.2 | The Non-Abelian Recipe Book..... | 104 |
| 1.3 | The Lagrangian of QCD..... | 107 |
| 2 | Glashow's Model $SU(2)_L \times U(1)_Y$..... | 108 |
| 2.1 | Kinetic Energy Terms for Glashow's Model..... | 113 |
| 3 | Spontaneous Symmetry Breaking..... | 114 |
| 3.1 | The Heisenberg Ferromagnet..... | 115 |
| 3.2 | SSB of gauge symmetry-general considerations | 115 |
| 3.3 | SSB of a global Gauge Symmetry: Nambu-Goldstone mechanism. | 116 |
| 3.4 | SSB of local Gauge Symmetry | 118 |
| 4 | The Higgs Mechanism for $SU(2)_L \times U(1)_Y$ | 119 |
| 4.1 | Yukawa terms for lepton masses..... | 122 |
| 4.2 | Electroweak quark sector..... | 123 |
| 4.3 | SM Lagrangian and independent parameter count..... | 125 |
| | Acknowledgements | 126 |
| 5 | Appendix of Feynman rules | 127 |

THE STANDARD MODEL

Chris Maxwell

Institute for Particle Physics Phenomenology, Durham University, Durham DH1 3LE, U.K.

Lectures presented at the STFC HEP Summer School,
University of Lancaster, September 2015.

1 Abelian and non-Abelian local gauge theories

The Standard Model is based on a product of groups $SU(3)_c \times SU(2)_L \times U(1)_Y$, describing QCD, the chiral $SU(2)_L$ electroweak sector and the hypercharge $U(1)_Y$ sector in which QED is embedded. The first two of these groups are non-abelian, and are based on non-commuting group generators. The final group is abelian. We shall review in what follows how such gauge theories can be constructed from the principle of local gauge invariance, beginning with the simplest case of QED, and generalising this recipe to the construction of the non-abelian $SU(N)$ theories.

1.1 QED Lagrangian from local gauge invariance

The QED Lagrangian can be defined more fundamentally by demanding **local gauge invariance**. The Dirac Lagrangian

$$\mathcal{L}_{Dirac} = i\bar{\psi}\gamma^\mu\partial_\mu\psi - m\bar{\psi}\psi, \quad (1.1)$$

has an obvious invariance under the **global** gauge transformation

$$\psi(x) \rightarrow \psi'(x) = e^{i\alpha}\psi(x), \quad \bar{\psi}(x) \rightarrow \bar{\psi}'(x) = e^{-i\alpha}\bar{\psi}(x), \quad (1.2)$$

where the phase $i\alpha$ is independent of spacetime position x . Each term is simply multiplied by $e^{i\alpha}e^{-i\alpha} = 1$. **Local** gauge invariance corresponds to demanding invariance with phases $i\alpha(x)$ which are chosen independently at each spacetime point.

$$\psi(x) \rightarrow \psi'(x) = e^{i\alpha(x)}\psi(x), \quad \bar{\psi}(x) \rightarrow \bar{\psi}'(x) = e^{-i\alpha(x)}\bar{\psi}(x). \quad (1.3)$$

One now finds that local gauge invariance does not hold since

$$\begin{aligned} i\bar{\psi}(x)\gamma^\mu\partial_\mu\psi(x) &\rightarrow i\bar{\psi}(x)e^{-i\alpha(x)}\gamma^\mu\partial_\mu[e^{i\alpha(x)}\psi(x)] \\ &= i\bar{\psi}(x)\gamma^\mu\partial_\mu\psi(x) - \bar{\psi}(x)\gamma^\mu\psi(x)[\partial_\mu\alpha(x)]. \end{aligned} \quad (1.4)$$

The $\partial_\mu\alpha(x)$ term violates the local gauge invariance. The resolution is that one needs to replace the ordinary derivative ∂_μ by the **covariant derivative** D_μ . To ensure local gauge invariance one needs to ensure that under a gauge transformation $D_\mu\psi(x)$ transforms in exactly the same way as $\psi(x)$ itself. It is in this sense that one has a “covariant derivative”.

$$D_\mu \psi(x) \rightarrow D'_\mu \psi'(x) = e^{i\alpha(x)}(D_\mu \psi(x)) . \quad (1.5)$$

This transformation rule holds if we define the covariant derivative

$$D_\mu \equiv \partial_\mu + ieA_\mu , \quad (1.6)$$

where under a local gauge transformation the **gauge field** A_μ transforms as

$$A_\mu \rightarrow A'_\mu = A_\mu - \frac{1}{e} \partial_\mu \alpha(x) . \quad (1.7)$$

The gauge transformation of A_μ is exactly the same as the classical EM transformation, but the idea will be that the covariant derivative D_μ and gauge fields A_μ can provide a general recipe for constructing general non-abelian gauge theories. Having changed ∂_μ to D_μ , and adding in the “kinetic energy” term $-\frac{1}{4}F_{\mu\nu}F^{\mu\nu}$ one has the QED Lagrangian

$$\begin{aligned} \mathcal{L}_{QED} &= -\frac{1}{4}F_{\mu\nu}F^{\mu\nu} + i\bar{\psi}\gamma^\mu D_\mu \psi - m\bar{\psi}\psi \\ &= -\frac{1}{4}F_{\mu\nu}F^{\mu\nu} + i\bar{\psi}\gamma^\mu \partial_\mu \psi - e\bar{\psi}\gamma^\mu \psi A_\mu - m\bar{\psi}\psi . \end{aligned} \quad (1.8)$$

Crucially $F_{\mu\nu}$ can be defined in terms of the commutator of covariant derivatives, D_μ . This involves introducing a “gauge comparator” and is analogous to parallel transport in General Relativity. The definition is

$$[D_\mu, D_\nu]\psi \equiv ieF_{\mu\nu}\psi . \quad (1.9)$$

In the case of abelian QED one finds the classical EM result

$$F_{\mu\nu} = \partial_\mu A_\nu - \partial_\nu A_\mu . \quad (1.10)$$

How does this generalise to non-Abelian gauge groups ?

1.2 The Non-Abelian Recipe Book

Local gauge transformations will be of the form

$$\psi(x) \rightarrow \psi'(x) = U(x)\psi(x) \quad , \quad \bar{\psi}(x) \rightarrow \bar{\psi}'(x) = \bar{\psi}(x)U^{-1}(x) . \quad (1.11)$$

Here $U(x)$ denotes an element of the gauge group \mathcal{G} chosen independently at each spacetime point. In the case of QED $\mathcal{G} = U(1)$ the group of 1×1 unitary ($MM^\dagger = I$) matrices (complex phases). We shall be interested in the non-Abelian Lie groups $SU(N)$ of $N \times N$ unitary matrices with $\det U = 1$. An element of such a Lie Group will have the form

$$U(x) = \exp(i \sum_{j=1}^{N^2-1} \alpha_j(x) T_j) . \quad (1.12)$$

Here the sum is over the $N^2 - 1$ **generators** of the Lie group. These satisfy the **Lie Algebra**

$$[T_i, T_j] = i c_{ijk} T_k . \quad (1.13)$$

Here the c_{ijk} are the real **structure constants** of the group. Abelian groups have commuting generators and so for the U(1) of QED $c_{ijk} = 0$. For SU(2) the generators involve the three Pauli matrices $T_i = \sigma_i/2$ and the structure constants are $c_{ijk} = \epsilon_{ijk}$, whilst for SU(3) the generators involve the eight Gell-Mann λ matrices $T_i = \lambda_i/2$. The spin- $\frac{1}{2}$ matter fields are N -plets in the **fundamental** representation of the gauge group. For instance (chiral) leptonic doublets of neutrinos and electrons in electroweak SU(2)_L

$$\begin{pmatrix} \nu_e \\ e \end{pmatrix} , \quad (1.14)$$

or quark colour triplets (red, green and blue, RGB) in SU(3) QCD.

$$\psi(x) = \begin{pmatrix} \psi_R(x) \\ \psi_G(x) \\ \psi_B(x) \end{pmatrix} . \quad (1.15)$$

The gauge fields are linear combinations of the generators of the gauge group

$$A_\mu = \sum_{i=1}^{N^2-1} A_\mu^i T_i . \quad (1.16)$$

One defines the covariant derivative

$$D^\mu = (\partial_\mu - ig A_\mu) . \quad (1.17)$$

Here g is the gauge coupling. For local gauge invariance one requires that

$$D^\mu \psi(x) \rightarrow D'^\mu \psi'(x) = U(x) [D^\mu \psi(x)] , \quad (1.18)$$

and hence A_μ transforms as

$$A_\mu \rightarrow A'_\mu = U(x) A_\mu U^{-1}(x) + \frac{i}{g} U(x) [\partial_\mu U^{-1}(x)] . \quad (1.19)$$

The locally gauge invariant Lagrangian is then obtained by replacing $\partial_\mu \rightarrow D_\mu$ in the free Dirac Lagrangian

$$\mathcal{L} = i\bar{\psi}\gamma^\mu D_\mu\psi - m\bar{\psi}\psi$$

The non-Abelian expression for $F_{\mu\nu}$ follows from

$$[D_\mu, D_\nu]\psi(x) = -igF_{\mu\nu}\psi(x) \quad (1.20)$$

which yields

$$\begin{aligned} F_{\mu\nu} &= \partial_\mu A_\nu - \partial_\nu A_\mu - ig[A_\mu, A_\nu] \\ &= \partial_\mu A_\nu - \partial_\nu A_\mu - igA_\mu^i A_\nu^j [T_i, T_j] \\ &= \partial_\mu A_\nu - \partial_\nu A_\mu + gA_\mu^i A_\nu^j c_{ijk} T_k . \end{aligned} \quad (1.21)$$

One can easily check that under a local gauge transformation

$$F_{\mu\nu} \rightarrow F'_{\mu\nu} = U(x)F_{\mu\nu}U^{-1}(x) , \quad (1.22)$$

and so the kinetic energy term

$$-\frac{1}{2}\text{Tr}[F_{\mu\nu}F^{\mu\nu}] , \quad (1.23)$$

is locally gauge invariant since the trace is cyclic.

$$\text{Tr}[F'_{\mu\nu}F'^{\mu\nu}] = \text{Tr}[UF_{\mu\nu}U^{-1}UF^{\mu\nu}U^{-1}] = \text{Tr}[F_{\mu\nu}F^{\mu\nu}] \quad (1.24)$$

$$-\frac{1}{2}\text{Tr}[F_{\mu\nu}F^{\mu\nu}] = -\frac{1}{2}F_{\mu\nu}^i F^{j\mu\nu} \text{Tr}[T_i T_j] . \quad (1.25)$$

Defining the generators so that $\text{Tr}[T_i T_j] = \frac{1}{2}\delta_{ij}$ one arrives at the kinetic energy term

$$-\frac{1}{4}F_{\mu\nu}^i F^{i\mu\nu} . \quad (1.26)$$

1.3 The Lagrangian of QCD

Quantum Chromodynamics (QCD) is a non-abelian gauge theory of interacting quarks and gluons. The gauge group is $SU(N_c)$, and there are $N_c^2 - 1$ gluons. Experimental indications are that $N_c = 3$. The Lagrangian density is

$$\mathcal{L}_{QCD} = \bar{\psi}(i\gamma^\mu \partial_\mu - m)\psi + g_s(\bar{\psi}\gamma^\mu T_a \psi)G_\mu^a - \frac{1}{4}G_{\mu\nu}^a G_a^{\mu\nu}. \quad (1.27)$$

Here $a = 1, 2, 3, \dots, 8$, and T_a are the generators of $SU(3)$, $T_a = \lambda_a/2$, where λ_a ($a = 1, 2, \dots, 8$) are the Gell-Mann λ -matrices. They satisfy the Lie algebra

$$[T_a, T_b] = if_{abc}T_c \quad (1.28)$$

The quark fields carry colour, R, G, B, and transform as a triplet in the fundamental representation

$$\psi(x) = \begin{pmatrix} \psi_R(x) \\ \psi_G(x) \\ \psi_B(x) \end{pmatrix} \quad (1.29)$$

\mathcal{L}_{QCD} is invariant under local $SU(3)$ gauge transformations

$$\psi(x) \rightarrow U(x)\psi = e^{iT^a\alpha_a(x)}\psi(x). \quad (1.30)$$

The field strength tensor $G_{\mu\nu}^a$ contains the abelian (QED) result and an extra term proportional to the structure constants f^{abc} which are responsible for three and four-point self-interactions of gluons, not present for photons in QED.

$$G_{\mu\nu}^a = \partial_\mu G_\nu^a - \partial_\nu G_\mu^a + g_s f^{abc} G_\mu^b G_\nu^c. \quad (1.31)$$

For QCD (but not QED) one also needs to include unphysical *ghost* particles. These are scalar Grassmann (anti-commuting) fields needed to cancel unphysical polarization states for the gluons. The required Fadeev-Popov extra term in \mathcal{L}_{QCD} is

$$\mathcal{L}_{\text{ghost}} = \bar{\eta}^a (-\partial^2 \delta^{ac} - g_s \partial^\mu f^{abc} G_\mu^b) \eta^c. \quad (1.32)$$

In both QED and QCD one needs also to include a gauge fixing term if inverse propagators are to be defined.

$$\mathcal{L}_{\text{gauge-fixing}} = \frac{1}{2\xi} (\partial^\mu G_\mu^a)^2 \quad (1.33)$$

There is only one other gauge-invariant structure that we could add involving the *dual* field strength tensor $\tilde{G}_{\mu\nu}^a$,

$$\mathcal{L}_\theta = \frac{\theta g_s^2}{64\pi^2} \tilde{G}^{a,\mu\nu} G_a^{\rho\sigma} \quad (1.34)$$

This is a total derivative and so produces no effects at the perturbative level. However, if $\theta \neq 0$ non-perturbative effects would induce a CP-violating electric dipole moment for the neutron, experimental constraints on this provide a bound $|\theta| < 3.10^{-10}$.

2 Glashow's Model $SU(2)_L \times U(1)_Y$

We begin by defining a weak isospin doublet containing a left-handed electron and electron neutrino

$$\chi_L = \begin{pmatrix} \nu_L \\ e_L \end{pmatrix} \equiv \begin{pmatrix} \nu \\ e \end{pmatrix}_L. \quad (2.1)$$

With an adjoint

$$\bar{\chi}_L = (\bar{\nu}_L \quad \bar{e}_L). \quad (2.2)$$

We shall introduce a weak isospin quantum number T . The doublet has $T = \frac{1}{2}$, the upper and lower members of the doublet have $T^3 = \pm \frac{1}{2}$, respectively.

These row and column matrices are acted on by isospin generators in the form of 2×2 Pauli matrices

$$\tau^1 = \begin{pmatrix} 0 & 1 \\ 1 & 0 \end{pmatrix}, \tau^2 = \begin{pmatrix} 0 & -i \\ i & 0 \end{pmatrix}, \tau^3 = \begin{pmatrix} 1 & 0 \\ 0 & -1 \end{pmatrix}. \quad (2.3)$$

The generators $\frac{1}{2}\tau^i$ satisfy the $SU(2)$ Lie Algebra

$$[\frac{1}{2}\tau^i, \frac{1}{2}\tau^j] = i\epsilon_{ijk} \frac{1}{2}\tau^k. \quad (2.4)$$

The isospin raising and lowering operators are $\tau^\pm = \frac{1}{2}(\tau^1 \pm i\tau^2)$.

One can then write an isospin triplet of weak currents

$$J_\mu^i = \bar{\chi}_L \gamma_\mu \frac{1}{2} \tau^i \chi_L \quad (i = 1, 2, 3). \quad (2.5)$$

Putting in row vectors, column vectors and matrices, we have explicitly on multiplying out

$$\begin{aligned} J_\mu^1 &= \frac{1}{2}(\bar{e}_L \gamma_\mu \nu_L + \bar{\nu}_L \gamma_\mu e_L) \\ J_\mu^2 &= \frac{i}{2}(\bar{e}_L \gamma_\mu \nu_L - \bar{\nu}_L \gamma_\mu e_L) \\ J_\mu^3 &= \frac{1}{2}(\bar{\nu}_L \gamma_\mu \nu_L - \bar{e}_L \gamma_\mu e_L). \end{aligned} \quad (2.6)$$

The charge raising and lowering V-A currents can be written in terms of J_μ^1 and J_μ^2

$$J_\mu^\pm = \bar{\chi}_L \gamma_\mu \tau^\pm \chi_L = J_\mu^1 \pm i J_\mu^2 . \quad (2.7)$$

The isospin triplet of currents have corresponding charges

$$T^i = \int d^3x J_0^i(x) , \quad (2.8)$$

and these satisfy an SU(2) algebra

$$[T^i, T^j] = i \epsilon_{ijk} T^k . \quad (2.9)$$

To construct a combined weak and electromagnetic theory we will also require the electromagnetic current

$$J_\mu^{em} = Q(\bar{e}_L \gamma_\mu e_L + \bar{e}_R \gamma_\mu e_R) , \quad (2.10)$$

where Q denotes the charge of the particle (in this case an electron) in units of $e \approx 0.303$ ($\alpha = e^2/4\pi$ is the fine structure constant). So $Q = -1$ for e^- . In terms of the net charge of interacting particles J_μ^3 and J_μ^{em} are neutral currents, whereas J_μ^1 and J_μ^2 are charged currents. J_μ^3 does not involve e_R whereas electromagnetism does, and so to have a gauge theory involving both weak and electromagnetic interactions we must add an extra current J_μ^Y to J_μ^3 . The simplest approach is to write

$$J_\mu^{em} = J_\mu^3 + \frac{1}{2} J_\mu^Y , \quad (2.11)$$

then putting in the expressions for J_μ^{em} and J_μ^3 we have

$$\begin{aligned} J_\mu^Y &= -\bar{\chi}_L \gamma_\mu \chi_L - 2\bar{e}_R \gamma_\mu e_R \\ &= -\bar{\nu}_L \gamma_\mu \nu_L - \bar{e}_L \gamma_\mu e_L - 2\bar{e}_R \gamma_\mu e_R . \end{aligned} \quad (2.12)$$

In virtue of the above identity between J_μ^{em} , J_μ^3 and J_μ^Y the corresponding charges, Q (electric charge in units of e), T^3 (third component of weak isospin) and Y (termed hypercharge) satisfy

$$Q = T^3 + \frac{Y}{2} . \quad (2.13)$$

This is identical to the Gell-Mann Nishijima relation obtained in the quark model of hadrons. The $\frac{1}{2}$ coefficient in front of J_μ^Y is purely conventional. T^3 , Q and Y may be read off from the coefficients of the $\bar{\nu}_L \gamma_\mu \nu_L$, $\bar{e}_L \gamma_\mu e_L$ and $\bar{e}_R \gamma_\mu e_R$ terms in J_μ^3 , J_μ^{em} and J_μ^Y above. The charge assignments (T, T^3, Q, Y) for the particles in the model are

$$\begin{aligned} \nu_L &= \left(\frac{1}{2}, \frac{1}{2}, 0, -1 \right) \\ e_L &= \left(\frac{1}{2}, -\frac{1}{2}, -1, -1 \right) \\ e_R &= (0, 0, -1, -2) \end{aligned} \quad (2.14)$$

Each generation of leptons will have a similar weak isospin doublet with the same quantum numbers,

$$\begin{pmatrix} \nu_e \\ e^- \end{pmatrix}_L, \begin{pmatrix} \nu_\mu \\ \mu^- \end{pmatrix}_L, \begin{pmatrix} \nu_\tau \\ \tau^- \end{pmatrix}_L. \quad (2.15)$$

We have an $SU(2)_L \times U(1)_Y$ structure where the generators of $U(1)_Y$ commute with those of $SU(2)_L$. This implies that members of an isospin doublet must have the same hypercharge.

We have the following commutation relations for the generators T^i, Q, Y ($i = 1, 2, 3$)

$$[T^i, Y] = 0, [Q, Y] = 0, [Q, T^i] = i\epsilon_{3ij}T^j, \quad (2.16)$$

so Q, T^3, Y , form a mutually commuting set of generators, but only **two** are independent because of the relation $Q = T^3 + \frac{Y}{2}$. The maximum number of independent mutually commuting generators defines the **rank** of the group. $SU(2)_L \times U(1)_Y$ has rank 2.

Notice that $U(1)_Y$ is chiral since e_L^- and e_R^- have **different** hypercharges whereas the electromagnetic charges are the same. To complete the specification of an $SU(2)_L \times U(1)_Y$ gauge theory invariant under local gauge transformations, we need to introduce suitable vector fields to couple to these currents.

QED is based on the interaction $-eJ_\mu^{em}A_\mu$ of the electromagnetic current $Q\bar{\psi}\gamma^\mu\psi$ with the photon field A_μ . This leads to a term in the Lagrangian $\bar{\psi}\gamma^\mu(i\partial_\mu + eA_\mu)\psi$. Analogously we introduce an isotriplet of vector gauge bosons W_μ^i , ($i = 1, 2, 3$), to gauge the $SU(2)_L$ symmetry with coupling g and a vector boson B_μ to gauge the $U(1)_Y$ symmetry with coupling $g'/2$. The interaction (analogous to QED) will be $-gJ^\mu W_\mu^i - \frac{g'}{2}J^\mu B_\mu$, leading to the lepton-gauge boson portion of \mathcal{L} ,

$$\mathcal{L}(e) = \bar{\chi}_L \gamma^\mu [i\partial_\mu - g \left(\frac{1}{2}\right) \vec{\tau} \cdot \vec{W}_\mu - \frac{g'}{2}(-1)B_\mu] \chi_L + \bar{e}_R \gamma^\mu [i\partial_\mu - \frac{g'}{2}(-2)B_\mu] e_R. \quad (2.17)$$

The $(\frac{1}{2}), (-1), (-2)$ in brackets are, respectively, the weak isospin of the doublet χ_L , $Y(e_L)$, and $Y(e_R)$. The notation $\vec{\tau} \cdot \vec{W}_\mu$ is shorthand for $\tau^i W_\mu^i = \tau^1 W_\mu^1 + \tau^2 W_\mu^2 + \tau^3 W_\mu^3$. The full lepton-gauge boson Lagrangian will contain $\sum_{l=e,\mu,\tau} \mathcal{L}(l)$, a sum over the three generations.

The $SU(2)_L$ and $U(1)_Y$ gauge transformations under which $\mathcal{L}(l)$ is invariant are

$$\begin{aligned} \chi_L &\rightarrow \chi'_L = \exp[-ig\frac{\vec{\tau}}{2} \cdot \vec{\Delta} + i\frac{1}{2}g'\Lambda] \chi_L \\ e_R &\rightarrow e'_R = \exp(ig'\Lambda) e_R \end{aligned}$$

$$\begin{aligned}
\vec{W}_\mu \rightarrow \vec{W}'_\mu &= \vec{W}_\mu + g\vec{\Delta} \times \vec{W}_\mu + \partial_\mu \vec{\Delta} \\
B_\mu \rightarrow B'_\mu &= B_\mu + \partial_\mu \Lambda .
\end{aligned} \tag{2.18}$$

Here $\Lambda(x)$ specifies the local $U(1)_Y$ gauge transformations and $\vec{\Delta}(x) = (\Delta^1(x), \Delta^2(x), \Delta^3(x))$ the local $SU(2)_L$ gauge transformations. The transformation of the \vec{W}_μ field is for an **infinitesimal** $SU(2)_L$ gauge transformation. Explicitly $W_\mu^{i'} = W_\mu^i + g\epsilon_{ijk}\Delta^j W_\mu^k + \partial_\mu \Delta^i$.

Separating off the interaction piece of $\mathcal{L}(l)$ we have

$$\mathcal{L}_I = \bar{\chi}_L \gamma^\mu [-g \frac{1}{2} \vec{\tau} \cdot \vec{W}_\mu + \frac{1}{2} g' B_\mu] \chi_L + \bar{e}_R \gamma^\mu g' B_\mu e_R . \tag{2.19}$$

We want to decompose this into a charged current (exchange of electrically charged W^\pm) and a neutral current (exchange of electrically neutral Z^0 .)

$$\mathcal{L}_I = \mathcal{L}_{CC} + \mathcal{L}_{NC} . \tag{2.20}$$

Consider the $\vec{\tau} \cdot \vec{W}_\mu$ term in \mathcal{L}_I . We have

$$\begin{aligned}
\frac{1}{2}(\vec{\tau} \cdot \vec{W}_\mu) &= \frac{\tau^1}{2} W_\mu^1 + \frac{\tau^2}{2} W_\mu^2 + \frac{\tau^3}{2} W_\mu^3 \\
&= \frac{1}{\sqrt{2}}(\tau^+ W_\mu^+ + \tau^- W_\mu^-) + \frac{\tau^3}{2} W_\mu^3 .
\end{aligned} \tag{2.21}$$

Here we have defined the charged vector fields $W_\mu^\pm = \frac{1}{\sqrt{2}}(W_\mu^1 \mp iW_\mu^2)$. The W_μ^3 term is neutral and so belongs in \mathcal{L}_{NC} . We therefore have

$$\begin{aligned}
\mathcal{L}_{CC} &= -\frac{g}{\sqrt{2}}[J_\mu^+ W^{+\mu} + J_\mu^- W^{-\mu}] \\
&= \bar{\chi}_L \gamma^\mu [-\frac{g}{\sqrt{2}}(\tau^+ W_\mu^+ + \tau^- W_\mu^-)] \chi_L .
\end{aligned} \tag{2.22}$$

So the $V - A$ charge raising and lowering currents of Eq.(2.7) couple to the charged W_μ^\pm fields. The rest of \mathcal{L}_I gives us

$$\begin{aligned}
\mathcal{L}_{NC} &= -gJ_\mu^3 W^{3\mu} - \frac{g'}{2} J_\mu^Y B^\mu \\
&= \bar{\chi}_L \gamma^\mu [-\frac{g}{2} \tau^3 W_\mu^3 + \frac{g'}{2} B_\mu] \chi_L + \bar{e}_R \gamma^\mu g' B_\mu e_R .
\end{aligned} \tag{2.23}$$

The next step is to identify the physical neutral vector fields Z_μ and A_μ . We therefore write W_μ^3 and B_μ as an orthogonal mixture of Z_μ and A_μ .

$$\begin{pmatrix} W_\mu^3 \\ B_\mu \end{pmatrix} = \begin{pmatrix} \cos \theta_w & \sin \theta_w \\ -\sin \theta_w & \cos \theta_w \end{pmatrix} \begin{pmatrix} Z_\mu \\ A_\mu \end{pmatrix} \tag{2.24}$$

The angle θ_w is the **weak mixing angle**. So in terms of Z_μ and A_μ

$$\mathcal{L}_{NC} = -gJ_\mu^3[\cos\theta_w Z^\mu + \sin\theta_w A^\mu] - \frac{g'}{2}J_\mu^Y[-\sin\theta_w Z^\mu + \cos\theta_w A^\mu] . \quad (2.25)$$

We must have that $J_\mu^{em} = J_\mu^3 + \frac{1}{2}J_\mu^Y$ is coupled to A_μ with strength e , so we need

$$\mathcal{L}_{NC} = -eA^\mu(J_\mu^3 + \frac{1}{2}J_\mu^Y) + \dots \quad (2.26)$$

So both $J_\mu^3 A^\mu$ and $\frac{1}{2}J_\mu^Y A^\mu$ terms must have coefficient $-e$ implying that

$$g \sin\theta_w = g' \cos\theta_w = e , \quad (2.27)$$

or equivalently

$$\frac{1}{g^2} + \frac{1}{g'^2} = \frac{1}{e^2} . \quad (2.28)$$

We then have

$$\mathcal{L} = -eJ_\mu^{em} A^\mu + Z^\mu[-g \cos\theta_w J_\mu^3 - g' \sin\theta_w J_\mu^3 + g' \sin\theta_w J_\mu^{em}] , \quad (2.29)$$

where J_μ^Y has been eliminated using $J_\mu^Y = 2(J_\mu^{em} - J_\mu^3)$. The terms in the square bracket coefficient of Z^μ can then be written as

$$\left[-g \frac{\cos^2\theta_w}{\cos\theta_w} J_\mu^3 - g \frac{\sin^2\theta_w}{\cos\theta_w} J_\mu^3 + g \frac{\sin^2\theta_w}{\cos\theta_w} J_\mu^{em} \right] \quad (2.30)$$

where $g' = g \sin\theta_w / \cos\theta_w$ has been used. Then setting $\sin^2 + \cos^2 = 1$ we get

$$\mathcal{L}_{NC} = -eJ_\mu^{em} A^\mu - \frac{g}{\cos\theta_w} [J_\mu^3 - \sin^2\theta_w J_\mu^{em}] Z^\mu . \quad (2.31)$$

So finally assembling all this we have

$$\mathcal{L}_I = -\frac{g}{\sqrt{2}}[J_\mu^+ W^{+\mu} + J_\mu^- W^{-\mu}] - eJ_\mu^{em} A^\mu - \frac{g}{\cos\theta_w} [J_\mu^3 - \sin^2\theta_w J_\mu^{em}] Z^\mu . \quad (2.32)$$

Expressing the currents in terms of the full fermion fields ν, e we obtain

$$\begin{aligned} \mathcal{L}_I = & -\frac{g}{\sqrt{2}}[\bar{\nu}\gamma_\mu \frac{1}{2}(1-\gamma_5)e W^{+\mu} + \bar{e}\gamma_\mu \frac{1}{2}(1-\gamma_5)\nu W^{-\mu}] + e(\bar{e}\gamma_\mu e A^\mu) \\ & - \frac{g}{2\cos\theta_w} \left[\bar{\nu}\gamma_\mu \frac{1}{2}(1-\gamma_5)\nu - \bar{e}\gamma_\mu \frac{1}{2}(1-\gamma_5)e + 2\sin^2\theta_w \bar{e}\gamma_\mu e \right] Z^\mu . \end{aligned} \quad (2.33)$$

From the coefficients of the $\bar{l}lV$ terms ($l = e, \nu$, $V = A(\gamma), W^\pm, Z$) multiplied by i we obtain the fermion-gauge boson vertex factors given in the Appendix.

2.1 Kinetic Energy Terms for Glashow's Model

To complete the Glashow model Lagrangian we need $SU(2)_L \times U(1)_Y$ gauge invariant kinetic energy terms for the vector boson fields. In QED we have the kinetic energy term $-\frac{1}{4}F_{\mu\nu}F^{\mu\nu}$ with $F_{\mu\nu} = \partial_\mu A_\nu - \partial_\nu A_\mu$. The relevant terms for the W_μ^i fields (\mathcal{L}_W) and B_μ (\mathcal{L}_B) are

$$\mathcal{L}_W = -\frac{1}{4}\vec{W}_{\mu\nu} \cdot \vec{W}^{\mu\nu} = -\frac{1}{4}\sum_i (\vec{W}_{\mu\nu})^i (\vec{W}^{\mu\nu})^i, \quad (2.34)$$

where

$$\vec{W}_{\mu\nu} = \partial_\mu \vec{W}_\nu - \partial_\nu \vec{W}_\mu - g\vec{W}_\nu \times \vec{W}_\mu, \quad (2.35)$$

and

$$\vec{W}_{\mu\nu}^i = \partial_\mu W_\nu^i - \partial_\nu W_\mu^i - gW_\mu^k W_\nu^l \epsilon_{ikl}. \quad (2.36)$$

Explicitly in terms of the fields W_μ^i ($i = 1, 2, 3$) which gauge $SU(2)_L$. For the $U(1)_Y$ field B_μ one has the Abelian field strength tensor $B_{\mu\nu} = \partial_\mu B_\nu - \partial_\nu B_\mu$, and the kinetic energy term

$$\mathcal{L}_B = -\frac{1}{4}B_{\mu\nu}B^{\mu\nu}. \quad (2.37)$$

These terms can of course be rewritten in terms of the physical fields W^+, W^-, Z_μ, A_μ .

$$\begin{aligned} W_\mu^1 &= \frac{1}{\sqrt{2}}(W_\mu^+ + W_\mu^-) \\ W_\mu^2 &= \frac{i}{\sqrt{2}}(W_\mu^- - W_\mu^+) \\ W_\mu^3 &= \cos\theta_w Z_\mu + \sin\theta_w A_\mu \\ B_\mu &= \cos\theta_w A_\mu - \sin\theta_w Z_\mu. \end{aligned} \quad (2.38)$$

Having so rewritten \mathcal{L}_W and \mathcal{L}_B we can pick out the $(\partial_\mu V)VV$ and $VVVV$ cross terms in the physical fields. The Feynman Rules are in momentum space so $i\partial_\mu V$ should be replaced by $p_\mu V$, where p_μ is the momentum of the vector boson V . We have therefore generated the three and four-point self-interactions of W^\pm , Z and γ . The relevant Feynman Rules are given in the Appendix.

We now have all the Feynman rules for the Glashow model Lagrangian

$$\mathcal{L} = \sum_{l=e,\mu,\tau} \mathcal{L}(l) + \mathcal{L}_W + \mathcal{L}_B. \quad (2.39)$$

Notice that there are no mass terms. If we want to have an $SU(2)_L \times U(1)_Y$ gauge invariant theory we cannot have them! For instance a mass term for the field B_μ would be $\frac{1}{2}M_B^2 B_\mu B^\mu$. Under the local gauge transformation in Eq.(2.18) $B_\mu \rightarrow B'_\mu = B_\mu + \partial_\mu \Lambda$ it is obvious

that $\frac{1}{2}M_B^2 B_\mu B^\mu \neq \frac{1}{2}M_B^2 B'_\mu B'^\mu$. Similarly for a term involving $M_W^2 = M_W^2 \vec{W}_\mu \vec{W}^\mu$ under an $SU(2)_L$ gauge transformation. This comment would apply in QED and forbid the photon mass term $\frac{1}{2}M_\gamma^2 A_\mu A^\mu$, of course this is not a problem since we know experimentally that $M_\gamma = 0$ and that photons are massless particles. A Dirac mass term for the leptons is also disallowed since $m\bar{\psi}\psi = m(\bar{\psi}_R\psi_L + \bar{\psi}_L\psi_R)$, written in terms of chiral L and R components. This is gauge invariant in QED which is L/R symmetric, but in the chiral $SU(2)_L \times U(1)_Y$ theory ψ_R and ψ_L have **different** gauge transformations in Eq.(2.18). Simply adding mass terms by brute force would lead to a sick theory. For massless vector bosons, e.g a photon in QED, one only has transverse polarization degrees of freedom, gauge invariance implies the absence of the longitudinal (L) modes. For massive W bosons one could consider the scattering of longitudinally polarized W pairs, $W_L^+ W_L^- \rightarrow W_L^+ W_L^-$. The propagator for a massive vector boson of virtuality q^2 involves $(g_{\mu\nu} - q_\mu q_\nu / M_W^2) / (q^2 - M_W^2)$. The longitudinally polarized W bosons are described by polarization vectors with $\epsilon_\mu^L \rightarrow \frac{q_\mu}{M_W}$ as $q^2 \rightarrow \infty$, so the propagator approaches a constant at large q^2 . This implies that the longitudinally polarized W scattering grows like the square of the c.m. energy and unitarity is violated since at most a logarithmic growth is allowed. We therefore need to generate mass more subtly. One possibility is to exploit the so-called Higgs mechanism suggested by Peter Higgs in 1964 and motivated by the generation of Cooper pairs in superconductivity, involving the concept of spontaneous symmetry breaking.

3 Spontaneous Symmetry Breaking

In what follows we shall introduce the concept of Spontaneous Symmetry Breaking (SSB) using the physical example of the Heisenberg spin chain model for a ferromagnet. This involves spontaneous breaking of rotational invariance. Treated in Landau mean field theory we shall see that the Free Energy of the ferromagnet below the critical Curie temperature T_c has a form similar to the wine-bottle or mexican-hat potential which we shall use later in the context of breaking local Gauge Symmetry. We will develop this idea via a series of toy models involving a complex doublet of scalar fields, first discussing SSB of a global gauge symmetry and then the more relevant SSB of local gauge invariance.

3.1 The Heisenberg Ferromagnet

We consider a ferromagnetic material in a zero external magnetic \vec{B} field. The Hamiltonian of the system is given by

$$H = -\frac{1}{2}J \sum_{(i,j)} \vec{\sigma}_i \cdot \vec{\sigma}_j , \quad (3.1)$$

where the sum is over nearest-neighbour pairs of spins (i, j) , $\vec{\sigma}_i$ denoting the spin on site i . This Hamiltonian is rotationally invariant so that it commutes with the unitary rotation operator of three-dimensional spatial rotations, $U(R)$.

$$U(R)H = HU(R) . \quad (3.2)$$

However, below a critical temperature T_c , the Curie temperature ($T_c = 1043$ K for Iron), the ground state of the system has an overall net magnetization $\vec{M} \neq 0$. This overall magnetization will be in a particular direction, and hence the rotational invariance has been broken. Heating up the ferromagnet so that $T > T_c$ one finds that above the Curie temperature the overall magnetization vanishes $\vec{M} = 0$ as the magnetic domains are randomized, and the system is rotationally invariant. Cooling down below T_c selects a new non-zero magnetization. It is interesting to study the free energy, F , of the ferromagnet. This may be analysed using Landau mean field theory. One finds

$$F = VN \left(\frac{T - T_c}{T_c} |\vec{M}|^2 + \beta |\vec{M}|^4 \right) . \quad (3.3)$$

Here V is the volume, N is a degeneracy of states normalization factor. $\beta > 0$ is a parameter. Plotting F versus $|\vec{M}|$ for $T > T_c$ reveals a monotonically increasing curve with a minimum at $|\vec{M}| = 0$. For $T < T_c$, however, one has a non-trivial minimum at $|\vec{M}| \neq 0$. So the system has a degenerate set of rotationally equivalent ground states. Rotating the $T < T_c$ curve around the F axis one finds a surface of the same form as the famous “wine-bottle” or “mexican hat” potential which we shall encounter in the Higgs Mechanism.

3.2 SSB of gauge symmetry-general considerations

The analogue of the ground state in the ferromagnet example will be the field theory vacuum. Crucially physical symmetries such as rotational and translational invariance must hold for the vacuum state. We want to spontaneously break the **internal** gauge symmetry leaving rotational invariance unbroken. If the vacuum is specified by a (Higgs) field we require a **scalar** field with $J = 0$, otherwise the vacuum has an intrinsic angular momentum and rotational invariance would be broken. We should therefore require a scalar operator $\hat{\phi}(x)$

with some non-vanishing vacuum expectation value (vev) $\phi_c(x)$,

$$\langle 0 | \hat{\phi}(x) | 0 \rangle = \phi_c(x) \neq 0 . \quad (3.4)$$

For translational invariance we must have a **constant** vev $\phi_c(x) = v$, so that

$$\langle 0 | \hat{\phi}(x) | 0 \rangle = v . \quad (3.5)$$

We now turn to some specific toy models of SSB involving complex scalar fields.

3.3 SSB of a global Gauge Symmetry: Nambu-Goldstone mechanism

We consider the Lagrangian

$$\mathcal{L} = (\partial_\mu \phi)^* \partial^\mu \phi - \mu^2 \phi^* \phi + \lambda (\phi \phi^*)^2 . \quad (3.6)$$

This has a global gauge invariance under $\phi \rightarrow \phi' = e^{i\alpha} \phi$ with α a constant. ϕ is a complex scalar field with real components ϕ_1 and ϕ_2 ,

$$\phi = \frac{1}{\sqrt{2}} (\phi_1 + i\phi_2) . \quad (3.7)$$

We can then write \mathcal{L} as

$$\mathcal{L} = \frac{1}{2} \partial_\mu \phi_1 \partial^\mu \phi_1 + \frac{1}{2} \partial_\mu \phi_2 \partial^\mu \phi_2 - V(\phi) , \quad (3.8)$$

where the scalar potential $V(\phi)$ is

$$V(\phi) = \frac{1}{2} \mu^2 (\phi_1^2 + \phi_2^2) - \frac{\lambda}{4} (\phi_1^2 + \phi_2^2)^2 . \quad (3.9)$$

We can distinguish between two cases. If $\lambda < 0$ and $\mu^2 > 0$ there is an overall minimum of $V(\phi)$ at $\phi_1 = \phi_2 = 0$. The term $-\mu^2 \phi^* \phi$ is then a conventional mass term for a scalar particle, as in the Klein-Gordon Lagrangian

$$\mathcal{L}_{\text{KG}} = \frac{1}{2} \partial_\mu \phi \partial^\mu \phi - \frac{1}{2} m^2 \phi^2 . \quad (3.10)$$

If, however, $\lambda < 0$ and also $\mu^2 < 0$ then we have a “wrong-sign” (imaginary) mass term. The true vacuum is no longer at $\phi = 0$, we obtain the mexican-hat (wine-bottle) potential with a degenerate circle of minima in the $\phi_1 - \phi_2$ plane. Introducing $X^2 = \phi_1^2 + \phi_2^2$ we find the minimum of

$$V(\phi) = \frac{\mu^2}{2} X^2 - \frac{\lambda}{4} X^4 \quad (3.11)$$

when

$$\frac{dV}{dX} = (\mu^2 - \lambda X^2)X = 0 \quad (3.12)$$

corresponding to

$$X^2 = \phi_1^2 + \phi_2^2 = \frac{\mu^2}{\lambda} \equiv v^2 \quad (3.13)$$

The minimum of the potential is

$$V|_{min} = \frac{\lambda}{4} < 0 . \quad (3.14)$$

A gauge transformation moves one around the degenerate circle of minima. By picking a particular vacuum state defined by a non-zero vev one spontaneously breaks the gauge invariance. We shall choose for simplicity to give a non-zero vev to the ϕ_1 direction with ϕ_2 having a zero vev.

$$\langle 0|\phi_1|0\rangle = v \quad \langle 0|\phi_2|0\rangle = 0 . \quad (3.15)$$

Correspondingly

$$\langle 0|\phi|0\rangle = \frac{v}{\sqrt{2}} . \quad (3.16)$$

We now rewrite the field ϕ in terms of new fields ξ and η reflecting the deviation from this *true vacuum* state,

$$\phi(x) = \frac{1}{\sqrt{2}}(v + \xi(x) + i\eta(x)) . \quad (3.17)$$

Rewriting $V(\phi)$ in terms of ξ and η we find

$$\begin{aligned} V(\phi) &= \frac{\mu^2}{2}[v^2 + \xi^2 + 2v\xi + \eta^2] - \frac{\lambda}{4}[v^2 + \xi^2 + 2v\xi + \eta^2]^2 \\ &= \frac{\mu^2}{2}[v^2 + \xi^2 + 2v\xi + \eta^2] - \frac{\mu^2}{4v^2}[v^4 + 4v^3\xi + 6v^2\xi^2 + 2v^2\eta^2] + \dots \\ &= -\mu^2\xi^2 + \dots \end{aligned} \quad (3.18)$$

Here the ellipsis denotes constant, cubic and quartic terms which we shall ignore. Substituting this back into the Lagrangian we have

$$\mathcal{L} = \frac{1}{2}\partial_\mu\xi\partial^\mu\xi + \frac{1}{2}\partial_\mu\eta\partial^\mu\eta + \mu^2\xi^2 + \dots \quad (3.19)$$

We see that we have a *correct* sign mass term, $\mu^2\xi^2$, for the ξ scalar boson corresponding to $m_\xi = \sqrt{-2\mu^2}$ (recall that $\mu^2 < 0$). ξ is the **Higgs boson** and corresponds to the field direction given a non-zero vev v . We have a massless η scalar boson. This is the **Goldstone Boson** which corresponds to a field direction given a zero vev. Thinking of these field directions as analogous to normal modes the Higgs excitations are around the circle of minima, whereas the Goldstone excitations are around the bottom of the well.

3.4 SSB of local Gauge Symmetry

We now consider the same scalar Lagrangian as in Eq.(3.6), but rewritten using the covariant derivative

$$D_\mu = \partial_\mu + ieA_\mu \quad (3.20)$$

Where under the local gauge transformation $\phi \rightarrow \phi' = e^{i\alpha(x)}\phi$ we have $A_\mu \rightarrow A'_\mu = A_\mu - \frac{1}{e}\partial_\mu\alpha(x)$. We have the locally gauge invariant Lagrangian

$$\mathcal{L} = (\partial_\mu - ieA_\mu)\phi^*(\partial_\mu + ieA_\mu)\phi - \mu^2\phi^*\phi + \lambda(\phi^*\phi)^2 - \frac{1}{4}F_{\mu\nu}F^{\mu\nu} . \quad (3.21)$$

We will perform SSB in exactly the same way as in the previous example so that ϕ_1 acquires a vev, and ϕ_2 is the Goldstone mode which doesn't. Substituting $\phi(x) = \frac{1}{\sqrt{2}}(v + \xi(x) + i\eta(x))$ into the Lagrangian then yields

$$\begin{aligned} \mathcal{L} &= \frac{1}{2}(\partial_\mu - ieA_\mu)(v + \xi - i\eta)(\partial^\mu + ieA_\mu)(v + \xi + i\eta) + \mu^2\phi^2 + \dots \\ &= \frac{1}{2}(\partial_\mu\eta)^2 + \frac{1}{2}(\partial_\mu\xi)^2 + \frac{1}{2}e^2A^\mu A_\mu v^2 + evA^\mu\partial_\mu\eta + \mu^2\xi^2 + \dots \end{aligned} \quad (3.22)$$

We see that we have successfully produced a mass term for the A_μ field, $\frac{1}{2}M_A^2A_\mu A^\mu$ with $M_A = ev$. We also have a massive Higgs ξ with $m_\xi = \sqrt{-2\mu^2}$. Less easy to interpret is the $+evA^\mu\partial_\mu\eta$ cross-term. The clue to how this unwanted cross-term can be removed lies in counting the number of field degrees of freedom before and after SSB. Rewriting the fields by identifying a different non-trivial vacuum cannot change this number. However, before SSB we have two longitudinal polarization states for the originally massless A_μ field, since the longitudinal polarization state is absent for massless vector particles, there are in addition two scalar fields, so overall we have **four** degrees of freedom before SSB. After SSB the A_μ field is now massive and so acquires an extra longitudinal polarization degree of freedom, so overall we have **five** field degrees of freedom after SSB. The explanation is that the Goldstone scalar field η is an unphysical spurion or ghost field which can be gauged away. We can say that it is “eaten” to provide the extra longitudinal polarization degree of freedom for the A_μ field. To see this we can locally gauge transform $\phi(x) \rightarrow \phi'(x) = e^{-i\eta(x)/v}\phi(x)$,

$$e^{-i\eta(x)/v}\frac{1}{\sqrt{2}}(v + \xi(x) + i\eta(x)) \approx \frac{1}{\sqrt{2}}(v + \xi(x)) , \quad (3.23)$$

where we have dropped $O(\eta^2)$ terms. We see that the η ghost field has been gauged away and is not present in the **unitary gauge**. We can also see that the unwanted cross-term is removed since

$$\frac{1}{2}e^2v^2A_\mu A^\mu + \frac{1}{2}\partial_\mu\eta\partial^\mu\eta + evA^\mu\partial_\mu\eta \quad (3.24)$$

can be rewritten as

$$\frac{1}{2}e^2v^2\left(A_\mu + \frac{1}{ev}\partial_\mu\eta\right)\left(A^\mu + \frac{1}{ev}\partial^\mu\eta\right) = \frac{1}{2}e^2v^2A'_\mu A'^\mu, \quad (3.25)$$

where A'_μ denotes the A_μ field in unitary gauge. In unitary gauge one finally has the Lagrangian

$$\mathcal{L} = \frac{1}{2}\partial_\mu\xi\partial^\mu\xi + \mu^2\xi^2 + \frac{1}{2}e^2v^2A_\mu A^\mu + \dots \quad (3.26)$$

The unitary gauge is not suitable for practical calculations, and one needs to introduce extra Feynman rules for the ghost scalars. We have not listed these rules in the Appendix, which assumes unitary gauge. In the next section we finally move on to discuss SSB for $SU(2)_L \times U(1)_Y$.

4 The Higgs Mechanism for $SU(2)_L \times U(1)_Y$

We begin by defining the $SU(2)_L \times U(1)_Y$ covariant derivative

$$D_\mu = \partial_\mu + \frac{i}{2}g\vec{\tau} \cdot \vec{W}_\mu + ig'\frac{Y}{2}B_\mu. \quad (4.1)$$

We introduce an $SU(2)_L$ doublet of complex scalar Higgs fields

$$\Phi = \begin{pmatrix} \phi^+ \\ \phi^0 \end{pmatrix}. \quad (4.2)$$

The doublet has weak isospin $T = \frac{1}{2}$ and hypercharge $Y = 1$ leading to electromagnetic charges $+1, 0$, for the $T^3 = \pm\frac{1}{2}$ upper and lower members of the doublet (recall $Q = T^3 + Y/2$).

In terms of real scalar fields ϕ_i one has

$$\phi^+ = \frac{\phi_1 + i\phi_2}{\sqrt{2}}, \quad \phi^0 = \frac{\phi_3 + i\phi_4}{\sqrt{2}}. \quad (4.3)$$

We then add to the massless Glashow model Lagrangian of Eq.(2.39) the scalar contribution

$$\mathcal{L}_\Phi = (D_\mu\Phi)^\dagger D^\mu\Phi - V(\Phi). \quad (4.4)$$

The conjugate Φ^\dagger contains the antiparticles $(\phi^-\bar{\phi}^0)$.

The most general $SU(2)_L \times U(1)_Y$ invariant and renormalisable scalar potential $V(\Phi)$ is

$$V(\Phi) = \mu^2(\Phi^\dagger\Phi) - \lambda(\Phi^\dagger\Phi)^2. \quad (4.5)$$

We arrange that as before $\lambda < 0$ and $\mu^2 < 0$ so that \mathcal{L}_Φ contains a wrong-sign $-\mu^2\Phi^\dagger\Phi$ mass term. $V(\Phi)$ is then bounded below so there will be an $SU(2)_L \times U(1)_Y$ invariant manifold of minima lying below $V(\Phi) = 0$, and we obtain the “wine-bottle” or “mexican hat” potential. \mathcal{L}_Φ is invariant under the $SU(2)_L \times U(1)_Y$ gauge transformations

$$\Phi \rightarrow \Phi' = \exp[-ig\frac{\vec{\tau}}{2} \cdot \Delta - i\frac{g'}{2}\Lambda]\Phi . \quad (4.6)$$

$V(\Phi)$ has minima specified by

$$\frac{dV}{d(\Phi^\dagger\Phi)} = 0 \Rightarrow \mu^2 - 2\lambda(\Phi^\dagger\Phi) = 0 \quad (4.7)$$

so that the degenerate minima are specified by

$$\Phi^\dagger\Phi|_{min} = \frac{\mu^2}{2\lambda} , \quad (4.8)$$

or in terms of real scalar fields ϕ_i

$$\frac{1}{2}(\phi_1^2 + \phi_2^2 + \phi_3^2 + \phi_4^2) = \frac{\mu^2}{2\lambda} . \quad (4.9)$$

We need to spontaneously break $SU(2)_L \times U(1)_Y$ by picking the vacuum from the set of minima of the potential V . We shall choose the vacuum expectation values (vev's) of the fields ϕ_1 , ϕ_2 and ϕ_4 to be zero

$$\langle 0|\phi_1|0\rangle = \langle 0|\phi_2|0\rangle = \langle 0|\phi_4|0\rangle = 0 . \quad (4.10)$$

We assign a non-zero vev v to the field ϕ_3

$$\langle 0|\phi_3|0\rangle^2 = v^2 = \frac{\mu^2}{\lambda} . \quad (4.11)$$

Of course, we should be able to pick the vacuum direction completely arbitrarily, but in order for the photon to remain massless, as it must do after the spontaneous symmetry breaking we need to give a non-zero vev to a neutral field. To do things generally we should only assign charges and other quantum numbers after performing the symmetry breaking. We shall proceed with these particular choices.

We now expand Φ around this chosen vacuum, setting $\phi_3 = H + v$, where H is the neutral scalar Higgs field. It is possible to choose a special gauge, the *unitary gauge*, in which

$$\Phi = \frac{1}{\sqrt{2}} \begin{pmatrix} 0 \\ H + v \end{pmatrix} . \quad (4.12)$$

That is the “Goldstone” fields with **zero vevs**, ϕ_1, ϕ_2, ϕ_4 can be eliminated. To see this we can apply the local gauge transformation $\exp(i\vec{\tau} \cdot \vec{\theta}(x)/v)$ to this unitary gauge form to obtain

$$\Phi' = \frac{1}{\sqrt{2}} \exp \left[\frac{i\vec{\tau} \cdot \vec{\theta}(x)}{v} \right] \begin{pmatrix} 0 \\ H + v \end{pmatrix}. \quad (4.13)$$

Expanding the exponential to $O(\theta)$ we find

$$\begin{aligned} \Phi' &= \frac{1}{\sqrt{2}} \begin{pmatrix} 1 + i\theta_3/v & i(\theta_1 - i\theta_2)/v \\ i(\theta_1 + i\theta_2)/v & 1 - i\theta_3/v \end{pmatrix} \begin{pmatrix} 0 \\ H + v \end{pmatrix} \\ &= \frac{1}{\sqrt{2}} \begin{pmatrix} \theta_2 + i\theta_1 \\ v + H - i\theta_3 \end{pmatrix}. \end{aligned} \quad (4.14)$$

So we see that the unitary gauge field of Eq.(4.12) is a gauge transformation of a general Φ with four independent scalar fields. The idea is that the three originally massless gauge fields W^\pm, Z^0 will become massive and acquire three extra longitudinal polarization degrees of freedom by “eating” the three unphysical Goldstone bosons. Notice that the above gauge transformation accordingly uses only three of the four possible $SU(2)_L \times U(1)_Y$ gauge transformation parameters. $\lambda = 0, \vec{\Delta} = -\frac{2\vec{\theta}}{v}$. As we noted earlier the unitary gauge is unsuited for calculations. One will need to add extra Feynman rules for the Goldstone bosons, analogous to the extra Feynman rules for Fadeev Popov ghost particles in QCD.

We can now evaluate \mathcal{L}_Φ in unitary gauge explicitly and exhibit the spontaneously generated mass terms for W^\pm and Z^0 . From Eq.(3.1) we find

$$\begin{aligned} D_\mu \Phi &= \begin{pmatrix} \partial_\mu + i\frac{g}{2}W_\mu^3 + i\frac{g'}{2}B_\mu & i\frac{g}{2}(W_\mu^1 - iW_\mu^2) \\ i\frac{g}{2}(W_\mu^1 + iW_\mu^2) & \partial_\mu - i\frac{g}{2}W_\mu^3 + i\frac{g'}{2}B_\mu \end{pmatrix} \begin{pmatrix} 0 \\ H + v \end{pmatrix} \\ &= \begin{pmatrix} \frac{ig}{2}(W_\mu^1 - iW_\mu^2)(H + v) \\ (\partial_\mu - \frac{ig}{2}W_\mu^3 + \frac{ig'}{2}B_\mu)(H + v) \end{pmatrix} \\ &= \begin{pmatrix} \frac{ig}{\sqrt{2}}W_\mu^+(H + v) \\ (\partial_\mu - \frac{i}{2}(g \cos \theta_w + g' \sin \theta_w)Z_\mu)(H + v) \end{pmatrix}. \end{aligned} \quad (4.15)$$

Notice that the photon field A_μ is no longer involved, only W_μ^\pm and Z_μ . The photon will therefore not acquire a $\frac{1}{2}M^2 A_\mu A^\mu$ mass term. The masslessness of the photon is guaranteed by the $U(1)_{em}$ gauge invariance of the Lagrangian. $U(1)_{em}$ is a residual symmetry. $SU(2)_L \times U(1)_Y$ has been spontaneously broken to $U(1)_{em}$, and the originally massless W^\pm, Z^0 gauge bosons have acquired masses in the process. The conjugate $(D_\mu \Phi)^\dagger$ is given by

$$(D_\mu \Phi)^\dagger = \frac{1}{\sqrt{2}} \left(-\frac{ig}{\sqrt{2}}W_\mu^-(H + v) \quad (\partial_\mu + \frac{i}{2}(g \cos \theta_w + g' \sin \theta_w)Z_\mu)(H + v) \right). \quad (4.16)$$

We finally obtain in the unitary gauge

$$\mathcal{L}_\Phi = (D_\mu \Phi)^\dagger D^\mu \Phi + \mu^2 \Phi^\dagger \Phi - \lambda (\Phi^\dagger \Phi)^2$$

$$\begin{aligned}
&= \frac{1}{2}\partial_\mu H \partial^\mu H + \frac{1}{4}g^2(H^2 + 2vH + v^2)W_\mu^+ W^{-\mu} \\
&+ \frac{1}{8}(g^2 + g'^2)(H^2 + 2vH + v^2)Z_\mu Z^\mu \\
&+ \mu^2 H^2 + \frac{\lambda}{4}(H^4 + 4vH^3) .
\end{aligned} \tag{4.17}$$

We have used the relation $(g \cos \theta_w + g' \sin \theta_w)^2 = g^2 + g'^2$. The masses of W^\pm and Z can now be read off by identifying the terms $M_W^2 W_\mu^+ W^{-\mu}$ and $\frac{1}{2}M_Z^2 Z_\mu Z^\mu$ in Eq.(4.17). We find

$$M_W = \frac{1}{2}gv \tag{4.18}$$

$$M_Z = \frac{1}{2}(g^2 + g'^2)^{1/2}v = \frac{1}{2}\frac{gv}{\cos \theta_w} . \tag{4.19}$$

For the Higgs scalar we identify the overall H^2 term $(\frac{1}{2}\mu^2 - \frac{3}{2}\lambda v^2)H^2$ coming from $\frac{\mu^2}{2}(H + v)^2 - \frac{\lambda}{4}(H + v)^4$, and recalling that $\mu^2 = \lambda v^2$ we obtain the H^2 coefficient $-\frac{1}{2}M_H^2 = \mu^2$ so that $M_H = \sqrt{-2\mu^2}$. There are also VVH, VVHH and HHH, HHHH Higgs self-interactions. The corresponding Feynman rules and vertex factors are contained in the Appendix.

An immediate consequence of the above vector boson masses is that

$$\frac{M_W}{M_Z} = \cos \theta_w . \tag{4.20}$$

This is often referred to as the “weak $\Delta I = \frac{1}{2}$ rule” and is connected with our choice of a Higgs doublet to perform the spontaneous symmetry breaking.

Notice that from the measured fine structure constant $\alpha = e^2/4\pi$ and the vector boson masses M_W and M_Z we can determine $\sin^2 \theta_w$, v and g , but **not** μ . This means that the Higgs mass M_H is not determined directly by other experimentally measured parameters. We shall return a little later to a discussion of the number of independent Standard Model parameters.

4.1 Yukawa terms for lepton masses

To give charged leptons a mass one adds a so-called Yukawa term to the Lagrangian, $\mathcal{L}_Y(l)$, where $l = e, \mu, \tau$ labels the lepton. We have for instance for an electron

$$\mathcal{L}_Y(e) = -G_e[\bar{\chi}_L \Phi e_R + \bar{e}_R \Phi^\dagger \chi_L] . \tag{4.21}$$

This is $SU(2)_L \times U(1)_Y$ invariant. G_e is the Yukawa coupling. On spontaneous symmetry breaking we have in the unitary gauge

$$\Phi = \frac{1}{\sqrt{2}} \begin{pmatrix} 0 \\ H + v \end{pmatrix}, \quad (4.22)$$

substituting this into $\mathcal{L}_Y(e)$ one has

$$\begin{aligned} \mathcal{L}_Y(e) &= -\frac{G_e}{\sqrt{2}}(v + H)(\bar{e}_L e_R + \bar{e}_R e_L) \\ &= -\frac{G_e}{\sqrt{2}}(H + v)\bar{e}e = -\frac{G_e v}{\sqrt{2}}(\bar{e}) - \frac{G_e}{\sqrt{2}}(\bar{e}eH). \end{aligned} \quad (4.23)$$

From which we can identify the electron mass $m_e = G_e v / \sqrt{2}$, and the lepton-Higgs coupling $g(H\bar{e}e) = m_e/v = gm_e/(2M_W)$. Notice that the ν_L upper element of the doublet does not appear since in unitary gauge the upper entry in Φ is zero, and so as required we do not generate a neutrino mass term or interaction with the Higgs. We see that the coupling between leptons and the Higgs is proportional to the lepton mass, so τ signatures involving the heaviest mass lepton will be important for Higgs searches at colliders. Similarly for quarks $b\bar{b}$, and $t\bar{t}$ signatures will be important. The vertex factor and Feynman rule for the Yukawa term is contained in the Appendix.

4.2 Electroweak quark sector

So far we have just considered the lepton sector. We also need to include a Lagrangian $\mathcal{L}(q)$ to describe electroweak quark interactions. We have six quarks (three generations) u, d, s, c, b, t . $Q_u = Q_c = Q_t = \frac{2}{3}$, and $Q_d = Q_s = Q_b = -\frac{1}{3}$. We can construct $SU(2)_L$ isospin doublets analogous to the leptonic case

$$\chi_L^f = \begin{pmatrix} U_f \\ D_f \end{pmatrix} \quad f = 1, 2, 3 \quad (4.24)$$

Here $U_1 = u, U_2 = c, U_3 = t$ and $D_1 = d, D_2 = s, D_3 = b$. However experimentally one observes $n \rightarrow pe^- \bar{\nu}_e$ and also $\Lambda \rightarrow pe^- \bar{\nu}_e$ decays, corresponding to $d \rightarrow u$ and $s \rightarrow u$ transitions. This implies that the weak interaction eigenstates are mixtures of flavour eigenstates. We therefore replace the above χ_L^f by

$$\chi_L^f = \begin{pmatrix} U_f \\ D'_f \end{pmatrix}, \quad f = 1, 2, 3, \quad (4.25)$$

where D'_f is a flavour rotated mixture

$$D'_f = \sum_{f'=1,2,3} V_{ff'} D_{f'}. \quad (4.26)$$

Here V is a 3×3 unitary matrix ($VV^\dagger = 1$) called the Cabibbo-Kobayashi-Maskawa **CKM** matrix. For two generations we have the Cabibbo model

$$\begin{aligned} D'_1 &= \cos \theta_c d + \sin \theta_c s \\ D'_2 &= -\sin \theta_c d + \cos \theta_c s . \end{aligned} \quad (4.27)$$

Here θ_c is the Cabibbo angle, and experimentally one finds $\theta_c \approx 13$ degrees or $\cos \theta_c \approx 0.97$. The full three generation CKM matrix has the following $|V_{ij}|$ structure for the magnitudes of the elements

$$V = \begin{pmatrix} |V_{ud}| = 0.97 & |V_{us}| = .23 & |V_{ub}| \approx 0 \\ |V_{cd}| = 0.24 & |V_{cs}| = 0.97 & |V_{cb}| = 0.06 \\ |V_{td}| \approx 0 & |V_{ts}| \approx 0 & |V_{tb}| \approx 1 \end{pmatrix} . \quad (4.28)$$

The matrix involves 4 parameters- 3 angles and 1 complex phase. The presence of this complex phase enables CP violation to occur.

In analogy with the leptonic isotriplet of currents one then defines the quark isotriplet

$$J_\mu^{fi} = \bar{\chi}_L^f \gamma_\mu \frac{1}{2} \tau_i \chi_L^f \quad (i = 1, 2, 3) . \quad (4.29)$$

As before $i = 1, 2$ are charged currents, and J_μ^{f3} is a neutral current.

$$\begin{aligned} J_\mu^{f3} &= \frac{1}{2} (\bar{U}_{fL} \gamma_\mu U_{fL} - \bar{D}'_{fL} \gamma_\mu D'_{fL}) \\ &= \frac{1}{2} (\bar{U}_{fL} \gamma_\mu U_{fL} - \bar{D}_{fL} \gamma_\mu D_{fL}) . \end{aligned} \quad (4.30)$$

Notice that D'_{fL} the rotated flavour mixture has been replaced by D_{fL} in the final line. This follows from the unitarity property $VV^\dagger = 1$. It has the important consequence that flavour changing neutral current processes are forbidden. We can now determine the electromagnetic quark currents

$$J_\mu^{f(em)} = \left(\frac{2}{3}\right) \bar{U}_{fR} \gamma_\mu U_{fR} + \left(\frac{2}{3}\right) \bar{U}_{fL} \gamma_\mu U_{fL} + \left(\frac{-1}{3}\right) \bar{D}_{fR} \gamma_\mu D_{fR} + \left(\frac{-1}{3}\right) \bar{D}_{fL} \gamma_\mu D_{fL} . \quad (4.31)$$

Here the $(\frac{2}{3})$, $(-\frac{1}{3})$ in brackets denote the electric charges of the quarks. If we define the hypercharge current J_μ^{fY} in the same way as for the leptons, so that $J_\mu^{f(em)} = J_\mu^{f3} + \frac{1}{2} J_\mu^{fY}$, then we can infer that

$$J_\mu^{fY} = \left(\frac{1}{3}\right) (\bar{U}_{fL} \gamma_\mu U_{fL} + \bar{D}_{fL} \gamma_\mu D_{fL}) + \left(\frac{4}{3}\right) \bar{U}_{fR} \gamma_\mu U_{fR} + \left(\frac{-2}{3}\right) \bar{D}_{fR} \gamma_\mu D_{fR} . \quad (4.32)$$

Again the $(\frac{1}{3})$ etc. numbers in brackets refer to the hypercharges of the particles. One can then read off for each generation U_f , D_f the charges (T, T^3, Q, Y)

$$U_L = \left(\frac{1}{2}, \frac{1}{2}, \frac{2}{3}, \frac{1}{3}\right)$$

$$\begin{aligned}
D_L &= \left(\frac{1}{2}, -\frac{1}{2}, -\frac{1}{3}, \frac{1}{3}\right) \\
U_R &= \left(0, 0, \frac{2}{3}, \frac{4}{3}\right) \\
D_R &= \left(0, 0, -\frac{1}{3}, -\frac{2}{3}\right)
\end{aligned} \tag{4.33}$$

So analogous to $\mathcal{L}(l)$ for leptons one obtains the quark electroweak lagrangian $\mathcal{L}(q)$

$$\begin{aligned}
\mathcal{L}(q) &= \sum_{f=1,2,3} (\bar{\chi}_L^f \gamma^\mu \left[i\partial_\mu - \frac{1}{2} \vec{\tau} \cdot \vec{W}_\mu - \left(\frac{1}{3}\right) B_\mu \right] \chi_L^f \\
&+ \bar{U}_{fR} \gamma^\mu \left[i\partial_\mu - \frac{g'}{2} \left(\frac{4}{3}\right) B_\mu \right] U_{fR} + \bar{D}_{fR} \gamma^\mu \left[i\partial_\mu - \frac{g'}{2} \left(\frac{-2}{3}\right) B_\mu \right] D_{fR}) .
\end{aligned} \tag{4.34}$$

To give masses to the quarks we shall require a corresponding quark Yukawa term $\mathcal{L}_Y(q)$.

$$\mathcal{L}_Y(q) = \sum_{f=1,2,3} -[\bar{\chi}_L^f G_{ff'}^D \Phi D_{f'R} + \bar{\chi}_L^f G_{ff'}^U \Phi^c U_{f'R} + \text{h.c.}] . \tag{4.35}$$

Here the $G_{ff'}^U$ and $G_{ff'}^D$ are the matrix of quark Yukawa couplings. To give a mass to the upper U_{fL} members of the chiral doublet one needs to use the conjugate scalar field

$$\Phi^c = \begin{pmatrix} \bar{\phi}^0 \\ -\phi^- \end{pmatrix} . \tag{4.36}$$

After spontaneous symmetry breaking one has in unitary gauge

$$\Phi^c = \begin{pmatrix} H + v \\ 0 \end{pmatrix} . \tag{4.37}$$

In this way one generates a quark mass matrix and $q\bar{q}H$ interactions. We shall not pursue the details any further.

4.3 SM Lagrangian and independent parameter count

Assembling all the pieces we have discussed we can now arrive at the Glashow-Weinberg-Salam Standard Model Lagrangian

$$\mathcal{L}_{SM} = \mathcal{L}_W + \mathcal{L}_B + \sum_{l=e,\mu,\tau} \mathcal{L}(l) + \sum_{l=e,\mu,\tau} \mathcal{L}_Y(l) + \mathcal{L}(q) + \mathcal{L}_Y(q) + \mathcal{L}_\Phi + \mathcal{L}_{QCD} + \dots . \tag{4.38}$$

The ellipsis denotes further gauge-fixing and ghost contributions. The Standard Model as specified by this Lagrangian has been shown to be renormalisable by 't Hooft and Veltmann. The unitarity problem for $W_L^+ W_L^- \rightarrow W_L^+ W_L^-$ scattering is also cured. It is solved by extra diagrams involving virtual Higgs exchange which now appear due to the WWH interaction

terms.

It is interesting to count how many of the parameters in the Standard Model are independent. There are fifteen parameters overall if we ignore the quark sector, which may be divided into couplings: $e(\alpha), g, g', G_e, G_\mu, G_\tau$. Masses: $M_W, M_Z, M_H, m_e, m_\mu, m_\tau$. Higgs sector parameters μ^2, λ ($v^2 = \frac{\mu^2}{\lambda^2}$), and last but not least the weak mixing angle $\sin^2 \theta_w$. There are clearly many relations between the parameters, such as $M_W = \frac{1}{2}gv$ or $e = g \sin \theta_w$ for instance. It turns out that there are in fact **seven** independent parameters which if specified can then predict all fifteen. One can choose for instance the set $g, g', G_e, G_\mu, G_\tau, \mu^2, \lambda$. Alternatively $\alpha, M_W, M_Z, M_H, m_e, m_\mu, m_\tau$ or $\alpha, \sin^2 \theta_w, M_H, v, G_e, G_\mu, G_\tau$ are possible sets.

Including the electroweak quark sector adds the CKM matrix V (three angles and one complex phase) and mass matrices $m(U), M(D), (m_u, m_c, m_t, m_d, m_s, m_b)$ making $4 + 3 + 3 = 10$ extra parameters. Including QCD we have in addition Λ_{QCD} and the QCD θ -parameter involved in the strong CP problem. So overall there are 19 independent free parameters in $SU(3)_c \times SU(2)_L \times U(1)_Y$.

A model with at least 19 undetermined parameters, in which the particular representations containing fermions and scalars are not compellingly motivated, and with a mysterious replication of three generations, does not seem a likely candidate for a complete theory of everything, even though it has proved consistent with experiment in essentially every detail checked, with the Higgs, confirmed by LHC earlier this year, being the last ingredient to fall into place.

Acknowledgements

It is a pleasure to thank Paul Dauncey for organizing a very enjoyable and productive school. The students were keen and motivated and the atmosphere made for a perfect learning environment.

5 Appendix of Feynman rules

The following pages summarize the Feynman Rules in unitary gauge for one generation of leptons. All the Lagrangian terms needed to derive the vertex factors for the different interactions are contained in these lecture notes.

Feynman Rules in the Unitary Gauge (for one Generation of Leptons)

Propagators:

All propagators carry momentum p .

$$\mu \overset{\text{W}}{\sim} \nu \qquad -i (g_{\mu\nu} - p_\mu p_\nu / M_W^2) / (p^2 - M_W^2)$$

$$\mu \overset{\text{Z}}{\sim} \nu \qquad -i (g_{\mu\nu} - p_\mu p_\nu / M_Z^2) / (p^2 - M_Z^2)$$

$$\mu \overset{\text{A}}{\sim} \nu \qquad -i g_{\mu\nu} / p^2$$

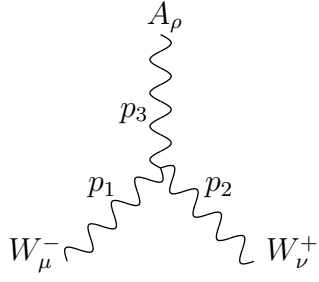
$$\overset{\text{e}}{\longrightarrow} \qquad i (\gamma \cdot p + m_e) / (p^2 - m_e^2)$$

$$\overset{\nu}{\longrightarrow} \qquad i \gamma \cdot p / p^2$$

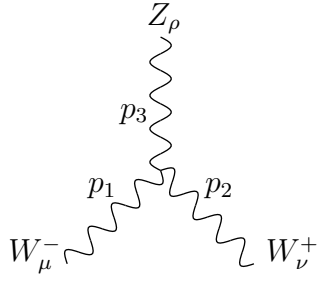
$$\overset{\text{H}}{---} \qquad i / (p^2 - m_H^2)$$

Three-point gauge-boson couplings:

All momenta are incoming

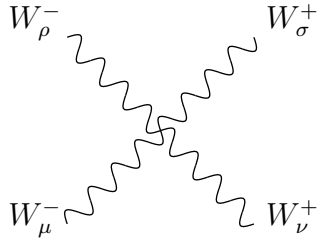


$$i g \sin \theta_W \left((p_1 - p_2)_\rho g_{\mu\nu} + (p_2 - p_3)_\mu g_{\nu\rho} + (p_3 - p_1)_\nu g_{\rho\mu} \right)$$

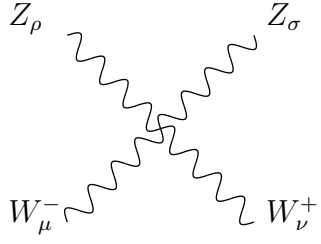


$$i g \cos \theta_W \left((p_1 - p_2)_\rho g_{\mu\nu} + (p_2 - p_3)_\mu g_{\nu\rho} + (p_3 - p_1)_\nu g_{\rho\mu} \right)$$

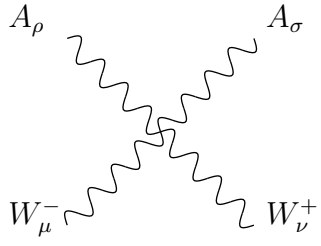
Four-point gauge-boson couplings:



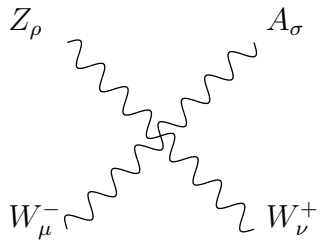
$$i g^2 (2g_{\mu\rho} g_{\nu\sigma} - g_{\mu\nu} g_{\rho\sigma} - g_{\mu\sigma} g_{\nu\rho})$$



$$i g^2 \cos^2 \theta_W (2g_{\mu\nu} g_{\rho\sigma} - g_{\mu\rho} g_{\nu\sigma} - g_{\mu\sigma} g_{\nu\rho})$$

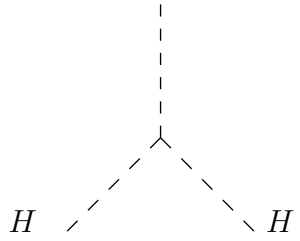


$$i g^2 \sin^2 \theta_W (2g_{\mu\nu} g_{\rho\sigma} - g_{\mu\rho} g_{\nu\sigma} - g_{\mu\sigma} g_{\nu\rho})$$



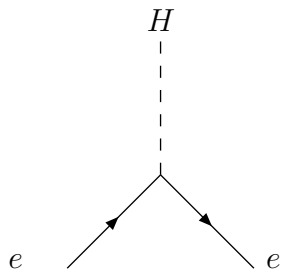
$$i g^2 \cos \theta_W \sin \theta_W (2g_{\mu\nu} g_{\rho\sigma} - g_{\mu\rho} g_{\nu\sigma} - g_{\mu\sigma} g_{\nu\rho})$$

Three-point couplings with Higgs scalars:



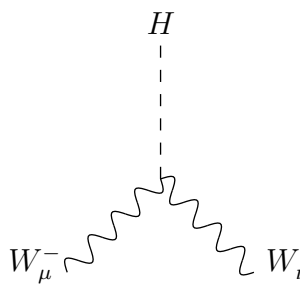
A Feynman diagram representing the trilinear Higgs coupling. It consists of a central vertex from which three dashed lines extend outwards. One dashed line goes vertically upwards, and two others go downwards and outwards at approximately 45-degree angles. Each of the three dashed lines is labeled with the letter H .

$$-\frac{3}{2} i g m_H^2 / M_W$$



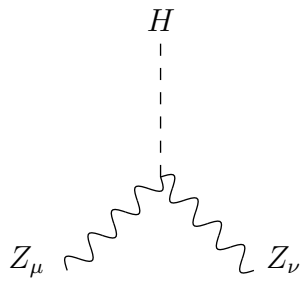
A Feynman diagram representing the Higgs-electron coupling. It consists of a central vertex. A dashed line labeled H extends vertically upwards from the vertex. Two solid lines extend downwards and outwards at approximately 45-degree angles from the vertex. Each solid line has an arrow pointing away from the vertex and is labeled with the letter e .

$$-\frac{1}{2} i g m_e / M_W$$



A Feynman diagram representing the Higgs-WW coupling. It consists of a central vertex. A dashed line labeled H extends vertically upwards from the vertex. Two wavy lines extend downwards and outwards at approximately 45-degree angles from the vertex. The left wavy line is labeled W_μ^- and the right wavy line is labeled W_ν^+ .

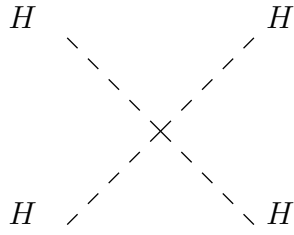
$$i g M_W g_{\mu\nu}$$



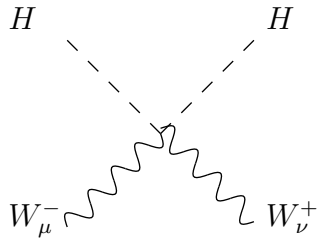
A Feynman diagram representing the Higgs-ZZ coupling. It consists of a central vertex. A dashed line labeled H extends vertically upwards from the vertex. Two wavy lines extend downwards and outwards at approximately 45-degree angles from the vertex. The left wavy line is labeled Z_μ and the right wavy line is labeled Z_ν .

$$i (g / \cos^2 \theta_W) M_W g_{\mu\nu}$$

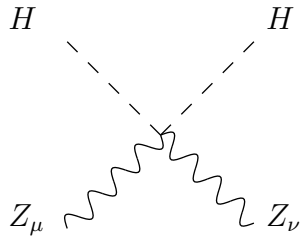
Four-point couplings with Higgs scalars:



$$-\frac{3}{4} i g (m_H^2/M_W^2)$$

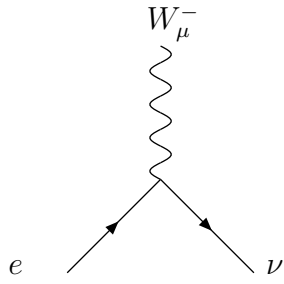


$$\frac{1}{2} i g^2 g_{\mu\nu}$$

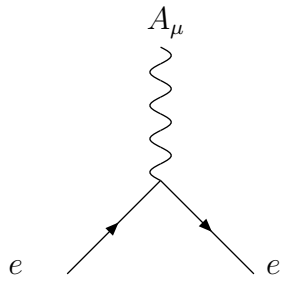


$$\frac{1}{2} i (g^2/\cos^2 \theta_W) g_{\mu\nu}$$

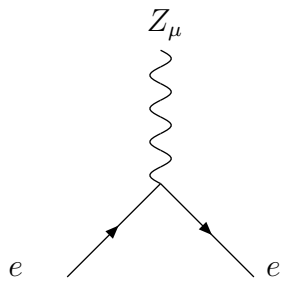
Fermion interactions with gauge bosons:



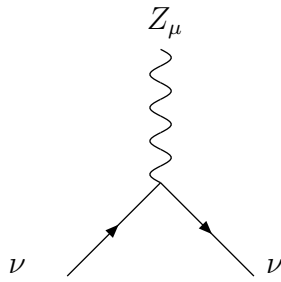
$$-i \left(g/2\sqrt{2} \right) \gamma_\mu (1 - \gamma^5)$$



$$+i g \sin \theta_W \gamma_\mu$$



$$+ \frac{1}{4} i \left(g / \cos \theta_W \right) \gamma_\mu \left(1 - 4 \sin^2 \theta_W - \gamma^5 \right)$$



$$- \frac{1}{4} i \left(g / \cos \theta_W \right) \gamma_\mu (1 - \gamma^5)$$

PHENOMENOLOGY

Dr Simon Badger (University of Durham)

Contents

| | | |
|----------|--|------------|
| 1 | Introduction | 138 |
| 2 | e^+e^- Annihilation..... | 139 |
| 2.1 | Leading Order | 139 |
| 2.1.1 | The Z resonance..... | 140 |
| 2.2 | Higher Order Corrections..... | 142 |
| 2.2.1 | Real Emission..... | 142 |
| 2.2.2 | Virtual Corrections..... | 145 |
| 3 | Running Coupling..... | 147 |
| 3.1 | Higher order calculations | 147 |
| 3.2 | Infrared safety | 148 |
| 3.3 | Event Shapes | 149 |
| 4 | Deep Inelastic Scattering..... | 153 |
| 5 | Hadron Collisions..... | 156 |
| 6 | Jets..... | 158 |
| 6.1 | Cone Algorithms..... | 160 |
| 6.2 | Sequential Recombination Algorithms..... | 161 |
| 6.3 | Jet Cross Sections | 162 |
| 6.4 | Jet Properties..... | 165 |
| 7 | Electroweak Physics | 167 |
| 7.1 | Quantum Corrections to Masses | 169 |
| 7.2 | Electroweak Observables..... | 170 |
| 7.2.1 | W mass measurements | 171 |
| 7.2.2 | ρ parameter | 172 |
| 8 | Higgs Boson | 173 |
| 8.1 | Unitarity | 174 |
| 8.2 | Higgs Searches | 175 |
| 8.3 | The effective Higgs coupling to gluons | 178 |
| 8.4 | Extended Higgs Sectors | 179 |
| 8.4.1 | The Two Higgs Doublet Model..... | 179 |
| 9 | Beyond the Standard Model Physics | 180 |
| 9.1 | Models | 181 |
| 9.1.1 | Grand Unified Theories..... | 181 |
| 9.1.2 | Hierarchy Problem..... | 183 |
| 9.1.3 | Technicolor..... | 183 |
| 9.1.4 | Supersymmetry | 184 |
| 9.1.5 | Extra Dimensions | 190 |
| 9.1.6 | Little Higgs Models..... | 192 |
| 9.1.7 | Unparticles | 192 |
| 9.2 | Beyond the Standard Model Signatures..... | 193 |
| 9.2.1 | Deviations from the Standard Model..... | 193 |
| 9.2.2 | Monojets | 194 |
| 9.2.3 | New Particle Production..... | 194 |
| 9.2.4 | Resonance Production | 195 |

| | | |
|----------|---|------------|
| 9.2.5 | SUSY-like models | 196 |
| 9.2.6 | Model Independent Searches | 199 |
| A | Kinematics and Cross Sections | 200 |
| A.1 | Kinematics..... | 200 |
| A.2 | Cross Sections..... | 201 |
| A.3 | Cross Sections in Hadron Collisions | 202 |
| A.3.1 | Resonance production ($2 \rightarrow 1$ processes) | 202 |
| A.3.2 | $2 \rightarrow 2$ Scattering Processes | 203 |
| B | Flavour Physics..... | 204 |
| C | Color algebra..... | 207 |
| | References..... | 209 |

Phenomenology

Lectures given at the 2016 HEP Summer School

Simon Badger,
IPPP, Durham University.

1 Introduction

Historically the lecture notes for the phenomenology course have consisted of the slides presented in the lectures. These notes are intended to provide additional information, and more mathematical detail, on the more theoretical aspects of the course which don't change from year to year. The recent experimental results, which as the LHC experiments take more and more data change from day-to-day, will continue to be presented solely on the slides used in the lectures.

These notes have been adapted from notes from Daniel Maître and Peter Richardson.

In order to study hadron collisions we need to understand the basics of cross section calculations, Quantum Chromodynamics (QCD) and jets which we will first consider in the simpler environment of e^+e^- and lepton-hadron collisions before we go on to study hadron-hadron collisions.

Unfortunately there is no single good book on modern phenomenology. Two old classics but now a bit dated are:

- *Quarks and Leptons* Halzen and Martin [1];
- *Collider Physics* Barger and Phillips [2].

Two good books, although mainly focused on QCD and probably at a bit too high a level for this course, are:

- *QCD and Collider Physics* Ellis, Stirling and Webber [3];
- *Quantum Chromodynamics* Dissertori, Knowles and Schmelling [4];

and of course the classic on Higgs physics

- *The Higgs Hunter's Guide* Gunion, Haber, Kane and Dawson [5].

In addition the recent reviews:

- *Towards Jetography* [6] which provides a good primer on jet physics;
- *General-purpose event generators for LHC physics* [7] which gives a detailed description of the physics of Monte Carlo event generators;

are good sources of additional information.

2 e^+e^- Annihilation

While electron-positron colliders are less relevant for current phenomenology than they were before, they are a good starting point to discuss many concepts one also finds at hadron colliders.

If we consider what happens when electrons and positrons collide, then the most likely thing is that some hadrons are produced. However, none of the Lagrangians or Feynman rules you've learnt involve hadrons. This is the key issue in most collider physics, we can calculate things for quarks and gluons but we observe hadrons.

2.1 Leading Order

We will start by studying one of the simplest possible processes, e^+e^- annihilation via the exchange of a photon or Z^0 boson, as shown in Fig. 1. This process can produce either



Figure 1: Feynman diagrams for e^+e^- annihilation into leptons and quarks.

quarks or leptons. Unfortunately due to quark confinement we cannot observe free quarks directly, instead quarks and antiquarks will produce hadrons with unit probability. Much of what we will study in this course will be concerned with the question, given that we observe hadrons how do we infer what was going on in the fundamental process involving quarks?

We will start with the simplest example. Given that quarks and antiquarks produce hadrons with unit probability we can measure the cross section for the process $e^+e^- \rightarrow q\bar{q}$, which we can calculate perturbatively, by measuring the cross section for $e^+e^- \rightarrow \text{hadrons}$. This is the case because gluons (which also produce hadrons) do not couple directly to the leptons. This is the basis of most collider phenomenology, we want to measure things using hadrons that we can calculate using partons. The total cross section for e^+e^- annihilation into hadrons is the simplest such observable.

Using the techniques you have learnt in the other courses you can now calculate the total cross section for e^+e^- annihilation. In reality it is more common to study the ratio

$$R \equiv \frac{\sigma(e^+e^- \rightarrow \text{hadrons})}{\sigma(e^+e^- \rightarrow \mu^+\mu^-)}, \quad (1)$$

as this reduces experimental uncertainties. At low energies this process is dominated by photon exchange so we can neglect the Z^0 boson. In this limit

$$\sigma(e^+e^- \rightarrow \mu^+\mu^-) = \frac{4\pi\alpha^2}{3s}, \quad (2)$$

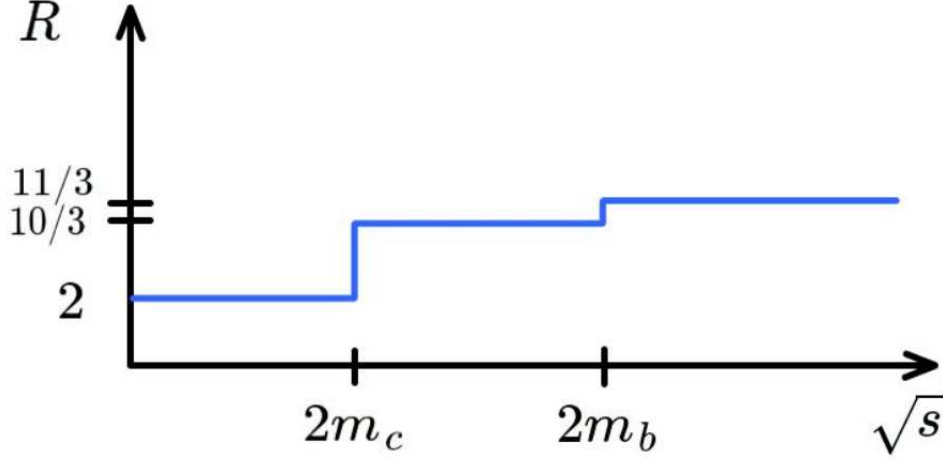


Figure 2: Expected shape for the R ratio.

where s is the centre-of-mass energy of the collision squared. The cross section for the production of quarks is

$$\sigma(e^+e^- \rightarrow \text{hadrons}) = \frac{4\pi\alpha^2}{3s} \sum_q e_q^2 N_c, \quad (3)$$

where e_q is the charge of the quark in units of the positron charge and the sum runs over all quarks for which the centre-of-mass energy $\sqrt{s} > 2m_q$, where m_q is the mass of the quark. Remember we must sum over all the quantum numbers of the quarks so the cross section is multiplied by number of colours, N_c . Therefore for centre-of-mass energies much less than the mass of the Z^0 boson, $\sqrt{s} \ll M_z$,

$$R = \sum_q e_q^2 N_c = N_c \underbrace{\left(\frac{4}{9} + \frac{1}{9} + \frac{1}{9} + \frac{4}{9} + \frac{1}{9} \right)}_{\substack{u,d,s \\ u,d,s,c \\ u,d,s,c,b}}. \quad (4)$$

The expected picture is shown in figure 2. The experimental measurement of this ratio is shown in Fig. 3 as a function of energy showing the thresholds for the production of the charm and bottom quarks. Below the charm threshold there are three active quarks down ($e_d = -\frac{1}{3}$), up ($e_u = \frac{2}{3}$) and strange ($e_s = -\frac{1}{3}$) giving $R = 2$. Above the charm ($e_c = \frac{2}{3}$) threshold $R = \frac{10}{3}$ while above the bottom ($e_b = -\frac{1}{3}$) threshold $R = \frac{11}{3}$.

2.1.1 The Z resonance

For energies $\sqrt{s} \sim m_Z$ we will need to include the effects of the second diagram in Fig. 1. The cross-section will then have three different contributions, the photon background, the

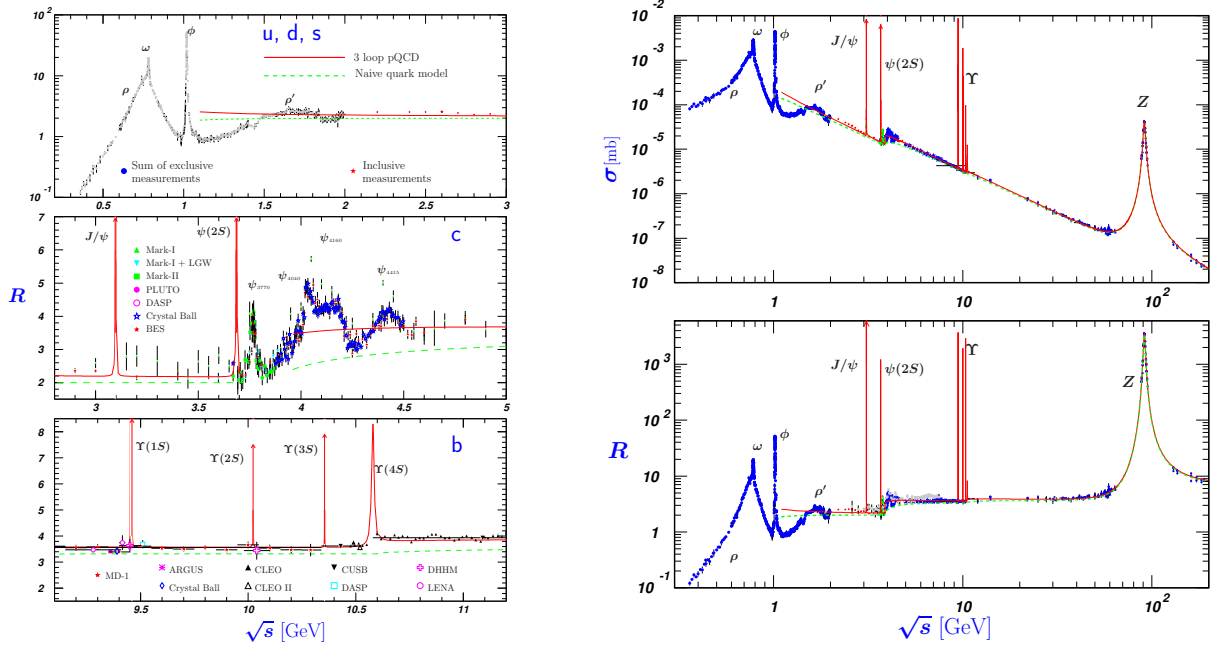


Figure 3: The ratio $R \equiv \frac{\sigma(e^+e^- \rightarrow \text{hadrons})}{\sigma(e^+e^- \rightarrow \mu^+\mu^-)}$ as a function of energy taken from Ref. [8].

Z-boson resonance and the photon-Z interference. The total cross-section, summed and averaged over spins can be written as (e.g. [3]):

$$\sigma(f\bar{f} \rightarrow f'\bar{f}') = \alpha^2 \frac{\pi}{2s} \int_{-1}^1 d(\cos\theta) \left\{ \begin{aligned} &(1 + \cos^2\theta) \left(q_f^2 q_{f'}^2 + \frac{g_Z^2}{4g_e^2} q_f q_{f'} v_f v_{f'} \chi_1 + \frac{g_Z^4}{16g_e^4} (a_f^2 + v_f^2)(a_{f'}^2 + v_{f'}^2) \chi_2 \right) \\ &+ \cos\theta \left(\frac{g_Z^2}{2g_e^2} a_f a_{f'} v_f v_{f'} \chi_1 + \frac{g_Z^4}{2g_e^4} a_f a_{f'} v_f v_{f'} \chi_2 \right) \end{aligned} \right\}$$

where

$$\frac{g_Z}{g_e} = \frac{1}{\cos\theta_w \sin\theta_w} \quad \chi_1 = \frac{s(s - m_Z^2)}{(s - m_Z^2)^2 + m_Z^2 \Gamma_Z^2} \quad \chi_2 = \frac{s^2}{(s - m_Z^2)^2 + m_Z^2 \Gamma_Z^2}$$

The axial ($v_f = T_f^3 - 2q_f \sin^2\theta_w$) and vector ($a_f = T_f^3$) couplings in the Standard Model are given in Table 1. T_f^3 is the 3rd component of the weak isospin as covered in the course on the Standard Model. The terms proportional to χ_2 come from the Z resonance while those proportional to χ_1 come from the photon-Z interference. Γ_Z is the width of the Z boson.

Later we will take a closer look at the EW sector of the Standard Model and use this measurement to find constraints on the number of neutrinos families below the Z mass threshold (see Figure 28).

| | q_f | a_f | v_f |
|--------------------|--------|--------|------------------------------|
| u, c, t | $2/3$ | $1/2$ | $1/2 - 4/3 \sin^2 \theta_w$ |
| d, s, b | $-1/3$ | $-1/2$ | $-1/2 + 2/3 \sin^2 \theta_w$ |
| e, μ, τ | -1 | $-1/2$ | $-1/2 + 2 \sin^2 \theta_w$ |
| ν_e, μ, τ | 0 | $1/2$ | $1/2$ |

Table 1: EW couplings in the Standard Model.

2.2 Higher Order Corrections

When we draw Feynman diagrams we are performing a perturbative expansion in the (hopefully) small coupling constant. Unfortunately the strong coupling often isn't very small, at the Z^0 mass, $\alpha_S(M_Z) = 0.118$. We therefore need to consider higher orders in the perturbative expansion. There are always two types of correction:

- real gluon emission;
- virtual gluon loops.

2.2.1 Real Emission

There are two possible diagrams for gluon emission, see Fig. 4. The matrix element, only



Figure 4: Feynman diagrams for $e^+e^- \rightarrow q\bar{q}g$.

considering photon exchange for simplicity, is

$$\mathcal{M} = e^2 e_q g_s t_{ij}^a \bar{v}(p_b) \gamma_\mu u(p_a) \frac{-g^{\mu\nu}}{q^2} \quad (5)$$

$$\bar{u}_i(p_1) \left[\gamma_\sigma \frac{\not{p}_1 + \not{p}_3}{(p_1 + p_3)^2} \gamma_\nu - \gamma_\nu \frac{\not{p}_2 + \not{p}_3}{(p_2 + p_3)^2} \gamma_\sigma \right] v_j(p_2) \epsilon_a^\sigma(p_3),$$

where $p_{a,b}$ are the 4-momenta of the incoming electron and positron, respectively. The outgoing quark, antiquark and gluon have 4-momenta $p_{1,2,3}$, respectively. The total momentum of the system $q = p_a + p_b = p_1 + p_2 + p_3$. The gluon has colour index $a = 1, \dots, N_c^2 - 1$ whereas the quark/antiquark have colour indices $i, j = 1, \dots, N_c$.

Summing/averaging over spins and colours

$$|\overline{\mathcal{M}}|^2 = \frac{4e^2 e_q^2 g_s^2 N_c}{s} C_F \frac{(p_1 \cdot p_a)^2 + (p_1 \cdot p_b)^2 + (p_2 \cdot p_a)^2 + (p_2 \cdot p_b)^2}{p_1 \cdot p_3 p_2 \cdot p_3}. \quad (6)$$

The colour algebra gives a colour factor

$$\sum_a^{N_c^2-1} t_{ij}^a (t_{ij}^a)^* = t_{ij}^a t_{ji}^a = \frac{1}{2} \delta^{aa} = \frac{1}{2} (N_c^2 - 1) = N_c C_F, \quad (7)$$

where the colour charges in the fundamental (quarks and antiquarks) and adjoint (gluons) representations are

$$C_F \equiv \frac{1}{2N_c}(N_c^2 - 1) \quad \text{and} \quad C_A \equiv N_c, \quad (8)$$

respectively. More about the colour algebra can be found in appendix C

The three-body phase space is

$$\begin{aligned} d\Phi_n(p_a + p_b; p_1, p_2, p_3) &= (2\pi)^4 \delta^{(4)}(p_a + p_b - p_1 - p_2 - p_3) \frac{d^3\vec{p}_1}{(2\pi)^3 2E_1} \frac{d^3\vec{p}_2}{(2\pi)^3 2E_2} \frac{d^3\vec{p}_3}{(2\pi)^3 2E_3} \\ &= \frac{1}{8(2\pi)^5} E_1 dE_1 d\cos\theta d\phi E_2 dE_2 d\cos\beta d\alpha \frac{1}{E_3} \delta(\sqrt{s} - E_1 - E_2 - E_3), \end{aligned}$$

where θ and ϕ are the polar and azimuthal angles, respectively, of the outgoing quark with respect to the beam direction. The polar and azimuthal angles of the antiquark with respect to the quark direction are β and α , respectively. We have integrated over p_3 using the δ -function and assumed that the outgoing particles are massless.

Using momentum conservation

$$E_3 = |\vec{p}_3| = |\vec{p}_1 + \vec{p}_2| = \sqrt{E_1^2 + E_2^2 + 2E_1 E_2 \cos\beta}. \quad (9)$$

Therefore the integral over the remaining δ -function is

$$\int d\cos\beta \delta(\sqrt{s} - E_1 - E_2 - E_3) = \frac{E_3}{E_1 E_2}, \quad (10)$$

so

$$\begin{aligned} d\Phi_n(p_a + p_b; p_1, p_2, p_3) &= \frac{1}{8(2\pi)^5} dE_1 d\cos\theta d\phi dE_2 d\alpha \\ &= \frac{s}{16(2\pi)^3} dx_1 dx_2 \frac{d\cos\theta d\phi d\alpha}{2(2\pi)^2}, \end{aligned} \quad (11)$$

where $x_i \equiv 2E_i/\sqrt{s}$. Momentum and energy conservation requires that $x_1 + x_2 + x_3 = 2$.

The total cross section is

$$\begin{aligned} \sigma &= \frac{1}{2s} \frac{s}{16(2\pi)^3} \int dx_1 dx_2 \frac{d\cos\theta d\phi d\alpha}{2(2\pi)^2} |\overline{M}|^2, \\ &= \frac{4\pi\alpha^2 e_q^2 N_c}{3s} C_F \frac{\alpha_S}{2\pi} \int dx_1 dx_2 \frac{x_1^2 + x_2^2}{(1-x_1)(1-x_2)}. \end{aligned} \quad (12)$$

The contribution from the Z^0 boson is the same except for σ_0 . This is divergent at the edge of phase space as $x_{1,2} \rightarrow 1$ so that the total cross section is $\sigma = \infty$!

This is a common feature of all perturbative QCD calculations. Configurations which are indistinguishable from the leading-order result are divergent. Physically there are two regions where this happens.

1. *Collinear limit:* If we take $x_1 \rightarrow 1$ at fixed x_2 or $x_2 \rightarrow 1$ at fixed x_1 . We can see what happens physically by considering the dot product of the antiquark and gluon 4-momenta, *i.e.*

$$2p_2 \cdot p_3 = \frac{sx_2x_3}{2}(1 - \cos \theta_{23}) = s(1 - x_1) \Rightarrow (1 - \cos \theta_{23}) = \frac{2(1 - x_1)}{x_2x_3} \rightarrow 0. \quad (13)$$

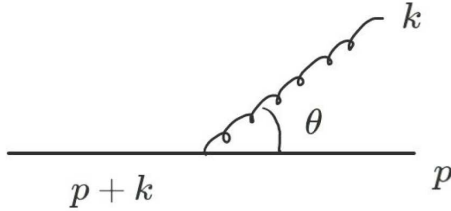
So the limit $x_1 \rightarrow 1$, where the matrix element diverges, corresponds to the angle between the antiquark and gluon $\theta_{23} \rightarrow 0$, *i.e.* collinear emission of the gluon from the antiquark. Similarly the limit $x_2 \rightarrow 1$ corresponds to collinear emission of the gluon from the quark.

2. *Soft limit:* $x_{1,2} \rightarrow 1$ at fixed $\frac{1-x_1}{1-x_2}$. We can consider what happens in this limit by considering the energy of the gluon

$$E_g = \frac{\sqrt{s}}{2}x_3 = \frac{\sqrt{s}}{2}(1 - x_1 + 1 - x_2) \rightarrow 0, \quad (14)$$

i.e. the matrix element diverges in the soft limit, when the energy of the gluon is small.

These are both universal features of QCD matrix elements. In general one can see how the divergencies appear by looking at the propagator just before the emission of a gluon.



$$P^2 = (k + p)^2 = 2|\vec{k}||\vec{p}|(1 - \cos \theta)$$

From this expression one can see that the propagator vanishes (and therefore divergences appear) when the gluon is either soft ($|k| \rightarrow 0$) or collinear ($\cos \theta \rightarrow 0$).

In these limits QCD matrix elements *factorize*, *i.e.* the matrix element including the emission of a soft or collinear gluon can be written as the convolution of the matrix element before the emission and a universal term describing collinear or soft emission.

Collinear Limit If we first consider collinear emission we take the momentum of the gluon p_3 parallel to p_2 ($\theta_{23} = 0$). We can therefore define

$$p_2 = (1 - z)\bar{p}_2, \quad p_3 = z\bar{p}_2, \quad \text{with } \bar{p}_2^2 = 0, \quad (15)$$

where \bar{p}_2 is the momentum of the antiquark before the gluon radiation and z is the fraction of the original antiquark's momentum carried by the gluon. In this limit the matrix element factorizes

$$|\mathcal{M}_{q\bar{q}g}|^2 = |\mathcal{M}_{q\bar{q}}|^2 \times \frac{g_s^2}{p_2 \cdot p_3} \times C_F \frac{1 + (1 - z)^2}{z}. \quad (16)$$

As does the phase space

$$dx_1 dx_2 \longrightarrow \frac{1}{4} z(1-z) dz d\theta_{23}^2. \quad (17)$$

Putting this together

$$\sigma = \sigma_0 \int \frac{d\theta_{23}^2}{\theta_{23}^2} dz C_F \frac{\alpha_S}{2\pi} \frac{1 + (1-z)^2}{z} = \sigma_0 \int \frac{d\theta_{23}^2}{\theta_{23}^2} dz \frac{\alpha_S}{2\pi} \hat{P}_{q \rightarrow gq}(z). \quad (18)$$

The Dokshitzer-Gribov-Lipatov-Altarelli-Parisi (DGLAP) splitting function is a universal probability distribution for the radiation of a collinear gluon in any processes producing a quark. The splitting functions are:

$$\begin{aligned} \hat{P}_{g \rightarrow gg}(z) &= C_A \left[\frac{1-z}{z} + \frac{z}{1-z} + z(1-z) \right]; & \hat{P}_{q \rightarrow qg}(z) &= C_F \frac{1+z^2}{1-z}; \\ p_{g \rightarrow q\bar{q}}(z) &= T_R [z^2 + (1-z)^2]; & \hat{P}_{q \rightarrow gq}(z) &= C_F \frac{1+(1-z)^2}{z}; \end{aligned} \quad (19)$$

where z is the fraction of the momenta carried by the first outgoing particle and $T_R = \frac{1}{2}$.

Soft Limit In the limit that $E_g \rightarrow 0$ the matrix element for the process factorizes

$$\mathcal{M}_{q\bar{q}g} = \mathcal{M}_{q\bar{q}} g_s t_{ij}^a \left(\frac{p_1}{p_1 \cdot p_3} - \frac{p_2}{p_2 \cdot p_3} \right) \cdot \epsilon_A(p_3), \quad (20)$$

the *eikonal current*. The matrix element squared therefore factorizes in this case

$$|\mathcal{M}_{q\bar{q}g}|^2 = |\mathcal{M}_{q\bar{q}}|^2 g_s^2 C_F \frac{2p_1 \cdot p_2}{p_1 \cdot p_3 p_2 \cdot p_3}. \quad (21)$$

The phase space is

$$dx_1 dx_2 \longrightarrow \frac{2}{s} E_g dE_g d\cos\theta. \quad (22)$$

So in the soft limit

$$\sigma = \sigma_0 \int C_F \frac{\alpha_S}{2\pi} \frac{dE_g}{E_g} d\cos\theta \frac{2(1 - \cos\theta_{q\bar{q}})}{(1 - \cos\theta_{qg})(1 - \cos\theta_{g\bar{q}})}, \quad (23)$$

the *dipole radiation pattern* a universal probability distribution for the emission of a soft gluon from any colour-connected pair of partons.¹

Figure 5 illustrates the dipole radiation pattern.

2.2.2 Virtual Corrections

There are three diagrams involving virtual gluon loops, see Fig. 6. This contribution is also divergent, but negative. This will cancel the real divergence to give a finite answer. To show this we need to regularize both the real and virtual cross sections and add them together. The result should be finite when we remove the regularization. The standard

¹Strictly this is only universal at the amplitude level, not as a probability distribution.

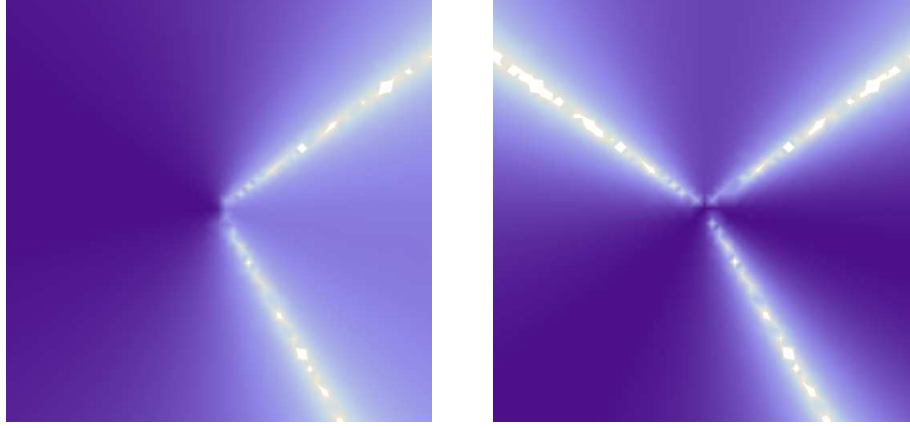


Figure 5: Dipole radiation pattern for $e^+e^- \rightarrow q\bar{q}\gamma$ and $e^+e^- \rightarrow q\bar{q}g$.

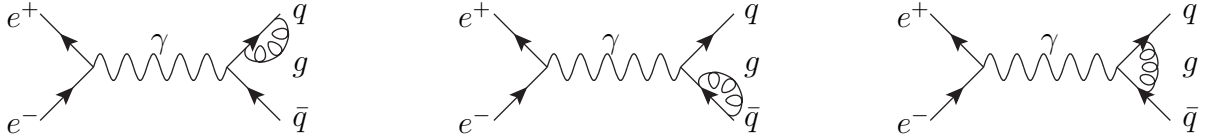


Figure 6: Virtual loop corrections to $e^+e^- \rightarrow q\bar{q}$.

way of doing this is to work in $d = 4 - 2\epsilon$ dimensions where to regularize these infrared divergences $\epsilon < 0$. In this case

$$\begin{aligned}\sigma_{\text{real}} &= \sigma_0 C_F \frac{\alpha_S}{2\pi} H(\epsilon) \left(\frac{4}{\epsilon^2} + \frac{3}{\epsilon} + \frac{19}{2} - \pi^2 + \mathcal{O}(\epsilon) \right), \\ \sigma_{\text{virtual}} &= \sigma_0 C_F \frac{\alpha_S}{2\pi} H(\epsilon) \left(-\frac{4}{\epsilon^2} - \frac{3}{\epsilon} - 8 + \pi^2 + \mathcal{O}(\epsilon) \right),\end{aligned}$$

where $H(0) = 1$. The sum

$$\sigma_{\text{total}} = \sigma_{\text{real}} + \sigma_{\text{virtual}} = \sigma_0 C_F \frac{3\alpha_S}{4\pi}, \quad (24)$$

is finite as $\epsilon \rightarrow 0$. So finally combining this correction with the leading-order result

$$R(e^+e^-) = R_0(e^+e^-) \left(1 + \frac{\alpha_s}{\pi} \right). \quad (25)$$

Measuring $R(e^+e^-)$ is one way of measuring the strong coupling giving²

$$\alpha_S(m_Z) = 0.1226 \pm 0.0038. \quad (26)$$

The second and third order corrections, and the results for the next-to-leading-order corrections including quark masses are also known.

This is the simplest example of an observable which we can calculate using perturbation theory involving quarks and gluons, but measure experimentally using hadrons. We now need to go on and consider more complicated observables.

²Taken from the Ref. [8].

3 Running Coupling

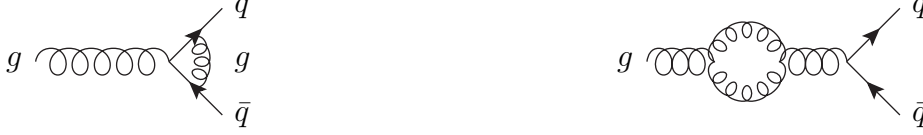


Figure 7: Example virtual corrections contributing to the evolution of the strong coupling constant.

In addition to the infrared, soft and collinear, divergences we saw in the calculation of $\sigma(e^+e^- \rightarrow \text{hadrons})$ it is possible to have ultraviolet divergences. The virtual corrections shown in Fig. 7 are divergent in the ultraviolet. These, and other similar corrections, lead to the strong coupling being *renormalized* to absorb the ultraviolet singularities. The renormalisation procedure introduces an unphysical renormalisation scale μ .

The leads to:

1. diagrams are dependent on μ ;
2. α_S is replaced by the running coupling $\alpha_S(\mu)$;
3. although we can't calculate the coupling we can calculate how it changes with scale:

$$\mu^2 \frac{d\alpha_S}{d\mu^2} \equiv \beta(\alpha_S) = -\beta_0 \alpha_S^2 + \dots \quad \beta_0 = \frac{11N_c - 4T_R n_f}{12\pi}, \quad (27)$$

where n_f is the number of active quark flavours.

For $\beta_0 > 0$ the coupling displays *asymptotic freedom*, i.e. $\alpha_S(\mu) \rightarrow 0$ as $\mu \rightarrow \infty$ which allows us to perform perturbative calculations at high energies where the coupling is small.

It is standard to quote the value of $\alpha_S(M_Z)$. The value at other scales can be found by solving the evolution equation. Recent experimental measurements of the strong coupling evolved to the Z^0 mass and the running of coupling are shown in Fig. 8.

It is common to define a scale Λ_{QCD} so that

$$\alpha_s(\mu) = \frac{4\pi}{\beta_0 \ln \left(\frac{\mu^2}{\Lambda_{\text{QCD}}^2} \right)} [1 + \dots]. \quad (28)$$

In general there is a choice of precisely how we perform the renormalisation, which leads to both *renormalisation scale* and *scheme* dependence. Physical observables don't depend on μ_F or the renormalisation scheme, but fixed order perturbative calculations do.

3.1 Higher order calculations

Since the strong coupling constant is not very small the perturbative series converges slower than it does in QED. To get reliable QCD predictions we need at least NLO precision and NNLO is preferable for important processes, but NNLO calculations are very

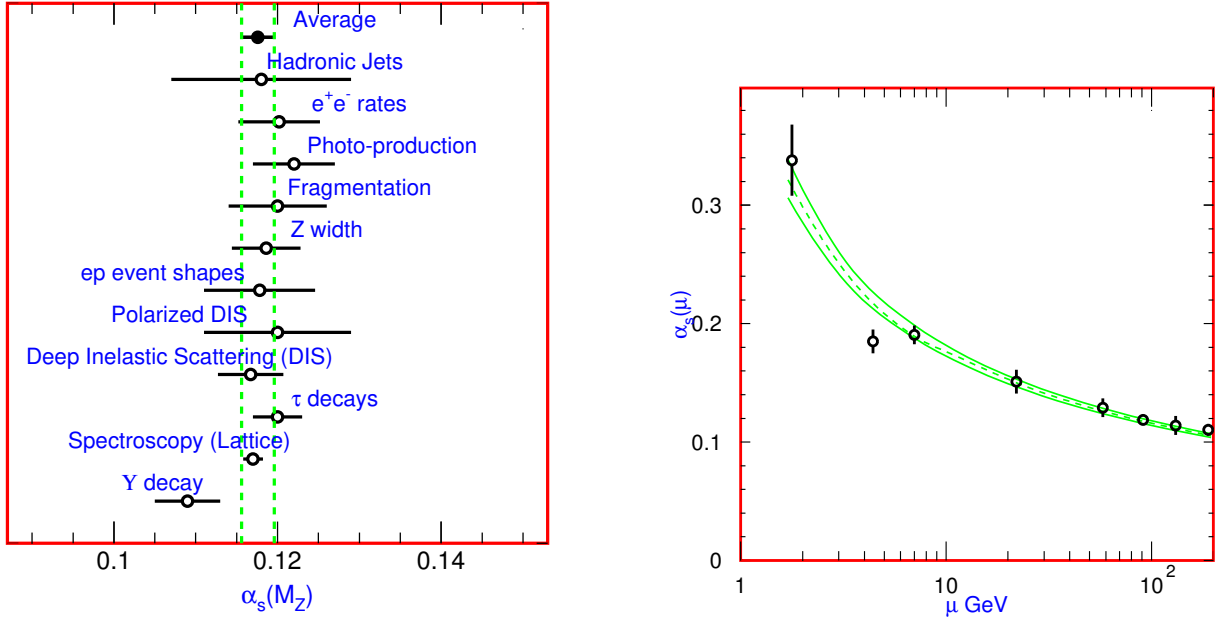


Figure 8: Measurements of the strong coupling at the Z^0 mass and the running of the coupling taken from Ref. [8].

challenging. Perturbative calculations for hadron colliders have two unphysical parameters: the factorisation and renormalisation scales. The former defines the separation between the perturbative and non-perturbative description of the proton and the latter is needed to remove the ultra-violet divergences and specifies at which scale the coupling constant should be evaluated. This dependence is an artefact of the truncation of the perturbative series, if we were able to compute the entire perturbative series to all orders, the dependence would drop out. Therefore the dependence on the factorisation and renormalisation scales is used as a gauge of the theoretical error due to the missing orders.

3.2 Infrared safety

To enable a meaningful comparison between theory and experiment it is important that the observable is defined in a way that allows the perturbative prediction to be carried out at higher orders. One requirement is that the observable should be infrared safe. By this we mean that the value of the observable does not change in the case of a collinear splitting or in the case of the emission of a soft particle. Mathematically it means that the observable \mathcal{O} has to fulfil the following properties. For a collinear splitting of the parton with momentum p_i we need

$$\mathcal{O}(p_1, \dots, p_i, \dots, p_n) = \mathcal{O}(p_1, \dots, zp_i, (1-z)p_i, \dots, p_n)$$

and in the case of a parton's momentum p_j becoming soft we require

$$\begin{aligned} \mathcal{O}(p_1, \dots, p_i, p_j, p_k, \dots, p_n) &\rightarrow \mathcal{O}(p_1, \dots, p_i, p_k, \dots, p_n) \\ \text{for } p_j &\rightarrow 0. \end{aligned}$$

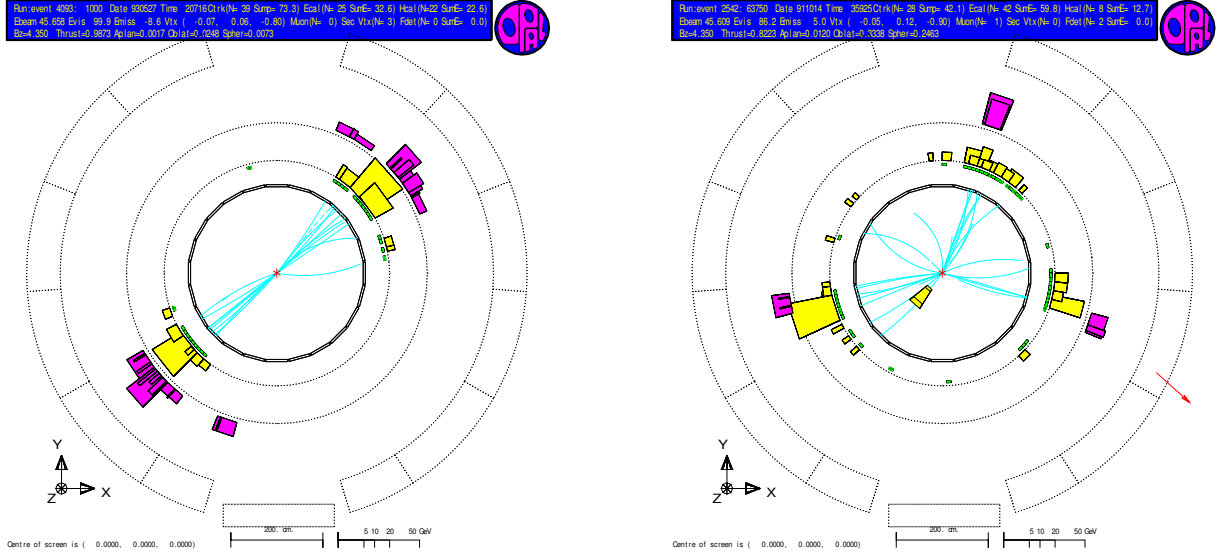


Figure 9: Example two and three jet e^+e^- events.

Examples of infrared unsafe observables or procedures are

- number of partons
- observables using incoming parton momentum fractions
- observables based on older jet algorithms
- using infrared unsafe observables as renormalisation or factorisation scale

It is not always easy to find out whether an observable/procedure is infrared safe, in order to do so correctly we will need to study the details of the jet clustering algorithm and the factorisation of the initial state in hadron collisions. The factorisation of short and long distance effects for hadronic initial states is covered in Section 4 while Section 6 covers details of different jet algorithms.

3.3 Event Shapes

If we consider the e^+e^- annihilation events shown in Fig. 9 we see a collimated bunch of hadrons travelling in roughly the same direction as the original quarks or gluons. Often you can “see” the jets without some fancy mathematical definition. We will come back and consider jets in more detail when we consider hadron–hadron collisions later in the course, in Section 6.

An alternative to defining jets is to define a more global measure of the event which is sensitive to the structure of the event. We need a number of properties to achieve this, the most important of which is *infrared safety*, *i.e.* if there is soft or collinear emission the answer doesn’t change. Formally if a parton splits into two collinear partons

$$p \rightarrow zp + (1 - z)p, \quad (29)$$

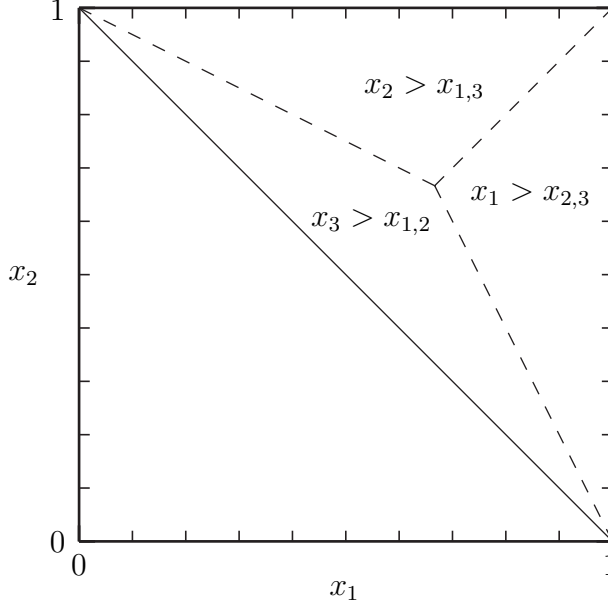


Figure 10: Phase space for $e^+e^- \rightarrow q\bar{q}g$. The requirement that $x_3 \leq 1$ ensures that $x_1 + x_2 \geq 1$ by momentum conservation so that physical phase space is the upper half plane.

or if a soft parton is emitted with momentum

$$p \rightarrow 0, \quad (30)$$

the result should not change.

After the total cross section, the simplest infrared safe observable is the thrust

$$T = \max_{\vec{n}} \frac{\sum_i |\vec{p}_i \cdot \vec{n}|}{\sum_i |\vec{p}_i|}, \quad (31)$$

where the sum is over all the final-state particles and the direction of the unit vector \vec{n} , the thrust axis, is chosen to maximize the projection of the momenta of the final-state particles along that direction.

For a two-jet *pencil-like* event all the particles lie along the thrust axis giving $T = 1$. For a totally *spherical* event the thrust can be calculated by taking a spherical distribution of particles in the limit of an infinite number of particles giving $T = \frac{1}{2}$. For three partons the thrust axis will lie along the direction of the most energetic parton, by momentum conservation there is an equal contribution to the thrust from the other partons giving $T = \max\{x_1, x_2, x_3\}$.

In order to calculate the differential cross section with respect to the thrust for $e^+e^- \rightarrow q\bar{q}g$ we can start from the differential cross section in Eqn. 12. In many cases when we wish to introduce a new quantity into a differential cross section it is easier to insert the definition using a δ -function rather than performing a Jacobian transform, in this case we use

$$1 = \int dT \delta(T - \max\{x_1, x_2, x_3\}), \quad (32)$$

to give

$$\frac{d\sigma}{dT} = \sigma_0 C_F \frac{\alpha_S}{2\pi} \int dx_1 dx_2 \frac{x_1^2 + x_2^2}{(1-x_1)(1-x_2)} \delta(T - \max\{x_1, x_2, x_3\}), \quad (33)$$

where σ_0 is the leading-order cross section for $e^+e^- \rightarrow q\bar{q}$. This expression can be evaluated in each of the three phase-space regions shown in Fig. 10. First in the region where $x_1 > x_{2,3}$

$$\begin{aligned} \left. \frac{d\sigma}{dT} \right|_{x_1 > x_{2,3}} &= \sigma_0 C_F \frac{\alpha_S}{2\pi} \int_{2(1-T)}^T dx_2 \frac{T^2 + x_2^2}{(1-T)(1-x_2)} \\ &= \sigma_0 C_F \frac{\alpha_S}{2\pi} \frac{1}{1-T} \int_{2(1-T)}^T dx_2 \frac{T^2 + 1}{(1-x_2)} - (1+x_2), \end{aligned} \quad (34)$$

where we have used the δ -function to integrate over x_1 and the limits on x_2 are given by $x_2 = x_1 = T$ for the upper limit and $T = x_1 = x_3 = 2 - x_1 - x_2 = 2 - T - x_2$ for the lower limit. Performing the integral gives

$$\left. \frac{d\sigma}{dT} \right|_{x_1 > x_{2,3}} = \sigma_0 C_F \frac{\alpha_S}{2\pi} \frac{1}{1-T} \left[(T^2 + 1) \ln \left(\frac{2T-1}{1-T} \right) + 4 - 7T + \frac{3}{2}T^2 \right]. \quad (35)$$

The same result is obtained in the region $x_2 > x_{1,3}$ due to the symmetry of the formulae under $x_1 \leftrightarrow x_2$.

In the final region we can take the integrals to be over $x_{2,3}$ and use the δ -function to eliminate the integral over x_3 giving

$$\begin{aligned} \left. \frac{d\sigma}{dT} \right|_{x_3 > x_{1,2}} &= \sigma_0 C_F \frac{\alpha_S}{2\pi} \int_{2(1-T)}^T dx_2 \frac{(2-T-x_2)^2 + x_2^2}{(T+x_2-1)(1-x_2)}, \\ &= \sigma_0 C_F \frac{\alpha_S}{2\pi} \int_{2(1-T)}^T dx_2 \frac{1}{T} [(2-T-x_2)^2 + x_2^2] \left[\frac{1}{T+x_2-1} + \frac{1}{1-x_2} \right], \\ &= \sigma_0 C_F \frac{\alpha_S}{2\pi} \frac{2}{T} \left[(2-2T+T^2) \ln \left(\frac{2T-1}{1-T} \right) + 2T - 3T^2 \right], \end{aligned} \quad (36)$$

where after the integral over x_3 , $x_1 = 2 - x_2 - T$ and the limits are calculated in the same way as before.

Putting the results from the three regions together gives

$$\frac{d\sigma}{dT} = \sigma_0 C_F \frac{\alpha_S}{2\pi} \left[\frac{2}{T(1-T)} (3T(T-1) + 2) \ln \left(\frac{2T-1}{1-T} \right) + \frac{3(3T-2)(T-2)}{1-T} \right]. \quad (37)$$

This result clearly diverges as $T \rightarrow 1$, indeed in this limit

$$\frac{1}{\sigma_0} \frac{d\sigma}{dT} \xrightarrow{T \rightarrow 1} -C_F \frac{\alpha_S}{2\pi} \left[\frac{4}{(1-T)} \ln(1-T) + \frac{3}{1-T} \right]. \quad (38)$$

We can use this result to define a two- and three-jet rate so that the three jet rate is

$$R_3(\tau) = \int_{\frac{1}{2}}^{1-\tau} \frac{1}{\sigma_0} \frac{d\sigma}{dT} \xrightarrow{\tau \rightarrow 0} C_F \frac{\alpha_S}{2\pi} 2 \ln^2 \tau, \quad (39)$$

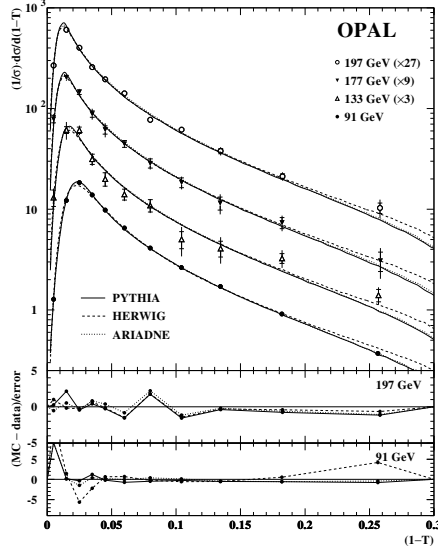


Figure 11: Thrust distribution at various centre-of-mass energies compared with Monte Carlo simulations, taken from Ref. [9].

and the two jet rate

$$R_2(\tau) = 1 - R_3(\tau) \xrightarrow{\tau \rightarrow 0} 1 - C_F \frac{\alpha_S}{2\pi} 2 \ln^2 \tau. \quad (40)$$

Similar logarithmically enhanced terms appear at all orders in the perturbative expansion giving an extra $\ln^2 \tau$ at every order in α_S , *i.e.*

$$R_2(\tau) \equiv \int_{1-\tau}^1 dT \frac{1}{\sigma} \frac{d\sigma}{dT} \xrightarrow{\tau \rightarrow 0} 1 - C_F \frac{\alpha_S}{2\pi} 2 \ln^2 \tau + \left(C_F \frac{\alpha_S}{2\pi} \right)^2 2 \ln^4 \tau + \dots \quad (41)$$

Although α_S is small, $\ln^2 \tau$ is large so the perturbative expansion breaks down. The solution is to resum the large $\alpha_S^n \ln^{2n} \tau$ terms to all orders giving the *Sudakov Form Factor*

$$R_2(\tau) \xrightarrow{\tau \rightarrow 0} \exp \left[-C_F \frac{\alpha_S}{2\pi} 2 \ln^2 \tau \right]. \quad (42)$$

This is finite (zero) at $\tau = 0$, *i.e.* the probability for no gluon radiation is zero. In general the Sudakov form factor gives the probability of no radiation

$$P(\text{no emission}) = \exp \left[-\hat{P}_{\text{naive}}(\text{emission}) \right]. \quad (43)$$

An example of the experimental measurement of the thrust distribution is shown in Fig. 11 compared to various Monte Carlo simulations which include resummation of these large logarithmic contributions..

4 Deep Inelastic Scattering

Historically measurements of deep inelastic scattering were very important for establishing the nature of QCD. Nowadays they are mainly important for the measurement of the parton distribution functions we need to calculate all cross sections for processes with incoming hadrons. As the proton isn't fundamental at sufficiently high energies the scattering is from the constituent quarks and gluons.

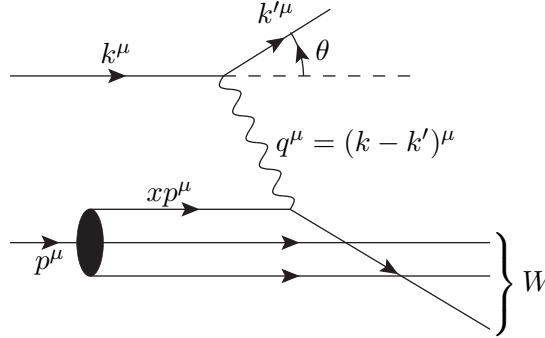


Figure 12: Deep inelastic scattering kinematics.

In deep inelastic scattering processes it is conventional to use the kinematic variables shown in Fig.12. The struck parton carries a fraction x of the four-momentum of the incoming hadron. The four-momentum of the exchanged boson is q and the virtuality of the boson $Q^2 = -q^2$. Using momentum conservation

$$xp + q = p', \quad (44)$$

where p' is the 4-momentum of the scattered quark. Therefore $(xp + q)^2 = 0$ giving $x = \frac{Q^2}{2p \cdot q}$. Similarly the mass of the hadronic system is $W^2 = (p + q)^2$. By definition $(k + p)^2 = 2k \cdot p = s$ and therefore $y = \frac{p \cdot q}{p \cdot k} = \frac{Q^2}{xs}$.

Deep inelastic scattering has $Q^2 \gg M^2$ (deep) and $W^2 \gg M^2$ (inelastic), where M is the proton mass. Historically the observation and understanding of DIS was one of the key pieces of evidence for quarks. On general grounds the cross section has the form

$$\frac{d^2\sigma}{dx dQ^2} = \frac{4\pi\alpha^2}{xQ^4} [y^2 x F_1(x, Q^2) + (1 - y) F_2(x, Q^2)], \quad (45)$$

which parameterizes the cross section in terms of two unknown structure functions, $F_{1,2}(x, Q^2)$. If we consider that the proton is a bound state of partons we can calculate these structure functions.

Suppose that the probability of a given type of quark carrying a fraction η of the proton's momentum is $f_q(\eta)$ the cross section for hadron scattering can be written in terms of those for partonic scattering

$$\frac{d^2\sigma(e + \text{proton})}{dx dQ^2} = \sum_q \int_0^1 d\eta f_q(\eta) \frac{d^2\sigma(e + q(\eta p))}{dx dQ^2}. \quad (46)$$

H1 and ZEUS

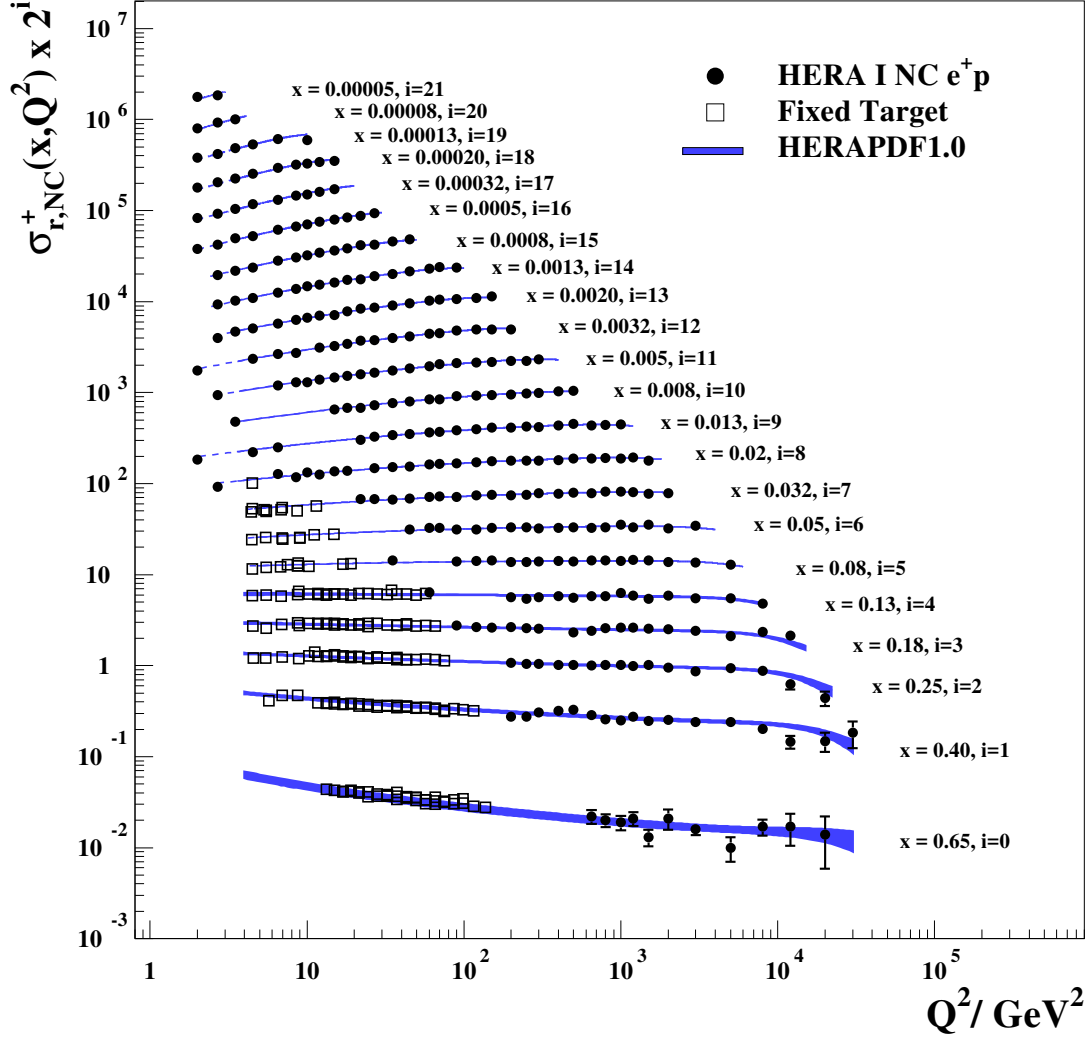


Figure 13: The reduced cross section, which is equivalent to F_2 up to some small corrections, measured by the H1 and ZEUS experiments from Ref. [10].

Taking the outgoing parton to be on-shell:

$$(q + \eta p)^2 = 2\eta p \cdot q - Q^2 = 0 \quad \Rightarrow \quad \eta = x.$$

Therefore

$$\frac{d^2\sigma(e + \text{proton})}{dx dQ^2} = \sum_q f_q(x) \frac{d^2\sigma(e + q(xp))}{dQ^2}. \quad (47)$$

The differential cross section for $e^\pm(k) + q(p) \rightarrow e^\pm(k') + q(p')$ via photon exchange which

dominates at low Q^2 for neutral current scattering is

$$\frac{d^2\sigma(e + q(xp))}{dQ^2} = \frac{2\pi\alpha^2 e_q^2}{Q^4} [1 + (1 - y)^2], \quad (48)$$

where e_q is the charge of the quark.

So in the naive parton model

$$\begin{aligned} 2xF_1(x) &= F_2(x), \\ F_2(x) &= x \sum_q e_q^2 f_q(x), \end{aligned} \quad (49)$$

are functions of x only, *Bjorken scaling*. Bjorken scaling works reasonably well, see Fig. 13, but the quantum corrections, lead to *scaling violations*.

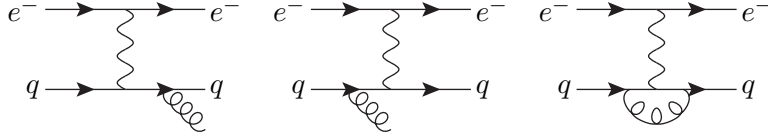


Figure 14: Real and virtual corrections to DIS.

If we consider the $\mathcal{O}(\alpha_S)$ corrections we have the following divergent contributions:

1. soft gluon, $E_g \rightarrow 0$;
2. gluon collinear to the final-state quark;
3. gluon collinear to the initial-state quark;
4. the virtual matrix element has a negative divergence;

corresponding to the diagrams shown in Fig. 14.

The contributions from (1), (2) and (4) are indistinguishable from the tree-level configuration and the divergences cancel between the real and virtual corrections. However (3) has momentum fraction $\eta > x$ and (4) $\eta = x$ so the initial-state divergences don't cancel.

Just as with final-state radiation in the collinear limit it can be shown that

$$d\sigma_{q \rightarrow qg} \rightarrow d\sigma_{q \rightarrow q} \times \frac{\alpha_S}{2\pi} C_F \frac{1 + z^2}{1 - z} \frac{dt}{t} \frac{dz}{z}. \quad (50)$$

Here we have the unregularized DGLAP splitting function $\hat{P}_{q \rightarrow qg}$, it is singular as $z \rightarrow 1$. The virtual contribution contains a compensating singularity at exactly $z = 1$. The

regularized splitting function is defined to be the sum of real and virtual contributions³

$$\begin{aligned} P_{qq}(z) &= C_F \frac{1+z^2}{1-z} + C_F \delta(1-z) \left\{ \frac{3}{2} - \int_0^1 dz' \frac{2}{1-z'} \right\}, \\ &\equiv C_F \left(\frac{1+z^2}{(1-z)_+} + \frac{3}{2} \delta(1-z) \right). \end{aligned} \quad (51)$$

The total contribution is

$$\begin{aligned} F_2(x, Q^2) &= x \sum_q e_q^2 \int_x^1 \frac{d\eta}{\eta} f_q(\eta) \left[\delta \left(1 - \frac{x}{\eta} \right) \right. \\ &\quad \left. + \frac{\alpha_S}{2\pi} P_{qq} \left(\frac{x}{\eta} \right) \int_0^1 \frac{dt}{t} + \bar{R}_{qq} \left(\frac{x}{\eta} \right) \right], \end{aligned} \quad (52)$$

where $\bar{R}_{qq} \left(\frac{x}{\eta} \right)$ is a calculable finite correction.

The integral over t is infrared divergent, comes from long timescales and should be part of the hadronic wavefunction. We therefore introduce a factorization scale μ_F and absorb contributions with $t < \mu_F$ into the parton distribution function so that $f_q(\eta)$ becomes $f_q(\eta, \mu_F^2)$.

$$\begin{aligned} F_2(x, Q^2) &= x \sum_q e_q^2 \int_x^1 \frac{d\eta}{\eta} f_q(\eta, \mu_F^2) \left[\delta \left(1 - \frac{x}{\eta} \right) \right. \\ &\quad \left. + \frac{\alpha_S}{2\pi} P_{qq} \left(\frac{x}{\eta} \right) \ln \frac{Q^2}{\mu_F^2} + R_{qq} \left(\frac{x}{\eta} \right) \right]. \end{aligned} \quad (53)$$

The finite piece is dependent on exactly how we define the parton distribution function, the factorization scheme dependence. Physical cross sections are independent of μ_F , however at any finite order in perturbation theory they do depend on the factorization scale.

Recall that in perturbation theory we cannot predict $\alpha_S(M_Z)$ but we can predict its evolution, Eqn. 27. Similarly for the PDFs

$$\mu_F^2 \frac{\partial f_q(x, \mu_F^2)}{\partial \mu_F^2} = \frac{\alpha_S(\mu_F^2)}{2\pi} \int_x^1 \frac{dy}{y} f_q(y, \mu_F^2) P_{qq} \left(\frac{x}{y} \right) + \dots \quad (54)$$

5 Hadron Collisions

In hadron collisions QCD processes dominate due to strength of the strong coupling. The cross sections for electroweak processes, W^\pm , Z^0 and Higgs production are much smaller. The values of x and Q^2 probed in hadron collisions and examples of the cross sections for various processes are shown in Fig. 15. In this section we will look at some of the basics

³The $+$ -prescription is defined by convolution with a well defined function, $g(z)$, such that

$$\int_0^1 dz [f(z)]_+ g(z) = \int_0^1 dz f(z) [(g(z) - g(1))].$$

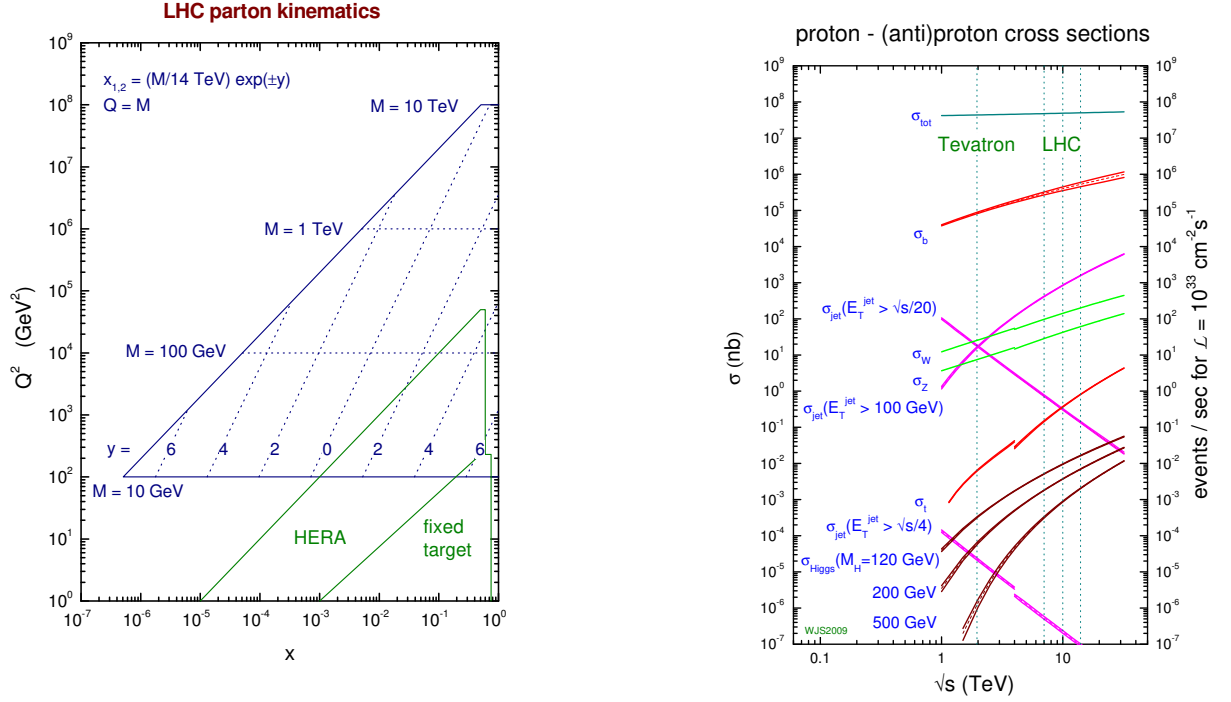


Figure 15: The values of x and Q^2 probed in hadron collisions and examples of the cross sections for various processes taken from Ref. [11].

of the production of the Z^0 boson, as a simple example of a hadron-hadron process, in the next section we will go on and study the physics of jets.

The calculation of the cross section for the production of an s -channel resonance in hadron-hadron collisions is described in more detail in Appendix A.3.1 where the cross section is given in Eqn. 128. The only dependence of the cross section on the rapidity of the Z^0 boson is via the PDFs, *i.e.* the rapidity distribution of Z^0 contains information on the PDFs of the partons a and b . The higher the mass of the produced system the more central it is, see Fig. 15. The Z^0 boson is centrally produced in both $p\bar{p}$ and pp collisions. The experimental results, for example those from the Tevatron shown in Fig. 16, are in good agreement with the theoretical predictions.

At leading order the transverse momentum of the gauge boson is zero. As before we have include real and virtual corrections, as shown in Fig. 17. In the same way as DIS the initial-state singularities must be factorized into the PDFs. At low transverse momentum we need to resum the multiple soft emissions whereas, as with the e^+e^- event shapes, at large p_\perp the fixed-order approach is more reliable. The transverse momentum of the Z^0 boson at the Tevatron is shown in Fig. 18.

In hadron-hadron collisions we would like at least next-to-leading order (NLO) calculations. This is the first order at which we have a reliable calculation of the cross section. If possible we would like next-to-next-to-leading order (NNLO) calculations but

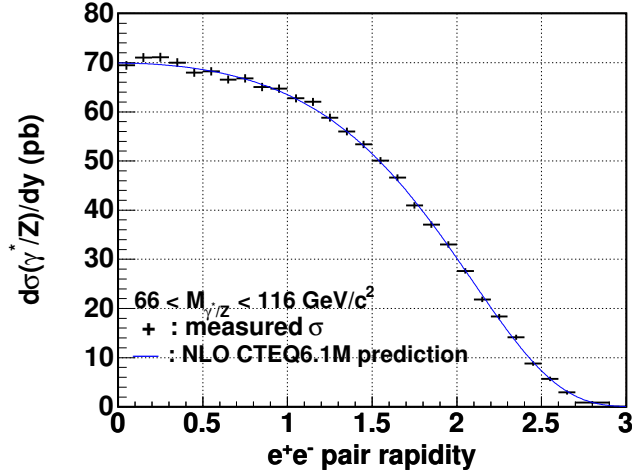


Figure 16: Rapidity of the Z^0 boson measured by the CDF experiment, taken from Ref. [12].

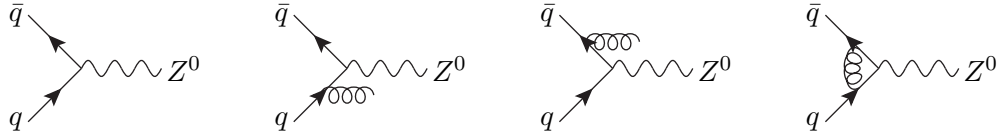


Figure 17: Real and virtual corrections to the production of the Z^0 boson.

that is much harder and takes a long time, *e.g.* $e^+e^- \rightarrow 3\text{jets}$ was calculated at: LO in 1974 [15]; NLO in 1980 [16]; NNLO in 2007 [17]. Calculating NNLO corrections is still extremely challenging in hadron collisions, only the Drell-Yan process and $gg \rightarrow H$ are known. However, we need higher order calculations because while the factorization scale uncertainty is significantly less at NLO when compared to leading order it can still be significant, see for example the scale uncertainty on the rapidity of the Z^0 boson shown in Fig. 19.

6 Jets

While we can often see the jets in an event when we look at an event display we need a precise definition to perform quantitative analyzes.⁴ Jets are normally related to the underlying perturbative dynamics, *i.e.* quarks and gluons. The purpose of a *jet algorithm* is to reduce the complexity of the final state, combining a large number of final-state particles to a few jets, *i.e.*

$$\{p_i\} \xrightarrow{\text{jet algorithm}} \{j_l\}. \quad (55)$$

We need a number of properties to achieve this (Snowmass accord):

⁴This section is based on the excellent review *Towards Jetography* [6].

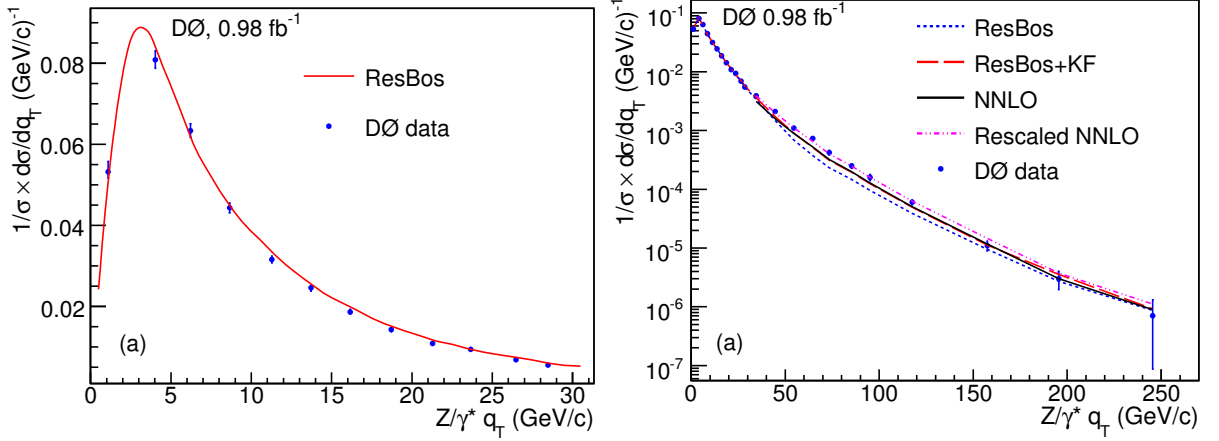


Figure 18: Transverse momentum of the Z^0 boson measured by the DØ experiment at the Tevatron, taken from Ref. [13].

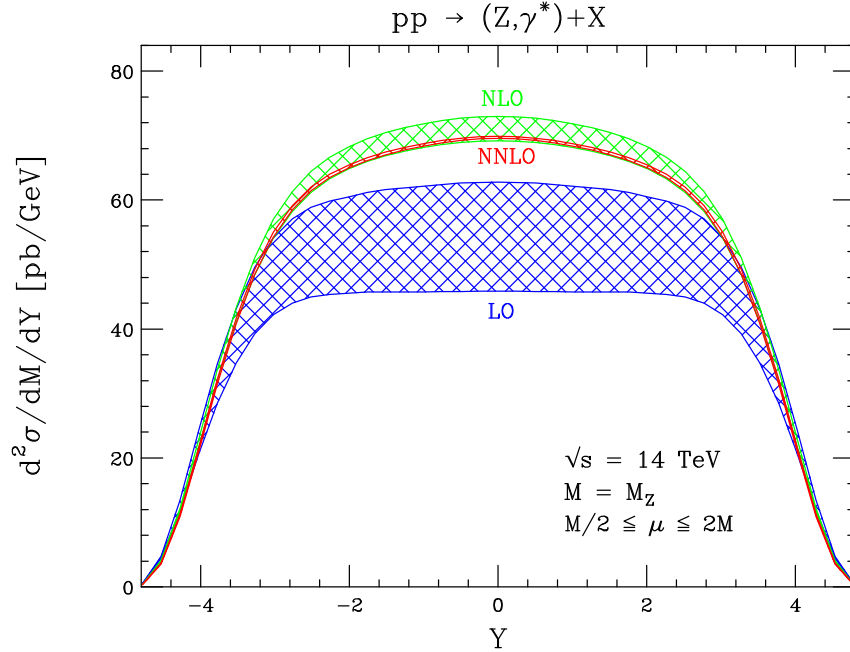


Figure 19: Rapidity distribution of the Z^0 boson for the LHC at $\sqrt{s} = 14$ TeV, taken from Ref. [14].

- simple to implement in experimental analyzes and theoretical calculations;
- defined at any order in perturbation theory and gives finite cross sections at any order in perturbation theory (*i.e.* infrared safe);
- insensitive to hadronization effects.

The most important of these properties is *infrared safety*, as with the event shapes we

considered earlier. Provided the jet algorithm is infrared safe there are a range of different approaches.

The two main types of jet algorithm are:

1. cone algorithms;
2. sequential recombination algorithms.

There is a long history to this subject with: theorists and e^+e^- experimentalists generally preferring recombination algorithms for their better theoretical properties; hadron collider experimentalists preferring cone algorithms for their more intuitive picture and because applying many experimental corrections was easier. However, with the start of the LHC we have converged on a specific recombination algorithm.

6.1 Cone Algorithms

The simplest, oldest, and most intuitively appealing idea is a cone algorithm. The most widely used algorithms are *iterative cone* algorithms where the initial direction of the cone is determined by a seed particle, i . The sum of the momentum of all the particles with a cone of radius R , the jet radius, in the azimuthal angle ϕ and rapidity⁵ y is then used as a new seed direction and the procedure iterated until the direction of the resulting cone is stable. In this approach the momenta of all the particles j such that

$$\Delta R_{ij}^2 = (y_i - y_j)^2 + (\phi_i - \phi_j)^2 < R^2, \quad (56)$$

are summed. As these algorithms are almost exclusively used in hadron–hadron collisions it is normal to use the kinematical variables defined in Appendix A.1.

While this may seem simple there are a lot of complications in the details of the algorithm in particular: what should be used as the seeds; what happens when the cones obtained from two different seeds share particles, *overlap*. The details of the treatment of these issues can lead to problems with infrared safety, which can often be very subtle.

Consider a simple approach where we take all the particles to be seeds. If we have two partons separated in (y, ϕ) by twice the cone radius then two jets, with the direction



Figure 20: Example of cone jets.

given by that of the original partons, are formed as shown in Fig. 20. However if there is an additional soft gluon emission between the two jets, as shown in Fig. 21, depending on

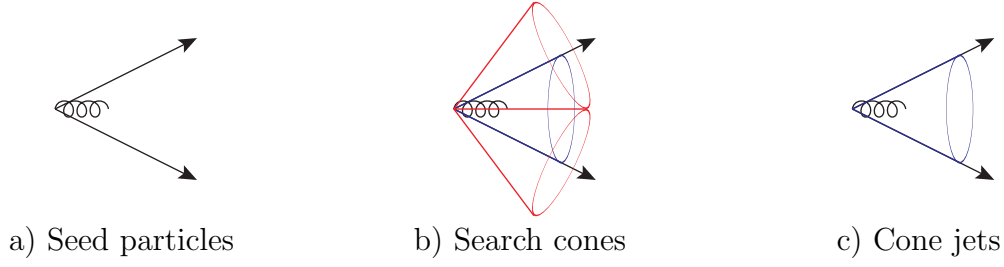


Figure 21: Example of cone jets with additional soft radiation.

the approach we can get only one jet, *i.e.* the algorithm is unsafe. A simple solution was to use the midpoint between all the seeds as a seed, the *midpoint algorithm*. This solves the problem at this level but similar problems appear for higher multiplicities. The final solution, for the only known infrared safe cone algorithm, SISCone, is to avoid the use of seeds and treat overlapping jets carefully.

6.2 Sequential Recombination Algorithms

In this approach jets are constructed by sequential recombination. We define a distance measure between two objects d_{ij} , in hadron collisions we must also define a distance measure d_{iB} with respect to the beam direction. There are two variants of the algorithm the *inclusive* where all jets are retained and *exclusive* where only jets above the cut-off value of the jet measure d_{cut} , the jet resolution scale, are kept. The algorithm proceeds as follows:

1. the distance measure is computed for each pair of particles, and with the beam direction in hadronic collisions, and the minimum found;
2. if the minimum value is for a final-state merging in the exclusive approach the particles i and j are recombined into a pseudoparticle if $d_{ij} \leq d_{\text{cut}}$, while in the inclusive algorithm they are always recombined;
3. otherwise if a beam merging is selected in the inclusive approach the particle is declared to be a jet, while in the exclusive approach it is discarded if $d_{iB} \leq d_{\text{cut}}$;
4. in the inclusive approach we continue until no particles remain, while in the exclusive approach we stop when the selected merging has $\min\{d_{iB}, d_{ij}\} \geq d_{\text{cut}}$.

In the inclusive approach the jets are all those selected from merging with the beam, whereas in the exclusive approach the jets are all the remaining particles when the iteration is terminated.

The choice of the distance measure, and to a lesser extent the recombination procedure,⁶ defines the algorithm.

⁵Or sometimes pseudorapidity η .

⁶In practice the so-called “E-scheme” where the four-momenta of the particles are added to give the pseudoparticle’s four-momentum is almost always used.

The earliest JADE algorithm for e^+e^- collisions uses the distance measure

$$d_{ij} = 2E_i E_j (1 - \cos \theta_{ij}), \quad (57)$$

where $E_{i,j}$ are the energies of the particles and θ_{ij} the angle between them. In e^+e^- collisions we have to use the exclusive algorithm and it is conventional to use a dimensionless measure $y_{ij} = d_{ij}/Q^2$, where Q is the total energy in the event. While this choice can easily be proved to be safe in the soft and collinear limits there are problems with the calculation of higher order corrections.

Therefore a class of k_T algorithms was developed in which the distance measure was chosen to be the relative transverse momentum of the two particles in the collinear limit, *i.e.*

$$d_{ij} = \min\{E_i^2, E_j^2\} \theta_{ij}^2 \simeq k_{\perp ij}^2 \quad \text{for } \theta_{ij} \rightarrow 0. \quad (58)$$

In e^+e^- collisions the conventional choice is

$$d_{ij} = 2 \min\{E_i^2, E_j^2\} (1 - \cos \theta_{ij}). \quad (59)$$

In hadron collisions it is best to use a choice which is invariant under longitudinal boosts along the beam direction. The standard choice is

$$d_{ij} = \min\{p_{i,\perp}^2, p_{j,\perp}^2\} \frac{\Delta R_{ij}^2}{R^2}, \quad (60)$$

where R is the ‘‘cone-size’’ and $p_{i,\perp}$ is the transverse momentum of particle i with respect to the beam direction. The standard choice for the beam distance is $d_{iB} = p_{i,\perp}^2$. There are other definitions, particularly of the distance d_{ij} , which are invariant under longitudinal boosts but that in Eqn. 60 is the most common choice.

In general there is a whole class of measures defined by

$$d_{ij} = \min\{p_{i,\perp}^{2p}, p_{j,\perp}^{2p}\} \frac{\Delta R_{ij}^2}{R}, \quad (61)$$

and $d_{iB} = p_{i,\perp}^{2p}$.

The parameter $p = 1$ for the k_T algorithm and 0 for the Cambridge/Aachen algorithm.

Recently a new approach, the anti- k_T algorithm, with $p = -1$, was proposed which favours clustering with hard collinear particles rather than clusterings of soft particles, as in the k_T and Cambridge/Aachen algorithms. The anti- k_T algorithm is still infrared safe and gives ‘‘conical’’ jets due to the angular part of the distance measure and is the algorithm preferred by both general-purpose LHC experiments.

6.3 Jet Cross Sections

All cone jet algorithms, except from SISCone, are not infrared safe. The best ones typically fail in processes where we consider extra radiation from three-parton configurations while some already fail when we consider radiation from two-parton configurations, see the summary in Table 2.

| Process | Last meaningful order | | Known at |
|--|-----------------------|----------------------|---------------------------|
| | JetClu Atlas cone | MidPoint CMS cone | |
| inclusive jet cross section | LO | NLO | NLO (\rightarrow NNLO) |
| $W^\pm/Z^0 + 1$ -jet cross section | LO | NLO | NLO |
| 3-jet cross section | none | LO | NLO |
| $W^\pm/Z^0 + 2$ -jet cross section | none | LO | NLO |
| jet masses in 3-jet and $W^\pm/Z^0 + 2$ -jet events | none | none | LO |

Table 2: Comparisons of various cone algorithms for hadron–hadron processes. Adapted from Ref. [6].

Examples of the jets, and their areas, formed using different algorithms on a sample parton-level event are shown in Fig. 22. As can be seen the k_T and Cambridge/Aachen algorithms tend to cluster many soft particles giving jets with an irregular area whereas the jets produced by the cone and anti- k_T algorithms are more regular making applying corrections for pile-up and underlying event contamination easier.

In order to study jet production in hadron collisions we need to understand both the jet algorithm and the production of the partons which give rise to the jets. The spin/colour summed/average matrix elements are given in Table 3. Many of these matrix elements have t -channel dominance, typically $t \rightarrow 0 \iff p_\perp^2 \rightarrow 0$. As a consequence the parton–parton scattering cross section grows quickly as $p_\perp \rightarrow 0$ an effect which is further enhanced by the running of α_s when using $\mu_R = p_\perp$ as the renormalisation scale. An example of the p_\perp spectrum of jets for different rapidities measured using the midpoint cone-algorithm is shown in Fig. 23.

| | |
|-----------------------------------|---|
| $qq' \rightarrow qq'$ | $\frac{4}{9} \frac{\hat{s}^2 + \hat{u}^2}{\hat{t}^2}$ |
| $q\bar{q} \rightarrow q'\bar{q}'$ | $\frac{4}{9} \frac{\hat{t}^2 + \hat{u}^2}{\hat{s}^2}$ |
| $q\bar{q} \rightarrow gg$ | $\frac{32}{27} \frac{\hat{t}^2 + \hat{u}^2}{\hat{t}\hat{u}} - \frac{8}{3} \frac{\hat{t}^2 + \hat{u}^2}{\hat{s}^2}$ |
| $qg \rightarrow qg$ | $\frac{\hat{s}^2 + \hat{u}^2}{\hat{t}^2} - \frac{4}{9} \frac{\hat{s}^2 + \hat{u}^2}{\hat{s}\hat{u}}$ |
| $gg \rightarrow q\bar{q}$ | $\frac{1}{6} \frac{\hat{t}^2 + \hat{u}^2}{\hat{t}\hat{u}} - \frac{3}{8} \frac{\hat{t}^2 + \hat{u}^2}{\hat{s}^2}$ |
| $gg \rightarrow gg$ | $\frac{9}{2} \left(3 - \frac{\hat{t}\hat{u}}{\hat{s}^2} - \frac{\hat{s}\hat{u}}{\hat{t}^2} - \frac{\hat{s}\hat{t}}{\hat{u}^2} \right)$ |
| $q\bar{q} \rightarrow g\gamma$ | $\frac{8}{9} \frac{\hat{t}^2 + \hat{u}^2 + 2\hat{s}(\hat{s} + \hat{t} + \hat{u})}{\hat{t}\hat{u}}$ |
| $qg \rightarrow q\gamma$ | $-\frac{1}{3} \frac{\hat{s}^2 + \hat{u}^2 + 2\hat{t}(\hat{s} + \hat{t} + \hat{u})}{\hat{s}\hat{u}}$ |

Table 3: Spin and colour summed/averaged matrix elements for $2 \rightarrow 2$ parton scattering processes with massless partons taken from Ref. [3]. A common factor of $g^4 = (4\pi\alpha_s)^2$ (QCD), $g^2 e^2 e_q^2$ (photon production) has been removed.

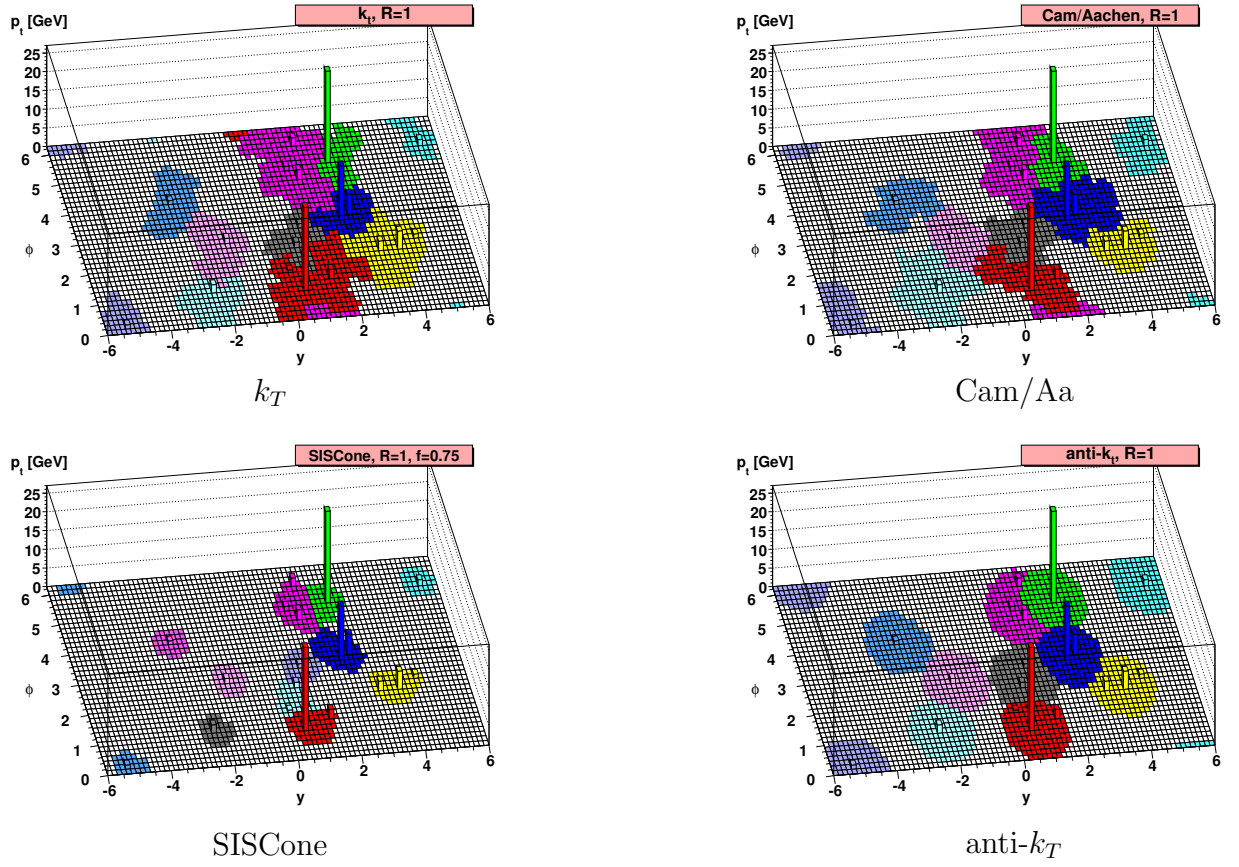


Figure 22: Examples of jets formed by different jet algorithms, taken from Ref. [6].

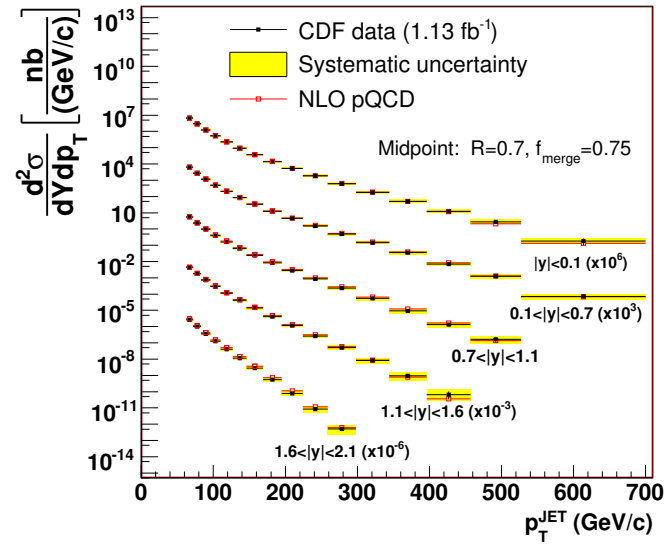


Figure 23: Transverse momentum spectrum of jets measured by the CDF experiment at the Tevatron, taken from Ref. [18].

6.4 Jet Properties

In general the computation of jet properties in hadron–hadron collisions is extremely complicated, however for some quantities we can get estimates of various effects. The simplest of these is to estimate the change in the p_\perp between a parton and the jet it forms.

We can start by considering the change due to perturbative QCD radiation. Suppose we have a quark with transverse momentum p_\perp which radiates a gluon such that the quark carries a fraction z of its original momentum and the gluon a fraction $1 - z$, as shown in Fig. 24. In this case after the radiation the centre of the jet will be the parton

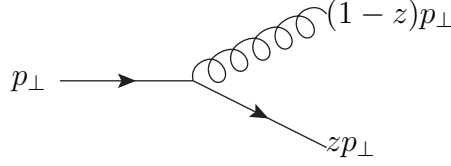


Figure 24: Kinematics of jet branching

with the highest transverse momentum after the branching, *i.e.* the quark if $z > 1 - z$ or the gluon if $z < 1 - z$. If the other parton is at an angular distance greater $\theta > R$ it will no longer be in the jet and the jet will have a smaller transverse momentum

$$\begin{aligned} \delta p_\perp &= (1 - z)p_\perp - p_\perp &= -zp_\perp & 1 - z > z \\ \delta p_\perp &= zp_\perp - p_\perp &= -(1 - z)p_\perp & z > 1 - z \end{aligned} \quad (62)$$

than the original parton.

We can use the splitting probabilities given in Eqn. 18 to compute the average transverse momentum loss

$$\begin{aligned} \langle p_\perp \rangle_q &= -\frac{C_F \alpha_S}{2\pi} p_\perp \int_{R^2}^1 \frac{d\theta^2}{\theta^2} \int_0^1 dz \frac{1+z^2}{1-z} \min\{1-z, z\}, \\ &= -\frac{C_F \alpha_S}{2\pi} p_\perp \ln\left(\frac{1}{R^2}\right) \left[\int_0^{\frac{1}{2}} \frac{1+z^2}{1-z} z + \int_{\frac{1}{2}}^1 \frac{1+z^2}{1-z} 1-z \right], \\ &= -\frac{C_F \alpha_S}{\pi} p_\perp \ln\left(\frac{1}{R}\right) \left[2 \ln 2 - \frac{3}{8} \right]. \end{aligned} \quad (63)$$

The loss of transverse momentum can be calculated for gluon jets in the same way using the gluon splitting functions giving

$$\langle p_\perp \rangle_g = -\frac{\alpha_S}{\pi} p_\perp \ln\left(\frac{1}{R}\right) \left[C_A \left(2 \ln 2 - \frac{43}{96} \right) + T_R n_f \frac{7}{48} \right]. \quad (64)$$

These calculations give

$$\frac{\langle p_\perp \rangle_q}{p_\perp} = -0.43 \alpha_S \ln \frac{1}{R}, \quad \frac{\langle p_\perp \rangle_g}{p_\perp} = -1.02 \alpha_S \ln \frac{1}{R}.$$

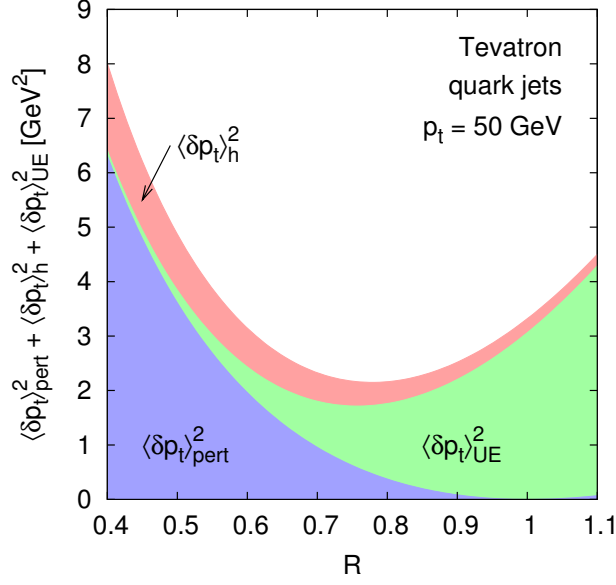


Figure 25: Example of various contributions to the shift of the transverse momentum, taken from Ref. [6].

So for a jet with $R = 0.4$ quark and gluon jets will have 5% and 11% less transverse momentum than the parent parton, respectively. These results are subject to significant finite R and higher order corrections. The result will also depend on the precise details of the recombination scheme, for example SISCONC has a different recombination scheme where the centre of the cone is the direction of the sum of the partons and we require one parton to fall outside the cone.

While this gives the perturbative energy loss by the jet there are other effects which can change the transverse momentum of the jet. In particular the jet can also lose energy in the hadronization process and can gain energy from the underlying event.

While these effects cannot be calculated from first principles we can use some simple models to gauge the size of the effects.

One model for the effect of hadronization on event shapes in e^+e^- collisions, due to Dokshitzer and Webber, is to perform a perturbative calculation and instead of stopping the calculation at some small energy scale μ_I because the strong coupling becomes non-perturbative continue the calculation into the infrared regime with a model of the strong coupling in this regime which does not diverge. They define

$$\mathcal{A}(\mu_I) = \frac{1}{\pi} \int_0^{\mu_I} dk_{\perp} \alpha_S(k_{\perp}). \quad (65)$$

This model can also be used to assess the size of the hadronization corrections for the jet transverse momentum. The hadronization is modelled by soft gluons with $k_{\perp} \sim \Lambda_{\text{QCD}}$. In this case the transverse momentum loss is

$$\delta p_{\perp} = z p_{\perp} - p_{\perp} = -(1 - z) p_{\perp}. \quad (66)$$

As before the transverse momentum loss is

$$\langle p_\perp \rangle_q = -\frac{C_F}{2\pi} p_\perp \int \frac{d\theta^2}{\theta^2} \int dz \alpha_S \frac{1+z^2}{1-z} (1-z). \quad (67)$$

As we are dealing with soft gluons $z \sim 1$ so $1+z^2 \simeq 2$. In this case we will not use a fixed value of α_S but need to evaluate it at the scale of the transverse momentum of the gluon with respect to the quark $k_\perp = p_\perp(1-z)\theta$. We also transform the integration variables to use k_\perp and θ giving

$$\langle p_\perp \rangle_q = -\frac{2C_F}{\pi} \int_R^1 \frac{d\theta}{\theta^2} \int_0^{\mu_I} dk_\perp \alpha_S(k_\perp) = -\frac{2C_F \mathcal{A}}{R}. \quad (68)$$

Using the coefficients from fits to the e^+e^- thrust distribution

$$\langle \delta p_\perp \rangle_q \sim -\frac{0.5 \text{ GeV}}{R}, \quad \langle \delta p_\perp \rangle_g \sim -\frac{1 \text{ GeV}}{R}. \quad (69)$$

The hadronization correction has a $\frac{1}{R}$ dependence on the size of the jet, unlike the $\ln \frac{1}{R}$ dependence of the perturbative radiation.

We can estimate the underlying event contribution by assuming there is Λ_{UE} energy per unit rapidity due to soft particles from the underlying event giving a correction to the transverse momentum of

$$\langle \delta p_\perp \rangle = \Lambda_{\text{UE}} \int_{\eta^2 + \phi^2 < R^2} d\eta \frac{d\phi}{2\pi} = \Lambda_{\text{UE}} \frac{R^2}{2}. \quad (70)$$

This is a useful estimate although strictly the area of the jet is only πR^2 for the anti- k_T algorithm.

An example of the various contributions to the shift between the partonic and jet transverse momentum is shown in Fig. 25.

7 Electroweak Physics

The Standard Model has 18 parameters (assuming massless neutrinos):

- 6 quark and 3 charged lepton masses;
- 3 quark mixing angles and 1 phase;
- 1 strong coupling;
- 1 electromagnetic coupling and 3 boson masses, m_W , m_Z , m_h .

All observables are a function of these 18 parameters. In principle we could choose 18 well-measured observables and define them to be the fundamental parameters of the theory, *e.g.*

$$\alpha, \quad G_F, \quad \alpha_S, \quad M_Z, \quad M_h, \quad m_f,$$

and calculate everything else in terms of them.

For the electroweak part of the theory we need m_t , m_h and three other parameters to specify everything, neglecting the masses of the other Standard Model fermions. Everything else can then be calculated from these parameters, *e.g.*

$$\cos \theta_W = \frac{m_W}{m_Z}, \quad e = g \sin \theta_W.$$

The current values of the electroweak parameters are

$$\begin{aligned} m_W &= 80.41 \text{ GeV}, & m_Z &= 91.188 \text{ GeV}, & \sin^2 \theta_W &= 0.231, \\ \alpha(m_Z) &= \frac{1}{128.89}, & G_F &= 1.16639 \times 10^{-5} \text{ GeV}^{-2}. \end{aligned}$$

It is common to include the Fermi constant, $G_F = \frac{\sqrt{2}g^2}{8m_W^2}$, from the effective theory of weak interactions at low energies as a parameter.

Different choices for the input parameters give different values for the calculated parameters.

1. input: $\alpha(m_Z)$, G_F , $\sin^2 \theta_W$, extracted:

$$g = \frac{4\pi\alpha(m_Z)}{\sin^2 \theta_W} = 0.6497,$$

$$m_W = \frac{g}{\sqrt{4\sqrt{2}G_F}} = 79.98 \text{ GeV}, \quad m_Z = \frac{m_W}{\cos \theta_W} = 91.20 \text{ GeV};$$

2. input: m_W , G_F , $\sin^2 \theta_W$ extracted:

$$m_Z = \frac{m_W}{\cos \theta_W} = 91.695 \text{ GeV},$$

$$g = \sqrt{4\sqrt{2}G_F m_W} = 0.653, \quad \alpha(m_Z) = \frac{g^2 \sin^2 \theta_W}{4\pi} = 1/127.51;$$

3. input: m_Z , $\alpha(m_Z)$, $\sin^2 \theta_W$ extracted:

$$m_W = \frac{m_Z}{\cos \theta_W} = 79.97 \text{ GeV}, \quad g = \frac{4\pi\alpha(m_Z)}{\sin \theta_W} = 0.6497;$$

4. input: m_Z , m_W , G_F extracted:

$$\sin^2 \theta_W = 1 - \left(\frac{m_W}{m_Z} \right)^2 = 0.2224,$$

$$g = \sqrt{4\sqrt{2}G_F m_W} = 0.653, \quad \alpha(m_Z) = \frac{g^2 \sin^2 \theta_W}{4\pi} = 1/132.42.$$

This is due to the quantum corrections.

It was the great triumph of the LEP/SLD and Tevatron physics programmes that the quantum corrections to the theory were probed. The normal choice of input parameters is:

1. $\alpha = 1/137.035999679(94)$ the fine-structure constant at $q^2 = 0$ is accurately measured, however the error on its evolution to $q^2 = m_Z^2$ has greater uncertainty due to hadronic corrections;
2. $G_F = 1.166367(5) \times 10^5 \text{ GeV}^{-2}$ is very accurately measured in muon decay $\mu^- \rightarrow e^- \nu_\mu \bar{\nu}_e$;
3. $m_Z = 91.1876 \pm 0.0021 \text{ GeV}$ from the LEP1 lineshape scan;

as these are the most accurately measured.

7.1 Quantum Corrections to Masses

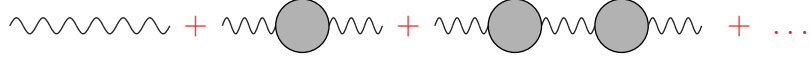


Figure 26: Example quantum corrections to the gauge boson propagator.

We have already considered the running of the coupling and corrections to cross sections and other observables. However masses are also renormalized in the Standard Model. If we consider the propagator for a massive gauge boson we get corrections of the form shown in Fig. 26. If we omit the Lorentz structures this gives a propagator

$$D(q^2) = \frac{i}{q^2 - m^2} + \frac{i}{q^2 - m^2} i\Pi(q^2) \frac{i}{q^2 - m^2} + \frac{i}{q^2 - m^2} i\Pi(q^2) \frac{i}{q^2 - m^2} i\Pi(q^2) \frac{i}{q^2 - m^2} + \dots,$$

where $\Pi(q^2)$ is the gauge boson self energy. This is a geometric progression, summing the series gives

$$D(q^2) = \frac{i}{q^2 - m^2} \frac{1}{1 - \frac{\Pi(q^2)}{q^2 - m^2}} = \frac{i}{q^2 - m^2 - \Pi(q^2)}. \quad (71)$$

If the particle can decay to the particles in the loop there is an imaginary part of the self energy $\Pi(q^2)$ which is related to the width of the particle

$$\text{Im } \Pi(q^2) = -iq\Gamma(q). \quad (72)$$

The real part of the self energy correction renormalizes the particle's mass giving

$$D(q^2) = \frac{i}{q^2 - m_R^2(q) + iq\Gamma(q)}. \quad (73)$$

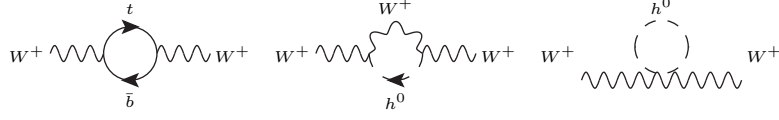


Figure 27: Quantum corrections to the W^\pm boson mass.

As we have defined to the mass of the Z^0 boson to be a fundamental parameter $\delta m_Z^2 = 0$, by definition.

The dominant corrections to the W mass come from top-bottom and Higgs loop corrections, as shown in Fig. 27.

The correction to the W^\pm boson mass is

$$\delta m_W^2 \sim \frac{4s_W^2}{1-2s_W^2} \frac{G_F}{8\pi^2\sqrt{2}} m_W^2 \times \frac{c_W^2}{s_W^2} N_c (m_t^2 - m_b^2) - \frac{4s_W^2}{1-2s_W^2} \frac{G_F}{8\pi^2\sqrt{2}} m_W^2 \times m_W^2 \frac{11}{3} \left(\ln \frac{M_h^2}{m_W^2} - \frac{5}{6} \right).$$

7.2 Electroweak Observables

A number of observables are used in the electroweak fit performed by the LEP Electroweak Working Group (LEPEWWG):

1. the Z^0 mass and width m_Z , Γ_Z ;
2. the hadronic cross section at the Z^0 pole $\sigma(\text{had}) \equiv \frac{12\pi\Gamma(e^+e^-)\Gamma(\text{had})}{m_Z^2\Gamma_Z^2}$;
3. the ratio of the hadronic to leptonic partial widths of the Z^0 , $R_\ell \equiv \frac{\Gamma(\text{had})}{\Gamma_{\ell^+\ell^-}}$, and the ratio of the bottom, $R_b \equiv \Gamma(b\bar{b})/\Gamma(\text{had})$, and charm, $R_c \equiv \Gamma(c\bar{c})/\Gamma(\text{had})$, quark partial widths to the hadronic partial width of the Z^0 ;
4. the forward-backward asymmetry for $e^+e^- \rightarrow f\bar{f}$

$$A_{fb}^{0,f} = \frac{\sigma_F - \sigma_B}{\sigma_F + \sigma_B}, \quad (74)$$

for charged leptons, $A_{fb}^{0,\ell}$, bottom $A_{fb}^{0,b}$, and charm $A_{fb}^{0,c}$ quarks;

5. the couplings of the fermions to the Z^0 can be extracted from the forward-backward asymmetry in polarized scattering at SLD

$$A_{LR}^{FB}(f) = \frac{\sigma_{LF}^f - \sigma_{LB}^f - \sigma_{RF}^f + \sigma_{RB}^f}{\sigma_{LF}^f + \sigma_{LB}^f + \sigma_{RF}^f + \sigma_{RB}^f} = \frac{3}{4} A_f. \quad (75)$$

The couplings for the bottom, A_b , and charm, A_c , quarks can be extracted from these measurements. There are a number of possible ways of extracting A_ℓ ;

6. $\sin^2 \theta_{\text{eff}}^{\text{lept}}(Q_{fb})$ is extracted from the hadronic charge asymmetry;
7. the W mass, m_W , and width, Γ_W are measured in a range of ways;

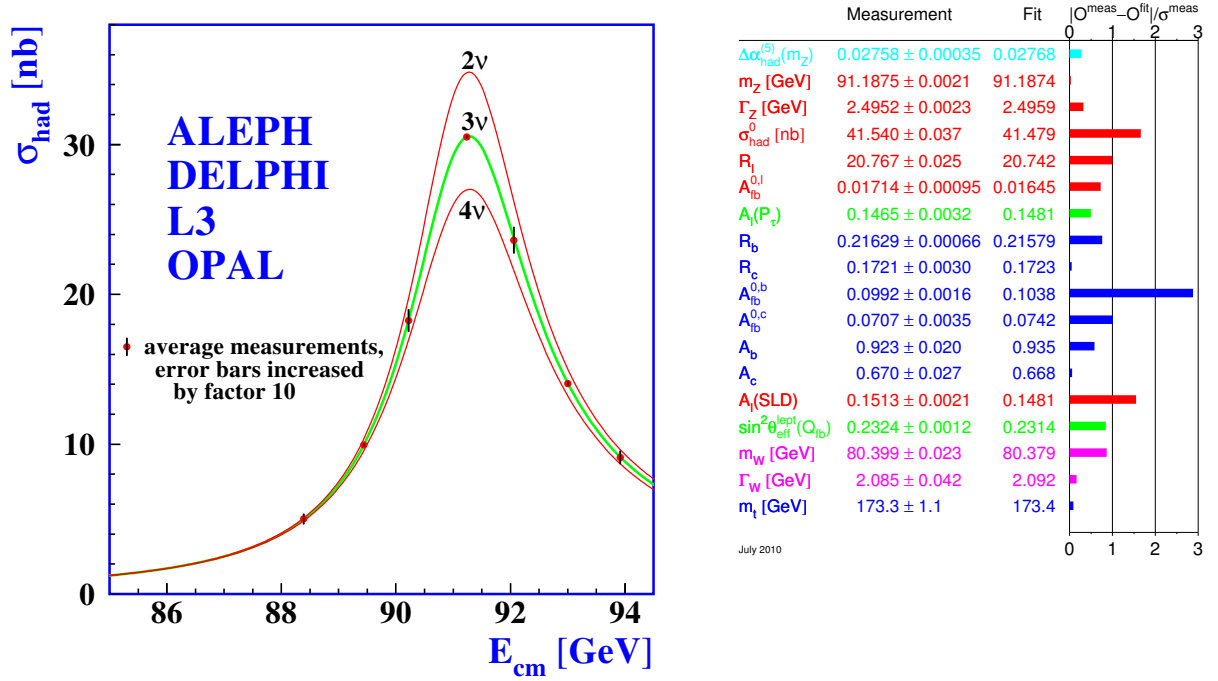


Figure 28: The lineshape of the Z boson and results of the precision electroweak fit taken from the LEPWWG.

8. the top quark mass, m_t , is measured at the Tevatron.

The results of the precision electroweak fit are in good agreement with the experimental results, as shown in Fig. 28, and for example shows that there are 3 massless neutrinos which couple to the Z boson.

7.2.1 W mass measurements

One of the most important quantities in electroweak sector is the mass of the W^\pm boson. The first measurements of the W mass were in hadronic collisions. The QCD backgrounds and resolution means that the hadronic W^\pm decay mode cannot be used. The mass cannot be directly reconstructed using the leptonic mode due to the unobserved neutrino. Instead the transverse mass

$$M_{\perp}^{\ell\nu 2} = 2p_{\perp}^{\ell} E_{\perp} (1 - \cos \phi_{\ell, \text{miss}}), \quad (76)$$

where p_{\perp}^{ℓ} is the transverse momentum of the observed lepton, E_{\perp} is the missing transverse energy and $\phi_{\ell, \text{miss}}$ is the azimuthal angle between the lepton and the direction of the missing transverse energy, is used.

The maximum value of the transverse mass is $M_{\perp}^{\ell\nu 2} \leq m_W^2$ and can be used to extract the W^\pm mass. This approach was used by the UA1 and UA2 experiments for the original W mass measurements and the recent results at the Tevatron, for example Fig. 29. The endpoint is smeared by the non-zero p_{\perp} and width of the W boson.

A major result of the LEP2 programme was the study of the production of pairs of electroweak gauge bosons, W^+W^- and Z^0Z^0 . The mass of the W can be extracted in two ways:

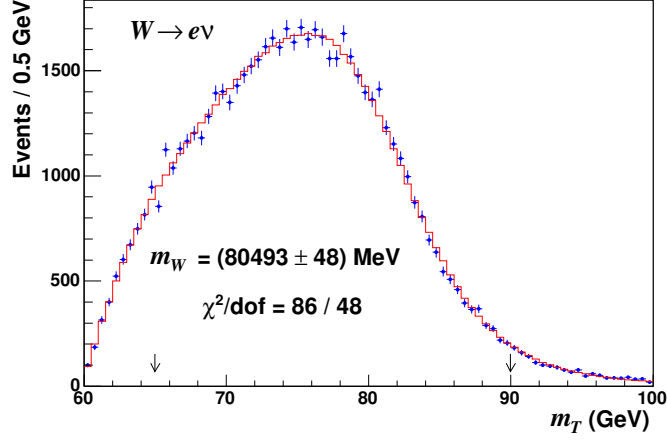


Figure 29: The transverse mass of the W at the Tevatron taken from Ref. [19].

1. measuring the cross section near the threshold

$$\sigma \sim \frac{G_F^2 m_W^2}{2\pi} \sqrt{1 - \frac{4m_W^2}{s}}, \quad (77)$$

which is clean theoretical but limited by statistics, see Fig. 30;

2. reconstructing the mass from the W decay products above threshold.

7.2.2 ρ parameter

In principle we should compare the full predictions of the Standard Model, or any model of new physics, with all the electroweak observables. However it is often useful, particularly in new physics models as corrections from new particles can lead to large corrections, to consider the ρ parameter. Naively

$$\rho = \frac{m_W^2}{m_Z^2 \cos^2 \theta_W} = 1, \quad (78)$$

connects the Z^0 and W^\pm masses with the weak mixing angle. The dominant loop corrections to it from self energies give

$$\Delta\rho = \frac{3G_F m_W^2}{8\sqrt{2}\pi^2} \left[\frac{m_t^2}{m_W^2} - \frac{\sin^2 \theta_W}{\cos^2 \theta_W} \left(\ln \frac{m_H^2}{m_W^2} - \frac{5}{6} \right) + \dots \right].$$

This relates m_W , m_t , and m_H . For a long time, m_t was most significant uncertainty in this relation; by now, m_W has more than caught up.

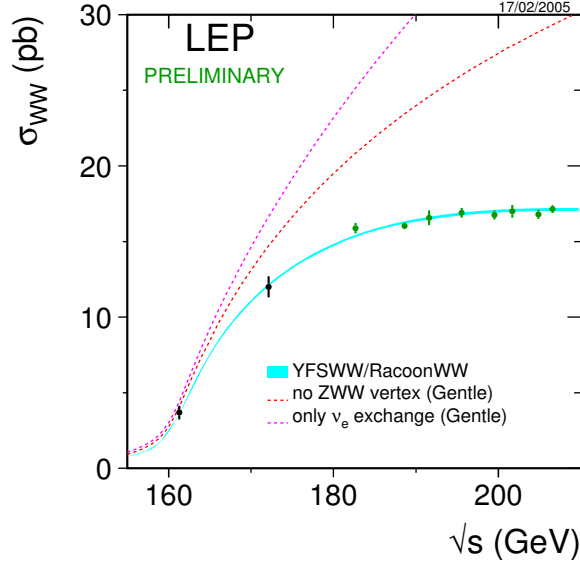


Figure 30: Cross section for the pair production of W^+W^- close to threshold from the LEPWWG.

8 Higgs Boson

The details of the Higgs mechanism with the SM are covered in the Standard model course. In this section we summarise the properties of the Standard Model Higgs Boson that are important for hadron collider measurements.

The SM contains spin-1 gauge bosons and spin- $\frac{1}{2}$ fermions. Massless fields ensure gauge invariance under $SU(2)_L \times U(1)_Y$ and renormalizability. While we could introduce mass terms “by hand”, *i.e.*

$$\mathcal{L} \propto m_A^2 A^\mu A_\mu + m_f (\bar{\Psi}_R \Psi_L + \bar{\Psi}_L \Psi_R), \quad (79)$$

this violates gauge invariance. Under the gauge transformation, $A^\mu \rightarrow A^\mu + \frac{1}{g} \partial^\mu \theta$, the mass term $A^\mu A_\mu$ gives terms proportional to the gauge transformation parameter θ , *i.e.* the gauge boson mass term is not gauge invariant. As the fields Ψ_L and Ψ_R transform differently under $SU(2)_L$ under the gauge transformation of the left-handed fermion field the fermion mass term is not gauge invariant.

Adding these mass terms by hand is obviously a bad idea. Instead we add a complex scalar doublet under the $SU(2)_L$ gauge group which introduces an additional four degrees of freedom. This scalar field can be coupled gauge invariantly to the gauge bosons, *i.e.*

$$\mathcal{L}_{\Phi A} = (D^\mu \Phi)(D_\mu \Phi). \quad (80)$$

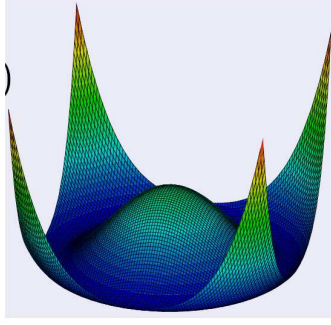


Figure 31: The Higgs boson potential.

A gauge-invariant interaction term with fermions can also be included⁷

$$\mathcal{L}_{\Phi\Psi} = g_f \bar{\Psi}_L \Phi \Psi_R + \text{h.c.} \quad (81)$$

In addition we need the Higgs potential

$$\mathcal{V}(\Phi) = \lambda (\Phi^\dagger \Phi)^2 + \mu^2 \Phi^\dagger \Phi. \quad (82)$$

For $\mu^2 < 0$ this potential has an infinite number of equivalent minima,

$$|\Phi| = \sqrt{\frac{-\mu^2}{2\lambda}} \equiv \frac{v}{\sqrt{2}}, \quad (83)$$

as shown in Fig. 31. We expand around one of these minima giving one radial and three circular modes. The circular modes are “gauged away” \rightarrow “eaten” by gauge bosons to give them mass via the vacuum expectation value (vev) the minimum of the potential.

From the structure above:

$$\begin{array}{llll} (D_\mu \Phi)^2 & \longrightarrow & \frac{g^2 v^2}{4} W_\mu W^\mu & \longrightarrow & M_W^2 = \frac{g^2 v^2}{4}; \\ g_f \bar{\Psi}_L \Phi \Psi_R & \longrightarrow & g_f \frac{v}{\sqrt{2}} \bar{\Psi}_L \Phi \Psi_R & \longrightarrow & m_f = \frac{g_f v}{\sqrt{2}}; \\ \lambda(|\Phi|^2 - v^2/2)^2 & \longrightarrow & \lambda v^2 H^2 & \longrightarrow & M_H^2 = 2\lambda v^2. \end{array}$$

This gives a fixed relation between the mass of the particles and their coupling to (surviving) scalar Higgs boson.

8.1 Unitarity

While in the Standard Model introducing the Higgs boson is the only way to give mass to the particles in a gauge invariant manner there are other arguments for the existence of the Higgs boson and it is interesting to ask what would happen if the Higgs boson did not exist.

⁷While we can use Φ to couple to the down-type fermions we need to use $i\sigma_2 \Phi^*$ to couple to the up-type fermions in a gauge invariant manner.

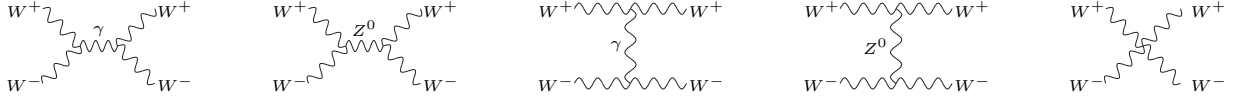


Figure 32: Feynman diagrams for WW scattering via gauge boson exchange.

If we consider $W^+W^- \rightarrow W^+W^-$ scattering, via the Feynman diagrams shown in Fig. 32, in the high energy limit the matrix element is

$$\mathcal{M} = g^2 \frac{s}{8M_W^2} \left(1 - \frac{4M_W^2}{s} \right) (1 + \cos \theta). \quad (84)$$

So without the Higgs boson the cross section

$$\sigma \sim \frac{s}{M_W^4}, \quad (85)$$

for $s \gg M_W$.



Figure 33: Higgs boson contributions to WW scattering.

This violates unitarity, so we need something to cancel the bad high energy behaviour of the cross section. We can arbitrarily invert a particle to cure this. This particle must be a scalar, suppose it has coupling, λ , to W^+W^- . This gives a contribution, via the Feynman diagrams in Fig. 33,

$$\mathcal{M} = \lambda^2 \left[-\frac{s}{8M_W^4} (1 + \cos \theta) - \frac{M_H^2}{4M_W^4} \left\{ \frac{s}{s - M_H^2} + \frac{t}{t - M_H^2} \right\} \right]. \quad (86)$$

This cancels the bad high energy behaviour if $\lambda = gM_W$, *i.e.* the Higgs coupling to the W^\pm boson. If we repeat the same procedure for $WW \rightarrow ZZ$ we need a coupling $g_{ZZH} \propto gm_Z$ and for $WW \rightarrow f\bar{f}$ we need a coupling $g_{f\bar{f}H} \propto gm_f$, *i.e.* the Higgs boson couplings to the Z^0 boson and Standard Model fermions.

So even if there was no Higgs boson we are forced to introduce a scalar interaction that couples to all particles proportional to their mass.

8.2 Higgs Measurements

To study the properties of the recently discovered Higgs boson we should focus our attention on,

- channels with a high signal rate;
- and a low background rate.

| Decay mode | Partial Width, Γ |
|------------------------------|---|
| $H \rightarrow f\bar{f}$ | $\frac{G_F M_H}{8\pi\sqrt{2}} \cdot 2m_f^2 N_c \left(1 - \frac{4m_f^2}{m_H^2}\right)^{\frac{3}{2}}$ |
| $H \rightarrow W^+W^-$ | $\frac{G_F M_H}{8\pi\sqrt{2}} \cdot m_H^2 \left(1 - \frac{4m_W^2}{m_H^2} + \frac{12m_W^4}{m_H^4}\right) \left(1 - \frac{4m_W^2}{m_H^2}\right)^{\frac{1}{2}}$ |
| $H \rightarrow ZZ$ | $\frac{G_F M_H}{8\pi\sqrt{2}} \cdot m_H^2 \frac{m_W^2}{2m_Z^2} \left(1 - \frac{4m_Z^2}{m_H^2} + \frac{12m_Z^4}{m_H^4}\right) \left(1 - \frac{4m_Z^2}{m_H^2}\right)^{\frac{1}{2}}$ |
| $H \rightarrow \gamma\gamma$ | $\frac{G_F M_H}{8\pi\sqrt{2}} \cdot m_H^2 \left(\frac{\alpha}{4\pi}\right)^2 \cdot \left(\frac{4}{3}N_c Q_t^2\right)^2 (2m_t > m_H)$ |
| $H \rightarrow gg$ | $\frac{G_F M_H}{8\pi\sqrt{2}} \cdot m_H^2 \left(\frac{\alpha_s}{4\pi}\right)^2 \cdot \left(\frac{2}{3}\right)^2 (2m_t > m_H)$ |
| $H \rightarrow VV^*$ | more complicated, but important for $m_H \lesssim 2m_V$ |

Table 4: Partial widths for various Higgs decay modes.

Unfortunately the channels with the highest signal rate often have the largest backgrounds. We need to be able to trigger on a given signal. Good mass resolution for the mass of the Higgs boson and its decay products can help to suppress backgrounds. We should also try and measure things that are well understood theoretically.

In order to consider the signals we need to understand how the Higgs boson is produced and then decays in hadron-hadron collisions.

The analytic results for the partial widths for various Higgs boson decay modes are given in Table 4 and the branching ratios are plotted as a function of the mass of the Higgs boson in Fig. 34. For $m_H < 2m_W$ the Higgs boson is quite narrow, $\Gamma_H = \mathcal{O}(\text{MeV})$, while for $m_H > 2m_W$ the Higgs boson becomes obese, $\Gamma_H(m_H = 1\text{TeV}) \approx 0.5 \text{ TeV}$. At large m_H the decay into vector boson pairs, W^+W^- and Z^0Z^0 , is dominant with $\Gamma_{H \rightarrow WW} : \Gamma_{H \rightarrow ZZ} \approx 2 : 1$, while for small m_H the decay into bottom quark pairs is dominant,

As the Higgs boson likes to couple to heavy objects (top, W , Z) there are a range of important Higgs production processes where the Higgs boson couples to heavy particles. The Feynman diagrams for the important processes are shown in Fig. 35 while the cross sections for the important processes are shown in Fig. 36 as a function of the Higgs boson mass.

The relative importance of different channels depend on the collider energy and the initial state (e.g. pp or $p\bar{p}$). At the Tevatron typical channels used for searches were:

- $gg \rightarrow H \rightarrow W^+W^- \rightarrow \ell\ell' + \cancel{E}_\perp$ this was the “golden plated” channel because although there is no mass peak the background can be reduced by using quantities, such as the angle between the leptons, which differ in the signal and background due to the different W boson production mechanisms;
- $q\bar{q} \rightarrow ZH \rightarrow \ell\ell b\bar{b}$ the key ingredient for this process is the b -tagging efficiency and mass resolution for jets in order to suppress the QCD backgrounds;
- $q\bar{q}' \rightarrow WH \rightarrow \ell\nu b\bar{b}$ has similar features to $q\bar{q} \rightarrow ZH \rightarrow \ell\ell b\bar{b}$;
- $q\bar{q}' \rightarrow ZH \rightarrow \cancel{E}_\perp + b\bar{b}$ the key feature is again the b -tagging efficiency and mass resolution for jets in order to suppress the QCD backgrounds;

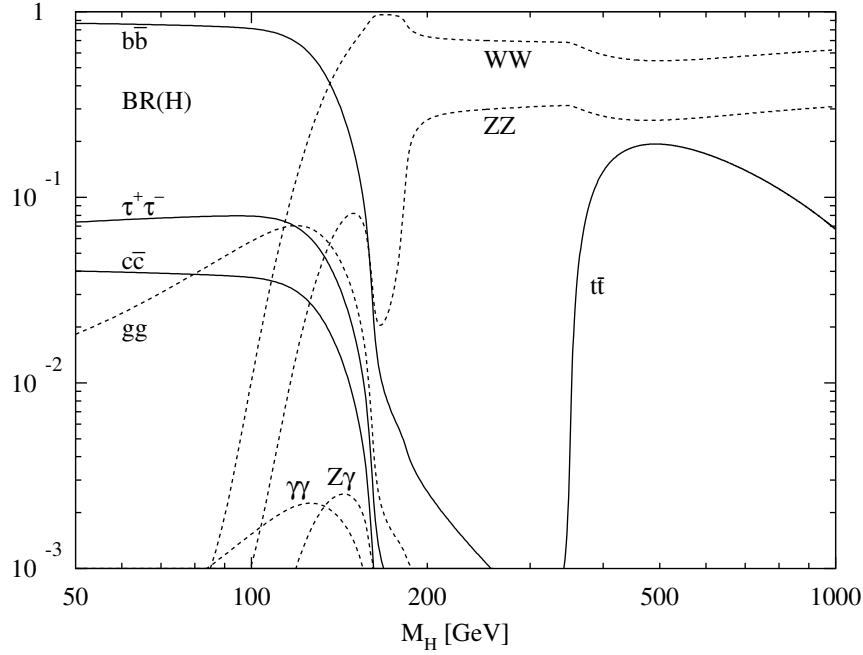


Figure 34: Branching ratios for the Higgs boson as a function of the Higgs boson mass, taken from Ref. [20], calculation by M. Spira.

- $q\bar{q}' \rightarrow W^\pm H \rightarrow W^\pm W^+ W^-$ in this case there is the possibility of same sign lepton production which has a low background together with the decay of remaining W to hadrons in order to increase the cross section.

Typical channels at the LHC include:

- $gg \rightarrow H \rightarrow ZZ \rightarrow 4\mu, 2e2\mu$ which is the “Golden plated” channel for $m_H > 140$ GeV, the key ingredient is the excellent resolution of the Z mass peak from the leptonic decay;
- $gg \rightarrow H \rightarrow W^+ W^- \rightarrow \ell\ell' + \cancel{E}_\perp$ is similar to the Tevatron analysis but with better statistics due to the larger production cross section;
- $gg \rightarrow H \rightarrow \gamma\gamma$ since Nature determined that the Higgs boson should have a mass around 120 GeV this is the easiest way to detect a Higgs boson in a collider experimnt. Although the branching ratio is small, the key ingredient is the mass resolution for photon pairs and a veto on photons from π^0 decays;
- $\text{VBF} \rightarrow H \rightarrow \tau\tau$ an important mode for determining couplings to the EW sector of the SM. The key ingredient is that QCD backgrounds are reduced by requiring a rapidity gap between the two tagging jets;
- $\text{VBF} \rightarrow H \rightarrow WW$ as for $\text{VBF} \rightarrow H \rightarrow \tau\tau$;
- $\text{VBF} \rightarrow H \rightarrow b\bar{b}$ is in principle similar to the other VBF modes but it is hard to trigger on pure QCD-like objects (jets).

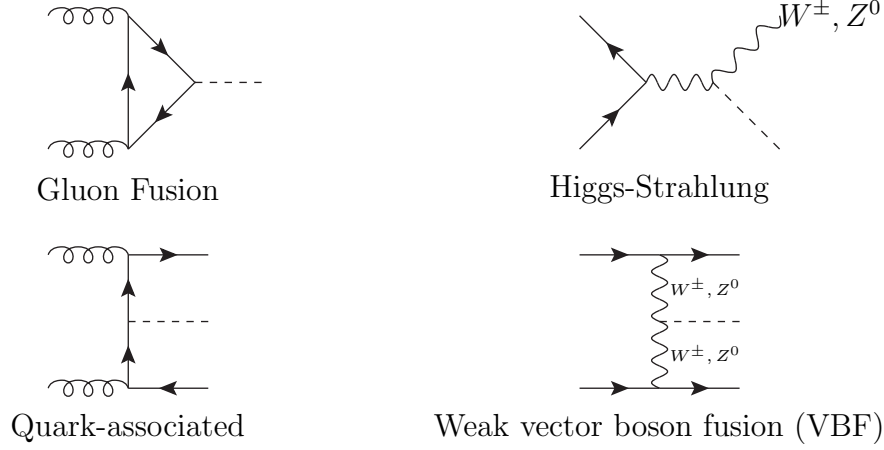


Figure 35: Feynman diagrams for important Higgs boson production processes.

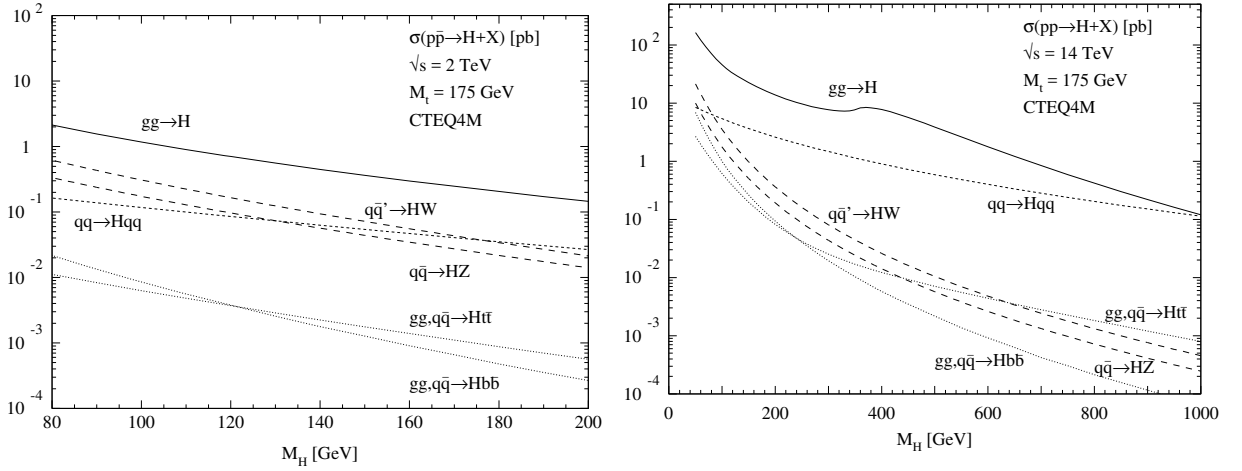


Figure 36: Higgs production cross sections at hadron colliders taken from Ref. [20], calculation by M. Spira.

8.3 The effective Higgs coupling to gluons

The loop induced coupling of gluons to the Higgs boson via a massive quark loop is one of the most important ingredients for Higgs studies at a proton-proton collider. Quantum corrections to this process can be extremely large but computations with the full dependence on the quark mass are extremely difficult.

For low transverse momenta, and inclusive quantities like the total cross section, it is popular to compute the quantum corrections in an effective field theory in the limit that the top quark mass is infinitely heavy, $m_t \rightarrow \infty$. The Lagrangian of the heavy quark Higgs effective theory (HEFT) proceeds through a dimension-five operator with the Higgs coupling directly to gluons and is derived via expansion in m_H/m_t ,

$$\mathcal{L}_{\text{HEFT}} = c_{\text{HEFT}} \frac{1}{4} H G^{a,\mu\nu} G_{\mu\nu}^a \quad (87)$$

where $c_{\text{HEFT}} = \frac{\alpha_s}{3\pi v} + \mathcal{O}(\alpha_s^2)$ for a Higgs vacuum expectation value v . It is possible to

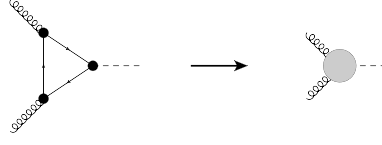


Figure 37: The triangle Feynman diagram for $gg \rightarrow H$ via a heavy quark loop can be used to extract the Wilson coefficient in the heavy quark effective Higgs Lagrangian.

extract the value of c_{HEFT} by considering the large mass limit of the triangle diagram in Figure 37. While the ratio of m_H/m_t is not particularly small the approximation often does a good job at matching data when the complete results for leading order are used as a normalisation. As the transverse momentum of the produced Higgs boson increases the approximation will break down.

Computations within this effective theory are now available for the total cross section $gg \rightarrow H$ through to N³LO [21, 22]. Figure 38 shows the convergence of the total cross-section by studying the dependence on the renormalisation and factorisation scale $\mu = \mu_R = \mu_F$. Further details on the approximation and other topics can be found in references [5, 23].

8.4 Extended Higgs Sectors

While current measurements show no significant deviations from a minimal SM Higgs sector adding a single Higgs doublet is the simplest choice for the Higgs sector. Many theoretically attractive models like SUSY naturally have a larger Higgs sector. However, we need to be careful to respect constraints from flavour changing neutral currents (FCNC) and the electroweak precision data.

8.4.1 The Two Higgs Doublet Model

The simplest extension to the Standard Model is the *Two Higgs Doublet Model* (THDM). In this model there are two Higgs doublets. There are a number of variants on the model depending on whether or not CP is conserved and how the Higgs bosons couple

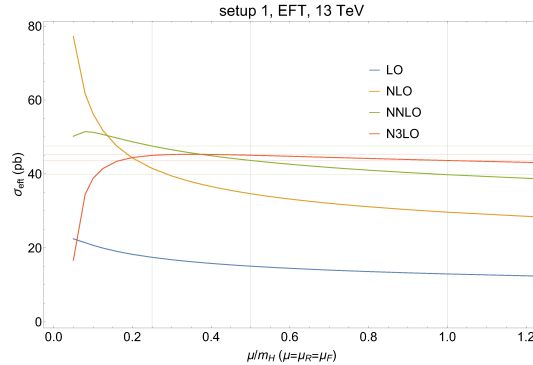


Figure 38: The scale dependence of the total cross section for Higgs production through gluon fusion up to N³LO in QCD. Figure taken from Ref. [22].

to the fermions. The most interesting variant (called Type-II) is that which occurs (in a constrained variant) in SUSY models. In the general version of the Type-II model there are ~ 10 new parameters, whereas in the constrained SUSY version there are only two m_{A^0} and $\tan\beta$. There are indirect constraints from rare processes, *e.g.* kaon and bottom mixing and decays, precision EW data and cosmology.

As there are two doublets there as two vevs: $v_{1,2}$. They are constrained by the requirement

$$v_1^2 + v_2^2 = v^2 \approx (246\text{GeV})^2, \quad (88)$$

in order to give the correct gauge boson masses as in the Standard Model. There is an additional parameter $\tan\beta = v_2/v_1$. In the Type-II mode the H_1 doublet gives mass to up-type fermions while the H_2 doublet gives mass to down-type fermions. Both doublets couple and give mass to the gauge bosons. After electroweak symmetry breaking there are five scalar boson mass eigenstates, two neutral scalars h^0, H^0 , one neutral pseudoscalar A^0 , and two charged scalars H^\pm . The coupling of all the Higgs bosons to the vector bosons are reduced. The couplings to the fermions are enhanced (up-type) and suppressed (down-type) as $\tan\beta$ increases. At tree level the masses are related by

$$m_{H^\pm}^2 = m_{A^0}^2 + m_W^2, \quad m_{H^0}^2 + m_{h^0}^2 = m_{A^0}^2 + m_Z^2. \quad (89)$$

At tree level in SUSY $m_{h^0} \leq M_Z$ however there are large quantum corrections ($m_{h^0} \lesssim 140\text{GeV}$).

9 Beyond the Standard Model Physics

As discussed in Section 7 the Standard Model has 18 free parameters, although in principle we should also include the Θ parameter of QCD. We now need more parameters to incorporate neutrino masses. Despite the excellent description of all current experimental data there are still a number of important questions the Standard Model does not answer.

- What are the values of these parameters?
- Why is the top quark so much heavier than the electron?
- Why is the Θ parameter so small?
- Is there enough CP-violation to explain why we are here, *i.e.* the matter-antimatter asymmetry of the universe?
- What about gravity?

While these are all important questions there is no definite answer to any of them.

There are however a large number of models of Beyond the Standard Model (BSM) physics which motivated by trying to address problems in the Standard Model. Given the lack of any experimental evidence of BSM physics the field is driven by theoretical and ascetic arguments, and unfortunately fashion.

All models of BSM physics predict either new particles or differences from the Standard Model, otherwise they cannot be distinguished experimentally from the Standard Model. There are a number of ways of looking for BSM effects:

Collider Experiments if the theory contains new particles these should be produced in collider experiments and decay to give Standard Model particles, currently the searches at the energy frontier are at the LHC general-purpose detectors ATLAS and CMS;

Precision Experiments measure something predicted by the Standard Model to very high accuracy and compare the results with the theoretical prediction, examples include the LEP/SLD precision measurements at the Z^0 pole and the anomalous magnetic moment, $g - 2$, of the muon;

Rare Decays or Processes measure the cross section or decay rate for some process which the Standard Model predicts to be small (or zero). Examples include: neutron electric dipole moment experiments, proton decay experiments, neutrino mixing experiments, rare B and kaon decay and CP-violation experiments (BELLE, BaBar, NA48/62, LHCb).

In many ways these approaches are complimentary. Some effects, *e.g.* CP-violation, are best studied by dedicated experiments but if the result of these experiments differs from the SM there should be new particles which are observable at collider experiments.

We will consider the collider signals of BSM physics in detail but only look at the constraints from low-energy physics as we look at various models. The most important low energy constraints are flavour changing neutral currents and proton decay. Often other constraints, *e.g.* from astrophysics and cosmology are also considered.

9.1 Models

We will briefly review some of the more promising models and then look at the implications of these models for collider physics taking a pragmatic view looking at the different possible signatures rather than the details of specific models.

There are a wide range of models: grand unified theories; Technicolor; supersymmetry; large extra dimensions; small extra dimensions; little Higgs models; unparticles Depending on which model builder you talk to they may be almost fanatical in their belief that one of these models is realized in nature.

9.1.1 Grand Unified Theories

The first attempts to answer the problems in the Standard Model were *Grand Unified Theories* (GUTs.) The basic idea is that the Standard Model gauge group $SU(3)_c \times SU(2)_L \times U(1)_Y$ is the subgroup of some larger gauge symmetry. The simplest group is $SU(5)$, which we will consider here, other examples include $SO(10)$. $SU(5)$ has $5^2 - 1 = 24$ generators which means there are 24 gauge bosons. In the Standard Model there are 8 gluons and 4 electroweak gauge bosons (W^\pm , W^0 , $B^0 \Rightarrow W^\pm$, γ , Z^0). Therefore there are 12 new gauge bosons $X^{\pm\frac{4}{3}}$ and $Y^{\pm\frac{1}{3}}$. The right-handed down type quarks and left

handed leptons form a $\bar{5}$ representation of $SU(5)$. The rest of the particles form a 10 representation of the gauge group

$$\begin{array}{c} \text{gluons} \\ W^\pm \end{array} \begin{array}{c} \rightarrow \\ \rightarrow \\ \rightarrow \\ \rightarrow \end{array} \begin{pmatrix} d \\ d \\ d \\ e^c \\ \bar{\nu}_e \end{pmatrix} \begin{array}{c} \leftarrow \\ \leftarrow \\ \leftarrow \\ \leftarrow \end{array} \begin{array}{c} X, Y \\ R \end{array} \quad \begin{pmatrix} 0 & u^c & -u^c & -u & -d \\ u^c & 0 & u^c & -u & -d \\ u^c & -u^c & 0 & -u & -d \\ u & u & u & 0 & -e^c \\ d & d & d & e^c & 0 \end{pmatrix}_L. \quad (90)$$

In this model there are two stages of symmetry breaking. At the GUT scale the $SU(5)$ symmetry is broken and the X and Y bosons get masses. At the electroweak scale the $SU(2) \times U(1)$ symmetry is broken as before. There are three problems with this theory: the couplings do not unify at the GUT scale; why is the GUT scale higher than the electroweak scale; and proton Decay. We will come back to the first two of these questions.

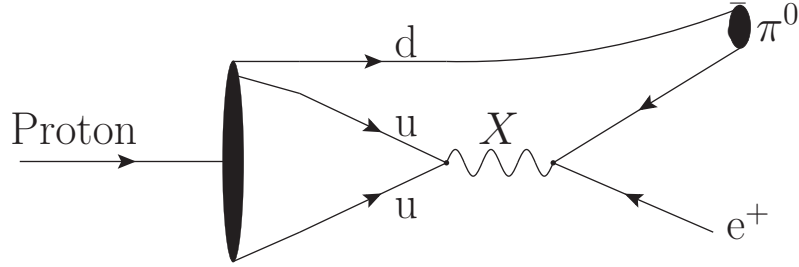


Figure 39: Proton Decay in a Grand Unified theory.

Proton Decay Grand unified theories predict the decay of the proton via the exchange of the X and Y bosons, as shown in Fig. 39. We would expect this decay rate to go like

$$\Gamma(p \rightarrow \pi^0 e^+) \sim \frac{M_p^5}{M_X^4}, \quad (91)$$

where M_X is the mass of the X boson and M_p the mass of the proton, on dimensional grounds.

There are limits on the proton lifetime from water Čerenkov experiments. The decay of the proton will produce an electron which is travelling faster than the speed of light in water. This will give Čerenkov radiation, just as the electron produced in the weak interaction of a neutrino does. This is used to search for proton decay. As there is no evidence of proton decay there is limit of

$$\tau_P \geq 1.6 \times 10^{32} \text{ years} \quad (92)$$

on the proton lifetime. This means $M_X > 10^{16-17} \text{ GeV}$ which is larger than preferred by coupling unification. Proton decay gives important limits on other models.

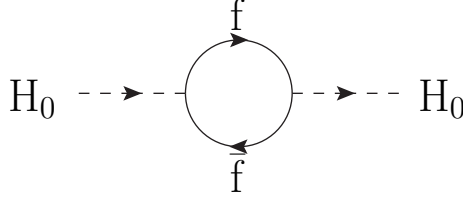


Figure 40: Quantum correction to the Higgs mass from a fermion loop.

9.1.2 Hierarchy Problem

The vast majority of new physics models are motivated by considering the hierarchy problem, *i.e.* why is the electroweak scale is so much less than the GUT or Planck (where gravity becomes strong) scales? It is more common to discuss the technical hierarchy problem which is related to the Higgs boson mass. If we look at the Higgs mass there are quantum corrections from fermion loops such as that shown in Fig. 40. This gives a correction to the Higgs mass,

$$\delta M_{Hf}^2 = i \frac{|g_f|^2}{4} \int \frac{d^4 k}{(2\pi)^4} \frac{\text{tr} [(k + \not{p} + m_f)(k + m_f)]}{[(k + p)^2 - m_f^2] [k^2 - m_f^2]}, \quad (93)$$

where p is the four-momentum of the Higgs boson, k the four-momentum flowing in the loop, g_f the coupling of the Higgs boson to the fermion and m_f the fermion mass. We need to introduce an ultra-violet cut-off, Λ , to regularize the integral giving

$$\delta M_{Hf}^2 = \frac{|g_f|^2}{16\pi^2} [-2\Lambda^2 + 6m_f^2 \ln(\Lambda/m_f)]. \quad (94)$$

So either the Higgs mass is the GUT/Planck scale or there is a cancellation

$$M_H^2 = M_{H\text{bare}}^2 + \delta M_H^2, \quad (95)$$

of over 30 orders of magnitude to have a light Higgs boson.

This worries a lot of BSM theorists, however there are values of the Higgs boson mass for which the Standard Model could be correct up to the Planck scale. The Higgs boson mass is $m_H^2 = \lambda v^2$. There are two constraints on the mass: the coupling should be perturbative, $\lambda \lesssim 1$; the vacuum must be non-trivial, $\lambda \rightarrow 0$ is forbidden. As can be seen in Fig. 41 there is an island of stability in the middle where the Standard Model can be valid to the Planck scale.

Many solutions to the hierarchy problem have been proposed. They come in and out of fashion and occasionally new ones are proposed. Examples include: Technicolor; supersymmetry; extra dimensions; and little Higgs models.

9.1.3 Technicolor

Technicolor is one of the oldest solutions to the hierarchy problem. The main idea is that as the problems in the theory come from having a fundamental scalar particle they can be solved by not having one. The model postulates a new set of gauge interactions *Technicolor*, which acts on new technifermions. We think of this interaction like QCD,

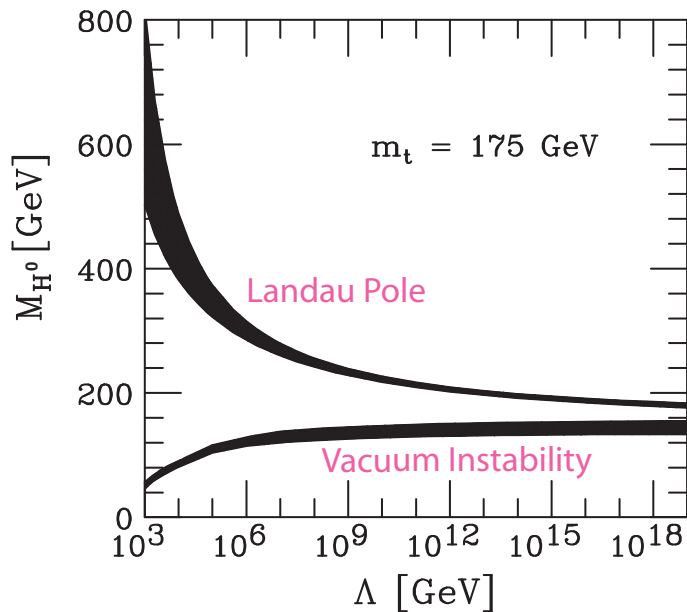


Figure 41: Region of stability for the Standard Model Higgs boson.

although different gauge groups have been considered. The technifermions form bound states, the lightest being technipions. Using the Higgs mechanism these technipions give the longitudinal components of the W^\pm and Z bosons, and hence generate the gauge boson masses. There must also be a way to generate the fermions masses, *Extended Technicolor*. It has proved hard to construct realistic models which are not already ruled out. For many years Technicolor fell out of fashion, however following the introduction of little Higgs models there has been a resurgence of interest and the new walking Technicolor models look more promising.

9.1.4 Supersymmetry

If there is a scalar loop in the Higgs propagator, as shown in Fig.42. We get a new

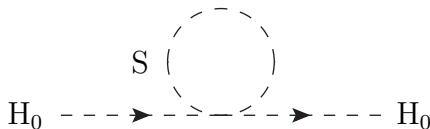


Figure 42: New scalar boson loop in the Higgs boson propagator.

contribution to the Higgs mass,

$$\delta M_{HS}^2 = \frac{\lambda_s}{16\pi^2} (\Lambda^2 - 2M_S^2 \ln(\Lambda/M_S)), \quad (96)$$

where M_S is the mass of the new scalar particle. If there are two scalars for every fermion, with the same mass and $\lambda_s = |g_f|^2$ the quadratic dependence cancels. Theorists like to

| SM particle | Spin | SUSY particle | Spin |
|----------------|------|---------------|-----------------|
| Electron | 1/2 | Selectron | 0 |
| Neutrino | 1/2 | Sneutrino | 0 |
| Up | 1/2 | Sup | 0 |
| Down | 1/2 | Sdown | 0 |
| Gluon | 1 | Gluino | 1/2 |
| Photon | 1 | Photino | 1/2 |
| Z | 1 | Zino | 1/2 Neutralinos |
| Higgs | 0 | Higgsino | 1/2 |
| W ⁺ | 1 | Wino | 1/2 Charginos |
| H ⁺ | 0 | Higgsino | 1/2 |

Table 5: Particle content of the Minimal Supersymmetric Standard Model.

have symmetries to explain cancellations like this, *Supersymmetry* (SUSY). For every fermionic degree of freedom there is a corresponding bosonic degree of freedom: all the SM fermions have two spin-0 partners; all the SM gauge bosons have a spin- $\frac{1}{2}$ partner. The full particle content of the theory is given in Table 5. In SUSY models we need to have two Higgs doublets to give mass to both the up- and down-type quarks in a way which is invariant under the supersymmetric transformations.

There are major two reasons, in addition to the solution of the hierarchy problem, to favour SUSY as an extension of the SM.

Coleman-Mandula theorem If we consider any extension to the Poincaré group any new generators which transform as bosons lead to a trivial S-matrix, *i.e.* scattering only through discrete angles. Later Haag, Lopuszanski and Sohnius showed that SUSY is the only possible extension of the Poincaré group which doesn't give a trivial S-matrix.

SUSY coupling unification In SUSY GUTS the additional SUSY particles change the running of the couplings and allow the couplings to truly unify at the GUT scale, as shown in Fig. 43. However, with increasingly accurate experimental measurements of the strong coupling this is no longer quite true.

In the modern view of particle physics we construct a theory by specifying the particle content and symmetries. All the terms allowed by the symmetries are then included in the Lagrangian. If we do this in supersymmetric models we naturally get terms which do not conserve lepton and baryon number. This leads to proton decay as shown in Fig. 44. Proton decay requires that both lepton and baryon number conservation are violated. The limits on the proton lifetime lead to very stringent limits on the product of the couplings leading to proton decay.

$$\lambda'_{11k} \cdot \lambda''_{11k} \lesssim 2 \cdot 10^{-27}. \quad (97)$$

Only natural way for this to happen is if some symmetry requires that one or both couplings are zero. Normally a multiplicatively conserved symmetry *R-parity*

$$R_p = (-1)^{3B+L+2S}, \quad (98)$$

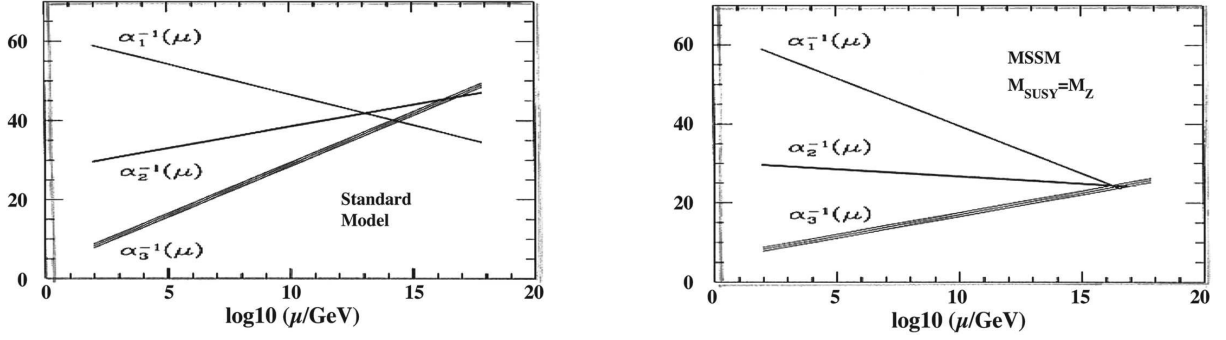


Figure 43: Coupling constant unification in the Standard and Minimal Supersymmetric Standard Models.

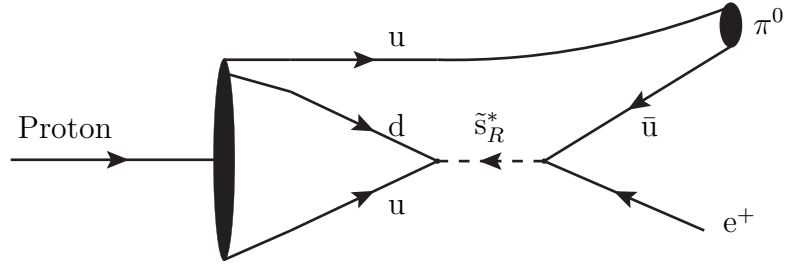


Figure 44: Proton decay in supersymmetric models.

such that Standard Model Particles have $R_p = +1$ and SUSY particles have $R_p = -1$, is introduced which forbids both terms.

Alternatively symmetries can be imposed which only forbid the lepton or baryon number violating terms. The simplest SUSY extension of the Standard Model has R_p conservation and is called the Minimal Supersymmetric Standard Model (MSSM). The multiplicative conservation of R-parity has two important consequences: SUSY particles are only pair produced; the lightest SUSY particle is stable, and therefore must be neutral on cosmological grounds. It is therefore a good dark matter candidate.

So far we haven't dealt with the biggest problem in SUSY. Supersymmetry requires that the SUSY particles have the same mass as their Standard Model partner and the SUSY partners have not been observed. SUSY must therefore be a broken symmetry in such a way that the Higgs mass does not depend quadratically on the ultraviolet cut-off, called *soft SUSY breaking*. This introduces over 120 parameters into the model. Many of these parameters involve either flavour changing or CP-violating couplings and are constrained by limits on flavour changing neutral currents.

Flavour Changing Neutral Currents In the Standard Model the only interactions which change the quark flavour are those with the W^\pm boson. So any processes which change the flavour of the quarks, but not the charge, *Flavour Changing Neutral Currents* (FCNCs), must be loop mediated.

There are two important types: those which change the quark flavour with the emission of a photon, *i.e.* $b \rightarrow s\gamma$; those which give meson-antimeson mixing, *e.g.* $B - \bar{B}$ mixing.

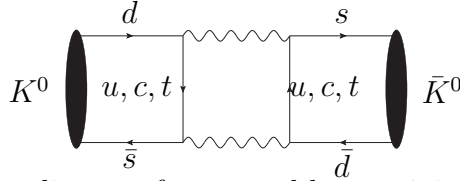


Figure 45: Feynman diagram for neutral kaon mixing in the Standard Model.

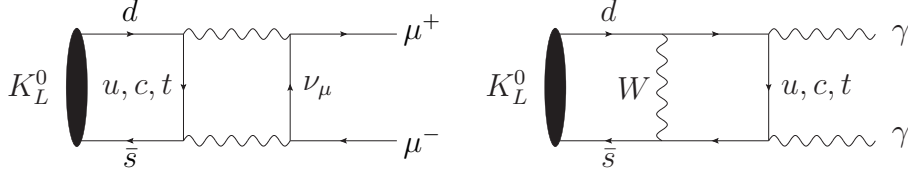


Figure 46: Feynman diagrams for the decay of the neutral kaon to $\mu^+\mu^-$ and $\gamma\gamma$ in the Standard Model.

Both are important in the Standard Model and in constraining possible new physics models.

In the Standard Model flavour changing neutral currents are suppressed by the Glashow-Iliopoulos-Maiani (GIM) mechanism. If we consider neutral Kaon mixing, as shown in Fig. 45, and the rare Kaon decays $K_L^0 \rightarrow \mu^+\mu^-$ and $K_L^0 \rightarrow \gamma\gamma$, as shown in Fig. 46.

Considering only two generations for simplicity all these diagrams go like

$$\frac{1}{M_W^2} \frac{m_u^2 - m_c^2}{M^2}, \quad (99)$$

times a factor due to the Cabibbo mixing angle where M is the largest mass left after the removal of one W propagator, *i.e.* M_W for $K^0 - \bar{K}^0$ mixing and $K_L^0 \rightarrow \mu^+\mu^-$, and m_c for $K_L^0 \rightarrow \gamma\gamma$. This suppression is called the GIM mechanism and explains why $\Gamma(K_L^0 \rightarrow \mu^+\mu^-) \sim 2 \times 10^{-5} \Gamma(K_L^0 \rightarrow \gamma\gamma)$. The current experimental results are in good agreement with the SM. This often proves a problem in BSM physics as there are often new sources of FCNCs.

In SUSY theories the SUSY partners also give contributions to FCNCs, as shown in Fig. 47. In this case the diagrams proportional to the mass difference of the squarks.

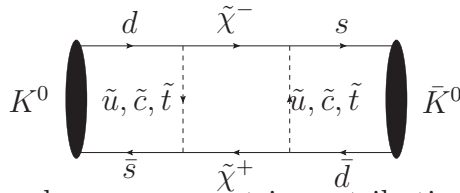


Figure 47: An example supersymmetric contribution to neutral kaon mixing.

Provide the SUSY breaking masses are flavour independent this is not a problem, as the mass differences are the same as the SM. It is also not a problem if there is no flavour mixing in the model. In general both these things are possible and must be considered.

SUSY Breaking What are the 120 SUSY breaking parameters? In general there are: SUSY breaking masses for the scalars; SUSY breaking masses for the gauginos; A terms which mix three scalars; mixing angles and CP-violating phases. We need a model of

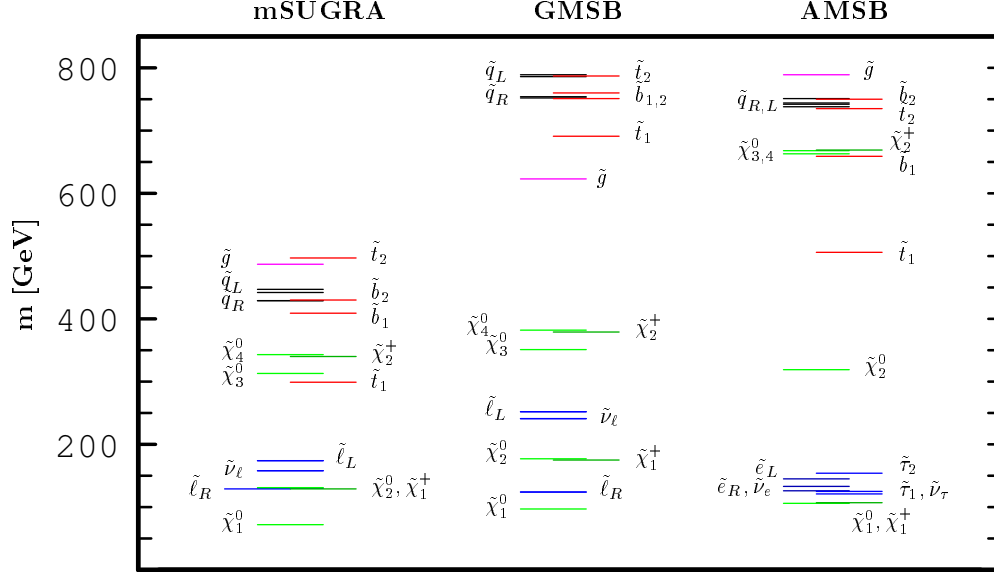


Figure 48: Examples of the mass spectra in different SUSY breaking models.

where these parameters come from in order to do any phenomenological or experimental studies. We therefore use models which predict these parameters from physics at higher energy scales, *i.e.* the GUT or Planck scale. In all these models SUSY is broken in a hidden sector, *i.e.* the MSSM particles.

SUGRA SUSY breaking is transmitted via gravity. All the scalar (M_0) and gaugino ($M_{1/2}$) masses are unified at the GUT scale. The A and B terms are also universal. The known value of M_Z is used to constrain the μ and B parameters leaving $\tan \beta = v_1/v_2$ as a free parameter. There are five parameters which give the mass spectrum: M_0 , $M_{1/2}$, $\tan \beta$, $\text{sgn } \mu$, A . The gluino mass is correlated with $M_{1/2}$ and slepton mass with M_0 .

GMSB In gauge mediated SUSY breaking (GMSB) the flavour-changing neutral current problem is solved by using gauge fields instead to gravity to transmit the SUSY breaking. The messenger particles, X , transmit the SUSY breaking. The simplest choice is a complete $SU(5)$ **5** or **10** of particles transmitting the SUSY breaking to preserve the GUT symmetry. The fundamental SUSY breaking scale $\lesssim 10^{10}$ GeV is lower than in gravity mediated models. The gaugino masses occur at one-loop, $M_{\tilde{g}} \sim \alpha_s N_X \Lambda$ while the scalar masses occur at two-loop, $M_{\tilde{q}} \sim \alpha_s^2 \sqrt{N_X} \Lambda$, where Λ is the breaking scale and N_X the number of messenger fields. The true LSP is the almost massless gravitino. The lightest superpartner is unstable and decays to gravitino and can be neutral, *e.g.* $\tilde{\chi}_1^0$, or charged, *e.g.* $\tilde{\tau}_1$.

AMSB The superconformal anomaly is always present and can give anomaly mediated SUSY breaking (AMSB). This predicts the sparticle masses in terms of the gravitino mass, $M_{3/2}$. The simplest version of the model predicts tachyonic particles so another SUSY breaking mechanism is required to get a realistic spectrum, *e.g.* adding universal scalar masses (M_0). The model has four parameters M_0 , $M_{3/2}$, $\tan \beta$ and $\text{sgn } \mu$. In this model the lightest chargino is almost degenerate with the lightest neutralino.

The mass spectrum in the models is different, as shown in Fig. 48. The main differences are: the mass splitting between gluino and electroweak gauginos; the mass splitting of the squarks and sleptons; and the nature of the LSP.

Muon g-2 Another important low energy constraint on BSM physics is the anomalous magnetic moment of the muon. The magnetic moment of any fundamental fermion is

$$\mu = g \left(\frac{e}{2m} \right) \mathbf{S}, \quad (100)$$

where g is the g -factor, m the mass and \mathbf{S} the spin of the particle. The Dirac equation predicts $g = 2$. However there are quantum corrections, as shown in Fig. 49, which lead to an anomalous magnetic moment, $g - 2$.

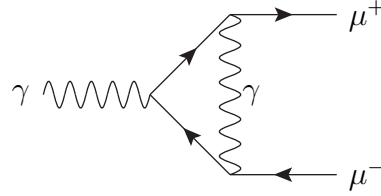


Figure 49: Vertex correction contributing to the anomalous muon magnetic moment in the Standard Model.

There are also quark loops in the photon propagator, as shown in Fig. 50. This is a low energy process so we can not use perturbative QCD. Instead we must use the measured e^+e^- total cross section and the optical theorem to obtain the corrections which leads to an experimental error on the theoretical prediction. In many BSM theories, for example

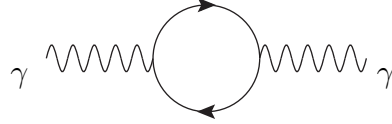


Figure 50: Quark loop in the photon propagator which contributes to the anomalous muon magnetic moment in the Standard Model.

in SUSY, there are additional corrections from diagrams, such as that shown in Fig. 51.

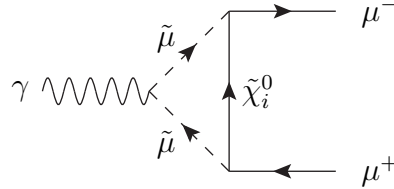


Figure 51: Example of a SUSY correction to the muon magnetic moment.

The original experimental result disagreed with the SM at 2.6σ , but there was an error in the sign in one of the terms in the theoretical calculation reducing the significance to about 1.4σ . However if you measure enough quantities some of them should disagree with the prediction by more the 1 sigma (about 1/3), and some by 2 sigma (4.6%) or 3 sigma (0.3%). This is why we define a discovery to be 5 sigma ($6 \times 10^{-50}\%$), so this is nothing to worry about.

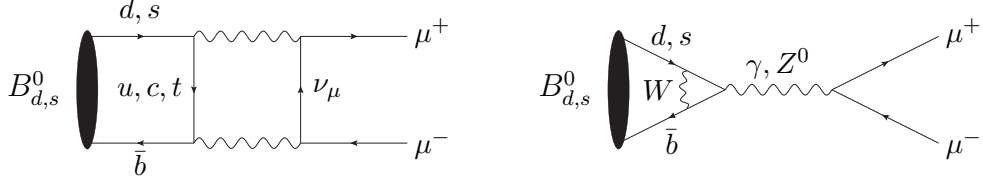


Figure 52: Standard Model Feynman diagrams for $B_s \rightarrow \mu^+ \mu^-$.

Rare B decays There is an amazing consistency of the current flavour physics measurements. However, many new physics models can have a similar pattern in their flavour sector, the new physics model must have this otherwise it is experimentally excluded. However, there can still be new physics in rare processes (like $B^+ \rightarrow \tau^+ \nu_\tau$) and CP-asymmetries. One promising examples is the decay $B_s \rightarrow \mu^+ \mu^-$. There are two Standard Model contributions from box and penguin diagrams as shown in Fig. 52. Both of these are suppressed by $V_{tb} V_{ts}^*$ giving a Standard Model branching ratio

$$\text{BR}_{B_s, d \rightarrow \mu\mu}^{(\text{SM})} \approx 10^{-9}. \quad (101)$$

This gives a simple leptonic final state with minor theoretical uncertainties but a huge background so the mass resolution is paramount, the expected mass resolution for the LHC experiments is given in Table 6.

| Exp. | ATLAS | CMS | LHCb |
|------------------|-------|-----|------|
| σ_m (MeV) | 77 | 36 | 18 |

Table 6: Expected mass resolution for $B_s \rightarrow \mu^+ \mu^-$.

In the MSSM, however, the amplitude involves three powers of $\tan^2 \beta$, so that

$$\text{BR}_{B_s \rightarrow \mu\mu}^{(\text{MSSM})} \propto \tan^6 \beta, \quad (102)$$

which leads to an enhancement over the SM value by up to three orders of magnitude.

9.1.5 Extra Dimensions

Many theorists believe there are more than 4 dimensions, for example string theories can only exist in 10/11 dimensions. The hierarchy problem can be solved (redefined?) in these models in one of two ways.

1. There is a large extra dimension with size $\sim 1\text{mm}$. In this case

$$M_{\text{Planck}}^2 \sim M^{n+2} R^n, \quad (103)$$

where M_{Planck} is the observed Planck mass, M is the extra-dimensional Planck mass and R the radius of the additional n dimensions. In this case the Planck mass is of order 1 TeV so there is no hierarchy problem. However the hierarchy in the sizes of the dimensions must be explained.

2. Small extra dimensions in which case the extra dimension is warped. The model has two branes, we live on one and the other is at the Planck scale. The Higgs VEV is suppressed by a warp factor, $\exp(-kr_c\pi)$, where r_c is the compactification radius of the extra dimension, and k a scale of the order of the Planck scale.

We can consider what happens in extra-dimensional models by studying a scalar field in 5-dimensions. In this case the equation of motion for the scalar field is

$$\left(\frac{\partial^2}{\partial t^2} - \nabla_5^2 + m^2\right) \Phi(x, y, z, x_5, t) = 0, \quad (104)$$

where

$$\nabla_5^2 = \frac{\partial^2}{\partial x^2} + \frac{\partial^2}{\partial y^2} + \frac{\partial^2}{\partial z^2} + \frac{\partial^2}{\partial x_5^2} \quad (105)$$

is the 5-dimensional Laplace operator. If the 5-th dimension is circular we can Fourier decompose the field,

$$\Phi(x, y, z, x_5, t) = \sum_n \Phi_n(x, y, z, t) \exp(inx_5/R). \quad (106)$$

The equation of motion therefore becomes,

$$\sum_n \left(\frac{\partial^2}{\partial t^2} - \nabla_4^2 + m^2 + \frac{n^2}{R^2}\right) \Phi_n(x, y, z, t). \quad (107)$$

This gives a Kaluza-Klein (KK) tower of states with mass splitting $\sim 1/R$. There are a number of different models.

Large Extra Dimensions Only gravity propagates in the bulk, *i.e.* in the extra dimensions. We therefore only get Kaluza-Klein excitations of the graviton. In large extra dimensional models the mass splitting between the KK excitations is small and all the gravitons contribute to a given process. Phenomenologically there are deviations from the SM prediction for SM processes.

Small Extra Dimensions Again only gravity propagates in the bulk so there are only KK excitations of the graviton. In this case the mass splitting is large leading to resonant graviton production.

Universal Extra Dimensions Another alternative is to let all the Standard Model fields propagate in the bulk, *Universal Extra Dimensions* (UED). All the particles have Kaluza-Klein excitations. It is possible to have a Kaluza-Klein parity, like R-parity in SUSY. The most studied model has one extra dimension and a similar particle content to SUSY, apart from the spins. There are also some 6-dimensional models.

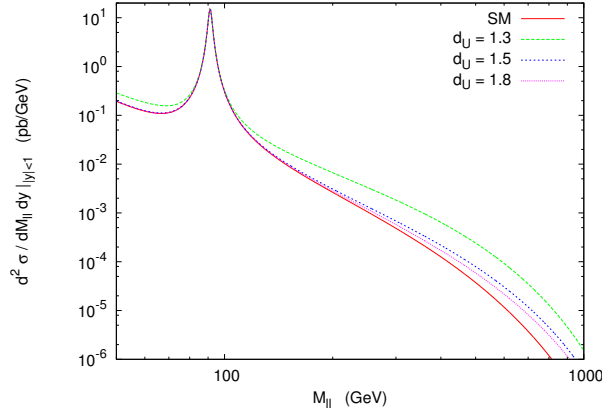


Figure 53: Drell-Yan mass spectrum including unparticle exchange taken from Ref. [24].

9.1.6 Little Higgs Models

In little Higgs models the Higgs fields are Goldstone bosons associated with breaking a global symmetry at a high scale, Λ_S . The Higgs fields acquire a mass and become pseudo-Goldstone bosons via symmetry breaking at the electroweak scale. The Higgs fields remain light as they are protected by the approximate global symmetry. The model has heavy partners for the photon, Z^0 , W^\pm bosons and the top quark as well as extra Higgs bosons. The non-linear σ -model used for the high energy theory is similar to the low energy effective theory of pions which can be used to describe QCD, or in Technicolor models. This similarity with Technicolor models is one of the reasons for the resurgence of Technicolor models in recent years.

The original Little Higgs models had problems with electroweak constraints. The solution is to introduce a discrete symmetry called T-parity, analogous to R-parity in SUSY models. This solves the problems with the precision electroweak data and provides a possible dark matter candidate. This model has a much larger particle content than the original Little Higgs model and is more SUSY-like with a partner for each Standard Model particle.

9.1.7 Unparticles

In these models a new sector at a high energy scale with a non-trivial infrared (IR) fixed point is introduced. This sector interacts with the Standard Model via the exchange of particles with a large mass scale leading to an effective theory

$$\frac{C_U \Lambda_U^{d_{BZ} - d_U}}{M_U^k} O_{SM} O_U, \quad (108)$$

where: d_U is the scaling dimension of the unparticle operator O_U ; M_U is the mass scale for the exchanged particles; O_{SM} is the Standard Model operator; d_{BZ} is the dimension of the operator in the high energy theory; k gives the correct overall dimension of the interaction term. This leads to new operators which give deviations from the Standard Model predictions for various observables.

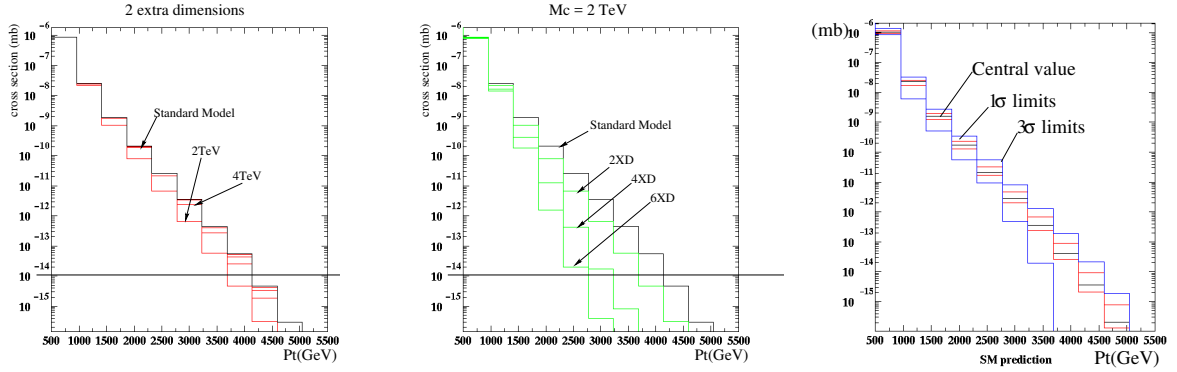


Figure 54: Jet p_{\perp} spectrum for various numbers of extra dimensions in the ADD model taken from Ref. [25].

9.2 Beyond the Standard Model Signatures

Before we go on and consider the signals of models of new physics in great detail it is worthwhile considering what we expect to see in general. Most models of new physics predict either the existence of more particles than the Standard Model or new operators which give deviations from the Standard Model predictions. The signatures of the model depend on either how these particles are produced and decay or the type of deviations expected. In any study of BSM physics the most important thing is to understand the Standard Model backgrounds. Often the signal is at the tail of some distribution and the limits of our ability to calculate or simulate it.

9.2.1 Deviations from the Standard Model

There can be deviations from what is expected in the Standard Model due to: compositeness; exchanging towers of Kaluza-Klein gravitons in large extra dimension models; unparticle exchange; This tends to give changes in the shapes of spectra. Therefore in order to see a difference you need to know the shape of the Standard Model prediction.

Example I: High p_{\perp} jets One possible signal of compositeness is the production of high p_{\perp} jets. At one point there was a disagreement between theory and experiment at the Tevatron. However, this was not due to new physics but too little high- x gluon in the PDFs. Now as well as looking in the p_{\perp} spectra at central rapidities where we expect to see a signal of BSM physics we also look at high rapidity as a disagreement at both central and high rapidities is more likely to be due to the parton distribution functions. An example of the jet p_{\perp} spectrum at a range of rapidities is shown in Fig. 23.

Example II: Unparticles Many models predict deviations in the Drell-Yan mass spectra, for example in an unparticle model with the exchange of virtual spin-1 unparticles, see Fig. 53. However, we need to be careful as higher order weak corrections which can also change the shape are often neglected.

| Background | Expected Events |
|-------------------------|--------------------------------|
| $Z \rightarrow \nu\nu$ | 130 ± 14 |
| $W \rightarrow \tau\nu$ | 60 ± 7 |
| $W \rightarrow \mu\nu$ | 36 ± 4 |
| $W \rightarrow e\nu$ | 17 ± 2 |
| $Z \rightarrow ll$ | 3 ± 1 |
| QCD | 15 ± 10 |
| Non-Collision | 4 ± 4 |
| Total Predicted | 265 ± 30 |
| Data Observed | 263 |

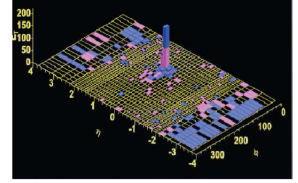
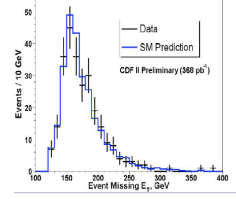


Figure 55: CDF results for monojet production taken from Fermilab wine and cheese seminar by K. Burkett.

Example III: PDF uncertainty or new physics In the ADD model of large extra dimensions there are changes in the shape of the jet p_\perp and dijet mass spectra due to the exchange of KK towers of gravitons and their destructive interference with SM, as shown in Fig. 54.

9.2.2 Monojets

There are a range of models which predict monojet signals with the production of a quark or gluon which is recoiling against either: a stable neutral particle; a tower of KK gravitons in large extra dimension models; unparticles;

Example IV: Mono-jets at the SppS In Ref. [26] the UA1 collaboration reported: 5 events with $E_{\perp, \text{miss}} > 40$ GeV and a narrow jet; 2 events with $E_{\perp, \text{miss}} > 40$ GeV and a neutral EM cluster. They could “not find a Standard Model explanation”, and compared their findings with a calculation of SUSY pair-production [27]. They deduced a gluino mass larger than around 40 GeV. In Ref. [28], the UA2 collaboration describes similar events, also after 113 nb^{-1} , without indicating any interpretation as strongly as UA1. In Ref. [29] S. Ellis, R. Kleiss, and J. Stirling calculated the backgrounds to that process more carefully, and showed agreement with the Standard Model.

There are many different Standard Model electroweak backgrounds and a careful comparison shows they are currently in agreement with the Standard Model, see Fig. 55.

9.2.3 New Particle Production

In general there are two cases for models in which new particles are produced.

1. The model has only a few new particles, mainly produced as s-channel resonances. Examples include: Z-prime models; little Higgs models; small extra dimension models,
2. The model has a large number of new particles. Examples include: SUSY; UED; little Higgs models with T-parity,

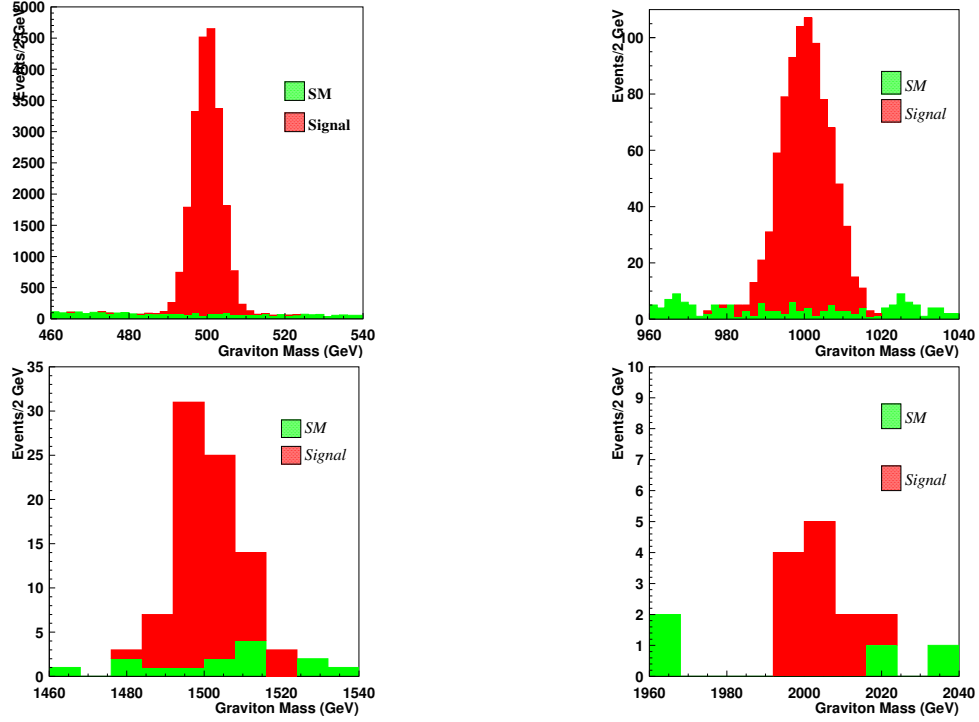


Figure 56: Example of resonant graviton production at the LHC for $\sqrt{s} = 14$ GeV taken from Ref. [30].

In the first type of model the main signal is the production of s -channel resonances while in the second class of models the signals are more varied and complex.

9.2.4 Resonance Production

The easiest and cleanest signal in hadron collisions is the production of an s -channel resonance which decays to e^+e^- or $\mu^+\mu^-$. Resonances in this and other channels are possible in: Little Higgs models; Z' models; UED; Small Extra Dimensions. Backgrounds can be removed using sideband subtraction.

Example V: Resonant Graviton Production The best channel, e^+e^- , gives a reach of order 2 TeV depending on the cross section for the LHC running at $\sqrt{s} = 14$ GeV. Other channels $\mu^+\mu^-$, gg , and W^+W^- are possible. If the graviton is light enough the angular distribution of the decay products can be used to measure the spin of the resonance. An example of the dilepton mass spectrum in this model is shown in Fig. 56.

A lot of models predict hadronic resonances. This is much more problematic due to the mass resolution which smears out narrow resonances and the often huge QCD backgrounds. Although background subtraction can be used the ratio of the signal to background is often tiny, for example Fig. 57 shows the measured $Z \rightarrow b\bar{b}$ peak at the Tevatron. 57

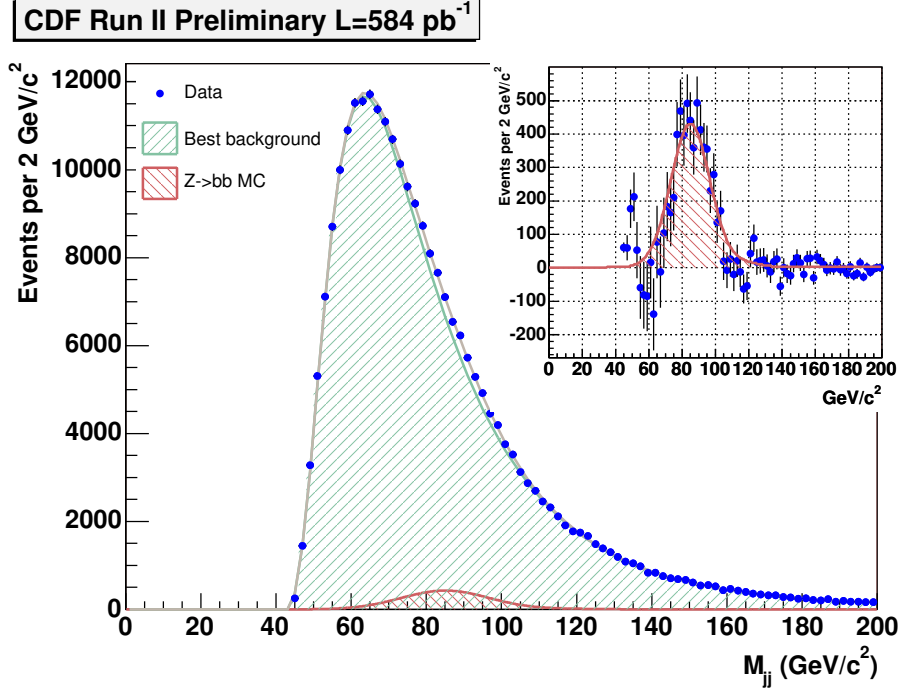


Figure 57: Dijet mass spectrum for bottom quark jets at the Tevatron taken from Ref. [31].

9.2.5 SUSY-like models

Most of the other models are “SUSY”-like, *i.e.* they contain: a partner of some kind for every Standard Model particle; often some additional particles such as extra Higgs bosons; a lightest new particle which is stable and a dark matter candidate.

A lot of new particles should be produced in these models. While some particles may be stable,⁸ the majority of these particles decay to Standard Model particles. Therefore we expect to see: charged leptons; missing transverse energy from stable neutral particles or neutrinos; jets from quarks, perhaps with bottom and charm quarks; tau leptons; Higgs boson production; photons; stable charged particles. It is worth noting that seeing an excess of these does not necessarily tell us which model has been observed.

The archetypal model containing large numbers of new particles which may be accessible at the LHC is SUSY. Other models are UED and the Little Higgs Model with T-parity. However, in practice UED is mainly used as a straw-man model for studies trying to show that a potential excess is SUSY.

Two statements which are commonly made are: the LHC will discover the Higgs boson; the LHC will discover low-energy SUSY if it exists. The first is almost certainly true, however the second is only partially true.

In hadron collisions the strongly interacting particles are dominantly produced. Therefore in SUSY squark and gluino production has the highest cross section, for example via the processes shown in Fig. 58.

⁸*i.e.* the decay length of the particle is such that the majority of the particles escape from the detector before decaying. In practice this happens for lifetimes greater than 10^{-7} s.

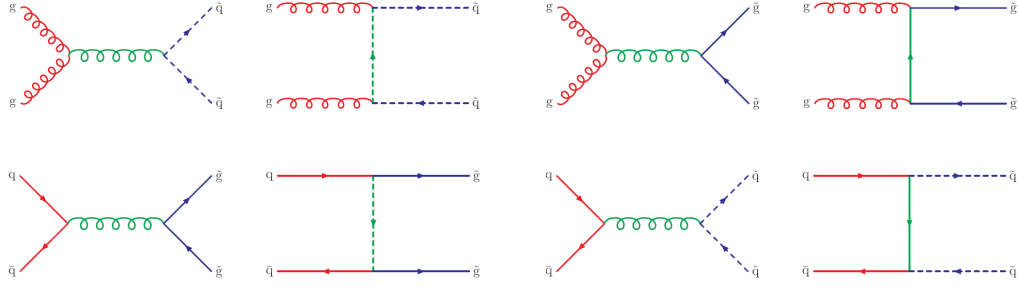


Figure 58: Example SUSY particle production processes.

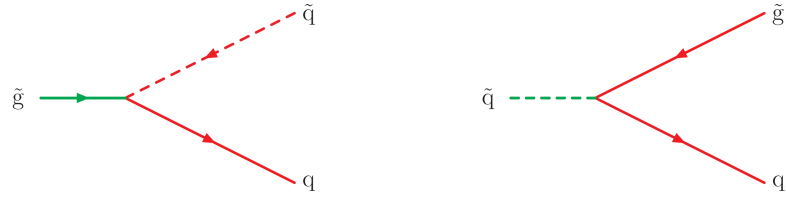


Figure 59: Example strong SUSY particle decays.

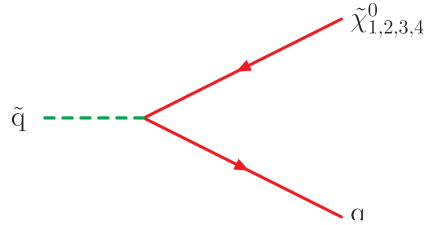


Figure 60: Example weak SUSY particle decays.

These particles then decay in a number of ways. Some of them have strong decays to other strongly interacting SUSY particles, for example via the processes shown in Fig. 59. However the lightest strongly interaction SUSY particle, squark or gluino, can only decay weakly, as shown in Fig. 60. The gluino can only have weak decays with virtual squarks or via loop diagrams. This is the main production mechanism for the weakly interacting SUSY particles.

The decays of the squarks and gluinos will produce lots of quarks and antiquarks. The weakly interacting SUSY particles will then decay giving more quarks and leptons. Eventually the lightest SUSY particle which is stable will be produced. This behaves like a neutrino and gives missing transverse energy. So the signal for SUSY is large numbers of jets and leptons with missing transverse energy. This could however be the signal for many models containing new heavy particles.

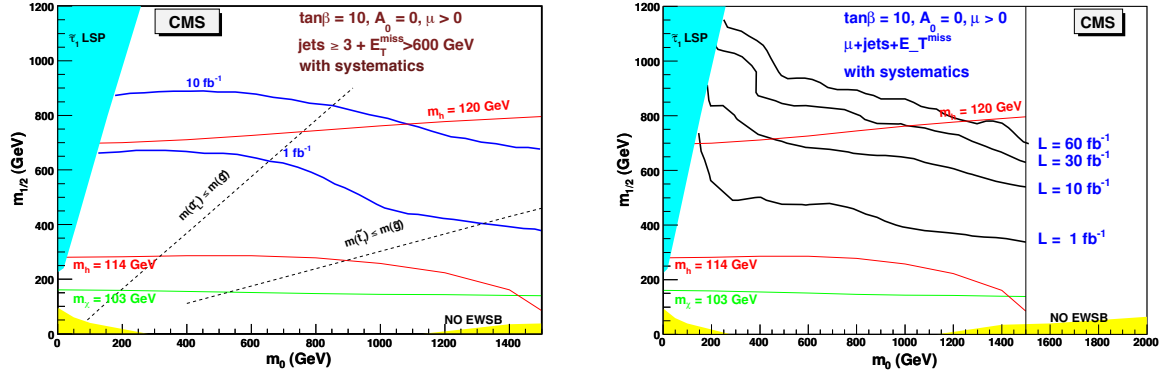


Figure 61: Expected limits in SUSY parameter space for searches using jets and missing transverse energy and jets, leptons and missing transverse energy for the LHC running at $\sqrt{s} = 14$ TeV taken from Ref. [32].

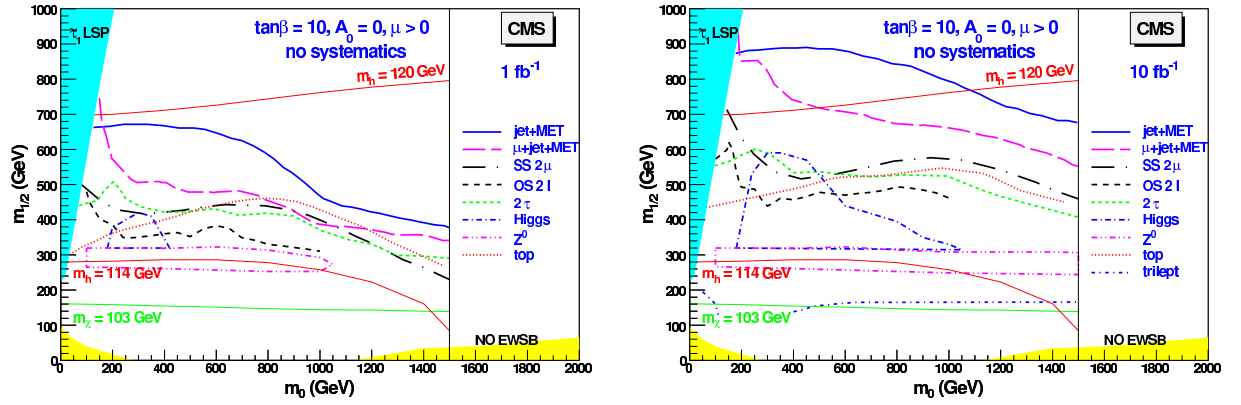


Figure 62: Expected limits in SUSY parameter space for searches using jets, leptons and missing transverse energy for the LHC running at $\sqrt{s} = 14$ TeV taken from Ref. [32].

All SUSY studies fall into two categories: search studies which are designed to show SUSY can be discovered by looking for a inclusive signatures and counting events; measurement studies which are designed to show that some parameters of the model, usually masses, can be measured.

There is a large reach looking for a number of high transverse momentum jets and leptons, and missing transverse energy, see Figs.61 and 62. It is also possible to have the production of the Z^0 and Higgs bosons and top quarks. In many cases the tau lepton may be produced more often than electrons or muons.

Once we observe a signal of SUSY there are various approaches to determine the properties of the model. The simplest of these is the effective mass

$$M_{\text{eff}} = \sum_{i=1}^n p_{\perp i}^{\text{jet}} + \cancel{E}_T, \quad (109)$$

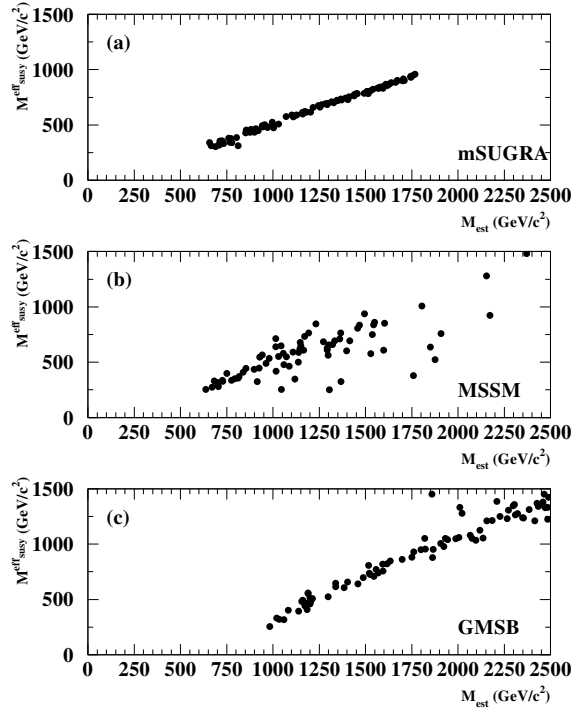


Figure 63: Correlation of the M_{eff} variable with the SUSY mass scale in various SUSY models taken from Ref. [33].

which is strongly correlated with the mass of strongly interacting SUSY particles and can be used to measure the squark/gluino mass to about 15%, see Fig. 63.

The analyzes we have just looked at are those that are used to claim the LHC will discover SUSY but this is not really what they tell us. They don't really discover SUSY. What they see is the production of massive strongly interacting particles, this does not have to be SUSY, it could easily be something else. In order to claim that a signal is SUSY we would need to know more about it. SUSY analyzes tend to proceed by looking for characteristic decay chains and using these to measure the masses of the SUSY particles and determine more properties of the model.

Given most of the searches are essentially counting experiments it is important to understand the Standard Model backgrounds which can be challenging, see Fig. 64.

9.2.6 Model Independent Searches

A popular approach in recent years has been to use experimental data to place constraints on general signatures of new physics parametrised by additional operators suppressed by a scale Λ ,

$$\mathcal{L}_{\text{eff}} = \mathcal{L}_{\text{SM}} + \sum_i \frac{1}{\Lambda^{d_i-4}} c_i \mathcal{O}_i. \quad (110)$$

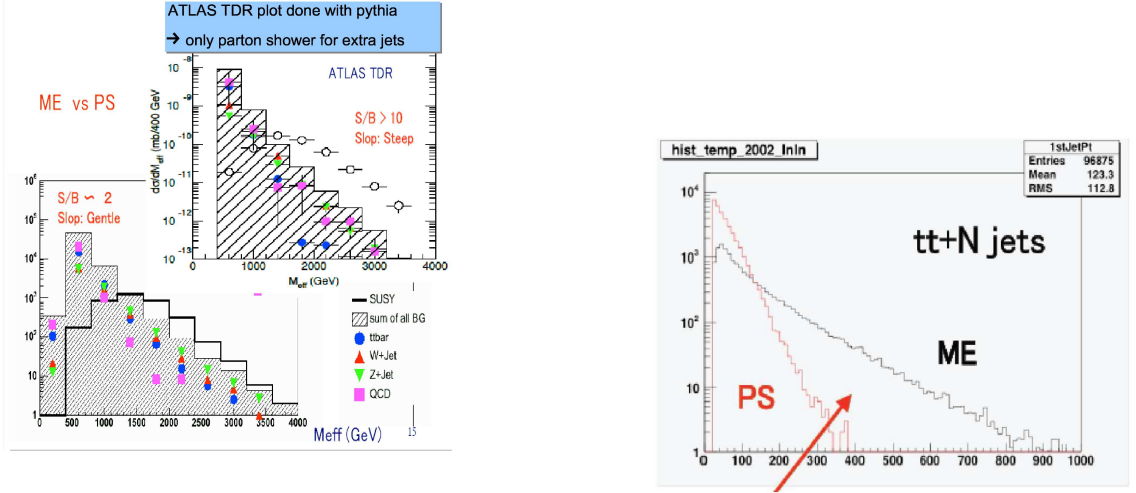


Figure 64: Backgrounds in inclusive SUSY searches.

where \mathcal{O}_i are a set of dimension d_i operators with Wilson coefficients c_i . The Wilson coefficients $c_i = c_i(\mu_R)$ run as functions of the renormalisation group scale μ_R .

Effective field theories: Even if we restrict ourselves to dimension-6 operators in our expansion the total number of Wilson coefficients is extremely large. Since we are only interested in operators that contribute to on-shell observables we can reduce to a set of independent operators by systematically using the equations of motion for each field and integration-by-parts identities. Nevertheless the number of independent dimension-6 operators for $SU(3) \times SU(2)_L \times U(1)_Y$ with 3 fermion generations is 3045 [34]. Constraining the Wilson coefficients will be a major challenge even with the large amount of new data coming from the LHC. In addition the expansion in the scale Λ must be carefully compared to the energy scales present in the observable. The EFT expansion will only be valid if $\Lambda \gg Q^2$ so that it may not be applicable to events with large transverse energy - which would hope to be of greatest sensitivity to new phenomena.

Simplified Models: While not completely model independent, identifying a limited set of additional operators and interactions that can parameterise potential new physics in particular observables is a useful technique. This intermediate point between a complete EFT and a specific model reduces the number of free parameters to a manageable level and at the same time retaining sensitivity to large classes of theories. Some further details and additional references can be found in [35].

A Kinematics and Cross Sections

A.1 Kinematics

The basic language of all phenomenology is that of relativistic kinematics, in particular four-vectors. In hadron collisions because we do not know what fraction of the beam

momenta is transferred to the partonic system it is preferable to use quantities, such as the transverse momentum, p_\perp , with respect to the beam direction which are invariant under longitudinal boosts along the beam direction to describe the kinematics. In addition to the transverse momentum we use the rapidity, y , and massless pseudorapidity, η ,

$$y = \frac{1}{2} \ln \frac{E + p_z}{E - p_z} \xrightarrow{\text{massless}} \eta = -\ln \tan \frac{\theta}{2}, \quad (111)$$

because rapidity differences are invariant under longitudinal boosts. Particles with small rapidities are produced at an angle close to 90° degrees to the beam direction while particles with large positive (negative) rapidities are travelling in the forward (backward) beam direction. The pseudorapidity is more often used experimentally as it is related to the measured scattering angle.

The four-momentum can be written as

$$p^\mu = (E, p_x, p_y, p_z) = (m_\perp \cosh y, p_\perp \cos \phi, p_\perp \sin \phi, m_\perp \sinh y), \quad (112)$$

where $m_\perp^2 = p_\perp^2 + m^2$. The one-particle phase-space element can also be rewritten in terms of y and p_\perp as

$$\frac{d^4p}{(2\pi)^4} \delta(p^2 - m^2) \theta(E) = \frac{d^3p}{(2\pi)^2 2E} = \frac{dy d^2p_\perp}{2(2\pi)^3}. \quad (113)$$

A.2 Cross Sections

The starting point of all collider physics calculations is the calculation of the scattering cross section. The cross section for a $2 \rightarrow n$ scattering processes, $a + b \rightarrow 1 \dots n$, is

$$d\sigma = \frac{(2\pi)^4}{4\sqrt{(p_a \cdot p_b)^2 - m_a^2 m_b^2}} d\Phi_n(p_a + p_b; p_1 \dots p_n) |\overline{\mathcal{M}}|^2, \quad (114)$$

where $p_{a,b}$ and $p_{i=1,\dots,n}$ are the momenta of the incoming and outgoing particles, respectively. The matrix element squared $|\overline{\mathcal{M}}|^2$ is summed/averaged over the spins and colours of the outgoing/incoming particles. The n -particle phase-space element is

$$d\Phi_n(p_a + p_b; p_1 \dots p_n) = \delta^4\left(p_a + p_b - \sum_{i=1}^n p_i\right) \prod_{i=1}^n \frac{d^3p_i}{(2\pi)^3 2E_i}, \quad (115)$$

where E_i is the energy of the i th particle. It is conventional to define $s = (p_a + p_b)^2$. For massless incoming particles $4\sqrt{(p_a \cdot p_b)^2 - m_a^2 m_b^2} = 2s$.

Although modern theoretical calculations involve ever higher multiplicity final states in these lectures we will primarily deal with $2 \rightarrow 2$ scattering processes in which case

$$\begin{aligned} d\Phi_2(p_a + p_b; p_1, p_2) &= \delta^4(p_a + p_b - p_1 - p_2) \frac{d^3p_1}{(2\pi)^3 2E_1} \frac{d^3p_2}{(2\pi)^3 2E_2}, \\ &= \delta(E_a + E_b - E_1 - E_2) \frac{1}{(2\pi)^6 4E_1 E_2} |p_1|^2 d|p_1| d\cos\theta d\phi, \\ &= \frac{1}{8\pi(2\pi)^4} \frac{|p_1|}{\sqrt{s}} d\cos\theta, \end{aligned} \quad (116)$$

where $|p_1|$ is the magnitude of the three-momenta of either of the outgoing particles and θ and ϕ are the polar and azimuthal scattering angles, respectively. The cross section

$$d\sigma = \frac{1}{16\pi s} \frac{|p_1|}{\sqrt{s}} d\cos\theta |\overline{\mathcal{M}}|^2. \quad (117)$$

It is conventional to describe the scattering process in terms of the Mandelstam variables

$$s = (p_a + p_b)^2, \quad t = (p_a - p_1)^2, \quad u = (p_a - p_2)^2. \quad (118)$$

There are only two independent Mandelstam variables

$$s + t + u = m_1^2 + m_2^2 + m_a^2 + m_b^2 \xrightarrow{\text{massless}} 0. \quad (119)$$

In terms of these variables

$$d\sigma = \frac{1}{16\pi s^2} dt |\overline{\mathcal{M}}|^2. \quad (120)$$

A.3 Cross Sections in Hadron Collisions

In hadron collisions there is an additional complication as the partons inside the hadrons interact. The hadron-hadron cross section is

$$d\sigma_{AB} = \sum_{ab} \int_0^1 dx_1 dx_2 f_{a/A}(x_1, \mu_F^2) f_{b/B}(x_2, \mu_F^2) \hat{\sigma}_{ab}(\hat{s}, \mu_F^2, \mu_R^2), \quad (121)$$

where $x_{1,2}$ are momentum fractions of the interacting partons with respect to the incoming hadrons, $\hat{s} = x_1 x_2 s$, $\hat{\sigma}_{ab}(\hat{s}, \mu_F^2, \mu_R^2)$ is the parton-level cross section for the partons a and b to produce the relevant final state, $f_{a/A}(x, \mu_F^2)$ is the parton distribution function (PDF) giving the probability of finding the parton a in the hadron A , and similarly for $f_{b/B}(x, \mu_F^2)$. The factorization and renormalisation scales are μ_F and μ_R , respectively.

In hadron collisions we usually denote the variables for partonic process with $\hat{}$, *e.g.* \hat{s} , \hat{t} and \hat{u} for the Mandelstam variables.

A.3.1 Resonance production ($2 \rightarrow 1$ processes)

The simplest example of a hadronic cross section is the production of an s -channel resonance, for example the Z^0 or Higgs bosons. We assume that the incoming partons are massless so that the 4-momenta of the incoming partons are:

$$p_{a,b} = x_{1,2}(E, 0, 0, \pm E), \quad (122)$$

where E is beam energy in the hadron-hadron centre-of-mass system of collider such that $s = 4E^2$. The Breit-Wigner cross section, *e.g.* for Z production, is

$$\hat{\sigma}_{q\bar{q} \rightarrow Z^0 \rightarrow \mu^+ \mu^-} = \frac{1}{N_C^2} \frac{12\pi \hat{s}}{M_Z^2} \frac{\Gamma_{q\bar{q}} \Gamma_{\mu^+ \mu^-}}{(\hat{s} - M_Z^2)^2 + M_Z^2 \Gamma_Z^2}. \quad (123)$$

In the limit that the width is a lot less than the mass

$$\frac{1}{(\hat{s} - M_Z^2)^2 + M_Z^2 \Gamma_Z^2} \approx \frac{\pi}{M_Z \Gamma_Z} \delta(\hat{s} - M_Z^2), \quad (124)$$

the *narrow width limit*. In this case the partonic centre-of-mass system is constrained to have $\hat{s} = M_Z^2$. The rapidity \hat{y} of the partonic system and \hat{s} are related to the momentum fractions $x_{1,2}$ by

$$\hat{s} = x_1 x_2, s \quad \text{and} \quad \hat{y} = \frac{1}{2} \ln \frac{x_1 + x_2 + x_1 - x_2}{x_1 + x_2 - x_1 + x_2} = \frac{1}{2} \ln \frac{x_1}{x_2}. \quad (125)$$

Inverting these relationships we obtain

$$x_{1,2} = \sqrt{\frac{\hat{s}}{s}} e^{\pm \hat{y}} \quad \text{and} \quad \hat{y} = \frac{1}{2} \ln \frac{x_1^2 s}{\hat{s}} \leq \ln \frac{2E}{\sqrt{\hat{s}}} = \hat{y}_{\max}. \quad (126)$$

This allows us to change the variables in the integration using

$$s dx_1 dx_2 = d\hat{s} d\hat{y}, \quad (127)$$

giving the differential cross section

$$\frac{d\sigma_{AB \rightarrow Z^0 \rightarrow \mu^+ \mu^-}}{d\hat{y}} = \sum_{a,b=q\bar{q}} x_1 f_{q/A}(x_1, \mu_F^2) x_2 f_{\bar{q}/B}(x_2, \mu_F^2) \frac{12\pi^2}{N_C^2 M_Z^3} \Gamma_{q\bar{q}} B_{\mu^+ \mu^-}. \quad (128)$$

A.3.2 $2 \rightarrow 2$ Scattering Processes

For most $2 \rightarrow 2$ scattering processes in hadron-hadron collisions it is easier to work in terms of the rapidities y_3, y_4 and transverse momentum, p_\perp , of the particles. We introduce average (centre-of-mass) rapidity and rapidity difference,

$$\bar{y} = (y_3 + y_4)/2 \quad \text{and} \quad y^* = (y_3 - y_4)/2, \quad (129)$$

which are related to the Bjorken x values by

$$x_{1,2} = \frac{p_\perp}{\sqrt{2}} (e^{\pm y_3} + e^{\pm y_4}) = \frac{p_\perp}{2\sqrt{s}} e^{\pm \bar{y}} \cosh y^*. \quad (130)$$

Therefore

$$\hat{s} = M_{12}^2 = 4p_\perp^2 \cosh y^* \quad \text{and} \quad \hat{t}, \hat{u} = -\frac{\hat{s}}{2} (1 \mp \tanh y^*).$$

The partonic cross section, assuming all the particles are massless, is

$$\begin{aligned} \hat{\sigma}_{ab \rightarrow 12} &= \frac{1}{2\hat{s}} \int \frac{d^3 p_1}{(2\pi)^3 2E_1} \frac{d^3 p_2}{(2\pi)^3 2E_2} |\overline{\mathcal{M}}_{ab \rightarrow 12}|^2 (2\pi)^4 \delta^4(p_a + p_b - p_1 - p_2), \\ &= \frac{1}{2\hat{s}^2} \int \frac{d^2 p_\perp}{(2\pi)^2} |\overline{\mathcal{M}}_{ab \rightarrow 12}|^2. \end{aligned} \quad (131)$$

Therefore once we include the PDFs, sum over a, b , and integrate over $x_{1,2}$ the hadronic cross section is

$$\sigma_{AB \rightarrow 12} = \sum_{ab} \int \frac{dy_1 dy_2 d^2 p_\perp}{16\pi^2 s^2} \frac{f_a(x_1, \mu_F) f_b(x_2, \mu_F)}{x_1 x_2} |\overline{\mathcal{M}}_{ab \rightarrow 12}|^2,$$

including the factor $1/(1 + \delta_{12})$ for identical final-state particles.

B Flavour Physics

While most of the interactions in the Standard Model preserve the flavour of quarks and leptons the interaction of fermions with the W boson can change the flavour of the quarks and violate CP-conservation.

In order to understand the interactions of the quarks with the W boson we first need to consider the generation of quark masses in the Standard Model. The masses of the quarks come from the Yukawa interaction with the Higgs field

$$\mathcal{L} = -Y_{ij}^d \overline{Q_{Li}^I} \phi d_{Rj}^I - Y_{ij}^u \overline{Q_{Li}^I} \epsilon \phi^* u_{Rj}^I + \text{h.c.}, \quad (132)$$

where $Y^{u,d}$ are complex 3×3 matrices, ϕ is the Higgs field, i, j are generation indices, Q_L^i are the left-handed quark doublets and, d_R^I and u_R^I are the right down- and up-type quark singlets. When the Higgs field acquires a vacuum expectation value $\langle \phi \rangle = (0, \frac{v}{\sqrt{2}})$ we get the mass terms for the quarks.

The physical states come from diagonalizing $Y^{u,d}$ using 4 unitary 3×3 matrices, $V_{L,R}^{u,d}$

$$M_{\text{diag}}^f = V_L^f Y^f V_R^{f\dagger} \frac{v}{\sqrt{2}}. \quad (133)$$

The interaction of the W^\pm and the quarks is given by

$$\mathcal{L}_W = -\frac{g}{\sqrt{2}} \left[\bar{d}_L^I \gamma^\mu W_\mu^- u_L^I + \bar{u}_L^I \gamma^\mu W_\mu^+ d_L^I \right]. \quad (134)$$

The interaction with the mass eigenstates, $f_L^M = V_L^f f_L^I$, is

$$\mathcal{L}_W = -\frac{g}{\sqrt{2}} \left[\bar{d}_L^M \gamma^\mu W_\mu^- V_{\text{CKM}}^\dagger u_L^M + \bar{u}_L^M \gamma^\mu W_\mu^+ V_{\text{CKM}} d_L^M \right], \quad (135)$$

where the Cabibbo-Kobayashi-Maskawa (CKM) matrix

$$V_{\text{CKM}} \equiv V_L^u C V_L^{d\dagger} = \begin{pmatrix} V_{ud} & V_{us} & V_{ub} \\ V_{cd} & V_{cs} & V_{cb} \\ V_{td} & V_{ts} & V_{tb} \end{pmatrix}, \quad (136)$$

is a 3×3 unitary matrix.

The CKM matrix can be parameterized in terms of three mixing angles, $(\theta_{12}, \theta_{13}, \theta_{23})$ and one phase, δ ,

$$V_{\text{CKM}} = \begin{pmatrix} c_{12}c_{13} & s_{12}c_{13} & s_{13}e^{-i\delta} \\ -s_{12}c_{23} - c_{12}s_{23}s_{13}e^{i\delta} & c_{12}c_{23} - s_{12}s_{23}s_{13}e^{i\delta} & s_{23}c_{13} \\ s_{12}s_{23} - c_{12}c_{23}s_{13}e^{i\delta} & -c_{12}s_{23} - s_{12}c_{23}s_{13}e^{i\delta} & c_{23}c_{13} \end{pmatrix}, \quad (137)$$

where $s_{ij} = \sin \theta_{ij}$ and $c_{ij} = \cos \theta_{ij}$. As experimentally $s_{13} \ll s_{23} \ll s_{12} \ll 1$ it is convenient to use the Wolfenstein parameterization: $s_{12} = \lambda$; $s_{23} = A\lambda^2$; and $s_{13}e^{i\delta} = A\lambda^3(\rho + i\eta)$.

In which

$$V_{\text{CKM}} = \begin{pmatrix} 1 - \frac{1}{2}\lambda^2 & \lambda & A\lambda^3(\rho - i\eta) \\ -\lambda & 1 - \frac{1}{2}\lambda^2 & A\lambda^2 \\ A\lambda^3(1 - \rho - i\eta) & -A\lambda^2 & 1 \end{pmatrix} + \mathcal{O}(\lambda^4). \quad (138)$$

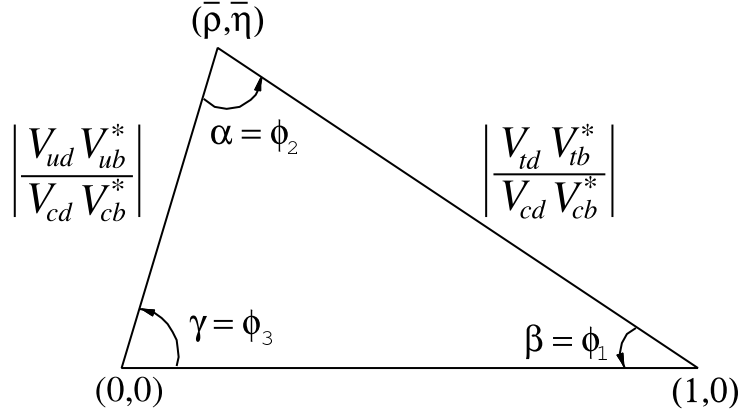


Figure 65: Unitary triangle.

If we assume that the neutrinos are massless there is no mixing for leptons. We now know that the neutrinos have small masses so there is mixing in the lepton sector. The analogy of the CKM matrix is the Maki-Nakagawa-Sakata (MNS) matrix U_{MNS} .

A number of unitarity triangles can be constructed using the properties of the CKM matrix. The most useful one is

$$V_{ud}V_{ub}^* + V_{cd}V_{cb}^* + V_{td}V_{tb}^* = 0, \quad (139)$$

which can be represented as a triangle as shown in Fig. 65. The area of all the unitary triangles is $\frac{1}{2}J$, where J is the Jarlskog invariant, a convention-independent measure of CP-violation,

$$J = \text{Im}\{V_{ud}V_{cs}V_{us}^*V_{cd}^*\}. \quad (140)$$

There are a large number of measurements which constrain the parameters in the unitarity triangle. They all measure different combinations of the parameters and over-constrain the location of the vertex of the unitarity triangle.

The magnitudes of the CKM elements control the lengths of the sides:

1. $|V_{ud}|$ is accurately measured in nuclear beta decay;
2. $|V_{cd}|$ can be measured using either semi-leptonic charm meson decays or using neutrino DIS cross sections;
3. $|V_{ub}|$ is measured using inclusive and exclusive semi-leptonic B meson decays to light mesons $B \rightarrow X_u \ell \bar{\nu}$ or $B \rightarrow \pi \ell \bar{\nu}$;
4. $|V_{cb}|$ is measured using inclusive and exclusive semi-leptonic B meson decays to charm mesons $B \rightarrow X_C \ell \bar{\nu}$ or $B \rightarrow D \ell \bar{\nu}$.

The CKM matrix elements which give the length of the remaining side can only be measured in loop-mediated processes. The most important of these, FCNCs, have already been discussed in the context of BSM physics in Section 9.1.4. These also gives rise to $B - \bar{B}$ mixing and oscillations, via the Feynman diagrams shown in Fig. 66.



Figure 66: Feynman diagrams giving $B^0 - \bar{B}^0$ and $B_s^0 - \bar{B}_s^0$ oscillations.

The oscillation probability is

$$P_{\text{oscillation}} = \frac{e^{-\Gamma t}}{2} \left[\cosh \left(\frac{\Delta\Gamma t}{2} \right) + \cos(\Delta m t) \right], \quad (141)$$

where Γ is the average width of the mesons, $\Delta\Gamma$ is the width difference between the mesons and Δm is the mass difference of the mesons. For both B_d and B_s mesons the Δm term dominates. From the box diagram

$$\Delta m_q = -\frac{G_F^2 m_W^2 \eta_B m_{B_q} B_{B_q} f_{B_q}^2}{6\pi^2} S_0 \left(\frac{m_t^2}{m_W^2} \right) (V_{tq}^* V_{tb})^2. \quad (142)$$

The decay constant f_{B_q} can be measured from leptonic decays $B_q \rightarrow \ell^+ \nu_\ell$ but B_{B_q} comes from lattice QCD results. The QCD correction $\eta_B \sim \mathcal{O}(1)$.

The B-factories have studied $B^0 - \bar{B}^0$ mixing in great detail giving

$$\Delta m_d = 0.507 \pm 0.005 \text{ps}^{-1}. \quad (143)$$

It is important to measure both $B_d - \bar{B}_d$ and $B_s - \bar{B}_s$ mixing as some hadronic uncertainties cancel in the ratio. The rate is $\propto |V_{ts} V_{tb}^*|^2$ due to the GIM mechanism. However, the high oscillation frequency makes $B_s - \bar{B}_s$ mixing tricky to observe. The Tevatron observation relied on tagging the flavour of the B meson at production by observing an associated kaon from the fragmentation. The final result is

$$\begin{aligned} \Delta m_s &= 17.77 & \pm 0.10(\text{stat}) & \pm 0.07(\text{sys}), \\ |V_{td}| |V_{ts}| &= 0.2060 & \pm 0.0007(\text{exp}) & \pm 0.008(\text{theo}). \end{aligned} \quad (144)$$

The only source of CP-violation in the Standard Model is the complex phase in the CKM matrix. In order to see any effect we need at least two diagrams for the process with different CP-phases. There are three possibilities: CP-violation in the decay (*direct*); CP-violating in the mixing (*indirect*); CP-violation in the interference between decay and mixing. Example amplitudes are shown in Fig. 67.

The simplest type of CP-violation is direct CP-violation. This is the only possible type of CP-violation for charged mesons and is usually observed by measuring an asymmetry

$$A_{f^\pm} \equiv \frac{\Gamma(M^- \rightarrow f^-) - \Gamma(M^+ \rightarrow f^+)}{\Gamma(M^- \rightarrow f^-) + \Gamma(M^+ \rightarrow f^+)} \xrightarrow{\text{CP conserved}} 0. \quad (145)$$

If CP-symmetry holds, then $|K_L\rangle = \frac{1}{\sqrt{2}}(|K^0\rangle + |\bar{K}^0\rangle)$ would be a CP-eigenstate with $|K_L\rangle = |\bar{K}_L\rangle$. If we take $|M\rangle = |K_L\rangle$ and $|f\rangle = |\pi^- e^+ \nu_e\rangle$ the corresponding CP-asymmetry is $A_{\text{CP}} = (0.327 \pm 0.012)\%$, which means that K_L is not a CP-eigenstate

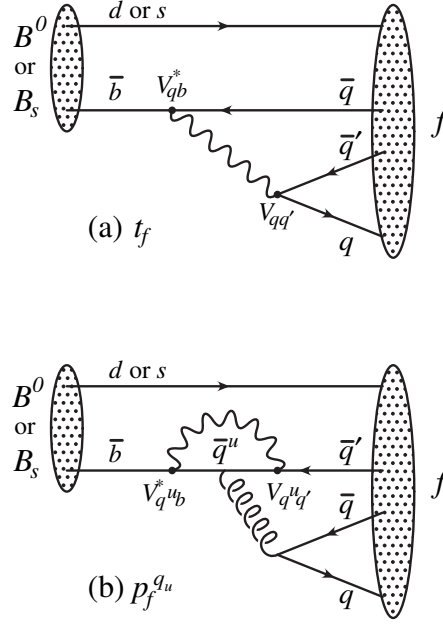


Figure 67: Examples of tree and penguin mediated processes, taken from Ref. [8].

and there is CP-violation. There are many possible modes which measure different combinations of the angles in the unitarity triangle. The observed flavour and CP-violation is consistent with the Standard Model, i.e. the description by the CKM matrix, see Fig. 68.

There is one final area of flavour physics which is important. The matter in the universe consists of particles and not antiparticles. There are three Sakharov conditions required for this to happen:

1. baryon number violation;
2. C-symmetry and CP-symmetry violation;
3. interactions out of thermal equilibrium.

There are non-perturbative effects in the SM which violate baryon number. However, the amount of CP-violation in the quark sector is not enough to give the observed matter-antimatter asymmetry, there might be more in the lepton sector, otherwise we need a new physics source of CP-violation.

C Color algebra

The color factors C_F and C_A correspond to the factors one gets for emitting a gluon off a quark or gluon line respectively.

$$\left| \underbrace{\text{gluon emission from quark line}}_n \right|^2 = N_c C_F^n \quad \left| \underbrace{\text{gluon emission from gluon line}}_n \right|^2 = (N_c^2 - 1) C_A^n$$

The color factor for the splitting of a gluon into a quark-antiquark pair is given by T_R .

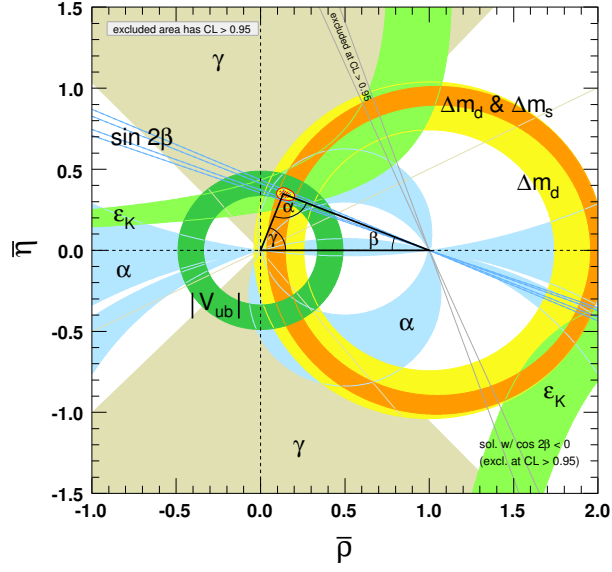


Figure 68: Experimental measurement of the unitarity triangle taken from Ref. [8].

$$\left| \text{Diagram} \right|^2 = (N_c^2 - 1) T_R$$

One can compute color factors using a set of pictorial rules (see [36] for more details.) All these rules follow from the properties of the SU(3) color group.

$$T_{ij}^a T_{jk}^a = \frac{1}{2} \left(\delta_{il} \delta_{jk} - \frac{1}{N_c} \delta_{ij} \delta_{kl} \right)$$

$$\text{Diagram} = \frac{1}{2} \left[\text{Diagram 1} - \frac{1}{N_c} \text{Diagram 2} \right]$$

The three-gluon vertex can be rewritten as:

$$if^{abc} = 2 \left(\text{Tr} [T^a T^b T^c] - \text{Tr} [T^a T^c T^b] \right)$$

$$\text{Diagram} = 2 \left[\text{Diagram 1} - \text{Diagram 2} \right]$$

Here is an example of a calculation of a color factor with the pictorial method.

$$\begin{aligned}
 \left(\text{diagram of a quark line with a gluon loop} \right)^2 &= \text{diagram of a quark loop with a gluon line} \\
 &= \frac{1}{2} \left[\text{diagram of a quark loop with a quark line} - \frac{1}{N_c} \text{diagram of a gluon loop} \right] \\
 &= \frac{1}{2} \left(N_c^2 - \frac{1}{N_c} N_c \right) = N_c C_F
 \end{aligned}$$

We have used the fact that a closed fermion loop with no gluon attachments amounts to a factor of N_c , while a closed gluon loop would give a factor of $N_c^2 - 1$.

$$\begin{aligned}
 \text{diagram of a closed fermion loop} &= N_c \\
 \text{diagram of a closed gluon loop} &= N_c^2 - 1
 \end{aligned}$$

A gluon loop on a gluon line can be written as the same line without the loop but with a factor of N_c .

$$\text{diagram of a gluon line with a gluon loop} = N_c \text{diagram of a gluon line}$$

References

- [1] F. Halzen and A. D. Martin, *Quarks and Leptons: An Introductory Course in Modern Particle Physics*, . ISBN-9780471887416.
- [2] V. D. Barger and R. J. N. Phillips, *Collider Physics*, . Redwood City, USA: Addison-Wesley (1987) 592 P. (Frontiers in Physics, 71).
- [3] R. K. Ellis, W. J. Stirling, and B. R. Webber, *QCD and Collider Physics*, *Camb. Monogr. Part. Phys. Nucl. Phys. Cosmol.* **8** (1996) 1–435.

- [4] G. Dissertori, I. G. Knowles, and M. Schmelling, *Quantum Chromodynamics: High energy experiments and theory*, . Oxford, UK: Clarendon (2003) 538 p.
- [5] J. F. Gunion, H. E. Haber, G. L. Kane, and S. Dawson, *The Higgs Hunter's Guide*, *Front. Phys.* **80** (2000) 1–448.
- [6] G. P. Salam, *Towards Jetography*, *Eur. Phys. J.* **C67** (2010) 637–686, [[arXiv:0906.1833](#)].
- [7] A. Buckley *et. al.*, *General-purpose event generators for LHC physics*, [arXiv:1101.2599](#).
- [8] **Particle Data Group** Collaboration, K. Nakamura *et. al.*, *Review of particle physics*, *J. Phys.* **G37** (2010) 075021.
- [9] **OPAL** Collaboration, G. Abbiendi *et. al.*, *Measurement of event shape distributions and moments in $e^+e^- \rightarrow \text{hadrons}$ at 91-209 GeV and a determination of α_S* , *Eur. Phys. J.* **C40** (2005) 287–316, [[hep-ex/0503051](#)].
- [10] **H1 and ZEUS** Collaboration, F. D. Aaron *et. al.*, *Combined Measurement and QCD Analysis of the Inclusive ep Scattering Cross Sections at HERA*, *JHEP* **01** (2010) 109, [[arXiv:0911.0884](#)].
- [11] J. M. Campbell, J. W. Huston, and W. J. Stirling, *Hard Interactions of Quarks and Gluons: A Primer for LHC Physics*, *Rept. Prog. Phys.* **70** (2007) 89, [[hep-ph/0611148](#)].
- [12] **CDF** Collaboration, T. A. Aaltonen *et. al.*, *Measurement of $d\sigma/dy$ of Drell-Yan e^+e^- pairs in the Z Mass Region from $p\bar{p}$ Collisions at $\sqrt{s} = 1.96$ TeV*, *Phys. Lett.* **B692** (2010) 232–239, [[arXiv:0908.3914](#)].
- [13] **D0** Collaboration, V. M. Abazov *et. al.*, *Measurement of the shape of the boson transverse momentum distribution in $p\bar{p} \rightarrow Z/\gamma^* \rightarrow e^+e^- + X$ events produced at $\sqrt{s} = 1.96$ -TeV*, *Phys. Rev. Lett.* **100** (2008) 102002, [[arXiv:0712.0803](#)].
- [14] C. Anastasiou, L. J. Dixon, K. Melnikov, and F. Petriello, *High precision QCD at hadron colliders: Electroweak gauge boson rapidity distributions at NNLO*, *Phys. Rev.* **D69** (2004) 094008, [[hep-ph/0312266](#)].
- [15] J. R. Ellis, M. K. Gaillard, and G. G. Ross, *Search for Gluons in e^+e^- Annihilation*, *Nucl. Phys.* **B111** (1976) 253.
- [16] R. K. Ellis, D. A. Ross, and A. E. Terrano, *The Perturbative Calculation of Jet Structure in e^+e^- Annihilation*, *Nucl. Phys.* **B178** (1981) 421.
- [17] A. Gehrmann-De Ridder, T. Gehrmann, E. W. N. Glover, and G. Heinrich, *Second-order QCD corrections to the thrust distribution*, *Phys. Rev. Lett.* **99** (2007) 132002, [[arXiv:0707.1285](#)].

- [18] **CDF** Collaboration, T. Aaltonen *et. al.*, *Measurement of the Inclusive Jet Cross Section at the Fermilab Tevatron p - \bar{p} Collider Using a Cone-Based Jet Algorithm*, *Phys. Rev.* **D78** (2008) 052006, [[arXiv:0807.2204](#)].
- [19] **CDF** Collaboration, T. Aaltonen *et. al.*, *First Run II Measurement of the W Boson Mass*, *Phys. Rev.* **D77** (2008) 112001, [[arXiv:0708.3642](#)].
- [20] V. Buescher and K. Jakobs, *Higgs boson searches at hadron colliders*, *Int. J. Mod. Phys.* **A20** (2005) 2523–2602, [[hep-ph/0504099](#)].
- [21] C. Anastasiou, C. Duhr, F. Dulat, F. Herzog, and B. Mistlberger, *Higgs Boson Gluon-Fusion Production in QCD at Three Loops*, *Phys. Rev. Lett.* **114** (2015) 212001, [[arXiv:1503.0605](#)].
- [22] C. Anastasiou, C. Duhr, F. Dulat, E. Furlan, T. Gehrmann, F. Herzog, A. Lazopoulos, and B. Mistlberger, *High precision determination of the gluon fusion Higgs boson cross-section at the LHC*, *JHEP* **05** (2016) 058, [[arXiv:1602.0069](#)].
- [23] S. Dawson, *Introduction to the physics of Higgs bosons*, in *Theoretical Advanced Study Institute in Elementary Particle Physics (TASI 94): CP Violation and the limits of the Standard Model Boulder, Colorado, May 29-June 24, 1994*, pp. 0445–506, 1994. [[hep-ph/9411325](#)].
- [24] K. Cheung, W.-Y. Keung, and T.-C. Yuan, *Collider Phenomenology of Unparticle Physics*, *Phys. Rev.* **D76** (2007) 055003, [[arXiv:0706.3155](#)].
- [25] **ATLAS** Collaboration, S. Ferrag, *Proton structure impact on sensitivity to extra-dimensions at LHC*, [[hep-ph/0407303](#)].
- [26] **UA1** Collaboration, G. Arnison *et. al.*, *Experimental Observation of Events with Large Missing Transverse Energy Accompanied by a Jet Or a Photon(s) in $p\bar{p}$ Collisions at $\sqrt{s} = 540$ -GeV*, *Phys. Lett.* **B139** (1984) 115.
- [27] J. R. Ellis and H. Kowalski, *Supersymmetric Particles at the CERN $p\bar{p}$ Collider*, *Nucl. Phys.* **B246** (1984) 189.
- [28] **Bern-CERN-Copenhagen-Orsay-Pavia-Saclay** Collaboration, P. Bagnaia *et. al.*, *Observation of Electrons Produced in Association with Hard Jets and Large Missing Transverse Momentum in $p\bar{p}$ Collisions at $\sqrt{s} = 540$ GeV*, *Phys. Lett.* **B139** (1984) 105.
- [29] S. D. Ellis, R. Kleiss, and W. J. Stirling, *Missing Transverse Energy Events and the Standard Model*, *Phys. Lett.* **B158** (1985) 341.
- [30] B. C. Allanach, K. Odagiri, M. A. Parker, and B. R. Webber, *Searching for narrow graviton resonances with the ATLAS detector at the Large Hadron Collider*, *JHEP* **09** (2000) 019, [[hep-ph/0006114](#)].
- [31] J. Donini *et. al.*, *Energy Calibration of b -Quark Jets with $Z \rightarrow b\bar{b}$ Decays at the Tevatron Collider*, *Nucl. Instrum. Meth.* **A596** (2008) 354–367, [[arXiv:0801.3906](#)].

- [32] **CMS** Collaboration, G. L. Bayatian *et. al.*, *CMS technical design report, volume II: Physics performance*, *J. Phys.* **G34** (2007) 995–1579.
- [33] D. R. Tovey, *Measuring the SUSY mass scale at the LHC*, *Phys. Lett.* **B498** (2001) 1–10, [[hep-ph/0006276](#)].
- [34] B. Henning, X. Lu, T. Melia, and H. Murayama, *2, 84, 30, 993, 560, 15456, 11962, 261485, ...: Higher dimension operators in the SM EFT*, [arXiv:1512.0343](#).
- [35] **LHC New Physics Working Group** Collaboration, D. Alves, *Simplified Models for LHC New Physics Searches*, *J. Phys.* **G39** (2012) 105005, [[arXiv:1105.2838](#)].
- [36] L. J. Dixon, *Calculating scattering amplitudes efficiently*, [hep-ph/9601359](#).

DARK MATTER

Dr David G. Cerdeño (University of Durham)

Contents

| | | |
|----------|--|------------|
| 1 | Motivation for Dark Matter | 217 |
| 1.1 | Evidence for Dark Matter | 217 |
| 1.1.1 | Galactic scale | 218 |
| 1.1.2 | Galaxy Clusters..... | 219 |
| 1.1.3 | Cosmological scale | 220 |
| 1.2 | Dark Matter Properties | 221 |
| 1.2.1 | Neutral | 221 |
| 1.2.2 | Nonrelativistic | 222 |
| 1.2.3 | NonBaryonic | 222 |
| 1.2.4 | Long-Lived | 223 |
| 2 | Freeze Out of Massive Species..... | 223 |
| 2.1 | Cosmological Preliminaries..... | 223 |
| 2.2 | Time evolution of the number density | 226 |
| 2.2.1 | Freeze out of relativistic species..... | 229 |
| 2.2.2 | Freeze out of nonrelativistic species..... | 230 |
| 2.2.3 | WIMPs | 231 |
| 2.3 | Computing the DM annihilation cross section..... | 231 |
| 2.3.1 | Special Cases | 234 |
| 3 | Direct DM Detection | 236 |
| 3.1 | Computation of the Dark Matter detection rate..... | 236 |
| 3.1.1 | DM flux..... | 236 |
| 3.1.2 | Kinematics..... | 236 |
| 3.2 | The master formula for direct DM detection..... | 237 |
| 3.2.1 | The scattering cross section | 237 |
| 3.2.2 | The importance of the threshold..... | 238 |
| 3.2.3 | Velocity distribution function | 239 |
| 3.3 | Coherent neutrino scattering | 239 |
| 3.4 | Inelastic scattering of DM particles | 240 |
| | References..... | 241 |

Dark Matter: From production to detection

David G. Cerdeno¹
IPPP, Durham University

These notes are a write-up of lectures given at the HEP Summer School, which took place at the University of Lancaster in September, 2015.

1 Motivation for Dark Matter

The existence of a vast amount of dark matter (DM) in the Universe is supported by many astrophysical and cosmological observations. The latest measurements indicate that approximately a 27% of the Universe energy density is in form of a new type of non-baryonic cold DM. Given that the Standard Model (SM) of particle physics does not contain any viable candidate to account for it, DM can be regarded as one of the clearest hints of new physics.

1.1 Evidence for Dark Matter

Astrophysical and Cosmological observations have provided substantial evidence that point towards the existence of vast amounts of a new type of matter, that does not emit or absorb light. All astrophysical evidence for DM is solely based on gravitational effects (either through the observation of dynamical effects, deflection of light by gravitational lensing or measurements of the gravitational potential of galaxy clusters), which cannot be accounted for by just the observed luminous matter. The simplest way to solve these problems is the inclusion of more matter (which does not emit light - and is therefore dark in the astronomical sense²). Modifications in the Newtonian equation relating force and accelerations have also been suggested to address the problem at galactic scales, but this hypothesis is insufficient to account for effects at other scales (e.g., cluster of galaxies) or reproduce the anisotropies in the CMB.

No known particle can play the role of the DM (we will later argue that neutrinos contribute to a small part of the DM). Thus, this is one of the clearest hints for Physics Beyond the Standard Model and provides a window to new particle physics models. In the following I summarise some of the main pieces of evidence for DM at different scales.

I recommend completing this section with the first chapters of Ref. [1] and the recent article [2].

¹ Email: davidg.cerdeno@gmail.com

²Since dark matter does not absorb light, a more adequate name would have been transparent matter.

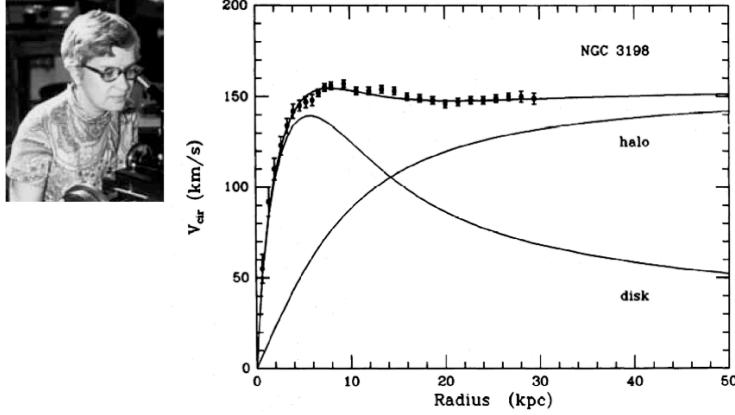


Figure 1: Left) Vera Rubin. Right) Rotation curve of a spiral galaxy, where the contribution from the luminous disc and dark matter halo is shown by means of solid lines.

1.1.1 Galactic scale

Rotation curves of spiral galaxies Rotation curves of spiral galaxies are probably the best-known examples of how the dynamical properties of astrophysical objects are affected by DM. Applying Gauss Law to a spiral galaxy (one can safely ignore the contribution from the spiral arms and assume a spherical distribution of matter in the bulge) leads to a simple relation between the rotation velocity of objects which are gravitationally bound to the galaxy and their distance to the galactic centre:

$$v = \sqrt{\frac{GM(r)}{r}}, \quad (1)$$

where $M(r)$ is the mass contained within the radius r . In the outskirts of the galaxy, where we expect that M does not increase any more, we would therefore expect a decay $v_{rot} \propto r^{-1/2}$.

Vera Rubin's observations of rotation curves of spiral galaxies [3, 4] showed a very slow decrease with the galactic radius. The careful work of Bosma [5], van Albada and Sancisi [6] showed that this flatness could not be accounted for by simply modifying the relative weight of the diverse galactic components (bulge, disc, gas), a new component was needed with a different spatial distribution (see Fig. 1).

Notice that the flatness of rotation curves can be obtained if a new mass component is introduced, whose mass distribution satisfies $M(r) \propto r$ in eq.(1). This is precisely the relation that one expects for a self-gravitational gas of non-interacting particles. This halo of DM can extend up to ten times the size of the galactic disc and contains approximately an 80% of the total mass of the galaxy.

Since then, flat rotation curves have been found in spiral galaxies, further strengthening the DM hypothesis. Of course, our own galaxy, the Milky Way is no exception. N-body simulations have proved to be very important tools in determining the properties of DM haloes. These can be characterised in terms of their density profile $\rho(r)$ and the velocity distribution function $f(v)$.

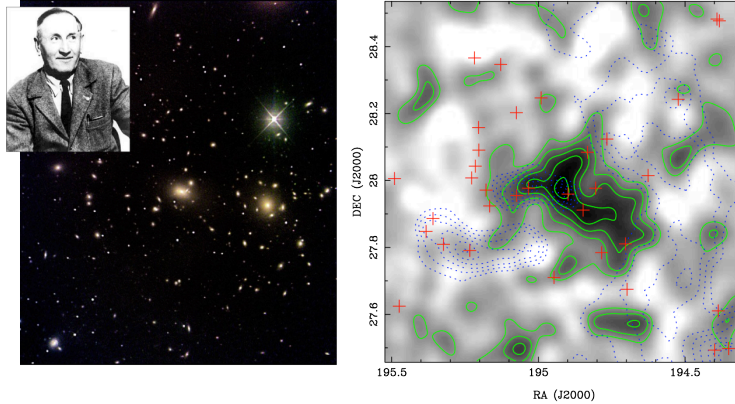


Figure 2: Left) Coma cluster and F. Zwicky, who carried out measurements of the peculiar velocities of this object. Right) Modern techniques [7], based on gravitational lensing, allow for a much more precise determination of the total mass of this object.

Observations of the local dynamics provide a measurement of the DM density at our position in the Galaxy. Up to substantial uncertainties, the local DM density can vary in a range $\rho_0 = 0.2 - 1 \text{ GeV cm}^{-3}$. It is customary to describe the DM halo in terms of a Spherical Isothermal Halo, in which the velocity distribution follows a Maxwell-Boltzmann law, but deviations from this are also expected. Finally, due to numerical limitations, current N-body simulations cannot predict the DM distribution at the centre of the galaxy. Whereas some results suggest the existence of a cusp of DM in the galactic centre, other simulations seem to favour a core. Finally, the effect of baryons is not easy to simulate, although substantial improvements have been recently made.

1.1.2 Galaxy Clusters

Peculiar motion of clusters. Fritz Zwicky studied the peculiar motions of galaxies in the Coma cluster [8, 9]. Assuming that the galaxy cluster is an isolated system, the virial theorem can be used to relate the average velocity of objects with the gravitational potential (or the total mass of the system).

As in the case of galaxies, this determination of the mass is insensitive to whether objects emit any light or not. The results can then be contrasted with other determinations that are based on the luminosity. This results in an extremely large mass-to-light ratio, indicative of the existence of large amounts of missing mass, which can be attributed to a DM component.

Modern determinations through weak lensing techniques provide a better gravitational determination of the cluster masses [10, 7] (see Fig. 2). I recommend reading through Ref.[9] for a derivation of the virial theorem in the context of Galaxy clusters.

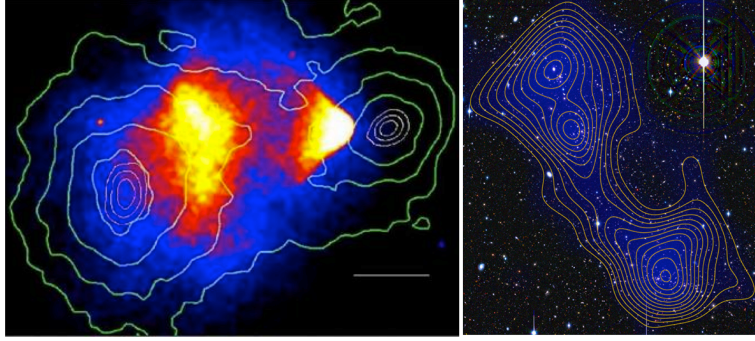


Figure 3: Left) Deep Chandra image of the Bullet cluster. Green lines represent mass contours from weak lensing. Right) Dark filament in the system Abell 222/223, reconstructed using weak lensing.

Dynamical systems. The Bullet Cluster (1E 0657-558) is a paradigmatic example of the effect of dark matter in dynamical systems. It consists of two galaxy clusters which underwent a collision. The visible components of the cluster, observed by the Chandra X-ray satellite, display a characteristic shock wave (which gives name to the whole system). On the other hand, weak-lensing analyses, which make use of data from the Hubble Space Telescope, have revealed that most of the mass of the system is displaced from the visible components. The accepted interpretation is that the dark matter components of the clusters have crossed without interacting significantly (see e.g., Ref. [11, 12]).

The Bullet Cluster is considered one of the best arguments against MOND theories (since the gravitational effects occur where there is no visible matter). It also sets an upper bound on the self-interaction strength of dark matter particles.

DM filaments. Observations of the distribution of luminous matter at large scales have shown that it follows a filamentary structure. Numerical simulations of structure formation with cold DM have been able to reproduce this feature. To date, it is well understood that DM plays a fundamental role in creating that filamentary network, gravitationally trapping the luminous matter. Recently, the comparison of the distribution of luminous matter in the Abell 222/223 supercluster with weak-lensing data has shown the existence of a dark filament joining the two clusters of the system. That filament, having no visible counterpart, is believed to be made of DM.

1.1.3 Cosmological scale

Finally, DM has also left its footprint in the anisotropies of the Cosmic Microwave Background (CMB). The analysis of the CMB constitutes a primary tool to determine the cosmological parameters of the Universe. The data obtained by dedicated satellites in the past decades has confirmed that we live in a flat Universe (COBE), dominated by dark matter and dark energy (WMAP), whose cosmological abundances have been determined with great precision (Planck).

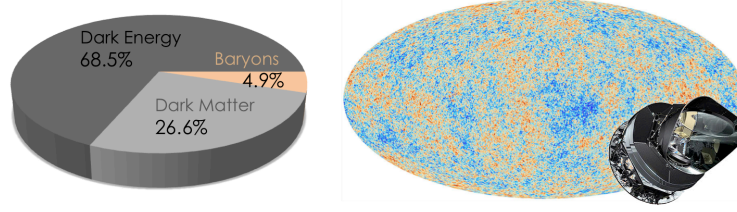


Figure 4: Left) Contribution to the energy density for each of the components of the Universe. Right) Planck temperature map.

The abundance of DM is normally expressed in terms of the cosmological density parameter, defined as $\Omega_{DM}h^2 = \rho_{DM}/\rho_c$ where ρ_c is the critical density necessary to recover a flat Universe and $h = 0.7$ is the normalised Hubble parameter. The most recent measurements by the Planck satellite, combined with data obtained from Supernovae (that trace the Universe expansion) yield

$$\Omega_{CDM}h^2 = 0.1196 \pm 0.0031 . \quad (2)$$

Given that $\Omega \approx 1$, this means that dark matter is responsible for approximately a 26% of the Universe energy density nowadays. Even more surprising is the fact that another exotic component is needed, *dark energy*, which makes up approximately the 69% of the total energy density (see Fig. 4).

1.2 Dark Matter properties

1.2.1 Neutral

It is generally argued that DM particles must be electrically neutral. Otherwise they would scatter light and thus not be dark. Similarly, constraints on charged DM particles can be extracted from unsuccessful searches for exotic atoms. Constraints on heavy millicharged particles are inferred from cosmological and astrophysical observations as well as direct laboratory tests [13, 14, 15]. Millicharged DM particles scatter off electrons and protons at the recombination epoch via Rutherford-like interactions. If millicharged particles couple tightly to the baryonphoton plasma during the recombination epoch, they behave like baryons thus affecting the CMB power spectrum in several ways [13, 14]. For particles much heavier than the proton, this results in an upper bound of its charge ϵ [14]

$$\epsilon \leq 2.24 \times 10^{-4} (M/1 \text{ TeV})^{1/2} . \quad (3)$$

Similarly, direct detection places upper bounds on the charge of the DM particle [16]

$$\epsilon \leq 7.6 \times 10^{-4} (M/1 \text{ TeV})^{1/2} . \quad (4)$$

1.2.2 Nonrelativistic

Numerical simulations of structure formation in the Early Universe have become a very useful tool to understand some of the properties of dark matter. In particular, it was soon found that dark matter has to be non-relativistic (cold) at the epoch of structure formation. Relativistic (hot) dark matter has a larger free-streaming length (the average distance traveled by a dark matter particle before it falls into a potential well). This leads to inconsistencies with observations.

However, at the Galactic scale, cold dark matter simulations lead to the occurrence of too much substructure in dark matter haloes. Apparently this could lead to a large number of subhaloes (observable through the luminous matter that falls into their potential wells). It was argued that if dark matter was *warm* (having a mass of approximately 2–3 keV) this problem would be alleviated.

Modern simulations, where the effect of baryons is included, are fundamental in order to fully understand structure formation in our Galaxy and determine whether dark matter is cold or warm.

1.2.3 NonBaryonic

The results of the CMB, together with the predictions from Big Bang nucleosynthesis, suggest that only 4 – 5% of the total energy budget of the universe is made out of ordinary (baryonic) matter. Given the mismatch of this with the total matter content, we must conclude that DM is non-baryonic.

Neutrinos. Neutrinos deserve special mention in this section, being the only viable non-baryonic DM candidate within the SM. Neutrinos are very abundant particles in the Universe and they are known to have a (very small) mass. Given that they also interact very feebly with ordinary matter (only through the electroweak force) they are in fact a component of the DM. There are, however various arguments that show that they contribute in fact to a very small part.

First, neutrinos are *too light*. Through the study of the decoupling of neutrinos in the early universe we can compute their thermal relic abundance. Since neutrinos are relativistic particles at the time of decoupling, this is in fact a very easy computation (we will come back to this in Section 2.2.1), and yields

$$\Omega_\nu h^2 \approx \frac{\sum_i m_i}{91 \text{ eV}}. \quad (5)$$

Using current upper bounds on the neutrino mass, we obtain $\Omega_\nu h^2 < 0.003$, a small fraction of the total DM abundance.

Second, neutrinos are *relativistic* (hot) at the epoch of structure formation. As mentioned above, hot DM leads to a different hierarchy of structure formation at large scales, with large objects forming first and small ones occurring only after fragmentation. This is inconsistent with observations.

1.2.4 Long-lived

Possibly the most obvious observation is that DM is a long-lived (if not stable) particle. The footprint of DM can be observed in the CMB anisotropies, its presence is essential for structure formation and we can feel its gravitational effects in clusters of galaxies and galaxies nowadays.

Stable DM candidates are common in models in which a new discrete symmetry is imposed by ensuring that the DM particle is the lightest with an exotic charge (and therefore its decay is forbidden). This is the case, e.g., in Supersymmetry (when R-parity is imposed), Kaluza-Klein scenarios (K-parity) or little Higgs models.

However, stability is not required by observation. DM particles can decay, as long as their lifetime is longer than the age of the universe. *Long-lived* DM particles feature very small couplings. Characteristic examples are gravitinos (whose decay channels are gravitationally suppressed) or axinos (which decays through the axion coupling).

2 Freeze Out of Massive Species

In this section we will address the computation of the relic abundance of dark matter particles, making special emphasis in the case of thermal production in the Early Universe.

2.1 Cosmological Preliminaries

This section does not intend to be a comprehensive review on Cosmology, but only an introduction to some of the elements that we will need for the calculation of Dark Matter freeze-out.

We can describe our isotropic and homogeneous Universe in terms of the Friedman- Lemaître- Robertson-Walker (FLRW) metric, which is exact solution of Einstein's field equations of general relativity

$$ds^2 = dt^2 - a^2(t) \left(\frac{dr^2}{1 - kr^2} + r^2(d\theta^2 + \sin\theta d\phi^2) \right) = g_{\mu\nu} dx^\mu dx^\nu. \quad (6)$$

The constant $k = \{-1, 0, +1\}$ corresponds to the spatial curvature, with $k = 0$ corresponding to a flat Universe (the choice we will be making in these notes). Remember that the affine connection, defined as

$$\Gamma_{\nu\lambda}^\mu = \frac{1}{2} g^{\mu\sigma} (g_{\sigma\nu, \lambda} + g_{\sigma\lambda, \nu} - g_{\nu\lambda, \sigma}), \quad (7)$$

is greatly simplified, since most of the derivatives vanish.

In the following we are going to work with a radiation-dominated Universe. Notice that matter-radiation equality only occurs very late (when the Universe is approximately 60 kyr) and dark matter freeze-out occurs before BBN. The Hubble parameter for a radiation-dominated Universe

reads

$$H = 1.66 g_*^{1/2} \frac{T^2}{M_P} , \quad (8)$$

where $M_P = 1.22 \times 10^{19}$ GeV.

It is customary to define the dimensionless parameter $x = m/T$ (where m is a mass parameter that we will later associate to the DM mass) and extract the explicit x dependence from the Hubble parameter to define $H(m)$ as follows

$$H(m) = 1.66 g_*^{1/2} \frac{m^2}{M_P} = H x^2 . \quad (9)$$

In this section we will try to compute the time evolution of the number density of dark matter particles, in order to be able to compute their relic abundance today and what this implies in the interaction strength of dark matter particles. The phase space distribution function f describes the occupancy number in phase space for a given particle in *kinetic* equilibrium, and distinguishes between fermions and bosons.

$$f = \frac{1}{e^{(E-\mu)/T} \pm 1} , \quad (10)$$

where the $(-)$ sign corresponds to bosons and the $(+)$ sign to fermions. E is the energy and μ the chemical potential. For species in chemical equilibrium, the chemical potential is conserved in the interactions. Thus, for processes such as $i + j \leftrightarrow c + d$ we have $\mu_i + \mu_j = \mu_c + \mu_d$. Notice then that all chemical potentials can be expressed in terms of the chemical potentials of conserved quantities, such as the baryon chemical potential μ_B . The number of independent chemical potentials corresponds to conserved particle numbers. This implies, for example, that given a particle with μ_i , the corresponding antiparticle would have the opposite chemical potential $-\mu_i$. For the same reason, since the number of photons is not conserved in interactions, $\mu_\gamma = 0$

Using the expression of the phase space distribution function (10), and integrating in phase space, we can compute a series of observables in the Universe. In particular, the number density of particles, n , the energy density, ρ , and pressure, p , for a dilute and weakly-interacting gas of particles with g internal degrees of freedom read

$$n = \frac{g}{(2\pi)^3} \int f(\mathbf{p}) d^3p, \quad (11)$$

$$\rho = \frac{g}{(2\pi)^3} \int E(\mathbf{p}) f(\mathbf{p}) d^3p, \quad (12)$$

$$p = \frac{g}{(2\pi)^3} \int \frac{|\mathbf{p}|^2}{3E(\mathbf{p})} f(\mathbf{p}) d^3p. \quad (13)$$

It is customary (and very convenient) to define densities normalised by the time dependent volume $a(t)^{-3}$. The reason for this is that in the absence of number changing processes, the density remains constant with time evolution (or redshift). Notice that since the evolution of the Universe is isentropic, the entropy density $s = S/a^3$ has precisely that dependence. Applying this prescription

to the number density of particles, we define the yield as a fraction of the number density and the entropy density as

$$Y = \frac{n}{s} . \quad (14)$$

Notice that, in the absence of number-changing processes, the yield remains constant. The evolution of the entropy density as a function of the temperature is given by ³

$$s = \frac{2\pi^2}{45} g_{*s} T^3 , \quad (15)$$

where the effective number of relativistic degrees of freedom for entropy is

$$g_{*s} = \sum_{\text{bosons}} g \left(\frac{T_i}{T} \right)^3 + \frac{7}{8} \sum_{\text{fermions}} g \left(\frac{T_i}{T} \right)^3 . \quad (16)$$

Remember also that we can express the energy density as

$$\rho = \frac{\pi^2}{30} g_* T^4 , \quad (17)$$

in terms of the relativistic number of degrees of freedom

$$g_* = \sum_{\text{bosons}} g \left(\frac{T_i}{T} \right)^4 + \frac{7}{8} \sum_{\text{fermions}} g \left(\frac{T_i}{T} \right)^4 . \quad (18)$$

In these two equations, T is the temperature of the plasma (in equilibrium) and T_i is the effective temperature of each species.

Solving the integral in eq. (11) explicitly for relativistic and non-relativistic particles, and expressing the results in terms of the Yield results in the following expressions.

- relativistic species

$$n = \frac{g_{eff}}{\pi^2} \zeta(3) T^3 , \quad (19)$$

where $g_{eff} = g$ for bosons and $g_{eff} = \frac{3}{4}g$ for fermions⁴. Then, using eq. (14), the Yield at equilibrium reads

$$Y_{eq} = \frac{45}{2\pi^4} \zeta(3) \frac{g_{eff}}{g_{*s}} \approx 0.278 \frac{g_{eff}}{g_{*s}} . \quad (20)$$

- non-relativistic species

$$n = g_{eff} \left(\frac{mT}{2\pi} \right)^{3/2} e^{-m/T} . \quad (21)$$

Then the Yield at equilibrium reads

$$Y_{eq} = \frac{45}{2\pi^4} \left(\frac{\pi}{8} \right)^{1/2} \frac{g_{eff}}{g_{*s}} \left(\frac{m}{T} \right)^{3/2} e^{-m/T} . \quad (22)$$

³To arrive at this equation, one can calculate $s = (p + \rho)/T$ for fermions and bosons, using the corresponding expression for the phase space distribution function.

⁴We are using here the approximation $E \approx |\vec{p}|$ in the relativistic limit, and the integrals $\int_0^\infty p^2/(e^p - 1) dp = 2\zeta(3)$, and $\int_0^\infty p^2/(e^p + 1) dp = 3\zeta(3)/2$, in terms of Riemann's Zeta function. Remember also that $\zeta(3) \approx 1.202$.

Exercise: It is easy to estimate the value of the Yield that we need in order to reproduce the correct DM relic abundance, $\Omega h^2 \approx 0.1$, since

$$\Omega h^2 = \frac{\rho_\chi}{\rho_c} h^2 = \frac{m_\chi n_\chi h^2}{\rho_c} = \frac{m_\chi Y_\infty s_0 h^2}{\rho_c}, \quad (23)$$

where Y_∞ corresponds to the DM Yield today and s_0 is today's entropy density. We can assume that the Yield did not change since DM freeze-out and therefore

$$\Omega h^2 = \frac{m_\chi Y_f s_0 h^2}{\rho_c}. \quad (24)$$

Using the measured value $s_0 = 2970 \text{ cm}^{-3}$, and the value of the critical density $\rho_c = 1.054 \times 10^{-5} h^2 \text{ GeV cm}^{-3}$, as well as Planck's result on the DM relic abundance, $\Omega h^2 \approx 0.1$, we arrive at

$$Y_f \approx 3.55 \times 10^{-10} \left(\frac{1 \text{ GeV}}{m_\chi} \right). \quad (25)$$

In Figure 5 represent the yield as a function of x for non-relativistic particles, using expression (22). As we can observe, the above range of viable values for Y_f correspond to $x_f \approx 20$.

Notice that this is a crude approximation and we will soon be making a more careful quantitative treatment.

2.2 Time evolution of the number density

The evolution of the number density operator can be computed by applying the covariant form of Liouville's operator to the corresponding phase space distribution function. Formally speaking, we have

$$\hat{L}[f] = C[f], \quad (26)$$

where \hat{L} is the Liouville operator, defined as

$$\hat{L} = p^\mu \frac{\partial}{\partial x^\mu} - \Gamma_{\sigma\rho}^\mu p^\sigma p^\rho \frac{\partial}{\partial p^\mu}, \quad (27)$$

and $C[f]$ is the collisional operator, which takes into account processes which change the number of particles (e.g., annihilations or decays). In the expression above, gravity enters through the affine connection, $\Gamma_{\sigma\rho}^\mu$.

One can show that in the case of a FRW Universe, for which $f(x^\mu, p^\mu) = f(t, E)$, we have

$$\begin{aligned} \hat{L} &= E \frac{\partial}{\partial t} - \Gamma_{\sigma\rho}^0 p^\sigma p^\rho \frac{\partial}{\partial E} \\ &= E \frac{\partial}{\partial t} - H |\mathbf{p}|^2 \frac{\partial}{\partial E}. \end{aligned} \quad (28)$$

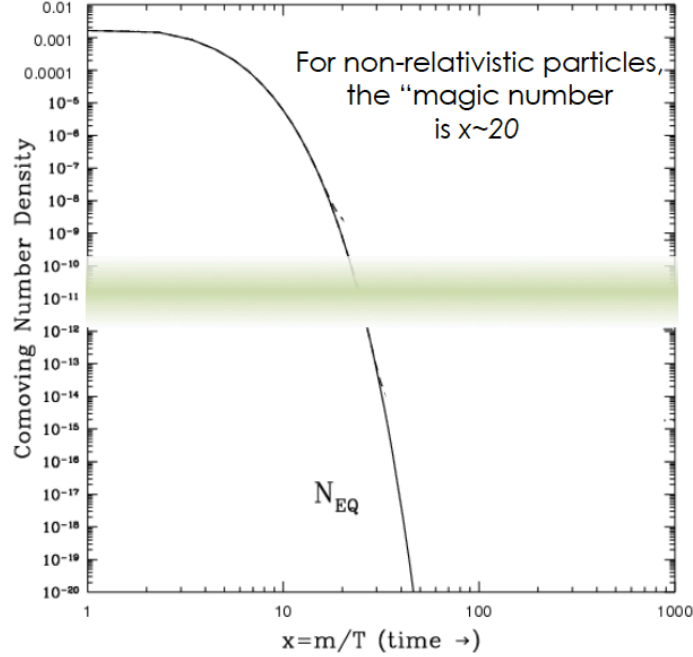


Figure 5: Equilibrium yield as a function of the dimensionless variable, x , for non-relativistic particles. The green band represents the freeze-out value, Y_f , for which the correct thermal relic abundance is achieved (for masses of order 1-1000 GeV).

Integrating over the phase space we can relate this to the time evolution of the number density

$$\frac{g}{(2\pi)^3} \int \frac{\hat{L}[f]}{E} d^3\mathbf{p} = \frac{g}{(2\pi)^3} \int \frac{C[f]}{E} d^3\mathbf{p} , \quad (29)$$

Exercise: We can show that

$$\frac{g}{(2\pi)^3} \int \frac{\hat{L}[f]}{E} d^3\mathbf{p} = \frac{dn}{dt} + 3Hn . \quad (30)$$

Regarding the collisional operator, it encodes the microphysical description in terms of Particle Physics, and incorporates all number-changing processes that create or deplete particles in the thermal bath. For simplicity, let us concentrate in annihilation processes, where SM particles (A, B) can annihilate to form a pair of DM particles (labelled 1, 2), or vice-versa ($A, B \leftrightarrow 1, 2$). The phase space corresponding to each particle is defined as

$$d\Pi_i = \frac{g_i}{(2\pi)^3} \frac{d^3\mathbf{p}_i}{2E_i} , \quad (31)$$

from where

$$\begin{aligned}
\frac{g}{(2\pi)^3} \int \frac{C[f]}{E} d^3\mathbf{p} &= - \int d\Pi_A d\Pi_B d\Pi_1 d\Pi_2 (2\pi)^4 \delta(p_A + p_B - p_1 - p_2) \\
&\quad [|\mathcal{M}_{12 \rightarrow AB}|^2 f_1 f_2 (1 \pm f_A)(1 \pm f_B) - |\mathcal{M}_{AB \rightarrow 12}|^2 f_A f_B (1 \pm f_1)(1 \pm f_2)] \\
&= - \int d\Pi_A d\Pi_B d\Pi_1 d\Pi_2 (2\pi)^4 \delta(p_A + p_B - p_1 - p_2) \\
&\quad [|\mathcal{M}_{12 \rightarrow AB}|^2 f_1 f_2 - |\mathcal{M}_{AB \rightarrow 12}|^2 f_A f_B] .
\end{aligned} \tag{32}$$

The terms $(1 \pm f_i)$ account for the viable phase space of the produced particles, taking into account whether they are fermions $(-)$ or bosons $(+)$. Assuming no CP violation in the DM sector (T invariance) $|\mathcal{M}_{12 \rightarrow AB}|^2 = |\mathcal{M}_{AB \rightarrow 12}|^2 \equiv |\mathcal{M}|^2$. Also, energy conservation in the annihilation process allows us to write $E_A + E_B = E_1 + E_2$, thus,

$$f_A f_B = f_A^{eq} f_B^{eq} = e^{-\frac{E_A + E_B}{T}} = e^{-\frac{E_1 + E_2}{T}} = f_1^{eq} f_2^{eq} . \tag{33}$$

In the first equality we have just used the fact that SM particles are in equilibrium. This eventually leads to

$$\frac{g}{(2\pi)^3} \int \frac{C[f]}{E} d^3\mathbf{p} = -\langle \sigma v \rangle (n^2 - n_{eq}^2) , \tag{34}$$

where we have defined the *thermally-averaged* cross-section as

$$\langle \sigma v \rangle \equiv \frac{1}{n_{eq}^2} \int d\Pi_A d\Pi_B d\Pi_1 d\Pi_2 (2\pi)^4 \delta(p_A + p_B - p_1 - p_2) |\mathcal{M}|^2 f_1^{eq} f_2^{eq} . \tag{35}$$

Collider enthusiasts would realise that this expression is similar to that of a cross-section, but we have to consider that the “initial conditions” do not correspond to a well-defined energy, but rather we have to integrate to the possible energies that the particles in the thermal bath may have. This explains the extra integrals in the phase space of incident particles with a distribution function given by $f_1^{eq} f_2^{eq}$. We are thus left with the familiar form of Boltzmann equation,

$$\frac{dn}{dt} + 3Hn = -\langle \sigma v \rangle (n^2 - n_{eq}^2) . \tag{36}$$

Notice that this is an equilibrium-restoring equation. If the right-hand-side of the equation dominates, then n traces its equilibrium value $n \approx n_{eq}$. However, when $Hn > \langle \sigma v \rangle n^2$, then the right-hand-side can be neglected and the resulting differential equation $dn/n = -3da/a$ implies that $n \propto a^{-3}$. This is equivalent to saying that DM particles do not annihilate anymore and their number density decreases only because the scale factor of the Universe increases.

It is also customary to define the dimensionless variable ⁵

$$x = \frac{m}{T} . \tag{37}$$

⁵It is important to point that this definition of x is not universal; some authors use T/m and care should be taken when comparing results from different sources in the literature.

Exercise: Using the yield defined in equation (14) we can simplify Boltzmann equation. Notice that

$$\frac{dY}{dt} = \frac{d}{dt} \left(\frac{n}{s} \right) = \frac{d}{dt} \left(\frac{a^3 n}{a^3 s} \right) = \frac{1}{a^3 s} \left(3a^2 \dot{a} n + a^3 \frac{dn}{dt} \right) = \frac{1}{s} \left(3Hn + \frac{dn}{dt} \right). \quad (38)$$

Here we have used that the expansion of the Universe is iso-entropic and thus $a^3 s$ remains constant. Also we use the definition of the Hubble parameter $H = \frac{\dot{a}}{a}$. This allows us to rewrite Boltzmann equation as follows

$$\frac{dY}{dt} = -s \langle \sigma v \rangle (Y^2 - Y_{eq}^2). \quad (39)$$

Now, since $a \propto T^{-1}$ and $s \propto T^3$,

$$\frac{d}{dt}(a^3 s) = 0 \rightarrow \frac{d}{dt}(aT) = 0 \rightarrow \frac{d}{dt} \left(\frac{a}{x} \right) = 0, \quad (40)$$

which in turns leads to

$$\frac{dx}{dt} = Hx, \quad (41)$$

and thus

$$\frac{dY}{dt} = \frac{dY}{dx} \frac{dx}{dt} = \frac{dY}{dx} Hx. \quad (42)$$

Using the results of Example (2.2) we can express Boltzmann equation (36) as

$$\begin{aligned} \frac{dY}{dx} &= \frac{-sx \langle \sigma v \rangle}{H(m)} (Y^2 - Y_{eq}^2) \\ &= \frac{-\lambda \langle \sigma v \rangle}{x^2} (Y^2 - Y_{eq}^2), \end{aligned} \quad (43)$$

where we have used the expression of the entropy density (15) in the last line and defined

$$\begin{aligned} \lambda &\equiv \frac{2\pi^2}{45} \frac{M_P g_{*s}}{1.66 g_*^{1/2}} m \\ &\approx 0.26 \frac{g_{*s}}{g_*^{1/2}} M_P m. \end{aligned} \quad (44)$$

Eq. (43) is a Riccati equation, without closed analytical form. Thus, to calculate its solutions we have to rely on numerical methods. However, it is possible to solve it approximately.

2.2.1 Freeze out of relativistic species

The freeze-out of relativistic species is easy to compute, since the yield (20) has no dependence on x_f . Neutrinos are a paradigmatic example of relativistic particles and one must in principle consider their contribution to the total amount of dark matter (after all, they are dark).

Since neutrinos decouple while they are still relativistic, their yield reads

$$Y_{eq} \approx 0.278 \frac{g_{eff}}{g_{*s}} . \quad (45)$$

Neutrinos decouple at a few MeV, when the species that were still relativistic are e^\pm , γ , ν and $\bar{\nu}$. Thus, the number of relativistic degrees of freedom is $g_* = g_{*s} = 10.75$. For one neutrino family, the effective number of degrees of freedom is $g_{eff} = 3g/4 = 3/2$. Using these values, the relic density today can be written as

$$\begin{aligned} \Omega h^2 &= \frac{\sum_i m_{\nu_i} Y_\infty s_0 h^2}{\rho_c} \\ &\approx \frac{\sum_i m_{\nu_i}}{91 \text{ eV}} . \end{aligned} \quad (46)$$

Notice that in order for neutrinos to be the bulk of dark matter, we would need $\sum_i m_{\nu_i} \approx 9 \text{ eV}$, which is much bigger than current upper limits (for example, obtained from cosmological observations). Notice, indeed, that if we consider the current bound $\sum_i m_{\nu_i} \leq 0.3 \text{ eV}$ we can quantify the contribution of neutrinos to the total amount of dark matter, resulting in $\Omega h^2 \leq 0.003$. This is less than a 3% of the total dark matter density.

2.2.2 Freeze out of non-relativistic species

We can define the quantity

$$\Delta_Y \equiv Y - Y_{eq} . \quad (47)$$

Boltzmann equation (43) is now easier to solve, at least approximately, as follows

- For early times, $1 < x \ll x_f$, the yield follows closely its equilibrium value, $Y \approx Y_{eq}$, and we can assume that $d\Delta_Y/dx = 0$. We then find

$$\Delta_Y = -\frac{\frac{dY_{eq}}{dx}}{Y_{eq}} \frac{x^2}{2\lambda\langle\sigma v\rangle} . \quad (48)$$

Thus, at freeze-out we obtain

$$\Delta_{Y_f} \approx \frac{x_f^2}{2\lambda\langle\sigma v\rangle} , \quad (49)$$

where in the last line we have used that for large enough x , using eq. (22) implies $\frac{dY_{eq}}{dx} \approx -Y_{eq}$.

- For late times, $x \gg x_f$, we can assume that $Y \gg Y_{eq}$, and thus $\Delta_{Y_\infty} \approx Y_\infty$, leading to the following expression,

$$\frac{d\Delta_Y}{dx} \approx -\frac{\lambda\langle\sigma v\rangle}{x^2} \Delta_Y^2 , \quad (50)$$

This is a separable equation that we integrate from the freeze-out time up to nowadays. In doing so, it is customary to expand the thermally averaged annihilation cross section in powers of x^{-1} as $\langle\sigma v\rangle = a + \frac{b}{x}$.

$$\int_{\Delta_{Y_f}}^{\Delta_{Y_\infty}} \frac{d\Delta_Y}{\Delta_Y^2} = - \int_{x_f}^{x_\infty} \frac{\lambda\langle\sigma v\rangle}{x^2} dx . \quad (51)$$

Taking into account that $x_\infty \gg x_f$, this leads to

$$\frac{1}{\Delta_{Y_\infty}} = \frac{1}{\Delta_{Y_f}} + \frac{\lambda}{x_f} \left(a + \frac{b}{2x_f} \right) . \quad (52)$$

The term $1/\Delta_{Y_f}$ is generally ignored (if we are only aiming at a precision up to a few per cent [17]) . We can check that this is a good approximation using the previously derived (49) for $x_f \approx 20$ (which, as we saw in Fig. 5 is the value for which the equilibrium Yield has the right value). This leads to

$$\Delta_{Y_\infty} = Y_\infty = \frac{x_f}{\lambda \left(a + \frac{b}{2x_f} \right)} . \quad (53)$$

The relic density can now be expressed in terms of this result as follows

$$\begin{aligned} \Omega h^2 &= \frac{m_\chi Y_\infty s_0 h^2}{\rho_c} \\ &\approx \frac{10^{-10} \text{ GeV}^{-2}}{a + \frac{b}{40}} \\ &\approx \frac{3 \times 10^{-27} \text{ cm}^3 \text{ s}^{-1}}{a + \frac{b}{40}} . \end{aligned} \quad (54)$$

This expression explicitly shows that for larger values of the annihilation cross section, smaller values of the relic density are obtained.

2.2.3 WIMPs

Equation (54) implies that in order to reproduce the correct relic abundance, dark matter particles must have a thermally averaged annihilation cross section (from now on we will shorten this to simply annihilation cross section when referring to $\langle\sigma v\rangle$) of the order of $\langle\sigma v\rangle \approx 3 \times 10^{-26} \text{ cm}^3 \text{ s}^{-1}$.

We can now consider a simple case in which dark matter particles self-annihilate into Standard Model ones through the exchange (e.g., in an s-channel) of a gauge boson. It is easy to see that if the annihilation cross section is of order $\langle\sigma v\rangle \sim G_F^2 m_{WIMP}^2$, where $G_F = 1.16 \times 10^{-5} \text{ GeV}^{-2}$, then the correct relic density is obtained for masses of the order of $\sim \text{GeV}$.

2.3 Computing the DM annihilation cross section

In the previous sections we have derived a relation between the thermally averaged annihilation cross section and the corresponding dark matter relic abundance. This is very useful, since it provides

an explicit link with particle physics. A central point in that calculation was the expansion in velocities of the thermally averaged annihilation cross section.

$$\langle \sigma v \rangle = \langle a + bv^2 + cv^4 + \dots \rangle = a + \frac{3}{2} \frac{b'}{x} + \frac{15}{8} \frac{c}{x^2} + \dots \quad (55)$$

Notice that in the expressions of the previous section we have defined $b \equiv 3b'/2$. As we also mentioned before, DM candidates tend to decouple when $x_f \approx 20$. For this value, the rms velocity of the particles is about $c/4$, thus corrections of order x^{-1} can in general not be ignored (they can be of order 5 – 10%). Moreover, some selection rules can actually lead to $a = 0$ for some particular annihilation channels and in that case $\langle \sigma v \rangle$ is purely velocity-dependent.

It is important to define correctly the relative velocity that enters the above equation. In Ref. [17] an explicitly Lorentz-invariant formalism is introduced where

$$g_1 \int C[f_1] \frac{d^3 p_1}{2\pi^3 E_1} = - \int \langle \sigma v \rangle_{\text{Mø}} (dn_1 dn_2 - dn_1^{eq} dn_2^{eq}) \quad (56)$$

where $\langle \sigma v \rangle_{\text{Mø}} n_1 n_2$ is invariant under Lorentz transformations and equals $v_{lab} n_{1,lab} n_{2,lab}$ in the rest frame of one of the incoming particles. In our case the densities and Møller velocity refer to the cosmic comoving frame. In terms of the particle velocities $\vec{v}_i = \vec{p}_i/E_i$,

$$v_{\text{Mø}} = [|\vec{v}_1 - \vec{v}_2|^2 + |\vec{v}_1 \times \vec{v}_2|^2]^{1/2} \quad (57)$$

The thermally-averaged product of the dark matter pair-annihilation cross section and their relative velocity $\langle \sigma v_{\text{Mø}} \rangle$ is most properly defined in terms of separate thermal baths for both annihilating particles [17, 18],

$$\langle \sigma v_{\text{Mø}} \rangle(T) = \frac{\int d^3 p_1 d^3 p_2 \sigma v_{\text{Mø}} e^{-E_1/T} e^{-E_2/T}}{\int d^3 p_1 d^3 p_2 e^{-E_1/T} e^{-E_2/T}} \quad (58)$$

where $p_1 = (E_1, \mathbf{p}_1)$ and $p_2 = (E_2, \mathbf{p}_2)$ are the 4-momenta of the two colliding particles, and T is the temperature of the bath. The above expression can be reduced to a one-dimensional integral which can be written in a Lorentz-invariant form as [17]

$$\langle \sigma v_{\text{Mø}} \rangle(T) = \frac{1}{8m_\chi^4 T K_2^2(m_\chi/T)} \int_{4m_\chi^2}^{\infty} ds \sigma(s) (s - 4m_\chi^2) \sqrt{s} K_1\left(\frac{\sqrt{s}}{T}\right) \quad (59)$$

where $s = (p_1 + p_2)^2$ and K_i denote the modified Bessel function of order i . In computing the relic abundance [19] one first evaluates eq. (59) and then uses this to solve the Boltzmann equation. The freeze out temperature can be computed by solving iteratively the equation

$$x_f = \ln \left(\frac{m_\chi}{2\pi^3} \sqrt{\frac{45}{2g_* G_N}} \langle \sigma v_{\text{Mø}} \rangle(x_f) x_f^{-1/2} \right) \quad (60)$$

where g_* represents the effective number of degrees of freedom at freeze-out ($\sqrt{g_*} \approx 9$). As explained in the previous section, one finds that the freeze-out point $x_f \equiv m_\chi/T_f$ is approximately $x_f \sim 20$.

The procedure can be simplified if we consider that the annihilation cross section can be expanded in plane waves. For example, consider the dark matter annihilation process $\chi\chi \rightarrow ij$ and assume

that the thermally averaged annihilation cross section can be expressed as $\langle\sigma v\rangle_{ij} \approx a_{ij} + b_{ij}x$. It can then be shown that the coefficients a_{ij} and b_{ij} can be computed from the corresponding matrix element. For example,

$$a_{ij} = \frac{1}{m_\chi^2} \left(\frac{N_c}{32\pi} \beta(s, m_i, m_j) \frac{1}{2} \int_{-1}^1 d \cos \theta_{CM} |\mathcal{M}_{\chi\chi \rightarrow ij}|^2 \right)_{s=4m_\chi^2}, \quad (61)$$

where θ_{CM} denotes the scattering angle in the CM frame, $N_c = 3$ for $\bar{q}q$ final states and 1 otherwise, and

$$\beta(s, m_i, m_j) = \left(1 - \frac{(m_i + m_j)^2}{s} \right)^{1/2} \left(1 - \frac{(m_i - m_j)^2}{s} \right)^{1/2} \quad (62)$$

The contribution for each final state is calculated separately.

2.3.1 Special cases

The derivation of equation (54) relied on the expansion of $\langle\sigma v\rangle$ in terms of plane waves. This expansion can be done when $\langle\sigma v\rangle$ varies slowly with the energy (we can express this in terms of the centre of mass energy s). However, there are some special cases in which this does not happen and which deserve further attention.

- **Annihilation thresholds**

A new annihilation channel $\chi + \chi \rightarrow A + B$ opens up when $2m_\chi \approx m_A + m_B$. In this case the expansion in velocities of $\langle\sigma v\rangle$ diverges (at the threshold energy) and it is no longer a good approximation [17]. Notice in particular that below the threshold, the expression of a_{ij} in Equation (61) is equal to zero (as it is only evaluated for $s > 4m_\chi^2$). A qualitative way of understanding this is of course that DM particles have a small velocity, which is here approximated to zero. In the limit of zero velocity, the total energy available is determined by the DM mass.

However, we are here ignoring that a fraction of DM particles (given by their thermal distribution in the Early Universe) have a kinetic energy sufficient to annihilate into heavier particles (above the threshold). In other words, $\langle\sigma v\rangle$ is different from zero below the corresponding thresholds. A very good illustration of this effect is shown in Ref. [17] and is here reproduced in Fig. 6.

The thin solid line corresponds to the approximate expansion in velocities and shows that not only $\langle\sigma v\rangle$ is zero below the threshold, but also diverges at the threshold, thereby not leading to a good solution. Expression (59), represented by a thick solid line, still provides a good solution.

- **Resonances**

The annihilation cross section is not a smooth function of s in the vicinity of an s-channel resonance. Thus, the velocity expansion of $\langle\sigma v\rangle$ will fail (although once more, expression (59) still provides a good solution). For a Breit-Wigner resonance (due to a particle ϕ) we have

$$\sigma = \frac{4\pi w}{p^2} B_i B_f \frac{m_\phi^2 \Gamma_\phi^2}{(s - m_\phi^2)^2 + m_\phi^2 \Gamma_\phi^2}, \quad (63)$$

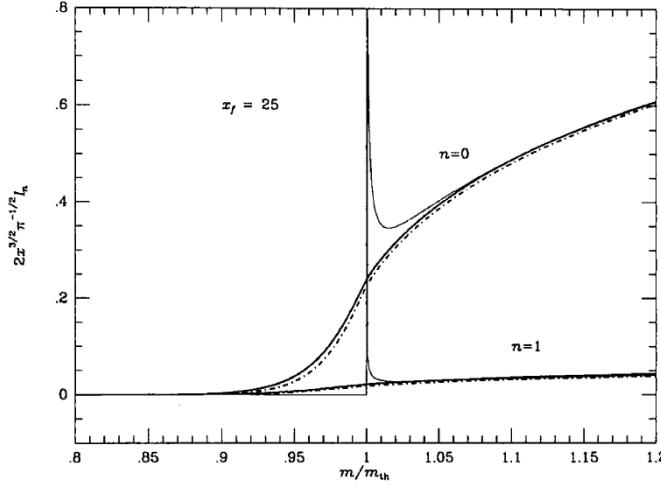


Figure 6: Relativistic thermal average near a threshold (thick solid line) compared to the result from the expansion in powers of x^{-1} (thin line). Figure from Ref. [17].

in terms of the centre of mass momentum $p = 1/2(s - 4m^2)^{1/2}$ and the statistical factor $w = (2J + 1)/(2S + 1)^2$. The quantities $B_{i,f}$ correspond to the branching fractions of the resonance into the initial and final channel.

We can define the kinetic energy per unit mass in the lab frame, ϵ , as

$$\epsilon = \frac{(E_{1,lab} - m) + (E_{2,lab} - m)}{2m} = \frac{2 - 4m^2}{4m^2} , \quad (64)$$

and rewrite the expression for σ in the lab frame (we want to use Equation (3.21) in Ref. [17] to compute $\langle \sigma v_{M\phi l} \rangle$). Summing to all final states, and using $v_{lab} = 2\epsilon^{1/2}(1 + \epsilon)^{1/2}/(1 + 2\epsilon)$, we obtain

$$\sigma v_{lab} = \frac{8\pi w}{m^2} b_\phi(\epsilon) \frac{\gamma_\phi^2}{(\epsilon - \epsilon_\phi^2)^2 + \gamma_\phi^2} , \quad (65)$$

with the definitions $b(\epsilon) = B_i(1 - B_i)(1 + \epsilon)^{1/2}/(\epsilon^{1/2}(1 + 2\epsilon))$, $\gamma_\phi = m_\phi \Gamma_\phi / 4m^2$, and $\epsilon_\phi = (m_\phi^2 - 4m^2)/4m^2$.

It can be shown that in the case of a very narrow resonance, $\gamma_\phi \ll 1$, the expression above can be approximated as

$$\sigma v_{lab} = \frac{8\pi w}{m^2} b_\phi(\epsilon) \pi \gamma_\phi \delta(\epsilon - \epsilon_\phi) , \quad (66)$$

the relativistic formula for the thermal average then reads [17]

$$\langle \sigma v_{M\phi l} \rangle = \frac{16\pi w}{m^2} \frac{x}{K_2^2(x)} \pi \gamma_\phi \epsilon_\phi^{1/2} (1 + 2e_\phi) K_1(2x \sqrt{1 + \epsilon_\phi}) b_\phi(e_\phi) \theta(\epsilon_\phi) . \quad (67)$$

Notice that $\epsilon_\phi > 0$ when $m < 2m_\phi$, i.e., when the mass of the DM is not enough to enter the resonance. The reason is easy to understand. Only through the extra kinetic energy provided

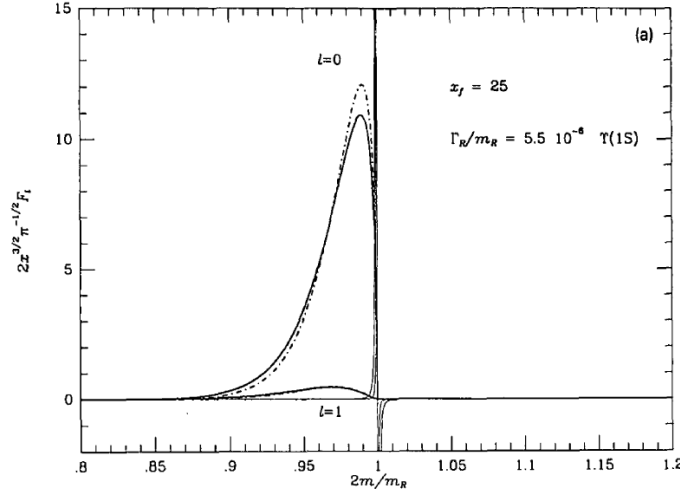


Figure 7: Relativistic thermal average in a resonance (thick solid line) compared to the result from the expansion in powers of x^{-1} (thin line). Figure from Ref. [17].

by the thermal bath, the resonance condition can be satisfied. However, when the mass of the DM exceeds the resonance condition, the kinetic energy only takes us further away from the resonant condition and the thermalised cross section tends to vanish. In other words, the centre of mass rest energy exceeds $m_\phi/2$. This can be seen in Figure 7.

For a large width the expression has to be computed numerically and can be found in [17].

- Coannihilations

When deriving Boltzmann equation (36) we have only considered one exotic species, but this needs not be the case. In fact, in most particle models for DM, there are more exotic species that we need to take into account. Notice that, in principle, this would lead to a system of coupled Boltzmann equations. If we label exotic species as χ_i , with $i = 0, 1 \dots k$, and SM particles as A, B , we have to consider all number changing processes for each species,

$$\begin{aligned} (i) \quad & \chi_i + \chi_j \rightarrow A + B \\ (ii) \quad & \chi_i + A \rightarrow \chi_j + B \\ (iii) \quad & \chi_j \rightarrow \chi_i + A \end{aligned}$$

If we consider the (usual) case in which the DM is protected by a symmetry (e.g., in the case of Supersymmetric theories) and that the exotic particles all must decay eventually into the lightest one χ_0 , then, we must only trace the evolution of the total number density of exotic species, $n = \sum_{i=0}^k n_i$. Under this assumption, processes (ii) and (iii) do not need to be considered, as they do not change the number of exotics. This is correct as long as the rate of these is faster than the expansion of the Universe.

Regarding process (i) we have to be aware that the cross section σ_{ij} is going to appear multiplied by the corresponding number densities, $n_i n_j$. Now, we are considering the case

in which both particles i and j are non-relativistic and as a consequence, $n_{i,j}$ are Boltzmann suppressed, $n_{i,j}/e^{-m_{i,j}/T}$. Thus, unless $m_j \approx m_i$, the abundance of χ_j is negligible and only the process $\chi_i + \chi_j \rightarrow A + B$ is important (and we are back to the case of a single exotic).

However, when $m_j \approx m_i$, there can be coannihilation effects and particle j may serve as a channel through which particles i can be more effectively depleted. This is the case, e.g., of the stau and the neutralino in supersymmetric theories.

3 Direct Dark Matter Detection

3.1 Computation of the Dark Matter detection rate

3.1.1 DM flux

We can easily estimate the flux of DM particles through the Earth. The DM typical velocity is of the order of $300 \text{ km s}^{-1} \sim 10^{-3} c$. Also, the local DM density is $\rho_0 = 0.3 \text{ GeV cm}^{-3}$, thus, the DM number density is $n = \rho/m$.

$$\phi = \frac{v\rho}{m} \approx \frac{10^7}{m} \text{ cm}^{-2} \text{ s}^{-1} \quad (68)$$

These particles interact very weakly with SM particles.

3.1.2 Kinematics

Direct DM detection is based on the search of the scattering between DM particles and nuclei in a detector. This process is obly observable through the recoiling nucleus, with an energy E_R . DM particles move at non-relativistic speeds in the DM halo. Thus, the dynamics of their elastic scattering off nuclei are easily calculated. In particular, the recoiling energy of the nucleus is given by

$$E_R = \frac{1}{2} m_\chi v^2 \frac{4m_\chi m_N}{(m_\chi + m_N)^2} \frac{1 + \cos \theta}{2} \quad (69)$$

It can be checked that for DM particles with a mass of the order of 100 GeV, this leads to recoil energies of approximately $E_R \sim 100 \text{ keV}$. Notice also that the maximal energy transfer occurs on a head-on-collision and when the DM mass is equal to the target mass. In such a case

$$E_R^{max} = \frac{1}{2} m_\chi v^2 = \frac{1}{2} m_\chi \times 10^{-6} = \frac{1}{2} \left(\frac{m_\chi}{1 \text{ GeV}} \right) \text{ keV} \quad (70)$$

where we have used that in a DM halo the typical velocity is $v \sim 10^{-3} c$.

Experiments must therefore be very sensitive and be able to remove an overwhelming background of ordinary processes which lead to nuclear recoils of the same energies.

3.2 The master formula for direct DM detection

The total number of detected DM particles, N , can be understood as the product of the DM flux (which is equal to the DM number density, n , times its speed, v), times the effective area of the target (i.e., the number of targets N_T times the scattering cross-section, σ), all of this multiplied by the observation time, t ,

$$N = t n v N_T \sigma. \quad (71)$$

We will be interested in determining the spectrum of DM recoils, i.e., the energy dependence of the number of detected DM particles. Thus,

$$\frac{dN}{dE_R} = t n v N_T \frac{d\sigma}{dE_R}. \quad (72)$$

Now, the DM velocity is not unique, and in fact DM particles are described by a local velocity distribution, $f(\vec{v})$, where \vec{v} is the DM velocity in the reference frame of the detector. We therefore have to integrate to all possible DM velocities, with their corresponding probability density,

$$\frac{dN}{dE_R} = t n N_T \int_{v_{min}} v f(\vec{v}) \frac{d\sigma}{dE_R} d\vec{v}, \quad (73)$$

where

$$v_{min} = \sqrt{m_\chi E_R / 2\mu_{\chi N}^2} \quad (74)$$

is the minimum speed necessary to produce a DM recoil of energy E_R , in terms of the WIMP-nucleus reduced mass, $\mu_{\chi N}$. Using $n = \rho/m_\chi$ and $N_T = M_T/m_N$ (where M_T is the total detector mass and m_N is the mass of the target nuclei), and defining the experimental exposure $\epsilon = t M_T$, we arrive at the usual expression for the DM detection rate

$$\frac{dN}{dE_R} = \epsilon \frac{\rho}{m_\chi m_N} \int_{v_{min}} v f(\vec{v}) \frac{d\sigma}{dE_R} d\vec{v}. \quad (75)$$

3.2.1 The scattering cross section

The scattering takes place in the non-relativistic limit. The cross section is therefore approximately isotropic (angular terms being suppressed by $v^2/c^2 \sim 10^{-6}$). This implies that

$$\frac{d\sigma}{d\cos\theta^*} = \text{constant} = \frac{\sigma}{2} \quad (76)$$

On the other hand,

$$E_R = E_R^{max} \frac{1 + \cos\theta^*}{2} \rightarrow \frac{dE_R}{d\cos\theta^*} = \frac{E_R^{max}}{2} \quad (77)$$

From this, we can see that

$$\frac{d\sigma}{dE_R} = \frac{d\sigma}{d\cos\theta^*} \frac{d\cos\theta^*}{dE_R} = \frac{\sigma}{E_R^{max}} = \frac{m_N}{2\mu_{\chi N}^2} \frac{\sigma}{v^2} \quad (78)$$

Notice finally that the momentum transfer from WIMP interactions reads (remember that we are considering non-relativistic processes and thus we neglect the kinetic energy of the nucleus)

$$q = \sqrt{2 m_N E_R} \quad (79)$$

and is typically of the order of the MeV. The equivalent de Broglie length would be $\lambda \sim 2\pi\hbar/p \sim 10 - 100$ fm. For light nuclei, the DM particle sees the nucleus as a whole, without substructure, only for heavier nuclei we have to take into account a suppression form factor. The nuclear form factor, $F^2(E_R)$, accounts for the loss of coherence

$$\frac{d\sigma}{dE_R} = \frac{m_N}{2\mu_{\chi N}^2} \frac{\sigma_0}{v^2} F^2(E_R) \quad (80)$$

Finally, the scattering cross section receives different contributions, depending on the microscopic description of the interaction.

In the end, we can

$$\frac{dN}{dE_R} = \epsilon \frac{\rho}{2 m_\chi \mu_{\chi N}^2} \sigma_0 F^2(E_R) \int_{v_{min}} \frac{f(\vec{v})}{v} d\vec{v} . \quad (81)$$

The inverse mean velocity

$$\eta(v_{min}) = \int_{v_{min}} \frac{f(\vec{v})}{v} d\vec{v} . \quad (82)$$

is the main Astrophysical input.

3.2.2 The importance of the threshold

From the kinematics of the DM-nucleus interaction, we see that, for a given recoil energy E_R , we require a minimal velocity of DM particles, given by expression (74).

Thus, given that experiments are only sensitive to DM interactions above a certain energy threshold, E_T , this means that we are only probing a part of the WIMP velocity distribution function (for a given DM mass). Conversely, given that DM particles have a maximum velocity in the halo (otherwise they become unbound and escape the galaxy), the experimental energy threshold is a limitation to explore low-mass WIMPs.

Exercise: Consider a germanium experiment and a xenon experiment with a threshold of 2 keV. Given the escape velocity in a typical isothermal halo, $v_{esc} = 554 \text{ km s}^{-1}$, determine the minimum DM mass that these experiments can probe.

This is the reason that experiments loose sensitivity for small masses.

3.2.3 Velocity distribution function

It is customary to consider the Isothermal Spherical Halo, which assumes that the Milky Way (MW) halo is an isotropic, isothermal sphere with density profile $\rho \propto r^{-2}$. The velocity distribution, in the galactic rest frame, for such a halo reads

$$f_{gal}(\vec{v}) = \frac{1}{(2\pi\sigma)^{3/2}} e^{-\frac{|\vec{v}|^2}{2\sigma^2}}, \quad (83)$$

where the one-dimensional velocity dispersion, σ , is related to the circular speed, v_c , as $\sigma = v_c/\sqrt{2}$. The canonical values are $v_c = 220 \text{ km s}^{-1}$, with a statistical error of order 10% (see references in [20])

Now, in order to use it for direct detection experiments we need to carry out a Galilean transformation $\vec{v} \rightarrow \vec{v} + \vec{v}_E$, such that

$$f(\vec{v}) = f_{gal}(\vec{v} + \vec{v}_E(t)). \quad (84)$$

where $\vec{v}_E(t)$ is the velocity of the Earth with respect to the Galactocentric rest frame.

$$\vec{v}_E(t) = \vec{v}_{LRF} + \vec{v}_\odot + \vec{v}_{orbit}(t) \quad (85)$$

Notice that v_E includes contributions from the speed of the Local Standard of Rest v_{LSR} , the peculiar velocity of the Sun with respect to v_{LSR} , and the Earths velocity around the Sun, which has an explicit time dependence.

Notice that if we work with the SHM, the angular integration in the computation of direct detection rates can be easily done as follows

$$\begin{aligned} \int \frac{f(\vec{v})}{v} d^3v &= \int d\phi \int d\cos\theta \int dv v \frac{1}{(2\pi\sigma^2)^{3/2}} e^{-\frac{|\vec{v}|^2 + |\vec{v}_E|^2}{2\sigma^2}} e^{\frac{|\vec{v}||\vec{v}_E|\cos\theta}{\sigma^2}} \\ &= 2\pi \int dv v \frac{2\sigma^2}{|v||\vec{v}_E|(2\pi\sigma)^{3/2}} e^{-\frac{|\vec{v}|^2 + |\vec{v}_E|^2}{2\sigma^2}} \sinh\left(\frac{|\vec{v}||\vec{v}_E|}{\sigma^2}\right) \\ &= \int dv \frac{\sqrt{2}}{\sqrt{\pi}\sigma|\vec{v}_E|} e^{-\frac{|\vec{v}|^2 + |\vec{v}_E|^2}{2\sigma^2}} \sinh\left(\frac{|\vec{v}||\vec{v}_E|}{\sigma^2}\right) \end{aligned} \quad (86)$$

3.3 Coherent neutrino scattering

Solar neutrinos might leave a signal in DD experiments, either through their coherent scattering with the target nuclei or through scattering with the atomic electrons.

In general, the number of recoils per unit energy can be written

$$\frac{dR}{dE_R} = \frac{\epsilon}{m_T} \int dE_\nu \frac{d\phi_\nu}{dE_\nu} \frac{d\sigma_\nu}{dE_R}, \quad (87)$$

where ϵ is the exposure and m_T is the mass of the target electron or nucleus. If several isotopes are present, a weighted average must be performed over their respective abundances.

The SM neutrino-electron scattering cross section is

$$\frac{d\sigma_{\nu e}}{dE_R} = \frac{G_F^2 m_e}{2\pi} \left[(g_v + g_a)^2 + (g_v - g_a)^2 \left(1 - \frac{E_R}{E_\nu}\right)^2 + (g_a^2 - g_v^2) \frac{m_e E_R}{E_\nu^2} \right], \quad (88)$$

where G_F is the Fermi constant, and

$$g_{v;\mu,\tau} = 2 \sin^2 \theta_W - \frac{1}{2}; \quad g_{a;\mu,\tau} = -\frac{1}{2}, \quad (89)$$

for muon and tau neutrinos. In the case $\nu_e + e \rightarrow \nu_e + e$, the interference between neutral and charged current interaction leads to a significant enhancement:

$$g_{v;e} = 2 \sin^2 \theta_W + \frac{1}{2}; \quad g_{a;e} = +\frac{1}{2}. \quad (90)$$

The neutrino-nucleus cross section in the SM reads

$$\frac{d\sigma_{\nu N}}{dE_R} = \frac{G_F^2}{4\pi} Q_v^2 m_N \left(1 - \frac{m_N E_R}{2E_\nu^2}\right) F^2(E_R), \quad (91)$$

where $F^2(E_R)$ is the nuclear form factor, for which we have taken the parametrisation given by Helm [21]. Q_v parametrises the coherent interaction with protons (Z) and neutrons ($N = A - Z$) in the nucleus:

$$Q_v = N - (1 - 4 \sin^2 \theta_W) Z. \quad (92)$$

3.4 Inelastic scattering of DM particles

WIMPs can also have inelastic scattering off nuclei [22]. The WIMP needs to have sufficient speed to interact with the nucleus and promote to an excited state (with energy separation δ)

$$\frac{1}{2} \mu_{\chi N} v^2 > \delta \quad (93)$$

This leads to the condition

$$v_{\min} = \sqrt{\frac{1}{2m_N E_R} \left(\frac{m_N E_R}{\mu_{\chi N}} + \delta \right)} \quad (94)$$

Therefore, the main effect at a given experiment is to limit the sensitivity only to a part of the phase space of the halo. This favours heavy nuclei (since they can transfer more energy to the outgoing WIMP) and can account for observation in targets such as iodine (DAMA/LIBRA) while avoiding observation in lighter ones such as Ge (CDMS)

References

- [1] J. Silk and Others, *Particle Dark Matter: Observations, Models and Searches*. 2010.
- [2] G. Bertone and D. Hooper, *A History of Dark Matter*, .
- [3] V. C. Rubin and J. Ford, W. Kent, *Rotation of the Andromeda Nebula from a Spectroscopic Survey of Emission Regions*, *Astrophys. J.* **159** (1970) 379.
- [4] V. C. Rubin, N. Thonnard, and J. Ford, W. K., *Rotational properties of 21 SC galaxies with a large range of luminosities and radii, from NGC 4605 $/R = 4\text{kpc}/$ to UGC 2885 $/R = 122\text{kpc}/$* , *Astrophys. J.* **238** (1980) 471.
- [5] A. Bosma, *21-cm line studies of spiral galaxies. II. The distribution and kinematics of neutral hydrogen in spiral galaxies of various morphological types.*, *Astron. J.* **86** (1981) 1825.
- [6] T. S. van Albada, J. N. Bahcall, K. Begeman, and R. Sancisi, *Distribution of dark matter in the spiral galaxy NGC 3198*, *Astrophys. J.* **295** (1985) 305.
- [7] R. Gavazzi, C. Adami, F. Durret, et al., *A weak lensing study of the Coma cluster*, *Astron. Astrophys.* **498** (2009) L33–L36, [[arXiv:0904.0220](#)].
- [8] F. Zwicky, *Die Rotverschiebung von extragalaktischen Nebeln*, *Helv. Phys. Acta* **6** (1933) 110–127.
- [9] F. Zwicky, *On the Masses of Nebulae and of Clusters of Nebulae*, *Astrophys. J.* **86** (1937) 217.
- [10] J. M. Kubo, A. Stebbins, J. Annis, et al., *The Mass Of The Coma Cluster From Weak Lensing In The Sloan Digital Sky Survey*, *Astrophys. J.* **671** (2007) 1466–1470, [[arXiv:0709.0506](#)].
- [11] M. Markevitch, A. H. Gonzalez, D. Clowe, et al., *Direct constraints on the dark matter self-interaction cross-section from the merging galaxy cluster 1E0657-56*, *Astrophys. J.* **606** (2003) 819–824, [[astro-ph/0309303](#)].
- [12] D. Clowe, M. Bradac, A. H. Gonzalez, et al., *A direct empirical proof of the existence of dark matter*, *Astrophys. J.* **648** (2006) L109–L113, [[astro-ph/0608407](#)].
- [13] S. D. McDermott, H.-B. Yu, and K. M. Zurek, *Turning off the Lights: How Dark is Dark Matter?*, *Phys. Rev. D* **83** (2010) 063509, [[arXiv:1011.2907](#)].
- [14] C. Kouvaris, *Composite Millicharged Dark Matter*, *Phys. Rev. D* **88** (2013) 015001, [[arXiv:1304.7476](#)].
- [15] A. D. Dolgov, S. L. Dubovsky, G. I. Rubtsov, and I. I. Tkachev, *Constraints on millicharged particles from Planck*, *Phys. Rev. D* **88** (2013) 117701, [[arXiv:1310.2376](#)].
- [16] E. Del Nobile, M. Nardecchia, and P. Panci, *Millicharge or Decay: A Critical Take on Minimal Dark Matter*, [arXiv:1512.05353](#).
- [17] P. Gondolo and G. Gelmini, *Cosmic abundances of stable particles: Improved analysis*, *Nucl. Phys. B* **360** (1991) 145–179.

- [18] M. Srednicki, R. Watkins, and K. A. Olive, *Calculations of relic densities in the early universe*, *Nucl. Phys. B* **310** (1988) 693–713.
- [19] T. Nihei, L. Roszkowski, and R. R. de Austri, *Exact Cross Sections for the Neutralino-Slepton Coannihilation*, *JHEP* **07** (2002) 46, [[hep-ph/0206266](#)].
- [20] F. Mayet, A. M. Green, J. B. R. Battat, et al., *A review of the discovery reach of directional Dark Matter detection*, *Phys. Rep.* **627** (2016) 1–49, [[arXiv:1602.03781](#)].
- [21] R. H. Helm, *Inelastic and Elastic Scattering of 187-Mev Electrons from Selected Even-Even Nuclei*, *Phys. Rev.* **104** (1956) 1466–1475.
- [22] D. Smith and N. Weiner, *Inelastic Dark Matter*, *Phys. Rev. D* **64** (2001) 043502, [[hep-ph/0101138](#)].